

University of Southampton Research Repository

Copyright © and Moral Rights for this thesis and, where applicable, any accompanying data are retained by the author and/or other copyright owners. A copy can be downloaded for personal non-commercial research or study, without prior permission or charge. This thesis and the accompanying data cannot be reproduced or quoted extensively from without first obtaining permission in writing from the copyright holder/s. The content of the thesis and accompanying research data (where applicable) must not be changed in any way or sold commercially in any format or medium without the formal permission of the copyright holder/s.

When referring to this thesis and any accompanying data, full bibliographic details must be given, e.g.

Thesis: Author (Year of Submission) "Full thesis title", University of Southampton, name of the University Faculty or School or Department, PhD Thesis, pagination.

Data: Author (Year) Title. URI [dataset]

UNIVERSITY OF SOUTHAMPTON
Faculty of Engineering and the Environment

Characterising the Creation of Defects in Large Scale Vacuum Assisted Resin Infusions in the Marine Industry

By

Mr Matthew Streeter

Thesis for the degree of Engineering Doctorate

25th June 2018

UNIVERSITY OF SOUTHAMPTON

ABSTRACT

FACULTY OF ENGINEERING AND THE ENVIRONMENT

Engineering Doctorate

Characterising the Creation of Defects in Large Scale Vacuum Assisted Resin Infusions in the Marine Industry

By Matthew Streeter

Utilisation of the Vacuum Assisted Resin Infusion (VARI) process has increased in recent years for the manufacture of large scale components for the transport industry. Quality control and repeatability are two key areas where the VARI process requires greater understanding due to the scale of the infusions. The marine industry has a history of being at the cutting edge of large scale composite manufacturing. This research focusses on utilising the processes and knowledge at Princess Yachts International (PYI) to monitor and analyse the process variability and uncertainty for large scale VARIs.

A detailed process review was conducted at PYI to evaluate the level of process monitoring and variability as well as the defect controls that are used in industry. Core samples were extracted from infusions where surface visible defects had been recorded. The core samples were analysed using Micro Computed Tomography (μ -CT) to generate a three-dimensional reconstruction of the defects. The location and structure of the defects indicated matrix failure towards the mould surface of the component, an area which is not monitored during the VARI process.

Having identified a requirement to monitor the manufacturing process, a review of available sensors was conducted identifying Fibre Bragg Grating (FBG) fibre optics as the most suitable monitoring method. The sensors measured the residual stress development during resin curing as well as the high loads exerted on the component during demoulding which were five times larger than during the infusion and resin curing process. The measured strains were lower than the failure strain of the resin suggesting the presence of defects that result in premature matrix failure.

A novel approach to monitoring resin flow was then developed to analyse the through thickness resin flow progress using μ -CT. Both monolithic and sandwich laminates were analysed both *in-situ* and *ex-situ* to evaluate the effect of variable laminate layup. The results further identified the high degree of variability during the infusion caused by changes in laminate schedule and the transition from sandwich to monolithic sections.

Supervisors: Dr James Blake, Dr Simon Quinn, Mr Julian Spooner (PYI)



Contents

List of Figures	ix
List of Tables	xv
Acknowledgements.....	xix
Nomenclature	xxi
1 Introduction	1
1.1 Motivation.....	1
1.2 Background	2
1.3 Large Scale VARI Defects.....	4
1.4 Composites in the Marine Industry	6
1.5 Composite Processes	7
1.5.1 Hand Layup	7
1.5.2 Prepreg Autoclave.....	7
1.5.3 Resin Infusion.....	8
1.5.4 Resin Transfer Moulding	8
1.5.5 Vacuum Assisted Resin Infusion.....	9
1.6 Research Area Summary.....	11
1.7 Research Statement.....	12
1.7.1 Research Aim	12
1.7.2 Research Objectives.....	12
1.7.3 Research Novelty	13
1.8 Thesis Structure	14
2 Related Work and Literature Review	15
2.1 Composite Defects	15
2.2 Resin System	22
2.2.1 Polyester Resin.....	22
2.2.2 Effect of Temperature on Viscosity.....	23
2.2.3 Cure Cycle.....	23
2.3 Void Structural Effects	31
2.4 Development of Computational Infusion Models	31
2.5 Commercial Flow Simulation Models	35
2.5.1 PAM-RTM.....	35
2.5.2 RTM-Worx.....	35
2.5.3 Liquid Injection Moulding Simulation	35

2.5.4	Limitations of Computational Infusion Models	36
2.6	Composite Manufacturing Sensor Review.....	38
2.6.1	Thermocouples	38
2.6.2	SMARTweave	40
2.6.3	Dielectric Measurement	42
2.6.4	Fibre Optic Sensors	45
2.6.5	Thermal Imaging	48
2.6.6	Linear Variable Differential Transformer	49
2.6.7	Ultrasonic.....	50
2.6.8	Videography	50
2.6.9	μ -CT	51
2.6.10	Sensor Summary	52
2.7	Discussion.....	54
3	Commercial Context	57
3.1	Princess Yachts Process Review and Reported Defects.....	57
3.1.1	Void Locations.....	58
3.1.2	Void Area and Infusion Parametric Variations.....	62
3.2	PVI and Scott Bader Production Experiments	68
3.2.1	Resin Flow Experiments	68
3.2.2	Curing Production Data and Experimental Assessment	75
3.2.3	Joint PVI and Scott Bader Investigations	82
3.3	Industry Process Review Discussion	82
4	Component Quality Assessment.....	85
4.1	Outer Skin Void Analysis.....	85
4.2	A3_S6_2 Large Void Sample	86
4.3	A3_S6_4 Void Sample	96
4.4	Y9_S8_1 Void Sample.....	99
4.5	Microstructural Analysis Discussions.....	100
4.6	Microstructural Analysis Conclusions	101
5	Process Monitoring.....	103
5.1	Carbon Fibre Conductive Sensors	103
5.1.1	Experimental Procedure	103
5.1.2	Discussion.....	105
5.2	Fibre Optic Flow and Cure Monitoring	107

5.2.1	Introduction	107
5.2.2	Temperature and Strain Sensitivity	107
5.2.3	Experimental Set-up.....	109
5.2.4	FBG and Thermocouple Positioning.....	115
5.2.5	Results.....	119
5.2.6	Discussion.....	128
5.3	Conclusions	134
6	Flow Front and Void Re-creation Experiment.....	137
6.1	Void Re-creation	137
6.2	Void Re-creation Experiment and μ -CT Analysis.....	142
6.2.1	Void Re-creation and μ -CT Analysis Objective.....	142
6.2.2	Experimental Procedure	142
6.2.3	μ -CT Analysis	148
6.2.4	Discussion.....	155
6.2.5	Conclusions	158
6.3	In-situ μ -CT Flow Analysis	159
6.3.1	In-situ μ -CT Flow Experiment Objectives	160
6.3.2	Vacuum Assisted Resin Infusion Partial Processing	160
6.3.3	Results.....	172
6.3.4	Discussion.....	181
6.4	Conclusions	184
7	Discussion	185
8	Conclusions and Future Work.....	195
8.1	Conclusions	195
8.2	Further Work.....	197
9	References	199
10	Appendices.....	213
	Appendix A-Princess Yachts Production Model Information.....	213
	Appendix B - Princess Yachts Hull Infusion Process and Material Data Sheets	214
	Appendix C- Princess Yachts International Defects and Void Recording Sheets	228
	Appendix D-Princess Yachts layup schematic.....	233
	Appendix E- μ -CT Outer Skin Void Analysis Settings.....	235
	Appendix F-Resin Flow and Void Re-creation μ -CT Settings.....	238
	Appendix G-In-situ Infusion μ -CT Settings	241

Appendix H-Fibre Optic Results 244

List of Figures

Figure 1: The largest yacht in the Princess Yachts International range, the M40.	3
Figure 2: Void Defects in VARI components at PYI.	4
Figure 3: Delamination surface in the outer reinforcement of the hull section above the chine.	5
Figure 4: Marine terminology for areas of the hull referred to during this research (Potgieter, 2016).	6
Figure 5: RTM Process (Jensen, 2003).	9
Figure 6: VARI layup (Ahlorn, 2009).	10
Figure 7: Micrograph of typical non-crimp-fabric composite laminate cross section (Edgren, 2006).	16
Figure 8: Mechanisms for micro and macrovoid formation: (a) and (c) show microvoids within the tows forming during longitudinal flow. (b) and (d) show macrovoids within the channels forming (Park & Lee, 2011).	17
Figure 9: Typical multi axial NCF composite structure (SAERTEX, 2016).	18
Figure 10: Void content as a function of capillary number, identifying the processing window where least voids will be produced (Gourichon, Binetruy & Krawczak, 2006).	19
Figure 11: PYI M40 infusion demonstrating the effects of non-uniform preform permeability resulting in flow front convergence at the rudder stock and race tracking due to bag bridging at the hull transom join.	20
Figure 12: Fibre bridging during the fibre layup process (Groh, 2016) and the bridging effect seen on the chine at PYI.	22
Figure 13: Cured and Uncured Unsaturated Polyester Resin (Cripps, 2017).	23
Figure 14: Schematic of basic phase transitions identifiable using cure monitoring (Lodeiro & Mulligan, 2005).	25
Figure 15: Void initiated fracture caused by shrinkage during cure.	26
Figure 16: a) Micromechanical stresses in fibre and resin. The average σ , is the ply stress. b) Macromechanical ply stresses. The average, N/h , is the laminate stress (Tsai & Hahn, 1980).	27
Figure 17: Residual strain recorded during the VARI process using fibre optic monitoring equipment (Nielsen et al., 2013).	28
Figure 18: Exothermic traces and shrinkage measurements for Crystic 703PA- 40g mass in 18 mm diameter tube (Cook, 2011).	28
Figure 19: Development of residual stress due to cure gradients. a) Initial state. b) Ply 1 has begun curing, shrinking and hardening whilst ply 2 is still pliant. c) Ply2 shrinks and hardens, whilst ply 1 has already cured, causing considerable stress development (Convergent Manufacturing Technologies, 2010).	29
Figure 20: A3 S11 Chine exotherm profile (Douglas, 2010).	30
Figure 21: Measured principal permeability value $Kp1$ as a function of the fibre volume fraction V_f , where the different symbols represent the experimental method used (Arbter et al., 2011).	36
Figure 22: Flow front progression monitoring set-up used by Aktas, Boyd & Shenoi (2012a).	39
Figure 23: Thermocouple flow front detection by Aktas, Boyd & Shenoi (2012b) on the left and lack of detection of the flow front at PYI on the right.	39
Figure 24: Schematic of the SMARTweave sensory set-up (Shepard, 1998).	41
Figure 25: Half-wavelength cross section with a superimposed equivalent circuit model.	43
Figure 26: Schematic of sensing configuration for resin flow monitoring used by Skordos and Partridge (2000).	44
Figure 27: FEF for single sided and double sided parallel plate measurements, showing variable penetration depths and edge effects with the parallel plate design (Hegg, 2004).	45

Figure 28: Basic structure of optical fibre with Bragg grating (Lodeiro & Mulligan, 2005).	47
Figure 29: Laminate specimen cross section with close-up of the inter-ply fibre optic placement (Nielsen et al., 2013).	48
Figure 30: Schematic indicating set-up for flash thermography inspection on an aircraft fuselage (NASA, 1996).	49
Figure 31: Thickness variations due to non-linear pressure variations during VARI.	50
Figure 32: Infusion Imperfection examples from PYI.....	59
Figure 33: Example void recording sheet from PYI.....	60
Figure 34: New void inspection sheet provided by the author to PYI to improve the reliability of the defect information being recorded.	60
Figure 35: Void locations and frequency of occurrence on the bottom of the hull components	61
Figure 36: Void locations and frequency of occurrence on the topside of the hull component.....	61
Figure 37: Chine cross section showing the transition from the topside sandwich layup to the monolithic structure below the chine.	62
Figure 38: Defect area for model A3 with respect to the chronological manufacturing number.	63
Figure 39: Defect area for model Y9 with respect to the chronological manufacturing number.	64
Figure 40: Top and bottom flow front experiment around a flat chine layup.....	69
Figure 41: Flow front experiment around a chine feature identifying the lead-lag between mould and bag face during infusion.....	70
Figure 42: Mould surface converging flow front from the flow front experiment around a chine feature.....	71
Figure 43: Core groove sandwich panel flow experiment.	72
Figure 44: Dry spots between the resin flow channels on the larger 40 mm spacing (left hand side) and smaller 20 mm spacing (right hand side) core material and the flow channels and distribution holes on the core material.....	73
Figure 45: Sandwich panel average flow front position at 50mbar pressure.....	74
Figure 46: Sandwich panel average flow front position at 250mbar pressure.....	74
Figure 47: Fibre layup on A3 Slot 11 chine region (Douglas 2010).	76
Figure 48: Exothermic cure temperatures for model A3 build 19.....	76
Figure 49: Exothermic cure temperatures for model A3 build 20.	77
Figure 50: Exothermic cure temperatures for model A3 build 27.....	77
Figure 51: Exotherm and Shore D Hardness curves for three infused tiles with varying thickness (Douglas 2010).	78
Figure 52: Cure temperature and shrinkage averages for Crystic 703pa large resin tube (Cook 2010).	79
Figure 53: Exotherm and shrinkage for Crystic 703pa – 20 g mass and 12 mm diameter test tube (Cook 2011).	79
Figure 54: Exotherm and shrinkage for Crystic 703pa – 20 g mass and 18 mm diameter test tube (Cook 2011).	80
Figure 55: Cracking and tearing seen in the resin mass post cure (Cook 2010).	80
Figure 56: Air bubbles in the top of the resin mass, and details of the upper section of cured resin (Cook 2011).	81
Figure 57: Micro computed tomography x-ray radiographs to three-dimensional volumetric rendering (Bruker, 2014).	86
Figure 58: A3_S6_2 extraction location and profile view.	87

Figure 59: Greyscale histogram of the μ -CT image with the greyscale value on the x-axis	88
Figure 60: Greys scale transition between fibre, resin and void volume in a μ -CT image.	88
Figure 61: A3_S6_2 Delamination surface in the outer reinforcement of the sample.	89
Figure 62: A3_S6_2 Extracted fibres from μ -CT volume.....	90
Figure 63: A3_S6_2 Fibre misalignment and waviness in the fabric positioning creating resin pockets.	90
Figure 64: Extracted voids from μ -CT volume.....	91
Figure 65: A3_S6_2 Extracted second layer of voids from μ -CT volume.....	92
Figure 66: A3_S6_2 through thickness void volume fraction where 0 depicts the mould surface and 1 the core surface.	94
Figure 67 A3_S6_2 through thickness fibre and resin void volume fraction where 0 depicts the mould surface and 1 the core surface.....	94
Figure 68: A3_S6_2 cylindrical voids formed between the fibre tows in the first layer of biaxial reinforcement from the mould surface.	95
Figure 69: A3_S6_4 extraction location and profile view.	96
Figure 70: A3_S6_4 through thickness radiograph.....	96
Figure 71: A3_S6_4 delamination regions highlighted in red illustrating the three delamination sections overlapping.	97
Figure 72: A3_S6_4 through thickness void volume fraction where 0 depicts the mould surface and 1 the core surface.	98
Figure 73: A3_S6_4 through thickness fibre and resin void volume fraction where 0 depicts the mould surface and 1 the core surface.	98
Figure 74: Sample Y9_S8_1 extraction location and profile.	99
Figure 75: Y9_S8_1 extracted void volume.	100
Figure 76: Carbon fibre linear voltage sensor circuit diagram.....	104
Figure 77: Carbon fibre linear sensor array.	104
Figure 78: Voltage against distance for the carbon fibre linear voltage sensors.	105
Figure 79: Princess Yachts V39.....	109
Figure 80: Reinforcement layup schedule.	111
Figure 81 Resin injection and high flow medium locations	112
Figure 82: Non-linear resin flow front after passing the propeller stern tubes.	113
Figure 83: Non-linear resin flow front at the FBG location.....	114
Figure 84: Fully infused component 100 minutes into the infusion process.....	114
Figure 85: Fibre optic location on the port topside of the hull.....	116
Figure 86: FBG rosette arrangement in the CSM surface tissue.....	116
Figure 87: Fibre optic 2 wavelength measurements from vacuum to demoulding.	119
Figure 88 Thermocouple recordings from the vacuum bag surface temperature and the ambient temperature.....	120
Figure 89: FBG 2 longitudinal strain measurements with change in temperature and change in wavelength from vacuum bag to demoulding.....	121
Figure 90: Average mechanical longitudinal, transverse and shear strain from fibre optics one and two.	122
Figure 91: Fibre optic 2 longitudinal FBG wavelength.	123
Figure 92: Polyester resin shrinkage and exothermic temperature during cure (Cook, 2011).	124
Figure 93: FBG2 Strain measurements during debuging and removal from the mould.....	125

Figure 94: During the demoulding process the component is supported by four lifting points and two reinforcing beams across the top to support the sagging effects on to topsides as shown by the arrows.	126
Figure 95: Mechanical strain measurements at fibre optic 2 after being removed from the mould and moved along the production line.....	126
Figure 96: Fibre optic 2 mechanical strain.....	127
Figure 97: Chine region cross section.	129
Figure 98 Vacuum bag temperatures recorded at the keel, bottom, chine and topsides on model A4 slot 1.....	130
Figure 99: Crystic 703pa Barcol hardness results comparing post cured samples and non-post cured samples.	131
Figure 100: Mechanical property and cure level development in unsaturated polyester resin (Norwood 2001).	132
Figure 101: Microscopic image of the flow front and voids observed by the visualisation method during RTM (Matsuzaki et al., 2013).	138
Figure 102: Resin flow front progressing from right to left through two layers of 1200g/m ² quad axial glass fibre.	138
Figure 103: Greyscale image of the flow front at one second intervals from a to h.	139
Figure 104: X-ray micrographs of the impregnation process recorded by Centea and Hubert (2011).	141
Figure 105: Experimental set-up showing location of the resin inlet and sandwich layup.	143
Figure 106: Laminate layup schedule.	144
Figure 107: Bag surface flow rate.	145
Figure 108: Mould surface flow rate.....	145
Figure 109: Flow front progression at a) 36:30, b) 46:00, c) 60:00 and d) 72:00 minutes.	146
Figure 110: Core butt joint illustrating the gap between the core sections which can impact resin flow.	146
Figure 111: Core sample extraction locations.	147
Figure 112: Extracted section of the component to be assessed.	147
Figure 113: Section 2 of the extracted samples top and bottom laminates including core resin distribution channels.	148
Figure 114: Vacuum bag surface laminate extraction.	149
Figure 115: Resin and void extraction from the bag surface laminate.....	150
Figure 116: Void extraction from the bag surface laminate.....	150
Figure 117: The first two lamina on the vacuum bag surface.	151
Figure 118: Vacuum bag surface flow front with the capillary flow dominance visible through the fibre saturation whilst the channel between the fibres are clearly unsaturated.....	152
Figure 119: Individual fibre, resin and void volumes at the resin flow front.....	152
Figure 120: Vacuum bag surface photograph of section one post infusion displaying a low level of porosity between fibre bundles.....	153
Figure 121: Section one of the resin flow experiment, volumetric reconstruction of the resin, fibres and voids.....	154
Figure 122: Section one μ -CT analysis of entire section, extracted void location and extracted void.	154

Figure 123: Bubbles drawn into a resin infusion behind the flow front caused by a leak, the voids visible in the right hand image fill the channels between the fibre bundles in the 0 ⁰ , -45 ⁰ and +45 ⁰ directions.	155
Figure 124: Resin flow front location at a) 72 minutes when the resin inlet was closed and b) once the resin had cured.	157
Figure 125: Visible fibre tow area and cure cycle temperature with processing time (Centea & Hubert, 2011).	161
Figure 126: Cylindrical infusion mould showing the effects of using a continuous lamina wrap.	163
Figure 127: μ -CT in-situ VARI experimental set-up.	163
Figure 128: Vertical cylinder VARI trials against a flat rectilinear permeability experiment.	165
Figure 129: VARI, flat plate and shrink wrapped infusion times.	166
Figure 130: μ -CT in-situ VARI experiment.	167
Figure 131: μ -CT in-situ VARI experiment elastic band locations.	167
Figure 132: In-situ μ -CT experiment speed.	168
Figure 133: Heat shrink vacuum bag application to the cylindrical mould for the μ -CT experiment.	169
Figure 134: In-situ μ -CT laminate schedule.	170
Figure 135: In-situ μ -CT Resin infusion experiment.	171
Figure 136: In-situ μ -CT scan of the dry fibre pre-impregnation.	172
Figure 137: Scan 3 with the resin flow front at 190 mm, polar transformation of the volumetric reconstruction of the in-situ μ -CT resin flow front experiment allowing for the identification of the resin flow front.	173
Figure 138: Resin flow front during the in-situ μ -CT resin infusion experiment.	174
Figure 139: Polar transformation of the resin flow front location for scans one to five from left to right.	174
Figure 140: μ -CT cross sections at 170 mm from the injection point when the resin flow front is at 150 mm (top) 190 mm (middle) and 230 mm (bottom).	176
Figure 141: μ -CT cross sections at 190 mm from the injection point when the resin flow front is at 150 mm (top) 190 mm (middle) and 230 mm (bottom).	177
Figure 142: μ -CT cross sections at 210 mm from the injection point when the resin flow front is at 150 mm (top) 190 mm (middle) and 230 mm (bottom).	177
Figure 143: μ -CT cross sections at 230 mm from the injection point when the resin flow front is at 150 mm (top) 190 mm (middle) and 230 mm (bottom).	178
Figure 144: Percentage saturation of the laminate at each of the four cross sections from scans one, three and five.	179
Figure 145: Third in-situ μ -CT VARI experiment conducted using two layers of reinforcement.	180
Figure 146: Capillary flow original and binary images of the resin flow front progression under capillary pressure alone (Morgan 2015).	182
Figure 147: In-situ μ -CT cross section identifying the resin distribution with the channels between the fibre bundles identifying voids fully surrounded by resin.	183
Figure 148: Crystic 703pa Data Sheet page 1	216
Figure 149: Crystic 703pa Data Sheet page 2	217
Figure 150: Crystic 703pa Data Sheet page 3	218
Figure 151: Butanox M50 Data Sheet page 1	219
Figure 152: Butanox M50 Data Sheet page 2	220
Figure 153: Butanox M50 Data Sheet page 3	221

Figure 154: Butanox M50 Data Sheet page 4	222
Figure 155 PYI Recorded Void Examples.....	228
Figure 156 PYI Void Recording Sheet	229
Figure 157 PYI Void Frequency of Occurrence and Location.....	230
Figure 158 Void area (%) against build number for models A3, Y9, S2 and T9.....	231
Figure 159 Void area (%) against build number for models N6, R2, B1 and Z7.....	232
Figure 160: Hull layup schematic.	233
Figure 161: Fibre optic one wavelength measurements from vacuum to demoulding	244
Figure 162: Fibre optic two wavelength measurements from vacuum to demoulding	244
Figure 163: Fibre optic three wavelength measurements from vacuum to demoulding.....	244

List of Tables

Table 1: Time taken for gelation to occur in different ambient temperatures using Crystic 703pa and Butanox M50.....	24
Table 2: Void recording sheets provided by PYI and the production model they relate to.	58
Table 3: Processing parameter spearman’s rank of correlation.....	65
Table 4: Core groove sandwich panel flow experiments.....	72
Table 5: Resin injection opening and closing times.....	112
Table 6: FBG properties.	117
Table 7: Reference times for each of the key phases during the production process.	121
Table 8: Partially processed laminate and their total processing times (Centea and Hubert 2011)..	161
Table: 9 Princess yachts production models.....	213

Academic Thesis: Declaration Of Authorship

I, MATTHEW STREETER [please print name]

declare that this thesis and the work presented in it are my own and has been generated by me as the result of my own original research.

[title of thesis]

Characterising the Creation of Defects in Large Scale Vacuum Assisted Resin Infusions in the Marine Industry
.....



I confirm that:

1. This work was done wholly or mainly while in candidature for a research degree at this University;
2. Where any part of this thesis has previously been submitted for a degree or any other qualification at this University or any other institution, this has been clearly stated;
3. Where I have consulted the published work of others, this is always clearly attributed;
4. Where I have quoted from the work of others, the source is always given. With the exception of such quotations, this thesis is entirely my own work;
5. I have acknowledged all main sources of help;
6. Where the thesis is based on work done by myself jointly with others, I have made clear exactly what was done by others and what I have contributed myself;
7. Either none of this work has been published before submission, or parts of this work have been published as: [please list references below]:

Acknowledgements

I would like to express my sincere gratitude to my supervisor's Dr James Blake and Dr Simon Quinn for their continuous support and guidance throughout this research. Without your guidance, patience and perseverance this research would not have been possible.

Besides my academic supervisors I would like to thank the team at Princess Yachts, Julian Spooner, Steven Douglas and Shaun Davy for their insight, knowledge and encouragement as well as providing me the opportunity to progress this research in an industry setting.

My sincere thanks also goes to Dr Mark Mavrogordato, commercial director of the X-ray imaging centre, without your enthusiasm and curiosity into the experiments being performed the research would never have reached its full potential.

I would like to thank my family for their encouragement throughout this research and for always believing in me.

Last but not least, I would like to thank my fiancé Lottie Coombs, without you this research would never have been completed, your support has been unwavering throughout this process and I am eternally grateful.

Nomenclature

Symbols are defined in the text at the first point of usage; all symbols used more than once are included in the nomenclature.

Acronyms

Ca	Capillary Number
CFD	Computational Fluid Dynamics
CSM	Chopped Strand Mat
CTE	Coefficient of Thermal Expansion
DWL	Designed Waterline
FBG	Fibre Bragg Grating
FEF	Fringing Electric Field
GRP	Glass Reinforced Plastic
ILSS	Inter Lamina Shear Strength
LCM	Liquid Composite Moulding
LVDT	Linear Variable Differential Transformer
MEL	Maximum Exposure Limits
NCF	Non Crimp Fabric
NDT	Non-destructive Testing
PPM	Parts Per Million
PYI	Princess Yachts International
RI	Resin Infusion
RTM	Resin Transfer Moulding
VARI	Vacuum Assisted Resin Infusion
VOC	Volatile Organic Compounds
μ -CT	Micro Computed Tomography

Symbol	Definition	unit
A	Cross-sectional area	m^2
d_i	Difference in statistical rank of corresponding variables	-
E	Young's Modulus	MPa
K_p	Permeability	m^2
K	Gauge factor	-
I_0	Intensity of the X-ray incident beam	-
I_x	Intensity of the beam at the distance x	-
L	Length	m
n	Number of samples	-
p	Photoelastic coefficient	-
P	Pressure	Pa
Q	Volumetric Flow rate	m^3/s
r_s	Spearman's rank of correlation	-
T	Temperature	$^{\circ}C$
v	Velocity	m/s
x	Distance from X-ray beam	m
V_f	Volume fraction	%
α_{δ}	Change of the refraction index	-
α_{sp}	Fibre optic expansion coefficient	RIU
γ	Surface tension	Nm
ϵ	Strain	$\mu m/m$
λ	Wavelength	nm
μ	Dynamic viscosity	cP
μ_C	Linear attenuation coefficient	cm^{-1}
ϕ	Porosity	%

Chapter 1

1 Introduction

1.1 Motivation

History shows us that transport demands have continually increased over the past century, whilst the world's natural petroleum reserves are decreasing. The requirement for more efficient forms of transportation has never been greater. The use of fibre reinforced plastic composite materials can drive improvements in fuel efficiency as a result of their strength to weight ratios (Adams, 2011).

For many years composite materials have been utilised across a broad range of marine applications. In recent years the aeronautic, military, electronics and automotive industries have sought greater knowledge of composite materials (Ngo, 2001). This is reflected in the increased use of composites in certain industries, for example the introduction of the Boeing 787 Dreamliner and Airbus A350XWB in the aerospace industry which are manufactured using composite materials for over 50% of their structures (Marsh, 2010).

A multitude of composite manufacturing techniques exist, traditionally open mould, hand layup techniques have been utilised by the marine industry for cost efficiency purposes. In 2000, 60% of composite manufacturers in the UK were utilising open moulding techniques, however this led to unacceptable levels of employee exposure to volatile organic compounds (VOCs), a group of carbon based chemicals which easily evaporate at room temperature (Nixon, 2000). As a result, self-imposed maximum exposure limits (MELs) were put in place for styrene, at 100 parts per million (ppm) averaged over 8 hours and a short term maximum of 250 ppm averaged over 15 minutes (HSE, 2003). Nixon (2000) found that although these limits were double those of other European countries, they were half of those often found through exposure from a gelcoat whilst hand laminating a yacht which often exceed 200 ppm. As a result, closed manufacturing techniques were sought to reduce the health and safety risks to those working around composites materials. The move to closed moulding techniques would also result in improved laminate quality as a result of increased compaction and fibre resin consolidation.

Liquid composite moulding in closed moulds offered advantages with respect to health and safety standards, weight, quality, repeatability and achieving reduced emissions (Walsh, 2011), resulting in the common implementation of Resin Transfer moulding (RTM), autoclave and vacuum assisted resin infusion (VARI) processes. Whilst there are benefits, each process does

compromise on processing efficiency, quality, production time, dimensional restrictions and fibre volume fraction control, as summarised in greater detail later in this research.

Autoclave manufacturing is a time intensive process that is difficult to automate as well as requiring a high level of investment. Size restrictions apply as well as restrictions on the complex shapes that can be laid-up by the stiff prepreg materials. RTM offers a decrease in production times as well as cost reductions, whilst only resulting in a moderate reduction in component properties and manufacturing repeatability. However, restrictions on component size have limited large scale applications to the automotive industry and smaller components in the aviation and marine industries. The VARI process offers a balance between cost, time and quality especially for the large scale components which are sought in the marine and wind turbine industries. However, the reduction in quality of the composite component compared to the results of autoclave and RTM techniques needs to be improved upon before the VARI process can be considered a more cost efficient technique for the automotive and aviation industries.

This research aims to identify the strengths and weaknesses of the VARI process and identify areas where processing improvements can be made to achieve improved quality, reduced costs, and improved production times. The knowledge, experience and information available at Princess Yachts International (PYI) will be used to examine production restrictions so that an industrial relevant solution can be proposed at the conclusion of the research.

1.2 Background

This research is supported and funded by Princess Yachts International (PYI), one of the UK's leading leisure boat builders. PYI's design and build a range of 13 to 40m composite luxury powerboats and boasts one of the UK's most advanced leisure composite boatbuilding manufacturing facilities. Since 2006 a closed mould VARI manufacturing process for hulls and decks has been utilised to achieve improved health and safety standards, weight, cost, quality, repeatability and emission controls (Walsh, 2011). PYI's continued research and development into the closed moulding composite manufacturing process has allowed for improvements in process control and component quality so that PYI were able to produce the M40 in 2011, Figure 1. The M40 is a 40m motor yacht with a displacement of 235 tonnes, which at the time of manufacture was the largest production VARI component in the world.



Figure 1: The largest yacht in the Princess Yachts International range, the M40.

However, the VARI process continues to result in variable component quality and is therefore yet to reach its full potential as an industrial composite manufacturing technique. A number of additional variables exist for the VARI process in comparison to closed moulding composite manufacturing techniques or those using pre-impregnated reinforcements and autoclaves. A summary of some of the additional variables are listed below (George, 2011):

- Variations in fabric compression
- Non-linear pressure distribution
- Vacuum irregularities
- Permeability variations
- Vacuum leaks

The increased inconsistencies in the VARI process lead to voids or defects being present in the final laminate as well as irregular surface geometries and inclusions. Due to the scale of the infusion being undertaken by PYI, the effects of these complications are exaggerated further, increasing the variability in the quality of the components being produced. As the infusions increase in size, so do the variations in dimensional stability and specific properties, namely those that are matrix dependent such as flexural, compressive and interlaminar shear strength (Park & Lee, 2011). Due to the luxury goods market that PYI operates in, the acceptable structural and aesthetic tolerances are very small and reduce further as the infusion sizes increase (Russell et al., 2000). This results in a timely and expensive re-work being required on the hulls and decks to ensure the surface finish meets customer expectations.

1.3 Large Scale VARI Defects

Post-infusion inspections are carried out on all composite mouldings so that imperfections can be identified. The location, type and dimensions of the imperfections are recorded and a repair process chosen and implemented. Figure 2 shows four examples of the type of voids recorded at PYI, with the first three examples appearing on the clear gelcoat areas of the hull form just above the chine (the location of the chine can be seen in Figure 4), and show similar delamination between the first and second layers of reinforcement on the mould surface. The fourth image shows an area where fibre bridging has occurred resulting in delamination between the core and the reinforcement.



Figure 2: Void Defects in VARI components at PYI.

In Chapter 4 further examination of core samples removed at locations where surface voids were identified has been completed using the μ -CT scanner at the University of Southampton. Figure 3 shows the delamination surface between the outer layers of reinforcement from a core sample removed from a 22m yacht hull produced by PYI. Similar defects occur across the range at PYI and are resulting in potential structural weaknesses requiring expensive rework carried out by hand which increases exposure to VOCs during the repair. The requirement to repair the components produced using the VARI are preventive the benefits of the infusion process being fully realised.

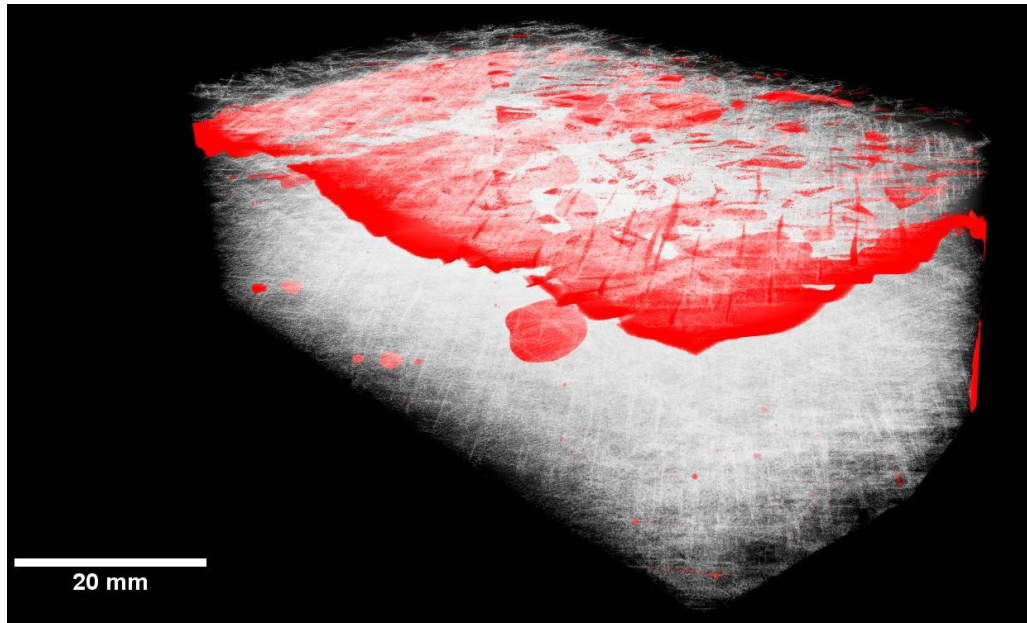


Figure 3: Delamination surface in the outer reinforcement of the hull section above the chine.

Void inspection and recording are currently limited to visual inspection techniques from above the chine to the keel, the location of these features can be seen in Figure 4. An example of the void recording sheets can be seen in Appendix C, Figure 156, as well as an example of the type of voids that are recorded.

The information obtained from PYI, which is analysed in greater detail in Chapter 3, identified the extent of the variability of the imperfections and the inconsistency between the same components. The lowest recorded void area on the infusions which PYI provided the void recording sheets for, identify a void area of 0.01%, this was preceded by a void area of 1.32% on the previous infusion. The high degree of variability in infusion quality limits PYI's ability to consistently produce infused hulls at the same rate and cost. The unknown factors effecting the variance in part quality are also limiting the ability for PYI to solve the issue and make improvements. These inconsistencies need to be further examined to establish if a statistical correlation exists between the recorded processing parameters and recorded void areas.

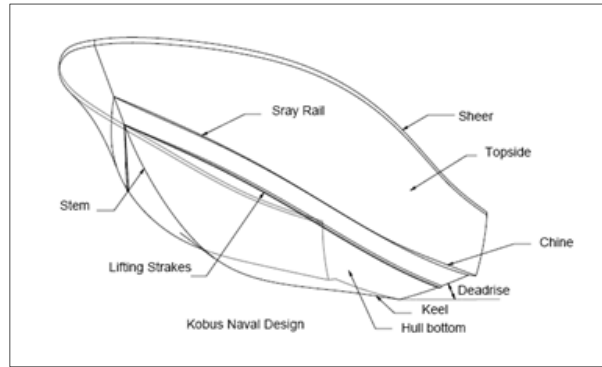


Figure 4: Marine terminology for areas of the hull referred to during this research (Potgieter, 2016).

Process improvements have continually taken place at PYI since the implementation of the VARI process to the hull and deck mouldings in 2006, however the level of inconsistency and variation between the infusions has resulted in the need for a more detailed study to be performed. This project has been instigated to provide a detailed analysis of the process used at PYI and assess potential improvements that can be made to reduce material waste and improve processing efficiency.

1.4 Composites in the Marine Industry

Over 95% of all composite marine crafts are manufactured using Glass Reinforced Plastic (GRP) due to their low costs, corrosion resistance and vibration/noise absorbing properties (Selvaraju & Ilaiyavel, 2011). The first application of composites in the marine industry dates back to the end of World War II where glass reinforced plastic (GRP) began to replace the use of timber due to increasing timber costs and supply issues as well as issues relating to the degradation of timber in salt water (Selvaraju & Ilaiyavel, 2011). The US Navy built a class of 28-foot personal water craft to test the benefits of reduced maintenance and production costs (Greene, 1999). In the mid 1960's GRP construction became mainstream in the leisure marine industry using single skin hand layup chop strand mat and roving reinforcement with stiffeners to maintain reasonable panel dimensions (Greene, 1999). In the early 1970's composite designers realised that a lighter structure could be produced by laminating an inner and outer skin to a low density core such as end grain balsa and PVC foam (Greene, 1999). In the late 1970's and early 1980's the type of resin and reinforcement used were focussed on in the continued search for reduced component weight. Vinylester and Epoxy resins were used for specialised composite vessels such as racing boats and power boats where the increased strength properties of Epoxy were necessary to justify the increased cost over polyester based resins (Greene 1999). The true advantages of fibre reinforced plastics were not available till the introduction of unidirectional and stitched fabrics. To reduce the negative effect of woven fabrics causing pre-buckling in the

reinforcement, unidirectional fibres were stitched together at different orientations resulting in superior shear strength (Greene, 1999).

The first use of resin infusion was documented in the 1950's although wider commercial application of the process did not begin until the 1990's (Rudd et al., 1997). After 40 years of hand layup and the use of chopped strand mat (CSM), the benefits of increased fibre volume fraction, manufacturing consistency and cleaner manufacturing conditions resulted in the first transition to closed infusion processes (Greene, 1999).

1.5 Composite Processes

The manufacturing process chosen for composite components has a direct influence on the quality, cost and repeatability of the manufacturing process. However, with improved quality and repeatability comes limitations on production time, scale and shapes. The three dominant composite manufacturing processes used in the marine, automotive and aviation industries are summarised below.

1.5.1 Hand Layup

Before 2006 PYI utilised a hand layup procedure to construct the hulls and decks of their motor yachts. Since the inception of fibre-reinforced composite materials, a number of creative methods have been used to wet fibres with a viscous resin (George, 2011). The most intuitive method, hand layup, consists of the application of resin using rollers, brushes or spray, onto fabric laid into a male or female mould. This is by far the cheapest method, however only one surface achieves a smooth finish, the volume fraction, voids, and thickness are poorly controlled and VOCs are released during the process. The process is also very labour intensive, each layer requires individual saturation and there are limitations on the number of layers that can be cured in one step. The use of hand layup techniques is decreasing in industry; however, due to the cost advantages, much of the marine industry still utilise the process for non-structural components or where the expected production volume is low.

1.5.2 Prepreg Autoclave

Resin pre-impregnated (prepreg) reinforcement materials used in parallel with autoclaves enables control of the temperature, resin and pressure during the manufacturing process. This results in high levels of repeatability and consistency in the properties of the component (George, 2011). Resin control comes from the prepreg material, which has a closely controlled quantity of resin infused into the dry reinforcement under high pressure before being partially cured. This however does induce a forming issue for prepreg materials, where the semi-cured impregnated fibres become less flexible and more difficult to lay into complex moulds. Once

the fibres are correctly placed in the mould, a vacuum bag is placed over the preform and placed into an autoclave, where the pressure and temperature can be controlled to ensure the correct cure cycle is applied. The pressure allows for a high level of resin fibre consolidation, resulting in fewer voids, a uniform preform thickness and repeatable material quality. The improved quality control and repeatability have resulted in the autoclave prepreg process being used in the aerospace industry.

Prepreg laminates are considerably more expensive than dry fibres. Prepregs also have limited shelf life whilst requiring permanent cooling to maintain the resin gel condition. The availability and size of autoclaves limits the scale of the components which can be manufactured using this technique. Out-of-autoclave prepreg manufacturing techniques have been developed so that the components can be cured in an oven using a vacuum pump and flexible vacuum bag to apply compaction to the component. However, the limiting factors of reinforcement cost, as well as limitations with the layup three-dimensional shape have restricted the use of prepreg reinforcements in the marine industry to high tech racing yachts and motor boats.

1.5.3 Resin Infusion

Resin infusion (RI) fills the middle ground between the high cost and high technology autoclave prepreg processes and the lower cost hand layup process. The development of the RI process has been driven by the industrial need for greater cost control and more repeatable and controllable processes. RI consists of resin infiltration using either a fully enclosed mould or a single sided mould and vacuum bag. Either a positive or negative pressure can be used to drive or draw resin into the mould containing the dry reinforcement. RI provides a more controllable process than hand layup, whilst also restricting the release of VOCs during manufacture. RI limits the physical contact with the resins and hardeners, resulting in substantial improvements in the working conditions for the composite engineers in industry. Due to the use of conventional fibre cloth, RI materials have a far superior shelf life over prepreg materials, whilst also being more flexible, which allows the production of complex shapes and geometries (George, 2011).

Multiple variations of the RI process exist, the two most common forms which are used by PYI are briefly outlined in the following sections of this research.

1.5.4 Resin Transfer Moulding

The resin transfer moulding (RTM) method uses a positive pressure to force resin into a cavity between two or more rigid moulds, Figure 5. The method is highly repeatable and produces constant component thickness. The ability to apply a higher injection pressure, limited by fabric

deformation and tooling allows RTM components to be infused quickly and they can be cured quickly using temperature controlled moulds. These factors all allow for the production of high quality components at a faster production rate than prepreg autoclave material, hand layup and VARI. Limitations on complex and large geometries and the increased costs associated with two rigid moulds limits the use of RTM to smaller components or those that require a high quality surface finish on all faces. RTM produces high quality components at reduced costs compared to the prepreg autoclave process. However, due to the closed nature of the process, resin fibre saturation cannot be visually monitored, leading to a reliance on sensors or injections simulations to guarantee that 100% resin impregnation is achieved before the component cures.

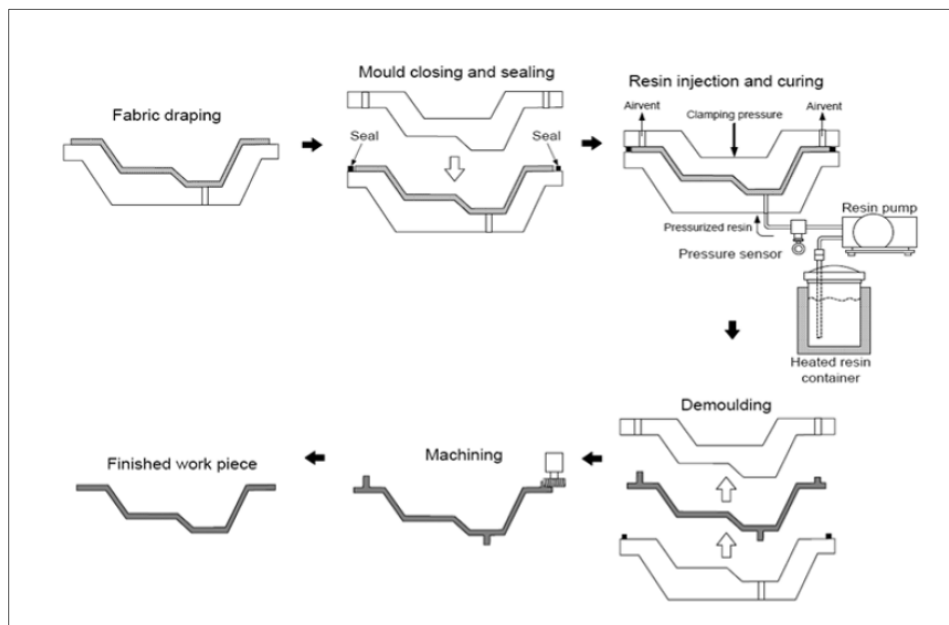


Figure 5: RTM Process (Jensen, 2003).

1.5.5 Vacuum Assisted Resin Infusion

VARI is a variation on the traditional RI process, which replaces the positive pressure used in the RTM process with a vacuum to draw the resin into the preform. The VARI process is highly repeatable and faster than hand layup for large components increasing production output whilst using the same laminating team and location (Gurit, 2011). VARI typically uses a single male or female mould, thus eliminating the costly requirement to have matching tools, which results in it being suitable for large components with low production volumes, hence why it was chosen by PYI as the process used to produce the hull and deck components. VARI was first used in the 1950's when the Marco infusion method was developed for use in the boat building industry (Rudd et al., 1997).

VARI is typically a three stage process, though variations exist depending on the required surface finish and laminate specification. The three stages are as follows (Hexcel, 2011):

1. Layup of fibre preform
2. Impregnation of the preform
3. Curing the impregnated preform

A typical VARI infusion layup is shown in Figure 6, where the requirement for additional consumables can be seen to support the VARI process (Gurit, 2011). The requirement to use vacuum membranes, distribution media, peel ply and breather fabrics increases the cost of the VARI due to the requirement for the majority of the materials to be disposable.

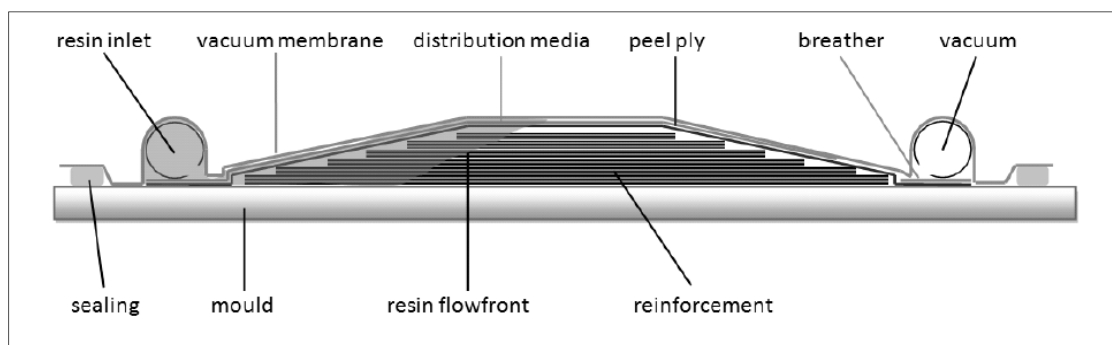


Figure 6: VARI layup (Ahlorn, 2009).

The reliance on a vacuum to draw the resin through the fibre preform, limits the potential pressure difference to one atmosphere due to the resin container being held at atmospheric pressure. This limits a number of factors, firstly the flow front advancing speed which controls the size of a component due to the quadratic relationship between length and time in Darcy's law: $t \propto L^2$ (George, 2011), which is discussed in more detail in the later sections. The resin advancing speed limitations have led to the use of high permeability distribution media, allowing for a faster in-plane flow front velocity. Higher in-plane resin flow velocities result in the relatively small through thickness infusion distances becoming a more important factor in the resistance to saturation and can become the most time consuming part of the process depending on the size and infusion strategy of the component (Stadtfield et al., 2002). Secondly the limited pressure applied to the component by the vacuum restricts the achievable preform compaction, resulting in a restriction on maximum achievable fibre volume fraction, hence limiting component quality.

Due to the large scale of the component and VARI being the preferred technique by PYI for the hull and deck components, the VARI process will be the focus of this research. VARI dominates

the wind turbine and marine industry, due to the size of the components that can be produced. Details of the materials and process used by PYI can be seen in Appendix B.

1.6 Research Area Summary

A range of voids are recorded in the components produced by PYI, some of which have been summarised in this Chapter with further examination of the defects and their causes in Chapter 3 and 4. Potential mechanisms that result in the defects have been researched previously and are discussed in Chapter 2. The complex nature of the VARI process limits the ability to establish causal relationships between processing parameters, materials and imperfections. The negative structural impact these defects can have on the components will be demonstrated in subsequent sections, which in general leads to increased material usage and unnecessary product mass. This, in all industries utilising composites to reduce component mass, affects product efficiency through increased fuel consumption, reduced load carrying capabilities and in the case of the wind turbine industry, less efficient energy conversion. The subsequent defect repair also leads to increased labour times, increasing exposure to VOCs and can lead to a reduced working life expectancy for the product.

This research focussed on identifying the causes of voids through the infusion steps of the VARI process. Both computational and experimental methods will be researched to deduce the most efficient, repeatable and accurate methods of assessing infusions and cure related voids. The knowledge learnt through extensive lab and computational research over the past four decades was investigated as well as its feasible application to the more restrictive nature of the commercial composites industry. An approach to combat one of the major disadvantages of the VARI process, the closed nature of the process, was investigated using non-intrusive sensory mechanisms. The commercial software that is available was evaluated in relation to its accuracy, usability and return on investment. This research approach connected the commercial side of the composites industry to the research carried out at research and academic institutions. Novel assessment processes were investigated to further the knowledge of the mechanisms causing defects in the RI process.

1.7 Research Statement

Large scale industrial VARI commonly results in voids, dry spots and dimensional variations, however the work at PYI has shown that there are few commercially viable resources available to monitor the developing defects during the infusion process. There is a lack of knowledge on how to assess and characterise void development, growth and movement in a non-contact and large scale application, as well as how to monitor dimensional variations during cure. This research will focus on utilising cutting edge research tools to monitor the processes involved with defect generation in a commercial application of a VARI.

1.7.1 Research Aim

The aim of this research is to generate guidance for the implementation of large scale VARI to maximise the structural and aesthetic quality of the composite components. Analytical and experimental tools will be reviewed and developed to monitor the infusion process in relation to the mould, layup and infusion parameters. These tools will be used to optimise the infusion process and material in a commercial environment.

An increased understanding of the effects that the processing parameters, materials and cure cycle have on voids and cure shrinkage will also aid in the design of future composite structures. Currently conservative design philosophies are applied to the design of VARI composite structures due to the unknown quantity and distribution of voids and dry spots. Analytical and experimental data can be applied during the design phase to quantify void levels, allowing for further optimisation of the structure, minimising material use and production times.

1.7.2 Research Objectives

In order to investigate the research statement a number of objectives are proposed:

- 1) To conduct a comprehensive literature review in the following areas.
 - a) Liquid composite manufacturing processes
 - b) Liquid composite moulding induced defects
 - c) Parameters affecting cure related defects
 - d) Research and commercial computational modelling methods for liquid composite moulding
 - e) Monitoring sensors for resin flow and cure characteristics
- 2) Full scale defect characterisation processing parameter study.
 - a) Manufacturing parametric/defect analysis
 - b) Three-dimensional defect characterisation using Micro Computed Tomography (μ -CT)
- 3) Assessment of the sensory technology available for large scale infusions.

- a) Full field, distributed and point sensors for flow, cure and stress monitoring
- b) Comparison between intrusive and non-intrusive sensors
- 4) Three-dimensional flow characterisation of the VARI process
 - a) Develop an experimental set-up to fully allow for three-dimensional flow characterisation

1.7.3 Research Novelty

A significant variation between academic and commercial based composite manufacturing knowledge currently exists. This research will focus on the application of state of the art technology to an industrial application, in order to optimise and maximise the capabilities of VARI in the marine industry, with transferable knowledge to the aeronautic, military, electronics, wind and automotive industries. Academic research has focussed on two dimensional experimental analysis to research the fluid dynamic effects occurring during VARI. The existence of a three-dimensional infusion experiment is required to firstly gain greater understanding of the complex effects occurring during resin infusion and secondly as a validation for any future three-dimensional modelling. The execution of an in-situ μ -CT VARI resin flow experiment will provide a novel contribution to knowledge in the composite industry. This research will allow comparison between lab scale experiments, computational analysis and industrial large scale infusions, maximising the capabilities of the infusion process. To the author's knowledge, no experiment like this exists for any RI process. In addition to the μ -CT experiment, fibre optic fibre Bragg grating strain sensors will be embedded into one of the hull infusions at PYI to measure the stress state of the component during the resin infusion process, the resin curing and during the demoulding process. Rarely in academic research can measurements be taken on large scale components under normal commercial manufacturing conditions.

1.8 Thesis Structure

The following sections of this thesis are structured as follows: A literature and current state of research is provided in Chapter 2 reviewing the resin infusion process, the techniques available to monitor and model the infusion process and the causes of the defects that are being found at PYI. Chapter 3 details the work that has already been conducted by PYI and their suppliers to understand the cause of the defects and implement process and material changes to reduce defect production. Chapter 4 provides a three-dimensional review of three core samples removed from the chine area of one of the A3 infusions and one of the Y9 infusions to assess the characteristics of the voids created at PYI. The information extracted from a defective composite sample identifies areas which require further monitoring and investigation. Chapter 5 details an approach to monitor the infusion and curing process to improve the level of information available during the manufacturing process. Fibre optics were used to monitor the key stages during the VARI process on one of the hulls infused at PYI. Chapter 6 uses μ -CT to investigate the generation of defects as a result of irregular flow characteristics which are commonly reported at PYI. A novel technique to monitor the resin infusion process three-dimensionally to improve the knowledge of how the irregular flow front relates to the generation and distribution of voids using μ -CT scanner has been developed and reviewed. Chapter 7 will review the research areas, relating the findings back to the industry related issues this research focusses on. Chapter 8 states the conclusions from the research with Chapter 9 detailing the further work which could be done to further develop the techniques used during this research project.

Chapter 2

2 Related Work and Literature Review

A substantial amount of previous research exists relating to the manufacturing of composite components. This Chapter will review some of the relevant research areas to the large scale VARI taking place at PYI and some of the causes of the defects which have been discussed in Chapter 1 and will be discussed further in Chapter 3 and 4. Types, causes and the effect of voids are discussed first, followed by the state of computational modelling of composite infusion and curing processes. Finally, the available sensors and monitoring techniques are reviewed to identify the most suitable to an industrial infusion.

2.1 Composite Defects

Defects can inadvertently be produced during the VARI process due to a number of mechanisms occurring during the infusion and curing process. Defects or voids can form at different scales during the VARI process depending on the cause of the voids. At the micro scale, voids can be created within the fibre bundles due to inconsistent resin flow progression. At the macro scale voids or defects can be affected by a number of variables which result in voids forming in the channels between the fibre bundles, known as porosity (Smith, 2009). At a larger scale, incomplete resin impregnation of the dry fibres caused by high viscosity resins combined with closely packed fibres result in dry areas in the infusion (Park & Lee, 2011; Guo et al., 2009). In addition to dry areas during the infusion, the curing process can result in matrix failures between reinforcements which results in delamination, a planar defect between ply boundaries. Delamination and dry areas are easily located using visual inspection techniques on thick laminates, but micro and macro scale voiding require non-destructive testing to be conducted on the component. Voids in the final cured part can be attributed to a number of factors, some of which are listed below (George, 2011; Smith, 2009):

- Entrapped air in the resin during mixing
- Leaks in the bag or connections
- Resin shrinkage
- Generation of volatile curing by-products
- Inter-tow and intra-tow entrapped air
- Foreign bodies
- Fabrication failures
- Inadequate vacuum source

- Fibre misalignment or wavy fibres
- Fibre defects
- Ply misalignment
- Incomplete cured matrix
- Converging flow fronts
- Resin flow restrictions
- Incorrect infusion strategy
 - Inlet and outlet positioning
 - Resin flow rate
 - Resin cure period
 - Resin distribution mesh locations

One of the main causes of micro and macrovoids are inter and intra tow entrapped air, which is caused by either mechanical entrapment or the release of volatile resin components during the curing process. Mechanical entrapment of gases in the fibre during infusion is caused by the heterogeneous nature of the fibre architecture. As the resin flows through the dry fibres the flow front can become non-uniform, this flow phenomenon is known as fingering, which traps air bubbles (Park & Lee, 2011). Fingering occurs where localised wetting is uneven due to the permeability variations between the fibre tows and the channels between the fibre tows which can be seen in Figure 7.

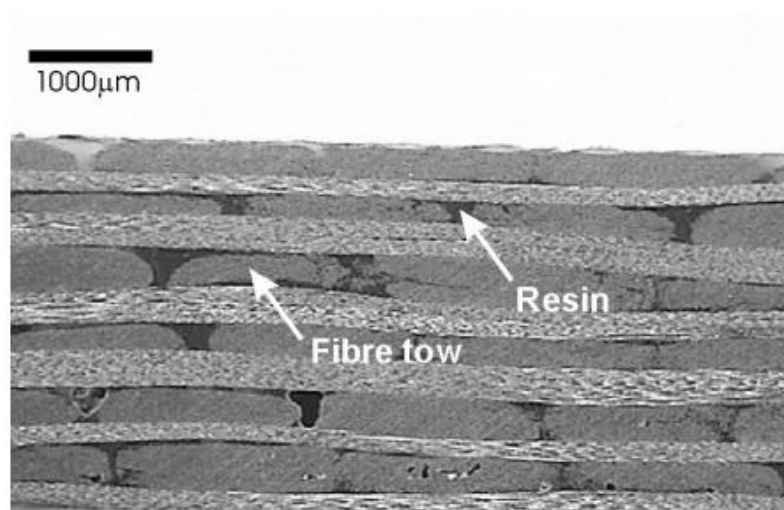


Figure 7: Micrograph of typical non-crimp-fabric composite laminate cross section (Edgren, 2006).

The bubble formation can be explained by the competition between the capillary and viscous forces; the consequence of the competing flow forces are locally induced differences between

the locations of the flow front. Consequently, the bubble formation occurs in two phases, intra-tow voids known as microvoids which are located within the fibre bundles, and inter-tow voids known as macrovoids within the channels between consecutive fibre bundles (Wielhorski, Abdelwahed & Bizet, 2012). Flow front velocity, which is dictated by infusion pressure, resin viscosity and fibre permeability, controls whether micro or macrovoids are created by the mechanical entrapment process. At low pressure, capillary flow dominates over the channel flow, leading to macrovoids, created as the resin is wicked from the leading flow front in the fibre bundles to the pore space in front of the channel flow front. At higher pressures, channel flow dominates due to hydrodynamic forces which result in a delay in the capillary flow (Pearce, Guild & Summerscales, 1998), causing complex micro flows as the resin is wicked from the channels into the tows, forming microvoids as shown in Figure 8 (Park & Lee, 2011).

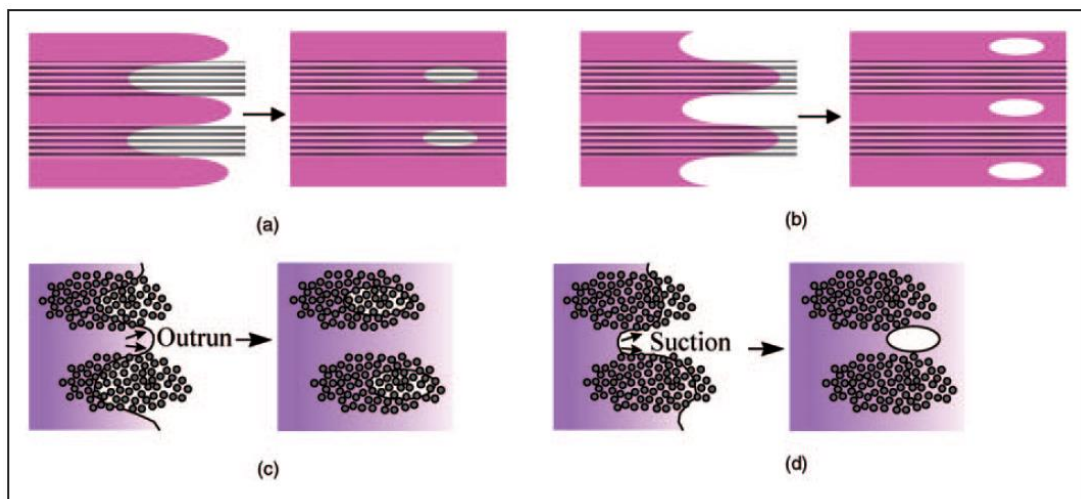


Figure 8: Mechanisms for micro and macrovoid formation: (a) and (c) show microvoids within the tows forming during longitudinal flow. (b) and (d) show macrovoids within the channels forming (Park & Lee, 2011).

The capillary pressure is the most important force of microscopic flow through the inner fibre bundles. The capillary pressure acts as a drag force on the infiltration of the fibre tows for a VARI (Li et al., 2010). Kuentzer, Simacek & Advani (2007) suggested that during the resin infusion process, where injection pressures are higher than the VARI process, the pores within the fibre bundle can take four to five times longer to saturate than the channels between the fibre bundles. However, for low resin flow velocities similar to those found above the chine on the VARI at PYI, the capillary flow will dominate within the fibre bundles, which results in macrovoids forming in the channels between fibre tows. The relationship between the dual micro and macro flows dictates the final microstructure of the composite part (Morgan, 2015).

Once the voids have formed, the physical obstructions within the fibre architecture can then block the void progression, which stops the voids being washed out of the system through resin bleeding. A number of physical obstructions exist, including the fibre tows and stitches in non-crimp fabrics (NCF), Figure 9.

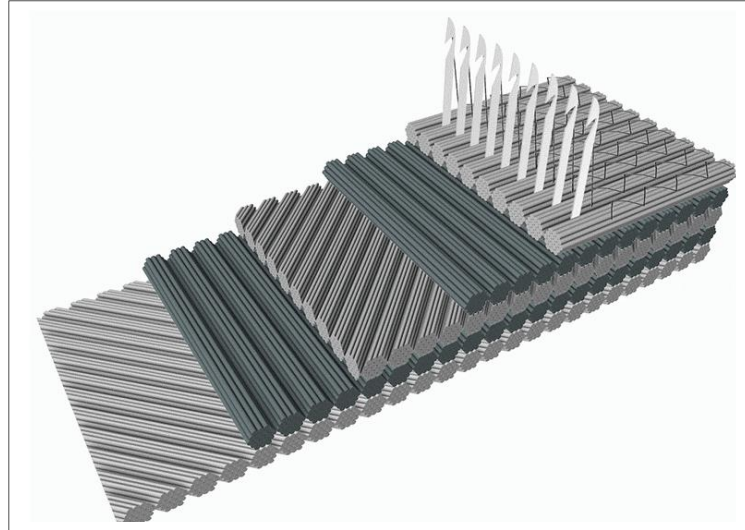


Figure 9: Typical multi axial NCF composite structure (SAERTEX, 2016).

The ability to combat mechanical entrapment can be achieved by increasing the fluids ability for capillary scale movement. A higher capillary number has been shown to aid void washout due to the reduced fluid resistance in the system (George, 2011).

Previous research has found that the fluid forces due to fluid viscosity and surface tension can be combined in a dimensionless number called capillary number (Ca), which when optimised results in the minimum number of voids for a specific laminate.

$$Ca = \frac{\mu v}{\gamma} \quad 2.1$$

In the above equation, μ represents the dynamic viscosity of the fluid, v is the velocity and γ represents the resin surface tension between the matrix and the ambient atmosphere. Void content can be represented as a function of Ca (Leclerc & Ruiz, 2008; Lee, Lee & Kang, 2006), which is shown in Figure 10 (Gourichon, Binetruy & Krawczak, 2006). The processing window section of the graph shows the conditions under which the infusions should take place in order to minimise the micro and macrovoids in the resulting infusion. Figure 10 identifies the occurrence of microvoids at high capillary numbers due to viscous flow dominating capillary forces, whilst macrovoids occur at lower capillary numbers due to capillary pressure dominating

viscous pressure, the optimum capillary number is different for different reinforcement layups and types (Young, 1996). The processing window is located above the x-axis which confirms that an optimum Ca will not prevent the existence of voids. Voids will always occur in composite parts; however, the optimum Ca allows for processing parameters to be set to reduce the void content to the lowest possible level for the laminate.

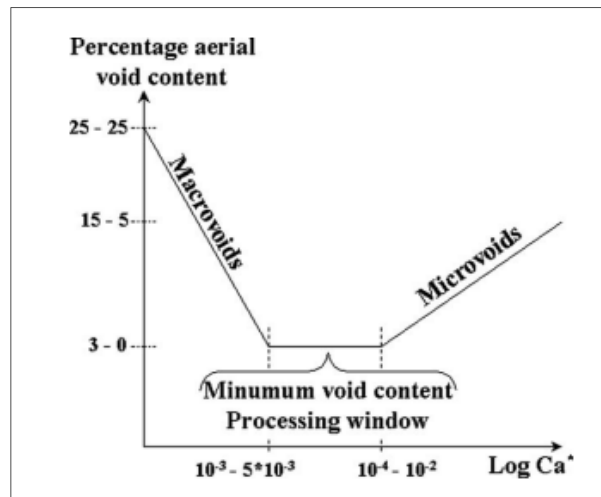


Figure 10: Void content as a function of capillary number, identifying the processing window where least voids will be produced (Gourichon, Binetruy & Krawczak, 2006).

Pressure not only drives the flow front velocity, affecting the mechanical entrapment of voids, the constantly changing pressure across the preform also affects the fluids gas concentration. Henry's law states that a fluids gas concentration at equilibrium increases linearly with respect to pressure, and that at absolute zero vacuum the gas concentration is zero (Sander, 1999). Due to the pressure field associated with VARI, the pressure continually increases as the flow front progresses, resulting in voids naturally occurring at the flow front, towards the vent and on the mould surface due to the lower pressure at these locations (Aranda et al., 2009). Some industrial applications infuse a preform at full vacuum, and then allow the inlet and vent to equalise at half vacuum, allowing for a reduction in thickness variations and for some gases to be reabsorbed into the resin (George, 2011).

Further to the effects of pressure and flow front velocity on voids, the resin infusion strategy can cause larger voids or dry spots. Dry spots can be created by the insufficient filling of the mould before gelation occurs (Park & Lee, 2011). These dry spots are caused by a number of factors, firstly the convergence of two flow fronts which results in the same effects as mechanical entrapment on a larger scale, trapping excess gases between the flow fronts as shown in Figure 11. Irregularities in preform permeability cause resin progression to be non-

uniform, causing large scale deflections in the flow front. An example of this is race tracking, which is commonly cited in experimental studies down the side of the panels where the bridging effect of the vacuum bag and the end of the fibre reinforcement changes the permeability and promotes resin flow. At PYI, the structural requirements dictate permeability variations due to the requirement for additional reinforcement in high load areas such as the bow thrusters, the rudder stock and the transom. The requirement for additional reinforcement or areas where holes are required in the hull leads to a transition from a sandwich layup to a monolithic structure. Sandwich and monolithic sections are constructed using very different laminate schedules which alter the permeability and quantity of the resin resulting in the irregular flow fronts seen in Figure 11. In addition to the changing laminate schedule, the joints between the high density foam cores also create channels for the resin to flow through which can result in resin flow accelerating ahead of the main resin flow front.



Figure 11: PYI M40 infusion demonstrating the effects of non-uniform preform permeability resulting in flow front convergence at the rudder stock and race tracking due to bag bridging at the hull transom join.

Insufficient pressure may result in deficient flow front velocity, meaning that all areas of the mould may not be reached. This is especially problematic on vertical infusion panels such as hull topsides, where the added effects of gravity slow the flow front progression, resulting in a maximum possible height of 6m in a VARI. Larger infusion heights have been recorded, but a double infusion had to be used to achieve a 10m topside height on a Russian Mine Sweeper, creating a natural weakness between the two injection joints (Gardiner, 2014).

Thirdly premature gelation may occur, leading to resin curing before the mould has fully impregnated. Infusion strategy is critical in guaranteeing that the mould is fully impregnated before the resin begins to cure. These problems of premature gelation are further accentuated by the scale of the infusions taking place at PYI.

The infusion strategy is also complicated by the semi-closed nature of the VARI process. Although the bag face of the mould is visible in the VARI process, the position and progression of the resin through the thickness and on the mould surface is unknown. The infusion strategy is often based on visual recordings of the flow front location, further information on the infusion process used by PYI can be seen in Appendix B. If a variation between the separate mould and bag surface flow fronts occur, the development of converging flow fronts can occur, this results in an increase in unnecessary voids.

In Chapter 4 the detrimental effects that fibre misalignment, waviness in the lamina layup and ply misalignments can have on void creation during the infusion and resin curing process are referred to. Fibre misalignment and ply misalignments both decrease the stiffness and strength of the final component as well as changing the resin flow due to permeability variations depending on the fibre orientation (Smith, 2009). Due to the scale and time constraints created by commercial pressures on the infusions undertaken by PYI, fibre misalignment can inadvertently occur. In addition to fibre misalignments, foreign objects can become embedded in the reinforcement layup restricting resin flow, inter lamina shear strength, reducing the fibre volume fraction as well as impacting the layup of the plies potentially inducing fibre waviness or a bridging effect. Fibre waviness is produced by in-plane kinking of the fibres in a ply; an example will be seen in Chapter 4 of this research, where the fibre waviness created a resin pocket between the first, second and third layers of reinforcement, which resulted in inconsistent curing rates and localised delamination.

The bridging effect can cause significant problems in three-dimensional moulding where the fibres are moulded around tight angles, this can result in the fibres bridging the radius. The result of the bridging effect is to decrease the consolidation pressure leading to reduced resin pressure beneath the bridged fibres (Groh, 2016). The bridging effect leads to a resin pocket which requires additional resin to fully impregnate the surrounding fibres, if this region is not fully impregnated a large dry spot can result. However the bridging effect also results in higher volumes of resin which in turn affect the thermally induced loads on the component due to the difference in thermal induced volumetric shrinkage of the fibres and the resin, Figure 12. As the resin begins to shrink during the curing process, the higher volume of resin will cause higher

exothermic cure temperatures which increases the level of shrinkage. Due to the constraints around the resin pocket, the bridged pocket will exert tensile stress on the surrounding fibres which can result in cracking in the brittle resin (Groh, 2016).

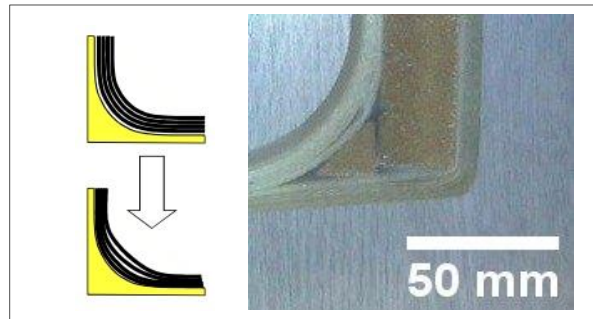


Figure 12: Fibre bridging during the fibre layup process (Groh, 2016) and the bridging effect seen on the chine at PYI.

A range of mechanisms exist which can result in defects being included in composite components manufactured using the VARI process. A review of the exact process used by PYI as well as the defects which are being reported needs to be conducted to identify which defect mechanisms exist before attempts can be made to remove them from the VARI process at PYI.

The resin impregnation, fibre arrangement and infusion strategy have been shown to be important to the quality of VARI components, the next section will demonstrate the importance of the resin cure cycle, temperature and resin choice on component quality.

2.2 Resin System

2.2.1 Polyester Resin

Polyester resins are the most widely used resin system in the marine industry, the majority of which are the unsaturated type (Cripps, 2017). Unsaturated polyester resin is a thermoset, capable of being cured from liquid or solid state under the right conditions. Unsaturated polyester resins are made up of reactive monomers the most commonly used is styrene which is added to reduce viscosity and to enable the resin to cure by cross-linking the molecular chains (Cripps, 2017). Viscosity is a critical factor for all resin infusions processes and has to be carefully controlled to ensure the preform is fully started before the resin reaches the gelation point. Polyester resins have an exponential relationship with temperature, which means that the viscosity will decrease by 33% for a 10°C increase in temperature and a 70% decrease for a 30°C increase in temperature (Potter, 2012).

Catalysts are added to the resin system shortly before the infusion process to initiate the polymerisation process, the catalyst solely activates the chemical reaction and does not take

part in the chemical reaction (Cripps, 2017). With the addition of styrene and a catalyst, the styrene cross-links the polymer chains at each of the reactive sites to create a complex three-dimensional network as can be seen in Figure 13.

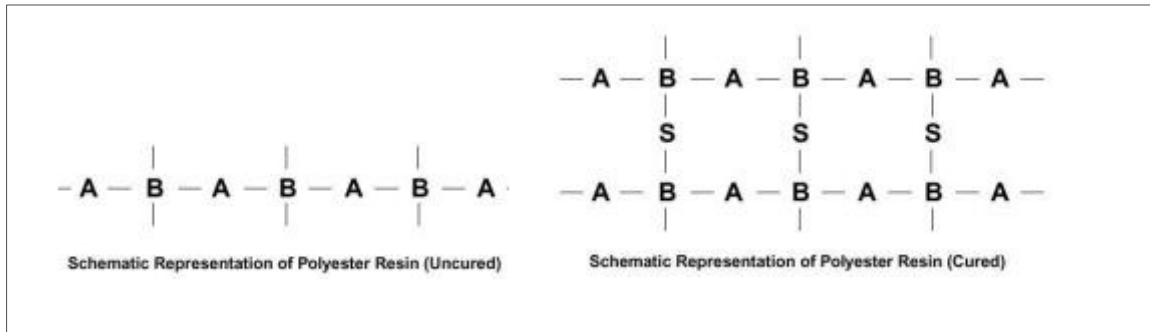


Figure 13: Cured and Uncured Unsaturated Polyester Resin (Cripps, 2017).

Before the polymerisation process has been complete, unsaturated resins release volatile organic compounds into the environment. The monomer cross linking agent used, styrene, contained in the liquid resin can evaporate into the air. As was discussed in Chapter 1, the release of VOCs during certain composite manufacturing processes are higher than acceptable for working environments. The composite manufacturing process directly effects the level of VOCs released due to the amount of resin surface exposed to air and the time exposed (Rogozen, 1982).

2.2.2 Effect of Temperature on Viscosity

The viscosity of polyester resins is directly linked to the resin temperature due to the motion of the atoms increasing with temperature. The relationship between temperature and viscosity is reversible as long as no change in molecular weight due to polymerisation has taken place (Summerscales, 2016). A typical relationship between temperature and viscosity is shown in equation 2.2:

$$\eta = \eta_0 e^{\alpha(T-T_0)} \quad 2.2$$

Where η is the viscosity, η_0 represents the viscosity at T_0 , a known viscosity for the resin. A typical value for α for a polyester resin is $-0.04 \text{ } ^\circ\text{C}$ (Summerscales, 2016)

2.2.3 Cure Cycle

The curing process is a critical aspect of the manufacturing cycle to ensure a high quality final component is produced. A fast, high temperature cure will result in a large build-up of residual

stress, whereas a slow, low temperature cure will lead to vitrification of the resin before gelation (Kim & Daniel, 2002). A uniform temperature is desirable across the laminate, however this is often not possible in thick composites which has been shown by PYI where they have measured a 44.9°C difference in cure temperature between the vacuum bag and mould surface, Figure 20 (Sorrentino & Tersigni, 2010). The difference in degree of cure between the mould surface and the bag surface can cause structural and geometrical inconsistencies. This can result in incomplete or non-uniform resin polymerisation, which has been shown to aid the development of residual stresses (Radford, 1993). Further still, an incorrect cure cycle can lead to peak cure temperatures being exceeded, invalidating the performance characteristics of the component (Antonucci, Regnault & Skrtic, 2010).

It is possible to design and optimise the thermal cycle to match the fibre layup schedule, resin systems and tooling under controlled manufacturing conditions. There are several performance parameters that need to be designed into the cure cycle to be fully optimised (Sorrentin & Tersigni, 2010; Kim & Daniel, 2002):

- Target cure degree
- Targeted maximum temperature
- Duration of cure cycle
- Production system limitation
 - Maximum allowable heating rate
 - Maximum allowable cooling rate
- Minimum energy consumption
- Residual stress control

Knowledge of how to set-up the time, temperature and pressure profiles so that the performance parameters are met is critical. Cure cycle optimisation is often restricted in industry due to the changing environmental conditions and the scale of the infusions taking place which leads to the incorrect design of the cure cycle, restricting the potential mechanical properties of the final component (Pantelalis, 2003). Table 1 illustrates how the ambient temperature and catalyst mixture can alter the resin cure characteristics substantially with a deviation of almost 200 minutes caused by a 10°C change in temperature.

Temperature	Gel time (minutes)		
	1.0%	1.5%	2.0%
15°C	317.9	195.9	149.0
20°C	207.3	123.8	83.4
25°C	128.4	84.1	64.4

Table 1: Time taken for gelation to occur in different ambient temperatures using Crystic 703pa and Butanox M50.

Sorrentino et al. (2009) focused on the thermal cycle design of thick composite components, and found that to reduce the effects of dishomogeneity it was necessary to carefully design the intersection of the thermal gradients to occur close after the gel point. Figure 14 shows the basic phase transformations during the curing process and indicates the gel point.

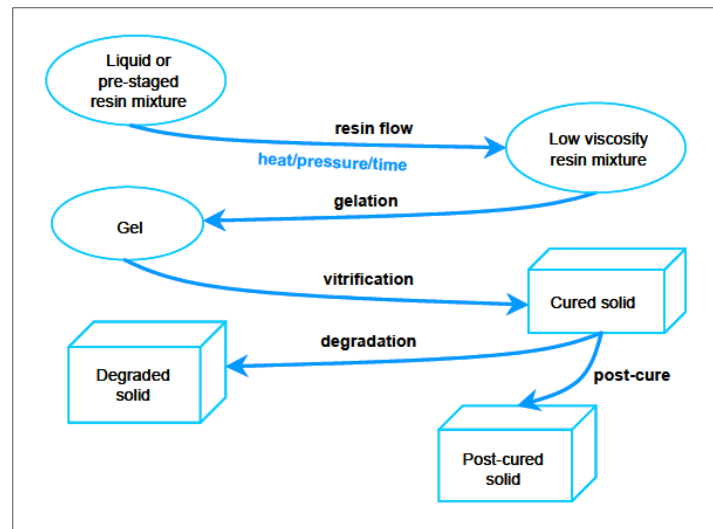


Figure 14: Schematic of basic phase transitions identifiable using cure monitoring (Lodeiro & Mulligan, 2005).

Unsaturated polyester resins exhibit high levels of volumetric cure shrinkage of between 5-9% (Khoun, Chaudhuri & Hubert, 2011), these effects are most common on thick and variable layup preforms (Kim & Daniel, 2002). The result of the high levels of geometric variations during heating and cooling is the development of residual stresses. In the manufacturing process there are four primary stages: gelcoat, barrier coat, skin coat and finally the resin infusion, at each stage of the process a unique cure cycle takes place, which results in residual stress development. These residual stresses result in relief mechanisms within the composite, leading to a number of possible defects, such as (Russell et al., 2000; Cao & Lee, 2003):

- Surface ripples
- Warping
- Sink marks
- Delamination
- Internal micro cracking
- Fabric print through
- Voids

Residual stresses generally exist in most composite structures; they can appear during the manufacturing process or during the service life of the component through viscoelastic creep

(Nielsen et al., 2013). The magnitude of residual stresses is dependent on a number of factors: the manufacturing process, fibre orientation and distribution, resin flow and resin volume variations, mould surface finish, tooling restrictions and resin dimensional changes (Khoun, Chaudhuri & Hubert, 2011). Residual stresses are self-equilibrated stresses and exist in a component without any external loading (Shokrieh, 2005). Two types of stresses are generally categorised for the purpose of residual stress analysis in composite materials: micromechanical stresses and macromechanical stresses (Johnston, 1997). Micromechanical stresses are those developed between fibre and matrix, caused by variations in thermal coefficients, resin shrinkage and matrix swelling during moisture absorption. Due to the higher thermal coefficient of expansion of the resin, these stresses are tensile in the resin and compressive in the fibres. Micromechanical stresses tend to be highly variable and difficult to evaluate due to the complex nature of the fibre and matrix arrangement within the laminate. However micromechanical stresses are comparatively small, and generally self-equilibrating and are therefore not important in relation to large scale composite deformation (Johnston, 1997). Macromechanical stresses cause large scale deformation, including warping and delamination, which can present as dry spots post infusion, as shown in Figure 15. This is due to internal micro cracking caused by the introduction of low profile additives (LPA) to the polyester resin to compensate for polymerisation shrinkage during cure (Khoun, Chaudhuri & Hubert, 2011).



Figure 15: Void initiated fracture caused by shrinkage during cure.

Macromechanical stresses are effectively the weighted average of the discontinuous local micromechanical stresses, as shown in Figure 16 (Tsai & Hahn, 1980). Macromechanical stresses are more easily measured and therefore more important whilst assessing large scale deformations and voids (Johnston, 1997).

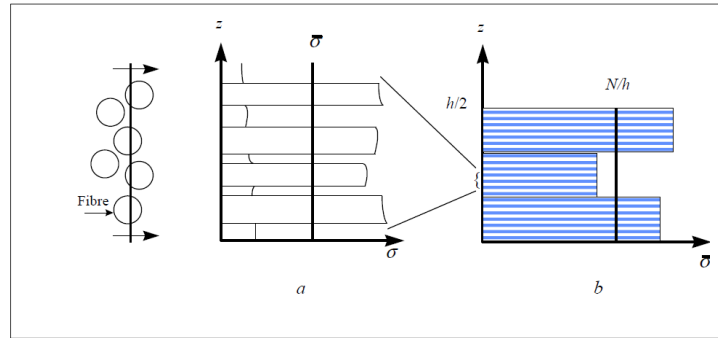


Figure 16: a) Micromechanical stresses in fibre and resin. The average σ , is the ply stress. b) Macromechanical ply stresses. The average, N/h , is the laminate stress (Tsai & Hahn, 1980).

During the manufacturing process, there are a number of sources and mechanisms that can lead to the development of residual stresses. These sources and mechanisms can generally be categorised under six dominating factors (Kim & Daniel, 2002; Johnston, 1997; Shokrieh, 2005):

- Thermal strains
- Resin cure shrinkage strains
- Gradients in component temperature and resin degree of cure
- Resin pressure gradient
- Tooling mechanical constraints
- Moisture

During the curing process, changes in the temperature of both the component and the tooling result in the development of thermal strains. The manufacturing process used by PYI utilises four individual cure cycles before post cure takes place. Figure 17 shows the recorded development of averaged residual strain during the resin infusion of 22 layers of unidirectional glass fibre with epoxy resin (Nielsen et al., 2013). Nielsen used multiple fibre optics to record the development of residual strain at each stage of the manufacturing process, vacuum, infusion, curing, demoulding and post cure. The application of gelcoat, skin coat and barrier coat before the infusion at PYI causes the development of residual stresses prior to the resin infusion. The process also results in the development of compressive stresses in the outer coats during the infusion and cure cycle, whilst the resin is in tension, which can result in delamination between the skin coat and the resin.

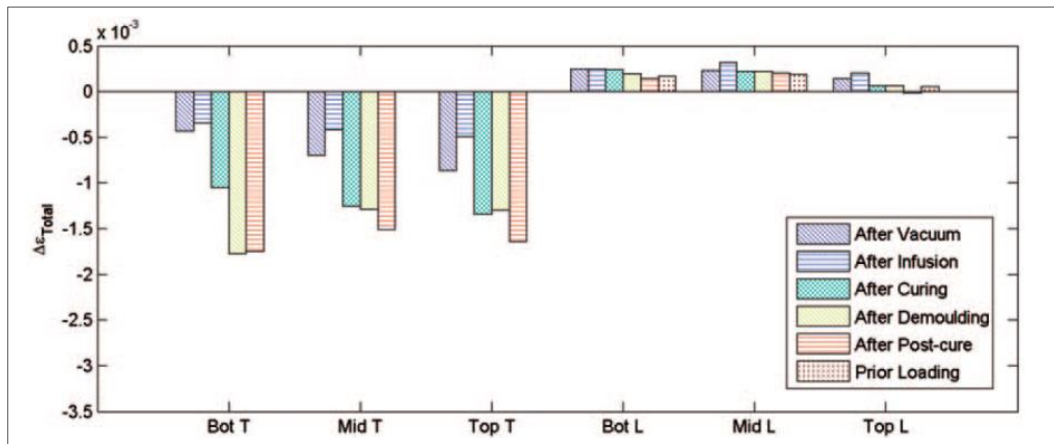


Figure 17: Residual strain recorded during the VARI process using fibre optic monitoring equipment (Nielsen et al., 2013).

In curved components, the variation in strains in both the through-thickness and in-plane directions will cause a reduction in dimensional stability. In addition to thermal strains, the increase in density and associated reduction in volume, more commonly known as cure shrinkage, can have a large effect on residual stress, depending on the vitrification point of the component (Johnston, 1997). Scott Bader carried shrinkage and exotherm temperature measurements using polyester resin catalysed with 1.5% Trignox 249 VR in a test tube, the results can be seen in Figure 18, (Cook, 2011).

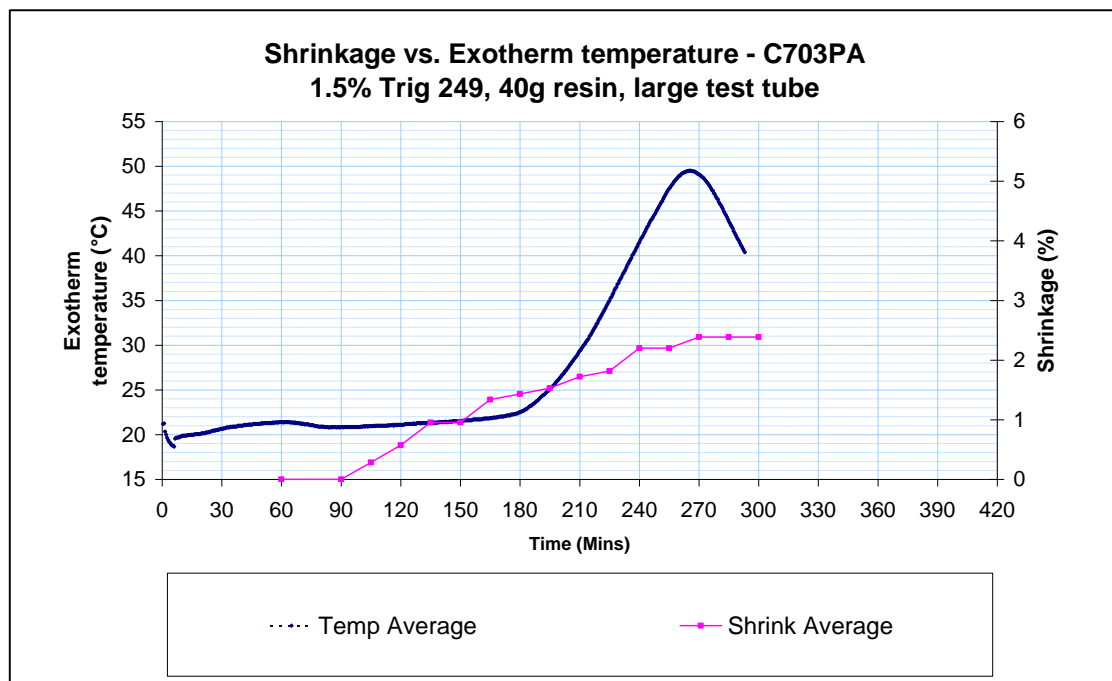


Figure 18: Exothermic traces and shrinkage measurements for Crystic 703PA- 40g mass in 18 mm diameter tube (Cook, 2011).

The average total shrinkage for Crystic 703pa was 2.4% in a 40 mm diameter tube, however the shrinkage in a given direction of a section of hull will be further affected by laminate thickness, resin/fibre content, temperature and moisture (Cook, 2011). Interesting observations of the resin tearing during the curing process were made during the study comparing vinylester (VE679-03PA) with polyester (Crystic 703pa) resins. This suggested that a shrinkage threshold exists above which delamination and voiding may occur depending on the resin mass and the boundary conditions (Cook, 2011).

In thick components, a through-thickness variation in temperature and resin cure, can lead to large scale deflections due to a continued build-up of residual stresses, as shown in Figure 19. In thicker composites the effects of temperature gradients are intensified by lower transverse thermal conductivity, coupled with the rapid heating process of the resin reaction.

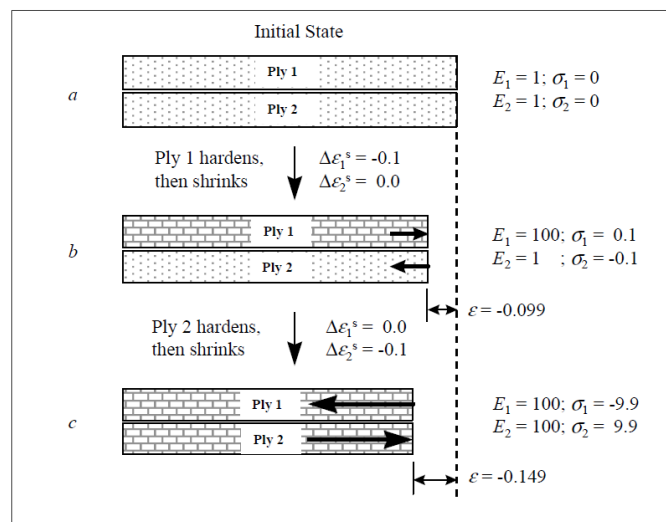


Figure 19: Development of residual stress due to cure gradients. a) Initial state. b) Ply 1 has begun curing, shrinking and hardening whilst ply 2 is still pliant. c) Ply2 shrinks and hardens, whilst ply 1 has already cured, causing considerable stress development (Convergent Manufacturing Technologies, 2010).

Residual stress development due to through thickness cure variations can be exaggerated by non-symmetric boundary conditions, potentially from tooling, causing an asymmetric stress state which can result in dimensional variations such as warping. The effects of through thickness cure variations can also be complicated by the effects of tooling and the insulating effects of the core, vacuum bagging, mould and distribution mesh layers. The previous measurements taken by PYI show a 44.9°C variation between the mould face (55.1°C) and the bag face (100°C) from production data taken from the model A3 (manufacturing number, Appendix A) slot 11 (build number) hull infusion as shown in Figure 20 (Douglas, 2010).

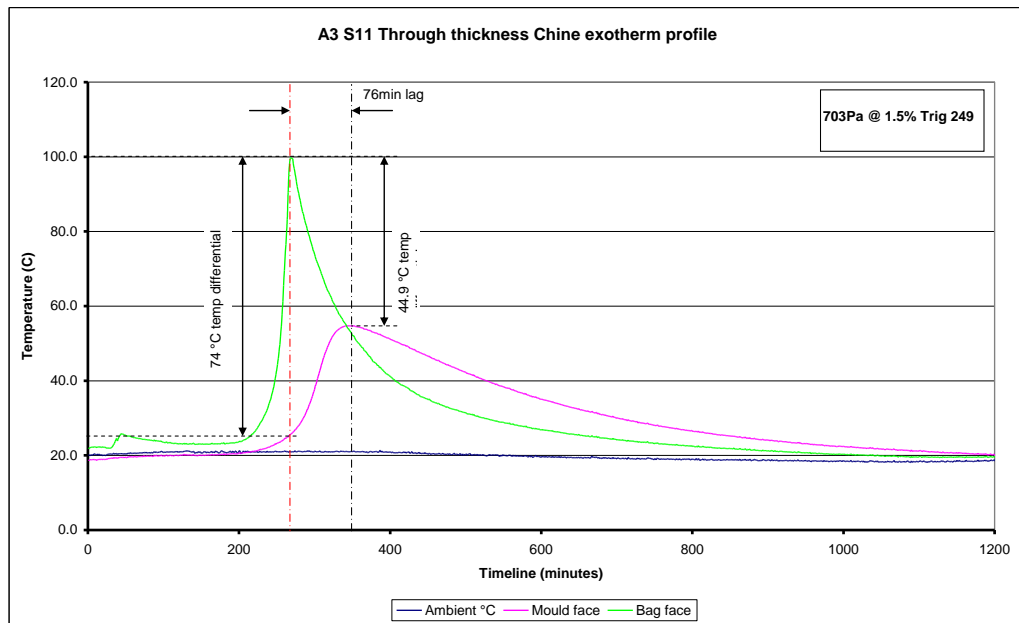


Figure 20: A3 S11 Chine exotherm profile (Douglas, 2010).

The effects of the uneven cure, can lead to an asymmetrical residual stress state (Bogetti & Gillespie, 1989). The tooling also leads to boundary constrictions on the component, resulting in the formation of shear and normal stresses, caused by variation in the thermal expansion coefficients of the tooling and the component (Nielsen et al., 2013).

The mould to laminate surface interface has been shown to develop high strain during cure (Kim & Daniel, 2002). Scott Bader found the resin adhering to the mould was aiding resin tearing, leading to defects in the resin mass post cure (Cook, 2011). Tooling mechanical constraints are therefore an important factor to consider whilst analysing residual stress development.

Resin flow characteristics also have a significant effect on residual stress development, and therefore voids, which are caused by resin tearing during cure. Uneven resin distribution and air entrapment can cause residual stress growth due to resin rich areas. Resin rich pockets have increased shrinkage levels and cause larger dimensional variations due to a higher level of pre-release, where the laminate releases from the mould surface before the resin has fully cured (Cook, 2011). This results in an uneven cure profile, leading to asymmetrical resin cure. Resin rich pockets are known to form in areas of complex fibre architecture due to sharp corner radii such as the chine or spray rails in a hull form (Dong, 2011). The resulting residual stress state and component defects caused by the resin cure characteristics can have a significant impact on the structural properties of the final component.

2.3 Void Structural Effects

The surface imperfections recorded at PYI could be caused by a number of individual factors or, more likely, a combination of factors. The results of the imperfections are not just aesthetic, the detrimental effects on the mechanical properties of the laminate caused by voids are well recorded and researched in the literature (e.g. Varna et al., 1995; Shenoi & Wellicome, 1993; Bowles & Frimpong, 1992; Ghiorse, 1993; Paul & Thomson, 1965; Judd & Wright, 1978; Yamada et al., 1992; Park & Lee, 2011). Voids are known to reduce the following properties:

- Interlaminar shear strength (ILSS)
- Longitudinal and transverse flexural modulus
- Longitudinal and transverse tensile strength
- Compressive strength and modulus
- Fatigue resistance
- Temperature resistance

Judd and Wright (1978) reported that the first 1% of voids can result in a decrease in strength of up to 3% in bending, 3% in tension, 9% in torsional shear and 8% for impact loading. It was also found that, independent of resin type, fibre type and fibre surface treatment, the ILSS of a composite is reduced by approximately 7% for each 1% increase in voids up to a maximum of 4% void content. Furthermore the localised effect of voids and void distribution will have a noticeable effect on material properties. A critical factor associated with the structural detriment of voids is the location of the voids in relation to the fibre reinforcement (Pearce, Guild & Summerscales, 1998). Therefore the density of voids and their locations are critical in order to understand the negative impact the voids will have on the component properties.

The risks associated with the inclusion of defects in a composite component have been discussed as well as the multitude of possible causes of the voids. Computational models have continued to develop as researchers attempt to further understand and develop the modelling capabilities of the composite manufacturing process. The current state of commercially available and research based computational models are reviewed in the subsequent section.

2.4 Development of Computational Infusion Models

Research into computational analysis techniques has been carried out in an effort to provide reliable simulations of the infusion processes. Historically these simulations have been limited to research institutions, who have concentrated on small scale lab experiment validations, rather than improving validity and accessibility to industry. A brief overview of both commercial

and research based models has been conducted to identify if a tool exists to improve the VARI process implemented at PYI.

Process models allow composite manufacturers to determine the effects of manufacturing variables, before any expensive prototyping occurs, which improves the overall efficiency of the manufacturing process. Various analytical models have been developed to aid in the process design of thick thermosetting composite materials, incorporating internal heat transfer, resin cure kinetics, resin flow, void generation and residual stress development (Sorrentino & Tersigni, 2010). Early examples used the one-dimensional finite difference method to analyse the curing process of flat plates (Loos & Springer, 1982). Technology has evolved so that both two dimensional and three-dimensional investigations using the finite element method are possible. A number of models have been developed utilising a variety of routes to assess and optimise the infusion cycle. Blest et al. (1999) developed a model that included resin flow, heat transfer and cure of a multilayer thermosetting composite laminate. Park and Lee (2001) concentrated on through thickness temperature distribution of arbitrary shapes using the finite element method. Zhang, Xu and Huang (2009) used the commercially available ABAQUS finite element software to create a three-dimensional heat transfer finite element model during the cure cycle. Other general purpose finite element software manufacturers have developed pre and post processors, allowing researchers to focus on the explanation and evaluation of the process. In the work of Zhang, to simplify and reduce the required programming time, the ABAQUS subroutines, HETVAL (heat flow), USDFLD (degree of cure), FILM (convection boundary condition) and DISP (temperature boundary condition) were used.

According to Mazumdar (2002), there are five available analytical tools: resin flow, degree of cure, degree of compaction, consolidation and residual stress. These tools are used to assess the simultaneous sub processes that occur during the infusion process, which fall under four sub-categories: thermochemical, flow, void and stress. Each sub-model has a distinct function, but they are each coupled to each other to provide a complete analysis.

Thermochemical sub-models allow for the assessment of temperature, viscosity, degree of cure (for thermosets) and crystallinity (for thermoplastics) as well as the time needed to complete the cure process (Abrams et al., 2000). The VARI process uses mostly thermosetting polymeric resins, which, as the process progresses, begins to cure and alters the resin viscosity (Song et al., 2004). A key component to achieving high quality large scale VARI is the ability to understand, predict and monitor the resin viscosity variations during the infusion. The resin viscosity variation during the infusion has a substantial impact on the flow front velocity, which directly

affects the ability to produce a fully impregnated component with a low void content. Another important aspect of large scale infusions is the through thickness temperature profiling that can be modelled using the finite element method (Slusar et al., 2005). The ability to predict and alter through thickness temperature variations can help to reduce resin shrinkage variations that lead to dimensional instability during cure (Song et al., 2004). To accurately predict the resin infiltration, the resin viscosity must be known as a function of both time and location of the resin flow.

Flow sub models evaluate the interaction between lamina, as well as the fibre position and fibre volume fraction (Morrison & Bader, 1989). Based on Darcy's law, flow models allow the simulation of the resin movement and impregnation through the reinforcement preform as well as the high-permeability distribution medium (Song et al., 2004). A brief overview of Darcy's law is given below.

Resin flow simulations in liquid composite mouldings for the past 35 years have been modelled using Darcy's law, which was devised during the 19th to study the flow of water through saturated porous sand beds. The law states that the superficial velocity (u) or volumetric flow rate (Q) divided by cross-sectional area (A) is proportional to the pressure gradient (P) applied along the length of the medium (L), and the permeability (K_p) divided by the fluid viscosity (μ) (George, 2011):

$$u = \frac{Q}{A} = -\frac{K_p}{\mu} \frac{\Delta P}{\Delta L} \quad 2.3$$

The superficial velocity, or the volume averaged velocity can be converted to the actual flow velocity through the pores (v) by relating the superficial velocity (u) to the fabric porosity (ϕ).

$$v = \frac{u}{\phi} \quad 2.4$$

where the porosity represents the fraction of the medium which the flow can pass through, which is equivalent to the inverse of the volume fraction.

According to Darcy's law, the permeability and porosity should be independent of all other flow conditions, and therefore represents the ease with which a fluid can pass through the fibre reinforcement, defined by the fibre architecture and porosity. For an anisotropic material the permeability can be defined by a tensor, including the magnitudes of permeability in each of the nine component directions.

$$\begin{pmatrix} u_x \\ u_y \\ u_z \end{pmatrix} = -\frac{1}{\mu} \begin{pmatrix} K_{pxx} & K_{pxy} & K_{pxz} \\ K_{pyx} & K_{pyy} & K_{pyz} \\ K_{pzx} & K_{pzy} & K_{pzz} \end{pmatrix} \begin{pmatrix} \partial P / \partial x \\ \partial P / \partial y \\ \partial P / \partial z \end{pmatrix} \quad 2.5$$

The one dimensional form of Darcy's law assumes an isotropic media, simplifying the equation to:

$$\frac{dL}{dt} = \frac{K_p \Delta P}{\phi \mu L} \quad 2.6$$

This can be integrated to form the basis for liquid composite moulding flow simulations.

$$t = \frac{L^2 \phi \mu}{2K_p \Delta P} \quad 2.7$$

Darcy's law ignores all variables except for porosity and resin viscosity, which fails to accurately model the VARI process, where fabric compressibility, dynamic viscosity, dual scale flow and permeability variations are common (George 2011). Both micro and macro impregnation can be modelled using Darcy's law although a large computation resource is required to carry out both scales simultaneously. In Darcy's law, the fluids are assumed to be Newtonian and incompressible, and the flow is quasi steady state. The infiltration into the porous medium is a moving boundary problem, therefore at each time step, the pressure distribution and velocities must be calculated. Due to the constantly changing compaction and therefore preform permeability, compaction models need to be incorporated into the flow model. Two compaction models need to be included due to the resin lubrication of the fibres which allow for a greater level of compaction to be achieved in the saturated and semi-saturated state.

Void sub models exist to quantify the effects of processing conditions on the presence and growth of voids during infusion and curing (Mazumdar, 2002). Void models identify the effects of the varying processing parameters on the production and mobility of voids. Utilising the results from the thermochemical and flow sub models, void models evaluate the processing parameters to identify likely void locations and sizes. Void sub models have focussed on the identification of dry spots, rather than macrovoid production, due to the extensive computational resources required to model macrovoids.

2.5 Commercial Flow Simulation Models

A number of commercially available flow models exist which include the thermochemical and flow sub models. The advantages and restrictions of three commercially available flow models are reviewed in the following section.

2.5.1 PAM-RTM

PAM-RTM is a software package developed by ESI group for the simulation of the resin infusion process based upon Darcy's law. The program has the ability to predict the effects of the following parameters in the final composite: preforming, resin, pre-heating, filling and curing (ESI, 2011). The software has been developed for the prediction of three-dimensional RTM simulations, however due to the added complexity, only a two dimensional assessment can be made of the VARI process. The PAM-RTM program cannot take into consideration the thickness variations between saturated and non-saturated regions, the local permeability variations in areas with large curvature and the influence of elastic film deformation; these factors mean that the predicted filling times are longer than reality. Due to the influence of a thick fibre layup used in the problematic regions at PYI, a two dimensional simulation is insufficient to accurately predict voids and dry spots.

2.5.2 RTM-Worx

RTM-Worx is flow simulation software that is based upon Darcy's law to solve the physical equations that govern flow through a porous medium using a finite element method. In the same way as PAM-RTM, RTM-Worx does not provide a three-dimensional VARI simulation due to the assumption that a linear pressure field exists and the resin flow velocity remains constant, both factors that are known to not be true for VARI (Koorevaar, 2002). Similarly to PAM-RTM, RTM-Worx is useful for assessing infusion strategies but lacks the infusion prediction accuracy required in this study.

2.5.3 Liquid Injection Moulding Simulation

Liquid Injection Moulding Simulation (LIMS), was designed by the University of Delaware to predict the RTM process in the same way as PAM-RTM and RTM-Worx. The unique feature of LIMS is a built in scripting language, LBASIC which allows boundary conditions to be modified during simulations. Correia (2004) used LBASIC to include the non-linear pressure field of a VARI process. However Correia used an averaging scheme, which assumes a weight averaged permeability of the preform, which eliminates the through thickness permeability, this has resulted in the LIMS only being able to accurately predict preforms with a uniform through thickness permeability.

2.5.4 Limitations of Computational Infusion Models

In addition to the identified limitations of the computational infusion models, it has also been shown that the accuracy of the input data can be questionable. A joint academic and industry study provided an assessment of the permeability variations of two reinforcements calculated using 16 different experimental procedures by a number of research institutions based around the world. The results showed a high degree of scatter, predominantly caused by human factors (Arbter et al., 2011).

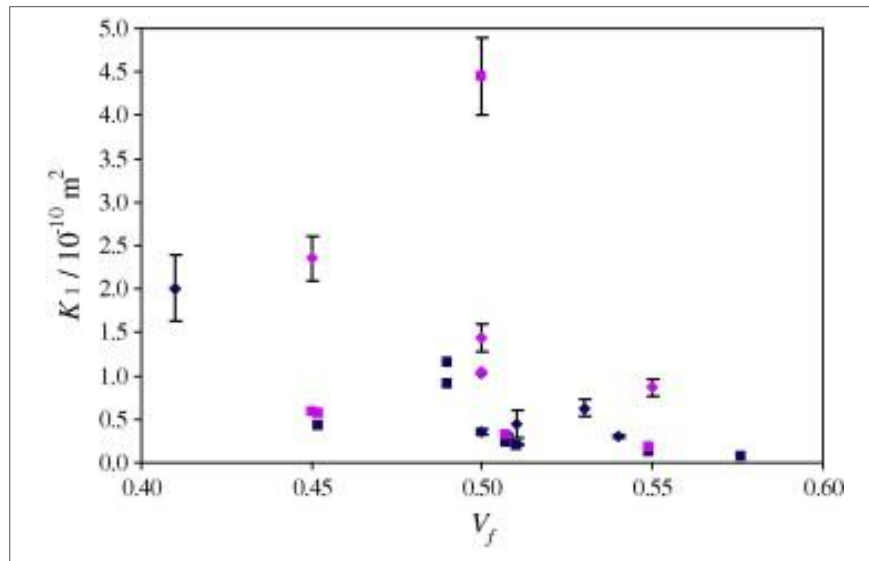


Figure 21: Measured principal permeability value K_{p1} as a function of the fibre volume fraction V_f , where the different symbols represent the experimental method used (Arbter et al., 2011).

The results show that a variation of a factor of 10 is seen between the maximum and minimum permeability results. A second study has subsequently been undertaken involving many of the same research institutions. The second study was conducted under tighter guideline control mechanisms to remove errors caused by inaccuracies in the different experimental methodologies. A guideline document was constructed in collaboration with all of the participants of the first study and the test conditions for a unidirectional unsaturated permeability test were defined.

A great deal of research is being carried out on methods of obtaining permeability through Computational Fluid Dynamics (CFD). A further problem relating to the computational models is their assumed permeability consistency from one infusion to the next and throughout the preform. In practice the parameters which affect dry spot formation change from cycle to cycle and accurate distribution of the permeability of the part within the mould is rarely known and highly changeable due to compaction, lubrication and layup inconsistencies (Hegg, 2004).

A key area of improving the information available to measure the input parameters to infusions models are the sensors used to monitor both lab scale and industrial resin infusions. The following sections investigates the available techniques to monitor the resin infusion process.

2.6 Composite Manufacturing Sensor Review

Multiple sensors are available to monitor the infusions process at either full-field, distributed or point measurements (Aktas, Boyd & Shenoi, 2012a), these sensors include the following:

- Thermocouples
- Dielectric
- Ultrasonic
- Fibre optics
- Point and lineal voltage sensors
- Pressure transducers
- Linear variable differential transformer (LVDT)
- Thermal imaging
- Videography
- SMARTweave

Many of these techniques have shown accurate and repeatable results on small scale infusions under controlled conditions, however for this research, a sensing device needs to be found that is effective for both industrial and lab applications. Key factors to review if a sensor is suitable for an industrial application are as follows: Set-up time, no delay to the layup or infusion time would be accepted for a full scale measurement. The cost of both the sensors and the measurement equipment is critical to balancing the accuracy and viability of further measurements in industry. Any sensors embedded into the component would need to be proven to not reduce the final mechanical properties of the component. The sensors would also need to be robust so that they can stand up to the harsher conditions experienced in an industrial setting.

A summary of the available sensor technology, along with an assessment of their potential applications to an industrial VARI process is included in the following sections.

2.6.1 Thermocouples

Thermocouples are widely used to monitor the VARI process as they provide both cure monitoring and flow progression information (Tuncol et al., 2007). Thermocouples have a fast response time, are cost effective, robust and can operate at high temperatures, all of which make them very attractive for industrial use (Lodeiro & Mulligan, 2005). Tuncol reported that a temperature variation is required between the mould and resin for the thermocouples to detect the resin flow front (Tuncol et al., 2007). Aktas however, found that with no artificially induced

temperature variation, the flow front was detected using multiple through thickness thermocouples using the experimental set-up shown in Figure 22 (Aktas, Boyd & Shenoi, 2012a).

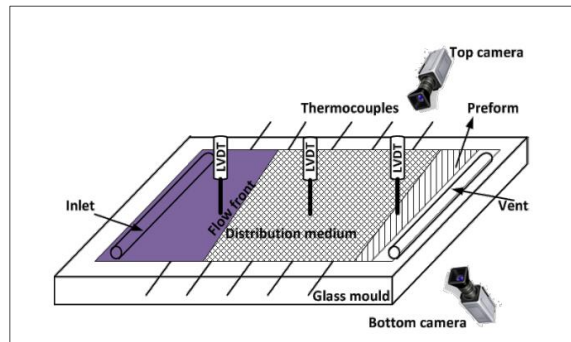


Figure 22: Flow front progression monitoring set-up used by Aktas, Boyd & Shenoi (2012a).

PYI have used thermocouples on the mould, core and vacuum bag surfaces to assess the exothermic temperatures during cure. Attempts to monitor the mould surface flow front progressions have however shown inconsistent results due to the gelcoat, skin coat and barrier coat which are applied and cured to the mould surface before the infusion starts. Without a large temperature difference between the resin and the mould, no change in mould temperature has been detected during the infusion stage. Both the results from Aktas and PYI are shown in Figure 23. The results show a change in temperature as the resin progresses, which represents the time when the flow front reaches the thermocouple sensors. The results from PYI are taken over a wide time frame in a less controllable environment, with the added complication of having to obtain temperature readings through both the vacuum bag and gelcoat.

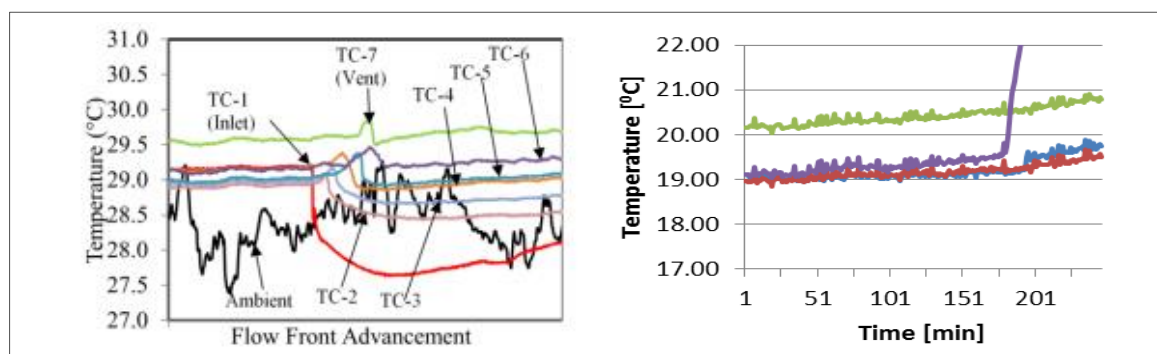


Figure 23: Thermocouple flow front detection by Aktas, Boyd & Shenoi (2012b) on the left and lack of detection of the flow front at PYI on the right.

In order to identify the resin flow front location, the thermocouples would need to be embedded into the component, which would introduce a foreign object into the infusion that

could affect the flow front progression. This increases the possibility of void development and lowers the mechanical properties of the resulting laminate. The wires connecting the thermocouple to the data acquisition box also need to exit the component, which could reduce the vacuum integrity and influence the fibre arrangement. Thermocouples also provide point rather than distributed measurements, which means that it would require a high number of sensors to measure a three-dimensional infusion. A higher number of sensors would increase expenses, production times and the risks associated with voids and vacuum integrity.

Thermocouples have been shown to be a reliable cost effective method of monitoring cure progression, however the through thickness flow detection, although possible at an experimental level, will not produce the flow front detection results required in an industry setting. Thermocouples may however be used to verify the results of other sensors during experiments and may be necessary to monitor component temperature for other sensor types.

2.6.2 SMARTweave

In the early 1990's the US military developed a distributed measurement technique which utilised a conductive measurement grid. It was found that two orthogonally placed conductive filaments laid either side of a fibre lamina can detect the presence of resin due to the bridging effect between the transverse filaments, which closes the electrical circuit at resin locations in the grid. The change in resistance between the two conductors allows the detection (or absence) of the resin at the point where the conductors are closest (Fink et al., 2001). Using a DC electric field to excite the mobile ions, the conductance across the sensing leads can be recorded as a function of resin temperature and viscosity, not only allowing for the flow front to be detected but also the identification of critical stages during the curing process (Fink, Roderic & Gillespie, 1999). Using a multiplexer, it is possible to detect if a specific node of the grid has been passed by the flow front, which allows for a global perspective of the flow pattern. Utilising a ten by ten grid, 100 points can be used to detect the resin progression, as shown in Figure 24 (Shepard, 1998). The location of each node is dependent on the spacing between the filaments, allowing for a variable resolution across a component depending on how the filaments are spaced.

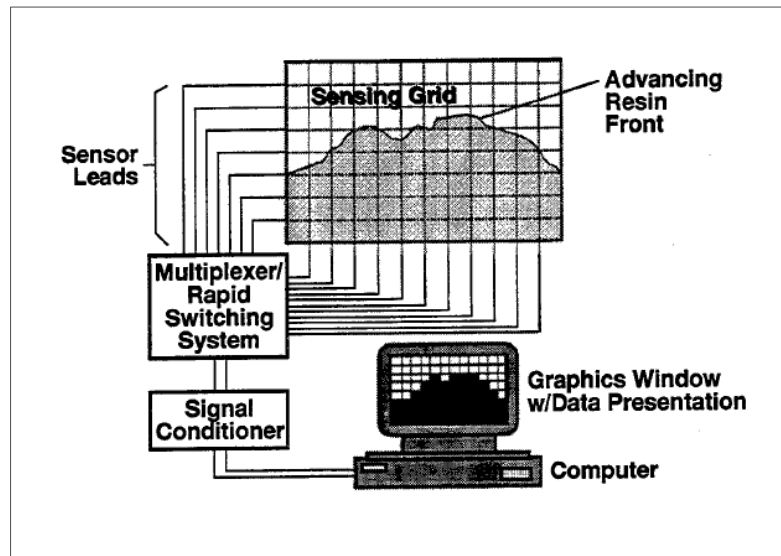


Figure 24: Schematic of the SMARTweave sensory set-up (Shepard, 1998).

The electrical circuit arrangement is dependent on the type of resin and reinforcement being used for the component. The resin electrical properties need to be quantified before use so that the relationship between resin conductivity, temperature and the extent of cure is known (Fink, Roderic & Gillespie, 1999). The ability to monitor the cure variations is possible due to the reduction in ionic mobility as the resin cures, which alters the DC conductivity of the resin and therefore affects the signal output. This recording method was first used by Walsh (1993) and was named SMARTweave (Sensor Mounted as Roving Threads). Figure 24 shows the set-up for the SMARTweave system. The sensor grid can be made out of any conductive material, the most commonly used for resin detection is carbon fibre or glass-fibre wrapped ultra-thin metallic wires (Fink, Roderic & Gillespie, 1999). A grid laid from carbon fibre tows and cured into the laminate would have little or no detrimental effect on the quality of the final product (Ragondet, 2005). Thibaudeau (2003) used a carbon fibre grid with epoxy resin to record the impedance changes with an impedance/gain-phase analyser, noting a positive result for resin detection, however the Thibaudeau commented on the reduced signal variation using polyester resins due to the reduced electrical conductivity of polyester resin.

The conductivity measurement method has shown potential over the past 20 years in both research and commercial application to monitor resin flow and cure as well as providing an online control system to aid infusion strategies. The ability to adapt the resin inlet locations and resin supply instantly to processing variations seen in the VARI process allows for greater control over repeatability and part properties. Analysis is required to test whether this approach would work with the polyester resin required for this research

The grid like sensors have several disadvantages, the major one of which is the relatively low recording resolution, which is limited by the sensor connections available. The embedded nature of the sensors also means that the manufacturing cycle time will be increased, with careful management required to ensure delays in fibre layup are minimised. The possibility of having carbon fibre bundles laid within the lamina rolls also needs to be explored to minimise disruptions. The vacuum integrity of the preform may also be reduced by the number of carbon fibre tows required to create the sensing grid. Each carbon tow will create a leak point due to the fibre arrangement and will also create weak points along the vacuum bag seal which may result in the component failing the pre-infusion leak tests. The grid does however still allow for the possibility of using an embedded but non-intrusive measurement system to obtain through thickness flow front and cure recordings.

2.6.3 Dielectric Measurement

2.6.3.1 Dielectric Permittivity

The previous sections identified the potential issues relating to the conductivity of polyester resins, an alternative is polarisation of the loose ions within the resin which may provide a comparable but more usable sensing system. All non-conducting or semi-conducting materials can be polarised, allowing two electrodes to detect the presence and changing state of the resin. Dielectric measurement is a powerful tool for electrical characterisation of non-conducting or semi-conducting materials, measuring the complex dielectric permittivity of the medium. By placing two electrodes on either side of the preform, the dielectric properties of the medium can be measured as a function of frequency. Dielectric measurement operates by shifting the ions from their equilibrium position resulting in dielectric polarisation. The difference between dielectric measurement and capacitance is that the electrical field does not flow through the medium as they would in a conductor, dielectric measurement records the interaction between the external electric field with the electrical dipole moment. As the resin passes between the electrodes the polarisability of the medium changes, which allows for the identification of the resin flow front. Further changes can be detected which are caused by changes in the environment between the electrodes as the resin cures. The general operating principles of dielectrics are given below (Hegg, 2004).

Dielectric measurements can be separated into two categories, parallel plate electrodes and fringe field electrodes. Fringe field electrodes can be described as parallel plate electrodes rotated around a central axis by 180° , the result is two electrodes that can penetrate a medium from a single side. For both parallel electrodes and fringe field electrodes, the two electrodes with equal but opposite surface charge densities have a potential difference.

The total charge on both plates is proportional to the potential difference between the plates. Figure 25 shows the conductance and capacitance equivalent circuit for a fringe field dielectric sensor.

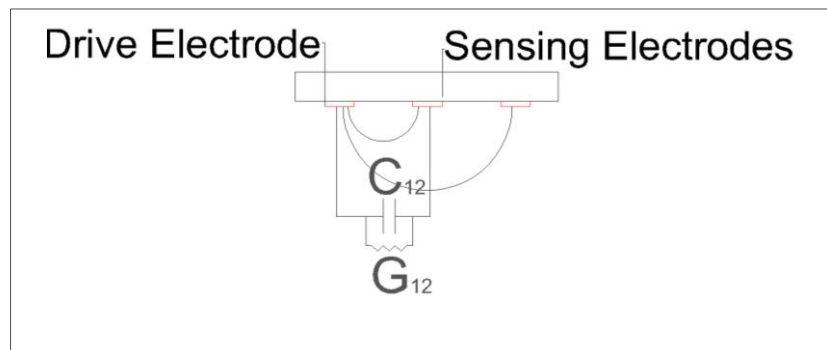


Figure 25: Half-wavelength cross section with a superimposed equivalent circuit model.

When the material between the electrodes is subjected to the external field, the material creates an internal electric field, in which state it is said to be polarised. To become polarised, the materials must be subjected to a frequency below the resonant frequency of the charge system. Because of this the AC voltage frequency is a critical choice depending on the resin and fibres being tested.

2.6.3.2 Dielectric sensors

The dielectric measurement method has shown to be one of the most promising methods for measuring processing points in the VARI process and has been shown to provide accurate and reliable detection of all the major cure process milestones: minimum viscosity, the gel point and vitrification (Pantelis & Maistros, 2006; Lodeiro & Mulligan, 2005).

The monitoring system has also already been proven by companies such as SP Systems, Dow Chemicals and Hexcel Composites. For flow monitoring, Skordos and Partridge (2000) placed dielectric sensors in parallel to the expected flow front movement along the mould surface of the preform to obtain continuous flow front positioning measurements. When the wires are placed into the mould, an electric field is formed between the conductive core and each wire. As impregnation takes place a difference in electrical properties between the initial air surrounding the sensors and the liquid resin results in a gradual change in electrical response, hence recording a continuous flow front position.

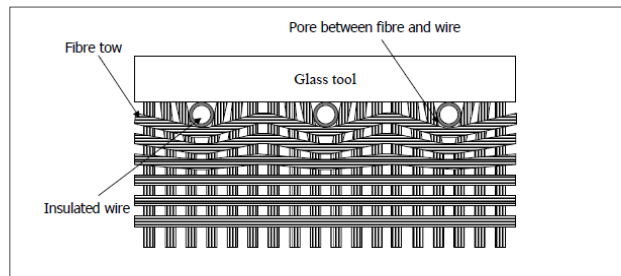


Figure 26: Schematic of sensing configuration for resin flow monitoring used by Skordos and Partridge (2000).

Similarly a discrete method was first used by Kranbuehl et al. (1994), where a number of integrated dielectric sensors were placed on the RTM mould face. As the flow front passed the sensors, a small jump in dielectric properties could be recorded, using a similar method to the thermocouple flow front detection technique. However dielectric sensors suffer the same drawbacks as the thermocouples: dielectric sensors are an embedded sensing system, which therefore cannot be used for commercial infusions unless the conductive filaments are made from similar materials to the fibre preform.

2.6.3.3 Dielectric Spectroscopy

Dielectric spectroscopy is a relatively recent development in RI sensing. Hegg (2004) developed two systems using fringing electrical field (FEF) sensing to measure multiple properties for both RTM and VARI. FEF works by measuring the capacitance change as the resin passes between the plates therefore detecting the dielectric material. A single sided and parallel plate fringing field dielectrometry were used for VARI and RTM respectively. The single sided FEF used for the VARI process is shown in Figure 27 where the ability to monitor multiple penetration depths is also shown. Figure 27 also shows the set-up for a parallel plate FEF experiment for the RTM process, using the mould bottom plate as one of the electrodes. The parallel plate dielectric spectroscopy sensor can be used for the VARI process either with an embedded electrode in the mould or by quantifying the mould effects on the dielectric response and placing the electrode on the outside of the mould.

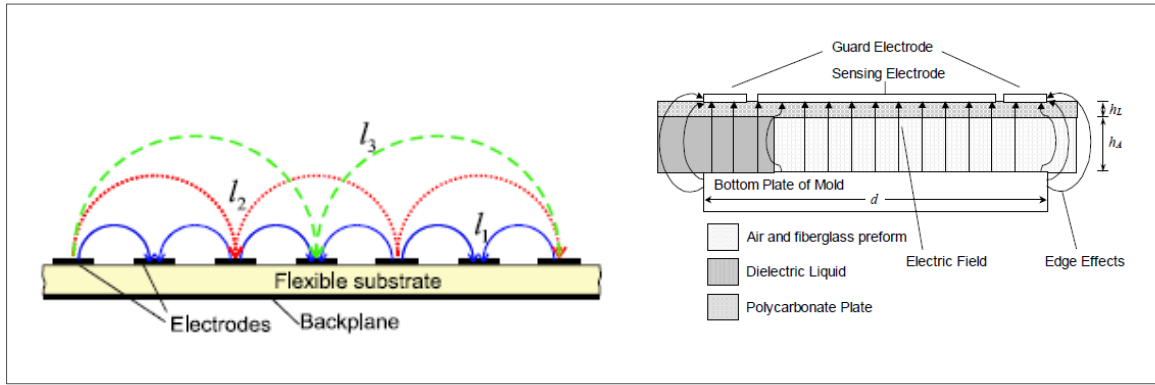


Figure 27: FEF for single sided and double sided parallel plate measurements, showing variable penetration depths and edge effects with the parallel plate design (Hegg, 2004).

Hegg demonstrated FEF's ability to monitor curing, temperature, viscosity and flow front location, both continuously and at point measurements from a non-contact sensor. The ability of the sensors to penetrate adequate depths in a VARI is questionable, especially on larger scale infusions. The scalability of the technology is also unknown. Hegg (2004) carried out experiments on one metre squared panels, only measuring a through thickness depth of 5mm. The component thickness at PYI varies from 20-50mm depending on layup schedules which is substantially larger than the thickness to which FEF sensors are proven to be reliable.

Utilising metallic dielectric sensors, in a similar way to thermocouples, introduces a foreign body sensor into the layup, affecting the same features as was noted for thermocouples. Dielectric sensors can also be very expensive, with costs potentially up to £2000. However the ability to record flow front progression and the cure cycle accurately as well as the option to re-use the same sensors multiple times justifies the higher cost of some of the lower cost disposable sensors.

Dielectric spectroscopy has shown to offer a potential solution to monitor VARIs, however further assessment including feasibility studies in to their use with the specific resin system and laminate schedule is required. The following areas would require further understanding before implementation on an industrial infusion: material sensitivity, processing applicability, part integration, capital and running costs and the volume of material needed to be analysed.

2.6.4 Fibre Optic Sensors

Fibre optic sensors offer a comparable solution to their electrical counterpart using light rather than electricity and glass fibre rather than wires (National Instruments, 2016). Fibre optics can therefore operate under extreme temperatures over long periods of time. Being passive sensors, fibre optics also have zero drift allowing for measurements to be repeated over many years

without the need to calibrate after the initial nulling has been carried out after embedding the sensors (Smartfibres, 2016; National instruments, 2016). The relationship between strain and the Bragg wavelength shift has been shown in literature to be linear and to follow the well documented gauge factor under variable operating conditions. The fibres used for fibre optic sensors are also very small in size, reducing the potential impact of embedding the fibres into a component. Fibre Bragg Grating (FBG) optical fibre sensors can be embedded into composite components with no effect on the structural performance of the composite (Smartfibres, 2016). Fibre optic sensors also offer the option to embed multiple sensors within one fibre, reducing the number of egress points from the vacuum bag. Tests on carbon fibre components resulted in no signs of fatigue or disbanding after one million cycles, leading to the expectation that fibre optic sensor will survive a service life of 25 years for large composite components, offering additional opportunities for the marine industry to investigate through life changes in strain as the vessel is used in different environmental conditions.

Research has shown that fibre optic sensors can be used to monitor temperature, strain and flow front location (Doyle et al., 1998; Lai et al., 1995; Lims & Lee, 2000; Dunkers et al., 2001). Fibre optic sensors work by sending an infrared light through the optical fibre, the wavelength of the infrared light is monitored and as the resin reaches the fibre optic, it refracts, allowing the flow front to be detected (Tuncol et al., 2007).

FBG fibre optics have the ability to accurately measure mechanical strain, therefore allowing the measurement of residual stresses built up during the manufacturing process (Maxwell et al., 2009). FBGs not only provide strain measurement during manufacturing, FBGs can continue to be used throughout the life of the component.

FBGs are written into single-mode fibres that consist of a very small inner core of approximately $9\mu\text{m}$ diameter and an outer cladding of pure glass of approximately $125\mu\text{m}$ diameter. The core has a high refractive index caused by high Germanium doping whilst the outer core has a lower refractive index, causing the light to propagate only inside the inner core (Nielsen et al., 2013). The outer coating has a breaking strain greater than $30,000\mu\text{m}/\text{m}$, and therefore protects the delicate inner core, which has a breaking strain of approximately $1,000\mu\text{m}/\text{m}$. FBGs have sections which act like a narrowband reflection filter which consists of multiple fringes, where each fringe reflects very small parts of all incoming wavelengths. Each fringe reflects light with a different phase shift, because of this the majority of light is being erased; however, the reflections with equal phase shift accumulate to create a strong reflection peak. The reflection of the whole grating is the sum of these thousands of very small single reflections. FBG sensors

back-reflect light within a specific predefined wavelength, modulation of the reflected wavelength is linearly related to the mechanical and thermal loads (Nielsen et al., 2013). A cross section of a typical FBG can be seen in Figure 28 (Leng & Asundi, 2002). The shift in peak position relates to variations in temperature and strain. The effects of temperature need to be removed to isolate the mechanical strain using independent temperature measurements at the location of the fibre optic (Lodeiro & Mulligan, 2005). FBGs show high temperature dependency, where the wavelength shift caused by a 1°C temperature change, is equivalent to the same wavelength shift caused by a $8\ \mu\text{m}/\text{m}$ change in mechanical strain (Nielsen et al., 2013).

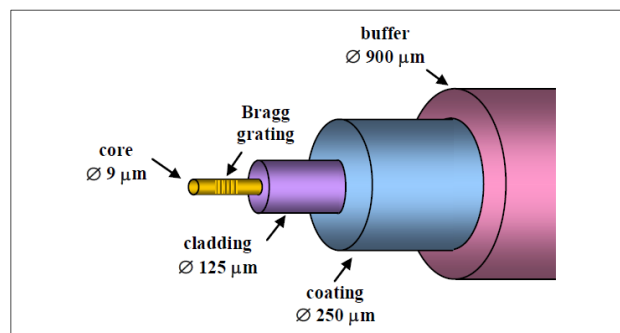


Figure 28: Basic structure of optical fibre with Bragg grating (Lodeiro & Mulligan, 2005).

FBGs are a costly and disposable sensor with a multiple FBG 10m fibre optic costing £562, whilst the additional equipment required for analysing the reflected light costs £1250 per month to rent (Smartfibres, 2016). FBGs also require the protective coating around the fibre optic to be removed, significantly reducing the strength of the fibre and making them very delicate to lay into the reinforcement, potentially delaying the production time, whilst the cost will also limit the repeatability of the experiment. Fibre sizes (128 or 80 micron) can also lead to possible flow obstructions as well as potential delamination regions (Todd, 2013). Previous research utilising fibre optics have conducted post manufacturing optical fibre microscopy and μ -CT to analyse the interference effects caused by the fibre optics. Nielsen et al. (2013) found the fibre optics did not increase the thickness of the matrix layer between reinforcement and did not introduce any voids around the optical fibre in a VARI process using glass fibre and epoxy resin, see Figure 29.

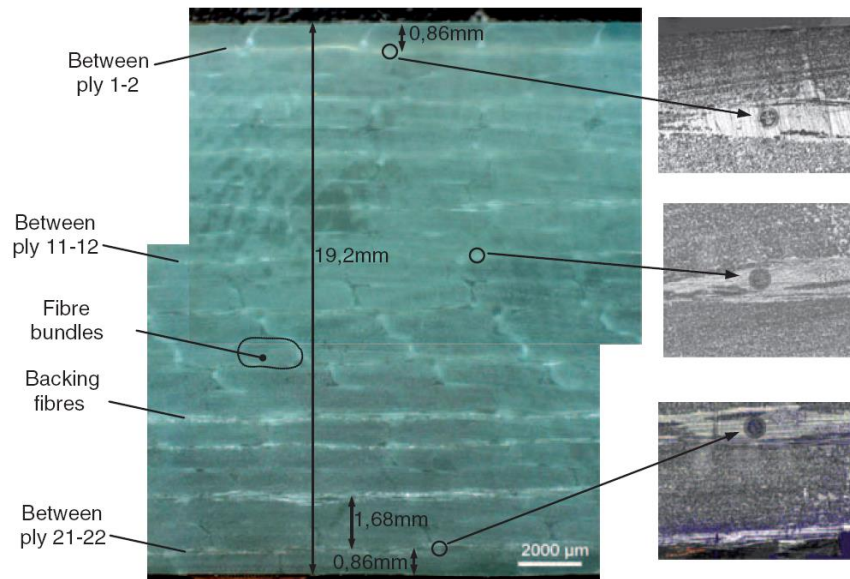


Figure 29: Laminate specimen cross section with close-up of the inter-ply fibre optic placement (Nielsen et al., 2013).

2.6.5 Thermal Imaging

Thermal imaging techniques have the advantage of being able to monitor the temperature over larger areas than point sensors, as well as being a non-contact measurement method. Very little published research has used thermal imaging for flow front progression detection, mainly due to the increased cost over the other visual detection techniques and the required variation between resin and preform temperatures to detect the resin movement.

Flash thermography imparts a pulse of thermal energy on to the surface of the specimen, Figure 30. The thermal energy on the surface is conducted through the cooler interior of the laminate, causing a reduction in surface temperature. The surface cooling should occur in a uniform manner, assuming the material properties are consistent. Sub surface defects possess different material properties, therefore affecting the flow of heat, altering the surface cooling of the specimen, which allows the identification of defects. Due to the nature of the thermal flow through the specimen, the depth at which the defects exist can also be estimated by the time at which the surface temperature anomaly is identified (Martin & Gyekenyesi, 2005).

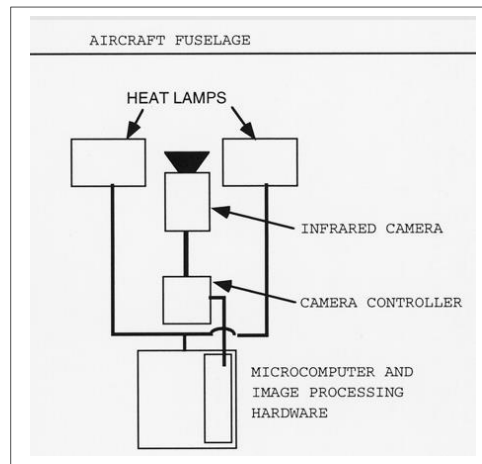


Figure 30: Schematic indicating set-up for flash thermography inspection on an aircraft fuselage (NASA, 1996).

Similarly to dielectric sensors, the added potential of multiple infusion stage measurements as well as the potential of defect detection post cure makes the thermal imaging very desirable.

2.6.6 Linear Variable Differential Transformer

Due to the known changes in preform thickness at different stages of the VARI process, linear variable differential transformers (LVDTs) can be used to measure the variations in preform thickness (Aktas, Boyd & Sheno, 2012a). As has been stated previously, VARI produces non-uniform and non-linear preform thicknesses. As the resin progresses through the preform, the pressure drop remains the same, therefore altering the pressure gradient; hence the preform thickness reduces the further the resin is from the resin inlet. Subsequent to the flow front passing a point, the vacuum release allows the preform to expand, resulting in the thickness variation shown in Figure 31.

Further to the expected changes in preform thickness during the infusion process, the preform is also expected to compress during the resin curing process. Polyester resin has been found to shrink by 5-9% whilst curing (Khoun, Chaudhuri & Hubert, 2011). The level of shrinkage or the thickness of the component could be used to estimate the resin cure state. The ability to monitor the preform thickness during the infusion and curing process would require a stable mould and LVDT mounting position so that the changes detected related to changes in the component not movements in the measurement tool. The scale of the infusions conducted by PYI may restrict the ability to mount stable sensors. LVDTs also only provide point measurements leading to multiple LVDTs to be mounted throughout the preform increasing costs and affecting the processing time.

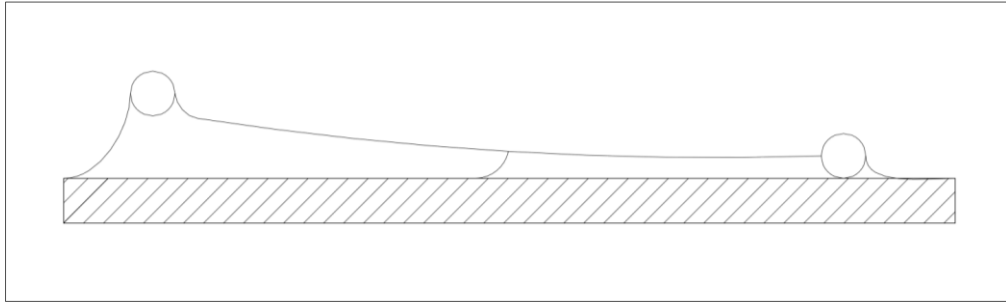


Figure 31: Thickness variations due to non-linear pressure variations during VARI.

2.6.7 Ultrasonic

Ultrasonic measurements provide the opportunity to assess resin fill, resin gel point, end of cure and the degree of cure using only one device. As the density and modulus of the laminate change, so does the ultrasonic velocity, allowing for the cure state to be evaluated. Due to access restrictions during the infusion process, a Pulse-echo ultrasonic transducer could be used, so that access would only be required on one side of the infusion. It could also be possible for mounting points to be integrated into the mould walls, allowing for the transducers to be used for multiple infusions in identical locations (Lodeiro & Mulligan, 2005). Ultrasonic equipment is highly reusable and repeatable, however costs are significant. Ultrasonic results also only show averaged values for the through thickness measurements, not allowing for through thickness variations. Ultrasonic measurements are affected by the dimensional changes during cure, so unless the shrinkage values can be quantified ultrasonic measurement error margins will increase. Ultrasonic measurement interpretation is critical to understanding the results, therefore skilled operators are required to correctly identify the key processing points as well as to identify post infusion defects.

2.6.8 Videography

The most common method for flow front detection is through visual monitoring using video cameras. Full field videography is used to assess the advance of the flow front, monitoring flow front convergence and advancing speeds (Aktas, Boyd & Sheno, 2012a). Matsuzaki et al. (2013) also used microscope videography to monitor mechanical entrapment at the flow front. A digital microscope was installed on the upper surface of the mould and then connected to a computer, due to the similarities in the optical refraction index of polymer resin and glass fibre, once the fibres are impregnated they become transparent. This allowed the successful identification of voids in thin laminates through the conversion of the image to binary, where the impregnated areas could be separated from the void areas. Pearce, Guild & Summerscales (1998) used a similar method to record the effects of converging flow front void entrapment. For thin laminates the benefits of videography are high, the mechanism is highly repeatable and is a low

cost procedure, whilst the larger full field monitoring technique is used to analyse the flow front advance around varying fibre layups. However the restrictions of using the technique on laminates with NCF quad axial layups and sandwich layup restricts the use of videography in an industry setting. Videography is a proven technique which can be used to monitor the surface flow front progressing through the component, however little information can be gathered for through thickness resin location and void locations.

2.6.9 μ -CT

μ -CT is a non-destructive imaging tool for the production of high resolution three-dimensional images. A micro focused X-ray source illuminates the sample and a planar X-ray detector collects magnified projection images. The three-dimensional reconstructions are based on hundreds of angular views acquired whilst the object rotates. Post processing software synthesises a stack of virtual cross section slices of an object to create a three-dimensional grey scale rendering of the scanned sample (Bruker, 2014). Reconstruction of the three-dimensional image is performed by rotating the sample to generate a series of two-dimensional projections which are transformed using a process called back projections (Boerckel et al., 2014). The volume reconstruction is reconstructed as a matrix of voxels which are volume pixels. Each voxel represents a local attenuation coefficient which represents a local X-ray absorption density. The grey scale levels in a μ -CT image relate to the X-ray attenuations, which reflect the proportion of X-rays scattered or absorbed as they pass through the sample (Ketcham, 2016). The attenuation levels depend on two primary factors, the sample material composition and density and the source energy of the X-ray. Combining the input energy and resulting grey scale variations, the density of the sample can be quantified (Boerckel et al., 2014). As the X-rays pass through the sample, the intensity of the incident X-ray beams is diminished according to the distance from the source and the intensity of the X-ray beam based on the following equation (Boerckel et al., 2014):

$$l_x = l_0 e^{-\mu_c x} \quad 2.8$$

Where l_0 is the intensity of the incident beam, l_x is the intensity of the beam at the distance x from the source and μ_c is the linear attenuation coefficient.

A number of factors affect the quality of the final three-dimensional reconstruction, depending on material being scanned and the X-ray strength, μ -CT resolution is limited to 1000-2000 times the cross sectional diameter of the sample. Therefore, the dimensions of the sample being scanned are critical to the achievable quality and resolution of the scan and should be minimised to improve contrast and resolution (Ketcham, 2016). To compensate for large sample sizes,

longer acquisition times are used to reduce the noise levels therefore limiting the ability to capture dynamic processes such as resin fibre impregnation during the VARI process.

Equation 2.8 identifies the reliance of the object being scanned to have sufficient variation in the density of its constituent materials to provide sufficiently large attenuation contrast to consistently and reliably segment and analyse the reconstruction. The thresholding applied to the volume reconstruction is critical to the accurate image segmentation and analysis of the resin impregnation (Cantatore & Muller, 2011).

2.6.10 Sensor Summary

The available composite process monitoring sensors have been investigated for their suitable implementation in an industrial scale VARI. Accuracy, invasiveness and cost are the critical factors involved with commercial process monitoring. Currently the two methods used by PYI, thermocouples and videography, are the cheapest available monitoring techniques. However, both monitoring techniques have provided limited processing information, especially regarding through thickness monitoring. It has been found that thermography, ultrasound and LVDT will only provide limited levels of improvement for infusion monitoring due to the limitations relating to measurement depth through the thickness of the component. Furthermore external factors can have considerable effects on all three measurement techniques, which would therefore require a high number of repeat experiments that would not be possible. Thermography and ultrasound measurements do provide additional post infusion measurements as a non-destructive testing tool to assess the laminate quality for voids and failure points. However, the primary purpose of these sensors is to gather information on the infusion process and the development of residual stresses during the resin cure process.

The non-contact monitoring techniques of dielectric spectroscopy and FEF measurements have been utilised in previous research to monitor flow and cure progress with proven results. However, penetration depth and the ability to distinguish between laminate depths requires further examination. The scalability of the process to monitor infusion over industrially relevant scales also needs to be verified. The ability to mount FEF sensors into a mould tool at PYI would also require significant time and cost, reducing the possibility of setting up a moulded mounted sensor array.

FBG sensors allow monitoring of the flow front location, cure temperatures and the development of residual stress during the manufacturing process. The dangers associated with embedded sensors have been investigated in previous research and found to be minimal by using optical imaging to assess the implications of embedding fibre optics. The optical

microscope image shown in Figure 29 shows that no voids were caused by the fibre optics, which is due to their relative size in comparison to the fibre bundles. Although the costs associated with fibre optic monitoring are high, the accuracy and ability to monitor through life strain variables coupled with the ability to make direct measurements within the preform allow the higher costs associated with the sensors to be justified. The optimal arrangement within the laminate needs to be investigated to maximise the data gathered associated with resin flow front progression and cure shrinkage. Furthermore, the ingress point through the vacuum bag needs to be investigated to ensure the fibre optics do not restrict the ability to maintain a vacuum during the manufacturing cycle.

SMARTweave and linear voltage sensors offer a low intrusive monitoring technique. Further investigation is required to assess the ability to implement these sensors into a NCF as well as the ability to monitor polyester resins.

2.7 Discussion

A review of the current state of research knowledge has been completed. The areas covered included, the creation of defects and the detrimental effect they have on structural properties, resin cure characteristics, computational modelling and the available sensors to monitor the infusion process has been undertaken. The first section identified the multiple defect sources during the resin infusion process which are summarised below:

- Entrapped air in the resin during mixing
- Leaks in the bag or connections
- Resin shrinkage
- Generation of volatile curing by-products
- Inter-tow and intra-tow entrapped air
- Foreign bodies
- Fabrication failures
- Inadequate vacuum source
- Fibre misalignment or wrinkles in the fibres
- Incomplete cured resin
- Converging flow fronts
- Resin flow restrictions
- Incorrect infusion strategies

Due to the scale of the infusions undertaken by PYI, the majority of the defect causes listed above could exist at PYI. In addition to the defect sources listed above, the resin curing process can also result in defects or reduced dimensional stability of the component due to the following:

- Surface ripples
- Warping
- Sink marks
- Delamination
- Internal micro cracking
- Fabric print through

The effect of the defects listed above can be detrimental to the mechanical properties of the final component. One of the obstacles to the wider adoption of the VARI process in the automotive and aviation industries are the risks associated with defects in the component and the inconsistency in the production of components using the VARI process. Matrix dominated

failure mechanisms such as the inter lamina shear strength of the component are impacted by the inclusion of voids in the laminate. Research suggests that for every 1% of voids included in a composite component, the inter laminar shear strength decreases by 7%.

The review of the current state of composite manufacturing computational modelling identified one of the biggest risks with computational modelling in many fields which is the reliability of the input data. Input parameters such as fibre permeability have been shown to be difficult to measure, the review into the process used to measure reinforcement permeability identified a difference by a factor of ten from one research institute to the next measuring the same fabric. It was also found that the application of the available computational resin flow models to complex large three-dimensional preforms was quite limited. The accurate inclusion of capillary flow effects and the influence of variable laminate schedules around the transition from monolithic to sandwich sections have not been sufficiently proven. It was therefore decided that the author should focus on experimental techniques to monitor the VARI process.

The review of the available sensors to monitor the VARI process identified that a range of sensors exist to suit both accuracy and cost requirements. A key consideration during the review of the sensor networks was the required application of these sensors into a commercial environment where additional consideration needs to be applied for sensor application times and their resilience to failure. The requirement of dielectric FEF, LVDTs, pressure transducers and ultrasound equipment to be mounted on or near the laminate surface restricts their application in commercial infusions. Dielectric FEF sensors have shown the possibility of providing long term repeat measurements through the integration of the sensor into the mould surface, however the ability of the sensor to penetrate through the thickness of the laminates manufactured by PYI has not been proven in the literature reviewed.

Fibre optic measurements have been shown to provide reliable measurements relating to both the manufacturing process and the through life condition of the components. The size of the fibre optic sensors has also been shown to have little or no impact on the material structure after being embedded between reinforcing layers. The requirement to monitor the temperature at the location of the fibre optic limits the ability to incorporate fibre optics into a commercial infusion due to the size of temperature compensated fibre optics or the requirement to use thermocouples which are also relatively large in size. Fibre optics are also expensive sensors which cannot be used multiple times, which would limit the range of information which can be captured using fibre optic sensors.

Research into the use of SMARTweave has shown that embedding carbon fibre tows into glass fibre preforms provides resin flow front locations during the infusion process. SMARTweave is limited by the effect the laying of the carbon fibre tows will have on the manufacturing process. SMARTweave also only provides point measurements around the preform, which would require a high number of sensing locations to monitor the large infusions carried out at PYI.

The review identified that a full field monitoring technique does not exist to monitor the VARI process. All the measurement techniques available provide localised measurements relating to resin flow and resin cure characteristics. It was also discovered that a number of the sensors needed to be embedded into the laminate in order to accurately measure the manufacturing process. Due to the commercial nature of this research, special permission would be required to embed any sensors within one of the composite components.

μ -CT material characterisation has proven in recent years to provide an accurate three-dimensional approach to non-destructive testing of composite parts. This technique will be used to analyse the voids reported at PYI, however the possibility of using this technique to monitor the resin infusion would provide a unique insight into the infusion and curing process. A three-dimensional technique to characterise the VARI process should be researched and developed as this would provide a higher level of information into the infusion process than can be achieved by the sensors reviewed in this Chapter.

Chapter 3

3 Commercial Context

Princess Yachts International (PYI) are a leading international composite boat manufacturer who have been using the VARI process since 2006. PYI have continued to push the boundaries of the VARI process with the scale of the infusions that they complete, the best example of this is the M40, a 40 metre hull form manufactured using a single infusion.

Despite the continued research and development in partnership with their resin and fibre suppliers, PYI have found the infusions process used to construct the composite hulls result in defects on the mould surface. Customer requirements dictate that the surface finish of the hull shows no signs of defects, whilst commercial pressures demand the hulls require no surface finishing post infusions to help increase production turnover. Growth in the leisure marine industry has increased demand for PYI yachts meaning that further time pressures are being placed on the manufacturing process used by PYI.

This Chapter reviews the processes undertaken by PYI, the type and frequency of the voids recorded and the research that has been previously undertaken investigating the defects recorded on the mould surface of the hull infusions.

3.1 Princess Yachts Process Review and Reported Defects

A detailed review of the infusion process, the reinforcement and resin used by PYI and any research that has already been undertaken by PYI and their suppliers was conducted. The review is required to evaluate the relationship between production parameters and voids, information relating to the following areas needs to be reviewed and analysed:

- Void sizes
- Void distribution
- Void microstructure
- Void frequency
- Laminate shrinkage
- Dry spots due to insufficient resin infiltration

The hull component represents the largest composite structure produced by PYI. The hulls consist of a mixture of monolithic and sandwich sections as well as complex three-dimensional shapes. An example of the reinforcement schedule used by PYI can be seen in Figure 160, where

the number of additional reinforcing layers can be seen around the chine, transom and keel. Details about the fibres and resin used by PYI can be seen in Appendix B, where the material data sheets have been added. In addition to the material data sheets, the infusion process followed by PYI has been defined in Appendix B.

A combination of visual recording methods, microstructural analysis and cure monitoring has been carried out by the research sponsors PYI, PYI's resin supplier Scott Bader and the author. The results of each investigation will be discussed in this Chapter, along with an identification of where further evaluation is required to identify the dominant processing parameters that affect the final part quality.

3.1.1 Void Locations

The hull components manufactured by PYI range from 13 to 40 metres in length. Post infusion the components are extracted from the mould and visually inspected to identify any laminate re-work that might be required before the component moves to the next stage of production. The visual inspections provide information relating to the location of the defect as well as their estimated dimensions which allows for a statistical analysis to be carried out. PYI provided the author with a range of defect review documents for the vessels displayed in Table 2. The model reference number relates to the production code used internally by PYI to differentiate between different yachts in their range. The details of each model can be found in Table: 9 in the Appendix A, where it can be seen that model A3 represents the 22.35m fly bridge motor yacht. PYI also allocate a production number to each hull, to maintain consistency with PYI, the components will be referred to by their model and production numbers throughout this Chapter. Table 2 shows that models A3 and Y9 have the largest number of sample data, these models are also comparable in dimensions and reinforcement schedule.

Production Model				Production data
Reference	Name	Length	Displacement	Number of Samples
		(m)	(tonnes)	
A3	Y 72	22.35	45.0	27
A4	MY 32	32.00	115.0	4
S1	V 78	23.83	47.5	6
S2	V 72	22.26	42.0	2
T9	Y 60	18.61	30.5	1
Y9	MY 78	24.10	58.5	17

Table 2: Void recording sheets provided by PYI and the production model they relate to.

The yachts produced by PYI use a gelcoat to colour the topsides of the yachts. All void inspections are carried out using a visual approach, however the gelcoat colouring located

above the waterline for each vessel hides any information relating to defects within the laminate. The inspection type limits the imperfections that can be identified to the following: areas of delamination, dry spots and high levels of porosity. Figure 32 shows two examples of the types of defect which are easily identified and recorded as part of the visual inspection. The depth of the imperfections is also not known, although it is possible to estimate the depth of the imperfection by assessing the level of clarity on the surface which gives an idea of the proximity to the mould surface.



Figure 32: Infusion Imperfection examples from PYI.

A visual inspection limited to only 25% of the component due to the gelcoat masking the laminate and an inspection procedure which does not review the laminate quality on the vacuum bag surface is inadequate to gain an accurate understanding of the laminate quality. Furthermore the review process is undertaken by different quality control engineers depending on locations using simple void recording sheets which limit the amount of information which can be recorded. The quality of the information recorded on the sample sheets provided by PYI ranged considerably from simple void numbers to details of the locations, dimensions and void types. A high proportion of the component goes untested due to the thickness of the laminate and procedure used. The data provided will be used for a qualitative review to gain an understanding of any underlying causes of the voids reported by PYI.

Samples of void recording sheets were supplied to the author, Figure 33, these were then collated into one schematic in order to identify the frequency of occurrences of the different void types, sizes and locations. The location of the imperfections relative to the chine and the gelcoat boundary were not differentiated in the void recording sheets. Due to this missing information the location of the voids vertically in relation to the chine and gelcoat boundary could not be reviewed. Additionally the imperfections recorded on the transom were also estimated due to lack of clarity from the recording sheets.

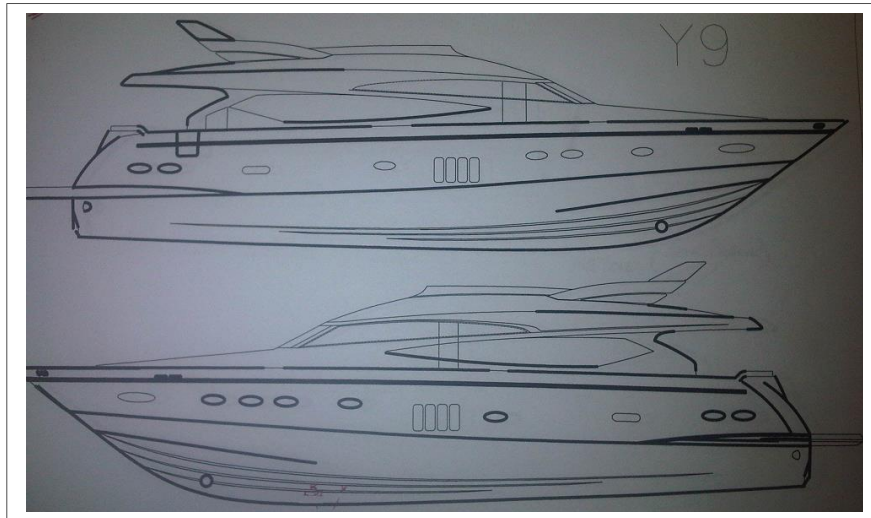


Figure 33: Example void recording sheet from PYI.

In order to improve the void information collected for each component a new void inspection sheet was created by the author and distributed to PYI, Figure 34. The new document provides clear instructions on how to record defect types to improve consistency from one production team to the next. A grid was added to the component so that the features on each hull could be used to improve the consistency of location recording. The transom and hull bottom were also added as these two surface represent the largest area not covered by the gelcoat.

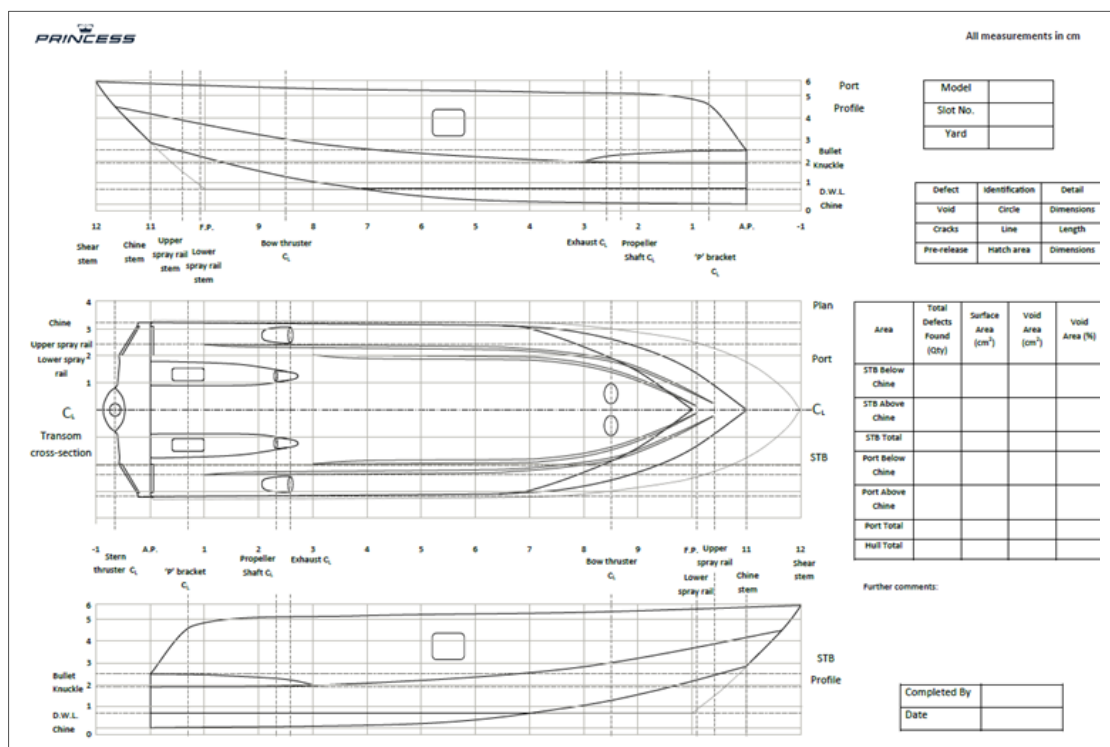


Figure 34: New void inspection sheet provided by the author to PYI to improve the reliability of the defect information being recorded.

The distribution and frequency of the defects can be seen in Figure 35 and Figure 36 where a relationship between complex geometric shapes and void locations can clearly be seen. Clusters of imperfections are located around the propeller tubes, exhaust outlets, bow thrusters and the transom features such as trim tabs and the chine where variations in the laminate schedule and component thickness exist.

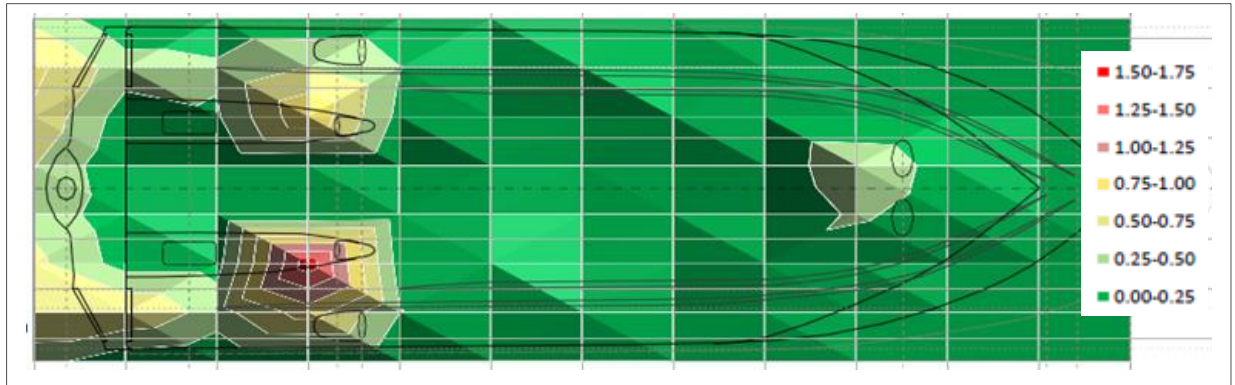


Figure 35: Void locations and frequency of occurrence on the bottom of the hull components

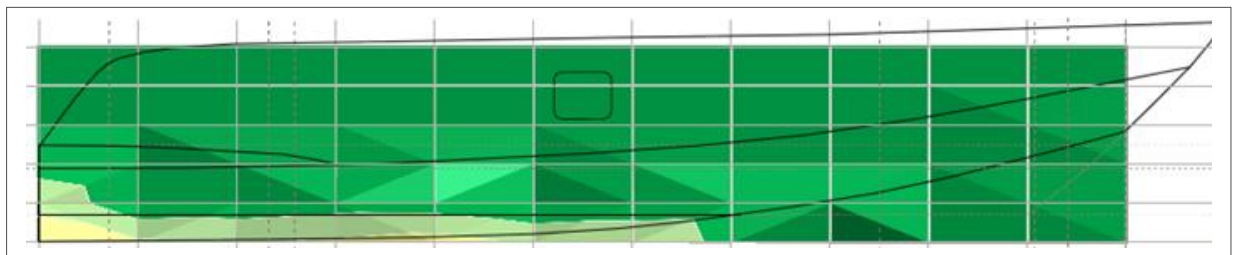


Figure 36: Void locations and frequency of occurrence on the topside of the hull component.

An example of a typical layup at the location of these design features such as the chine can be seen in Figure 37 where the lamina schedule changes from sandwich on the bottom of the hull to monolithic below the chine and sandwich section on the vertical section above the chine. Similar transitions occur at the propeller tubes, exhaust outlets, bow thrusters and the transom. To promote resin flow around these areas, high flow fabric is used on the vacuum bag surface, this can exaggerate the irregular flow front due to the delay on the mould surface, however the time to impregnate these thick monolithic sections is critical to guaranteeing the full saturation of the preform before the resin gels.

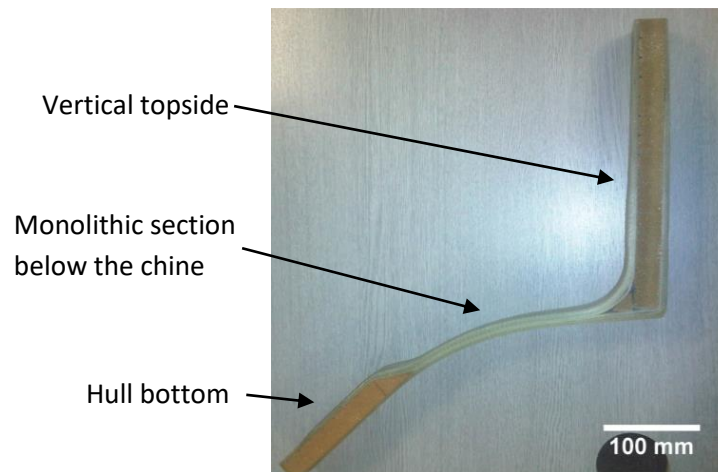


Figure 37: Chine cross section showing the transition from the topside sandwich layup to the monolithic structure below the chine.

In addition to the proximity to the design features in the hull, Figure 36 shows that the frequency of voids on the chine near the transom on the left is higher compared to the voids near the bow on the right. This suggests that the variable laminate schedule is not the only cause of the voids. The area closer to the transom aligns with other design features, whereas forward of amidships, the only feature affecting the lamina schedule are the bow thruster tubes. Due to the initial resin inlet being located at the keel, the resin flow has to pass the propeller shaft outlet point, exhaust outlet and chine before reaching the topsides in one section. The combination of variable permeability, resin and fibre distribution and resulting cure temperatures and shrinkage may be impacting the component quality.

The location of the frequent voids leads to a number of hypotheses to their specific cause in these regions. Firstly these features coincide with a transition region from monolithic to sandwich layup or visa-versa. These regions often include multiple ply variations at the transition from monolithic to sandwich construction. These variations have a number of impacts on the permeability and cure characteristics of the preform: they alter the resin flow front velocity and shape, the cure temperature, fibre volume fraction and resin volume. Each variable working individually or in combination may be the cause of the imperfections, however without further information to characterise the processes occurring during the infusion and cure, these hypotheses cannot be validated.

3.1.2 Void Area and Infusion Parametric Variations

In addition to the location information collected by PYI, critical information was also recorded during the production process relating to resin viscosity, vacuum pressure and resin quantity. It is expected that a relationship would exist between this information and the quantity of voids

recorded post production, which should help to identify some of the causes of the voids and imperfections. The analysis of this information will also help to identify any improvements that have occurred during the production cycle of each model.

The production data for each model were compared to the post infusion void recording sheet to identify any relationships between the number of voids and changing processing parameters. Due to the volume of data available for models A3 and Y9, and their similarity in size, 22m and 24m in length respectively, these models were focused upon for further analysis.

Comparisons between the total void areas reported for each production number chronologically were conducted to identify improvements in the component quality as the manufacturing process for each component matured. Improvements in the resin injection plan, core material layout and design and fibre layup would be expected to improve as the production team develop their skills and understanding of the different layup schedules and infusion plans. The results shown in Figure 158 and Figure 159 in Appendix C identify the inconsistency between chronological build numbers and the reported voids and imperfections. Improvements in the void areas reported for model A3 can be seen in Figure 38 where improvements have been made as the production number increases.

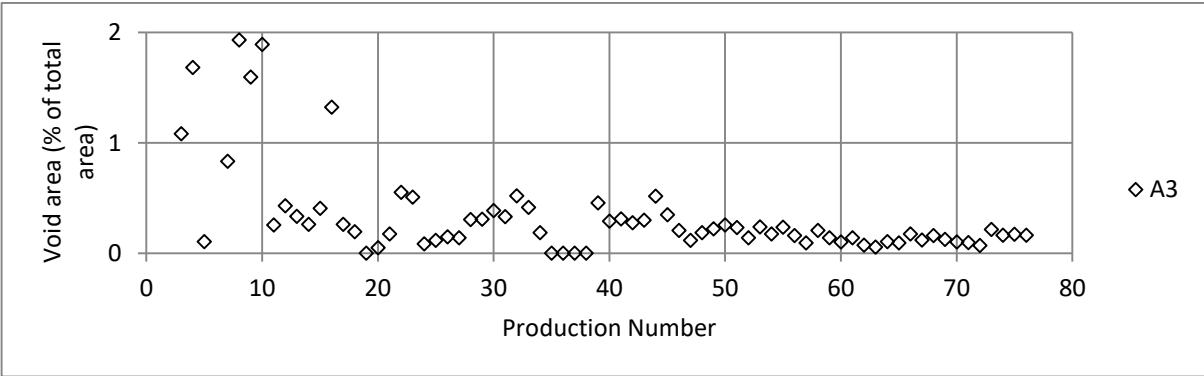


Figure 38: Defect area for model A3 with respect to the chronological manufacturing number.

Model Y9 however, having reached a lower production number, has not shown the same improvements as the A3 model. Inconsistencies between consecutive production numbers can be seen between build numbers eleven and thirteen where the void area increased from 0.24% to 1.72% as can be seen in Figure 39.

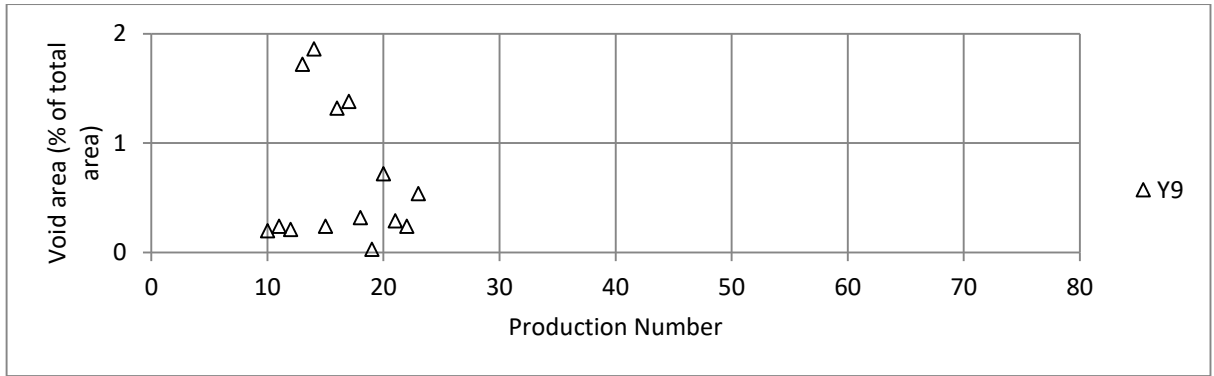


Figure 39: Defect area for model Y9 with respect to the chronological manufacturing number.

The reported void and imperfection areas vary by a factor of seven between the two components manufactured using the same mouldings, materials and instructed manufacturing process. The variability in the component quality reported for these composite structures identifies the high level of variability in the VARI process being used for these large component infusions. Limited control and monitoring data is available from these infusions, however a relationship between the component quality and the processing parameters needs to be investigated.

Both models identify a negative trend between production number and void areas, suggesting improvements are made as the manufacturing process matures for each component. The volume of data provided for models, T9, A4, S2 and S1 consists of high levels of variations between each production number. The variation in component quality is demonstrated by the high standard deviation of 0.415% for model A3 and 1.27% for model Y9 which results in a coefficient of variation of 2.66 and 2.10. A coefficient of variation greater than 1 indicates a relatively high variation in the data.

Variations in critical parameters such as vacuum pressure, flow front velocity and resin viscosity will cause a distinction between the distribution, size, shape and density of voids, therefore a statistical correlation between the variations in void area and processing parameter variations would be expected. A statistical analysis was carried out utilising a Spearman's coefficient of rank correlation (r_s). The Spearman coefficient of rank is a nonparametric method of measuring the association between two variables (Lehmann & D'Abbrera, 2006), chosen over a Pearson's correlation coefficient due to the non-linear distribution of the data, which could lead to misleading results. Spearman's coefficient of rank correlation is shown below;

$$r_s = 1 - \frac{6 \sum d_i^2}{n(n^2 - 1)} \quad 3.1$$

In Equation 3.1, r_s represents the Spearman's rank of correlation, d_i the difference in statistical rank of corresponding variables and n denotes the number of ranks.

Seven relationships were investigated to identify any quantifiable relationship between variations in the measured processing parameter and the final part quality judged by the surface defect visual inspection.

Spearman's coefficient can have a distribution between 1 and -1, and either of these results identifies a perfect association, whilst 0 represents no identifiable association. Significance levels were also calculated to determine the reliability of the association based on the sample size and the probability of the association happening by chance. Associations with a significance level lower than 95% should be rejected.

Processing parameter		r_s	Significance level greater than 95%
Void area	Fill rate	0.36	No
Void area	Boost % of fill time	0.49	No
Void area	Chine % of fill time	0.59	Yes
Void area	Knuckle % of fill time	0.41	No
Vacuum level	Fill rate	0.4	Yes
Fill rate	Resin Viscosity	-0.36	Yes
Resin temperature	Resin Viscosity	-0.27	Yes

Table 3: Processing parameter spearman's rank of correlation.

The final three associations in Table 3 were included to test the reliability of the data. A strong association would be expected between the vacuum level/ fill rate, fill rate/resin viscosity and resin temperature/resin viscosity due to the dependencies between each variable. Although the results do not identify the expected level of association, the anticipated positive or negative trends were produced. Increased vacuum levels have been shown to increase resin flow and therefore the fill rate, which is known to have an inverse relationship with resin viscosity. This inverse relationship is due to an increased resistance to flow with increased viscosity which is in turn strongly affected by the resin temperature. The results identify that the distinct relationship that should exist between the processing variables does not exist.

The three associations between the injection port openings of the boost, chine and knuckle as a percentage of total fill time, show a poor but not insignificant association to the percentage of voids. The relationship suggests there is a positive effect of opening the ports earlier in the

infusion cycle to reduce voids. The earlier opening also suggests a faster flow front progression on the bag surface, signifying an increased flow velocity, which has been shown to minimise macrovoids due to the reduction or elimination of inter bundle flow front lag behind the intra-bundle flow front (Beard, Saouab & Bouquet, 2003; Hattabi et al., 2005; Patel & Lee, 1995; Williams, Morris & Ennis, 1974). However the fill times only relate to the vacuum bag flow front as the infusion strategy is adjusted based on resin location on this surface. Without any data relating to the flow front progression on the mould surface and through the thickness of the component it is difficult to draw conclusions relating to the impact of different resin flow velocities. Further data collection is required to increase the quantity and accuracy of the data.

The inconclusive results of the processing parameters statistical correlation and the variability in the void recording sheets generates questions about the quality of the manually recorded data from PYI. The limitations associated with only reviewing 25% of the laminate post production as well as restricting the quality control personnel to surface visual checks raises concerns about the quality control procedure at PYI. The subjective nature of the process results in inconsistencies between different production locations that PYI operate at, which significantly reduces the reliability of the results used to compare component quality. The procedure followed by the quality control personnel also restricted the level of detail that could be provided about each defect. The void recording sheets appear to only be used to record that defects exist on each component and a rough location to help the laminating team to repair the defects. The revised defect recording sheet, Figure 34, provided to PYI allows for improved accuracy with respect to the location of the defects as well as the type of defects recorded.

The processing parameter review further identified these issues due to the poor correlation between the vacuum level, fill rate, viscosity and resin temperature. The processing information relies on the measurements taken by the laminating team. Depending on the infusion being carried out, the team may be more focussed on repairing leaks in the vacuum bag than recording production information. The results suggest that an automated data collection system would be beneficial to aiding the monitoring of the production process. The automated recording of the processing information would help to mitigate the risks associated with manual data, in addition to the processing information, data collection could also help to identify components which are likely to result in defects due to variations in the production process.

The results, although inconclusive, do identify the potential effects that variations in processing parameters may have on the laminate quality. A greater and more accurate data set is required to identify these relationships more conclusively. The challenges associated with the industrial

environment in which the infusions take place increases the number of unknowns and uncontrollable factors. Ideally a controlled working environment would be used with the same equipment, materials and personnel. In practise this is not possible due to the industrial nature of the infusions taking place.

3.2 PYI and Scott Bader Production Experiments

3.2.1 Resin Flow Experiments

In addition to the information relating to processing variables and void locations, PYI and their suppliers have carried out a number of resin flow and cure experiments. Due to the size of the VARI being undertaken by PYI and the variable laminate layup schedules used, understanding the changing resin flow behaviour and curing characteristics is very important. PYI have conducted a number of experiments investigating the effect of changing layup schedules, transitions from monolithic to sandwich layup, the use of different flow distribution methods and the changing resin cure characteristics of high and low volume resin regions. The outcome of each investigation has been reviewed in order to identify the effect each variable has on the final component quality as well as to link the results of each individual investigation.

Experimental characterisation of the flow front progression through a laminate with similar features to the chine has been carried out and can be seen in Figure 40 and Figure 41. Both experiments were conducted to investigate the effects of the distribution mesh on the monolithic region and core grooves in the sandwich section. A comparative laminate layup was used to mimic the ply drops used at the chine in a scaled experiment. Due to the size of the experiment, it was not possible to include the staggered lamina reduction technique used on the full scale infusions, which will affect the resin flow characteristics.

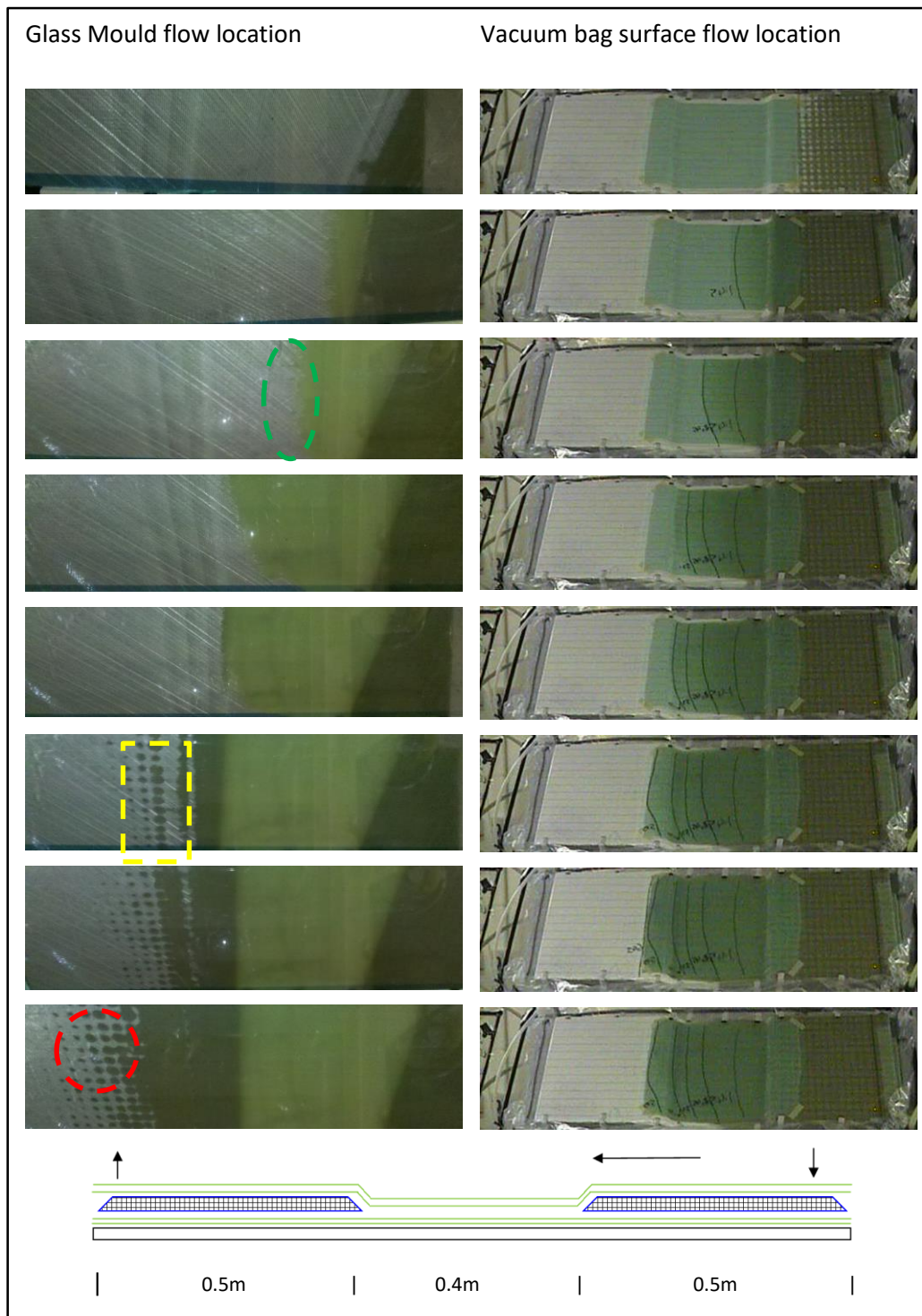


Figure 40: Top and bottom flow front experiment around a flat chine layup.

At the bottom of Figure 40 layup of the experiment can be seen, with the resin inlet on the right, vacuum outlet on the left and resin flowing from right to left. The resin inlet and outlet positions are located on the top of the sandwich sections, with a monolithic section in between both sandwich sections. The green section on the vacuum bag surface is where the high flow fabric has been used to promote resin flow over the monolithic section.

Time lapse photos of both the mould surface and vacuum bag surface of the flat chine layup are shown in Figure 40. The results highlight three important resin flow phenomena, firstly the through thickness flow caused by the core grooves and distribution holes result in converging flow fronts between each hole, circled in red, an effect previously investigated by Pearce, Guild & Summerscales (1998). The second flow effect, the lead-lag effects of the core grooves results in a leading flow front on the mould surface as the resin flow dominates in the core grooves after the monolithic laminate area, circled in yellow, this identifies the dangers of creating flow channels that allow the resin to accelerate past the saturated lamina. The third effect, the through thickness permeability, creates an initial lead-lag characteristic that occurs when using thick composites at the injection point, circled in green, where the mould surface flow front is delayed behind the vacuum bag surface flow front (Searl, 2003; Feiler, 2003). The lead-lag effect will likely be exaggerated on the full scale infusion due to the use of distribution mesh at the initial infusion point on the keel line.

A similar experiment using a mould with a 90° transition from horizontal to vertical flow was conducted to evaluate any variations caused by the geometric alterations which could result in fibre bridging as well as the gravitational effects at the chine. A mirror was used to the right of the infusion to show the mould surface flow front.

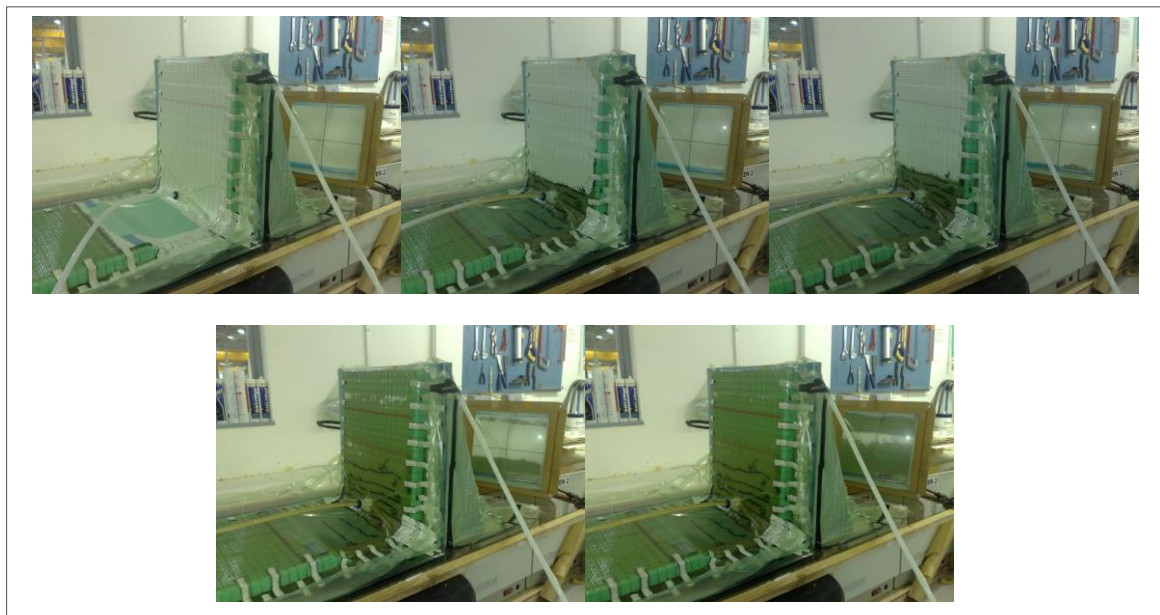


Figure 41: Flow front experiment around a chine feature identifying the lead-lag between mould and bag face during infusion.

The time lapse photos in Figure 41 show the results of the experiment where comparable flow features to Figure 40 are visible. The distribution holes used in the first experiment were not

repeated, resulting in a large delay in the mould flow front at the bottom of the topside section. The delayed flow front results in the parallel converging front seen in the mirror of the last two photos of Figure 41 and in the three images in Figure 42.

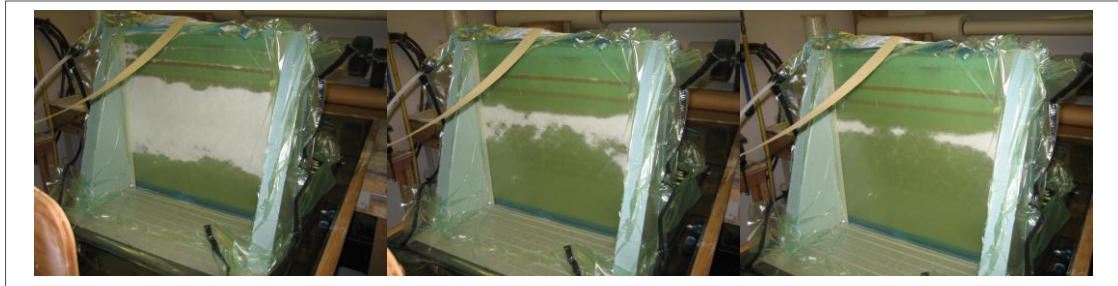


Figure 42: Mould surface converging flow front from the flow front experiment around a chine feature.

Large converging fronts have been proven in research and industrial applications to result in considerable dry spots and microvoids (Pearce, Guild & Summerscales, 1998). Adjustments to the infusion strategy are based upon visualisations of the flow front on the bag face. If these flow features are scaled to the full scale infusions, the infusion strategy may be exaggerating any flow lead-lag effects caused by the irregular layup. It appears necessary from this experiment to carry out flow monitoring on a full scale infusion to investigate the irregularity of the flow front.

Post infusion inspections revealed no visible surface voids caused by the non-uniform flow front. A number of reasons may exist for this; firstly void mechanisms such as mechanical entrapment are affected by the scale of the infusion, therefore a relatively small lab infusion will not result in the same volume of voids as a large hull infusion. Another factor is the ability for the voids to be dislodged and washout of the preform. A smaller infusion will promote a higher level of void washout compared to a larger infusion; these effects as well as the lowered probability of vacuum leaks, and a more controllable flow rate restrict the ability to recreate the voids. It is therefore thought that without an artificial injection of voids, experiments which are not at the scale of the VARI being undertaken by PYI will not replicate the void phenomena (Park & Lee, 2011).

Future investigation into flow distribution grooves on the core allowed a closer investigation into the effects of converging flow fronts, vacuum pressure and lamina thickness. Four experiments were carried out with both 20 and 40mm core grooves to assess the core groove distribution effects on flow rate whilst maintaining core groove volume. Details of the experiments performed are shown in Table 4.

Panel			Vacuum Pressure	Lamina Schedule
1	A	20mm Spacing	50 mbar	1 Ply of 1200 QD each side of core
	B	40mm Spacing		
2	A	20mm Spacing	50 mbar	4 plies of 1200 QD each side of core
	B	40mm Spacing		
3	A	20mm Spacing	250 mbar	1 Ply of 1200 QD each side of core
	B	40mm Spacing		
4	A	20mm Spacing	250 mbar	4 plies of 1200 QD each side of core
	B	40mm Spacing		

Table 4: Core groove sandwich panel flow experiments.

The experimental set-up and flow front can be seen in Figure 43 where the effects of the core grooves distribution on dry spots can be seen. The narrower core grooves appear to produce a reduced number of voids whilst in Figure 43 the wider core grooves result in a faster flow rate.

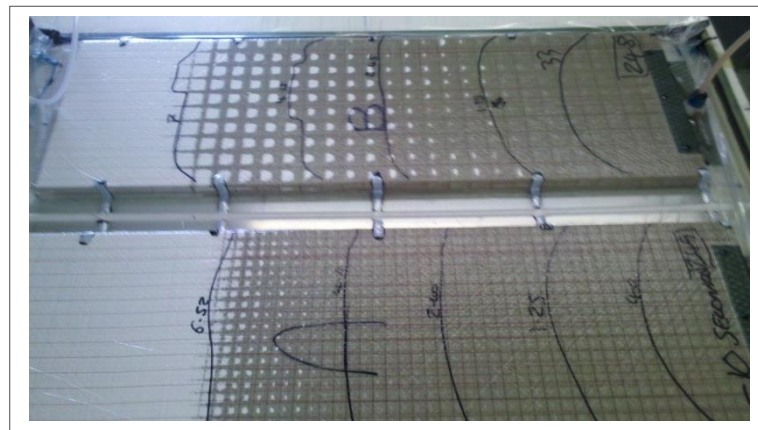


Figure 43: Core groove sandwich panel flow experiment.

Post infusion examination of the panel identified voids located below the through thickness distribution holes as a result of the converging flow fronts. The voids shown in Figure 44 are a result of the lower vacuum pressure infusions for both the thick and thin laminate layups. Pearce, Guild & Summerscales (1998) found that when converging flow fronts meet head on there is an increased volume of voids at the knit line. In addition to this increased volume, the voids formed in this manner were also found to retain their position during subsequent flow, due to the removal of the driving pressure. The 50mbar vacuum infusions however did not result in the same level of voids and appear to validate the void washout theory at higher vacuum pressure.

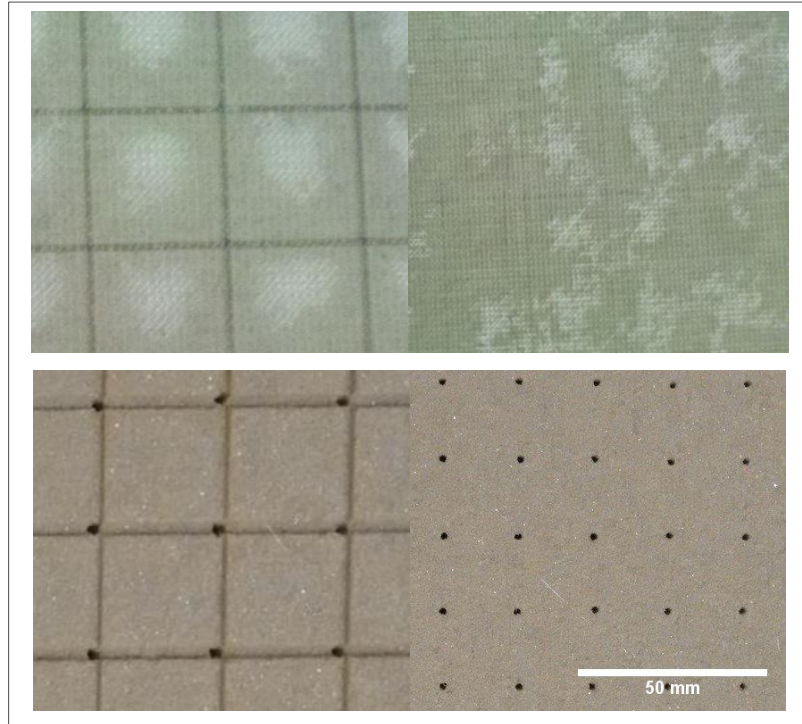


Figure 44: Dry spots between the resin flow channels on the larger 40 mm spacing (left hand side) and smaller 20 mm spacing (right hand side) core material and the flow channels and distribution holes on the core material.

For each experiment the flow rate was recorded on the vacuum bag surface using time lapse photos. The averaged results of each of the four experiments can be seen in Figure 45 and Figure 46. The results for the 250mbar infusion follows the expected pattern, with the single lamina layup resulting in a substantially faster flow speed of 0.00214 and 0.00220m/s for the 20 and 40mm core sections. The thick skin panel recorded an average flow speed of 0.00131 and 0.00119m/s, identifying a lack of consistent variation in flow rate between the 20 and 40mm core groove lay-outs. The results from the 50mbar vacuum pressure infusion however appear to identify two of the problems associated with vacuum infusion, variability and lack of repeatability. The higher flow speed on the 40mm single lamina and 20mm four lamina panels at 0.00309 and 0.00242m/s does not follow the expected reduced flow rate associated with thicker laminate layups. Each experiment was repeated three times, reducing the possibility of the flow rate anomaly resulting from an experimental error.

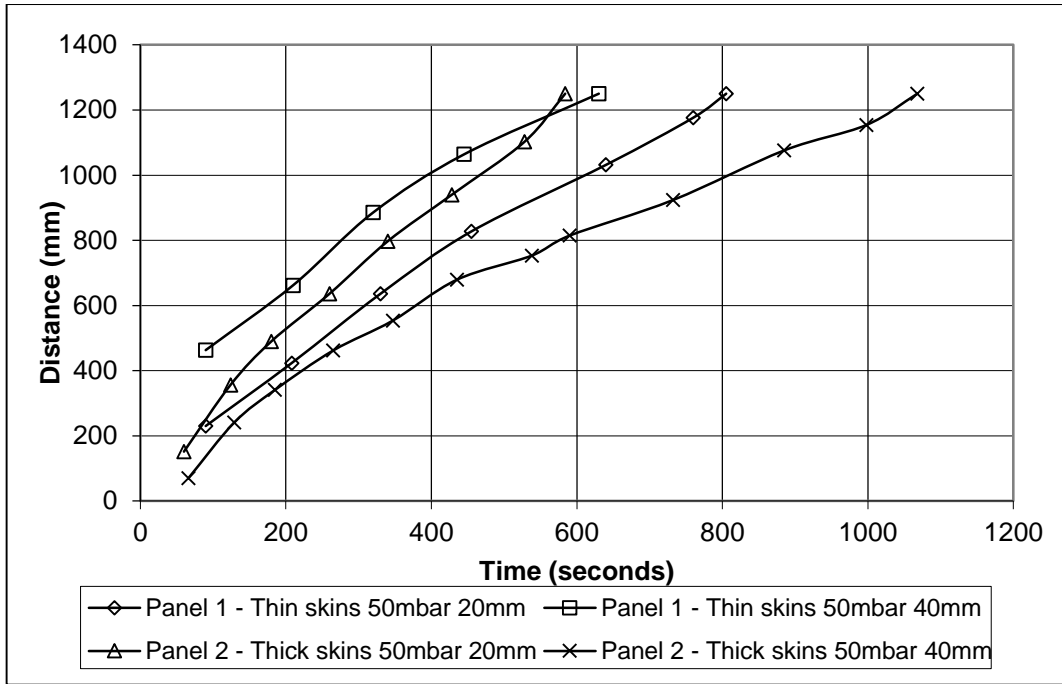


Figure 45: Sandwich panel average flow front position at 50mbar pressure.

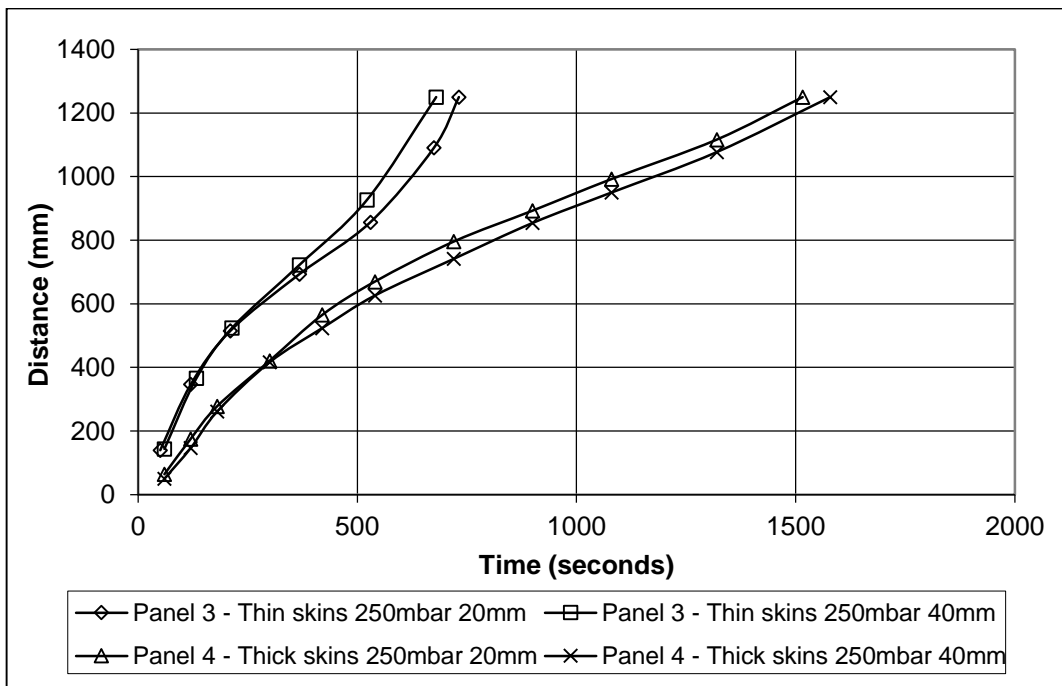


Figure 46: Sandwich panel average flow front position at 250mbar pressure.

Currently the core distribution grooves are placed on the vacuum bag surface to avoid any possibility of print through to the gelcoat surface, resulting in an inferior surface finish. Further analysis of the effects of the core grooves on the three-dimensional flow front is required to assess any improvements that could be made to reduce the level of converging flow fronts

within the preform. A method which could identify the location of the through thickness flow front would considerably improve the level of information provided to the infusion team.

3.2.2 Curing Production Data and Experimental Assessment

3.2.2.1 PYI experimental investigation

PYI have been working with their resin suppliers Scott Bader to reduce the number of voids and improve the dimension stability of the polyester resin. Over the past few years laboratory trials assessing the resin cure characteristics of the hull infusions have been carried out (Douglas 2011). To date, investigations have included:

- The relationship between exotherm and hardness using shore durometer. (PYI)
- The relationship between exotherm temperature and shrinkage. (SB)
- Through thickness exotherm profiling. (PYI)
- Investigation of hull core fractures. (PYI – University of Plymouth)
- Defining cure progression through thickness. (SB)
- Definition of physical state of resin system during cure stages. (SB)

3.2.2.2 Results of the experiments completed by PYI

A number of experimental techniques have been used in the aforementioned investigations. Firstly PYI completed a study to measure through thickness temperature profiles in the chine region where the most significant defects are occurring. Thermocouples were placed on the gelcoat surface of the mould tool and on the vacuum bag as shown in Figure 47 (Douglas, 2010). The results shown in Figure 20 show the thermal cure profile through the mould surface and the vacuum bag surface at the chine during cure. The through thickness temperature variations cause a continued build-up of residual stresses, the importance of which were discussed in Chapter 2.

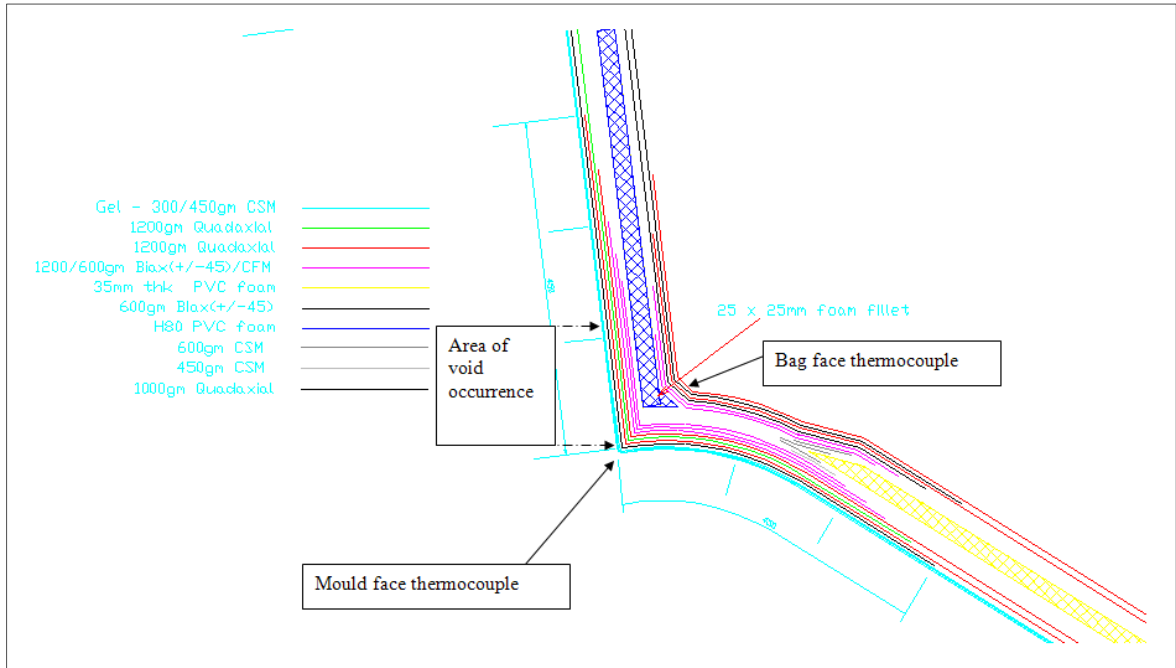


Figure 47: Fibre layup on A3 Slot 11 chine region (Douglas 2010).

Mould surface exothermic temperatures have also been recorded at the keel, bottom, chine and topsides for three A3 infusions, build numbers 19, 20 and 27. The thermocouple recorded temperatures can be seen in Figure 48, Figure 49 and Figure 50, these show that considerable temperature peaks can be seen at the chine region where the largest volume of resin and fibres are located. The second peak can be seen in the keel region, where a high volume of resin and fibre are located due to the monolithic layup. The peak temperature difference across the laminate of 40°C is likely to have a considerable effect on the laminate residual stress distribution as well as the cure shrinkage uniformity.

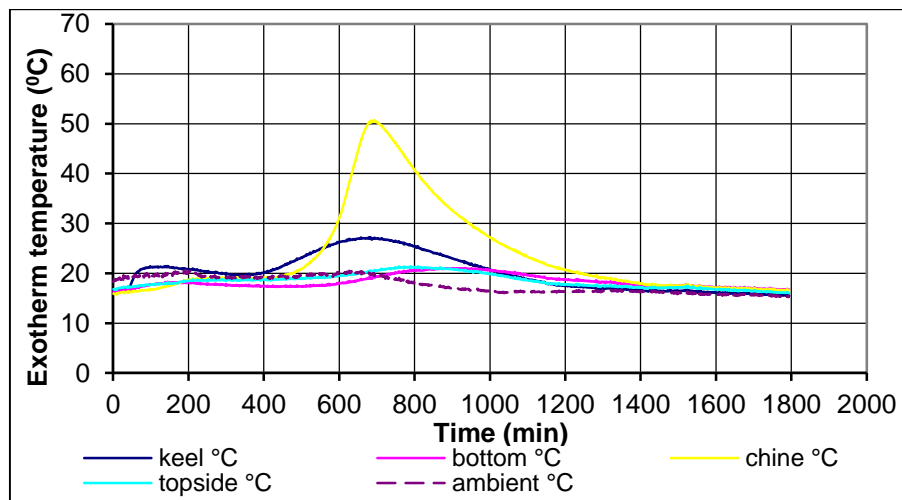


Figure 48: Exothermic cure temperatures for model A3 build 19.

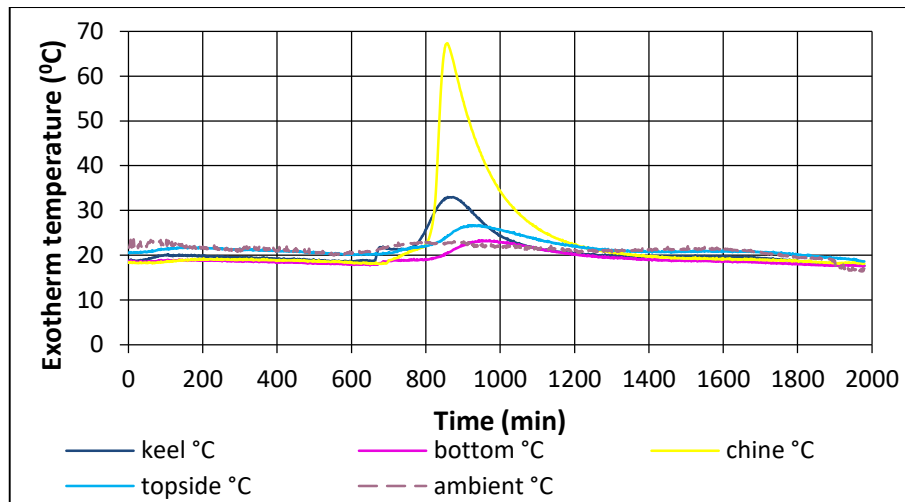


Figure 49: Exothermic cure temperatures for model A3 build 20.

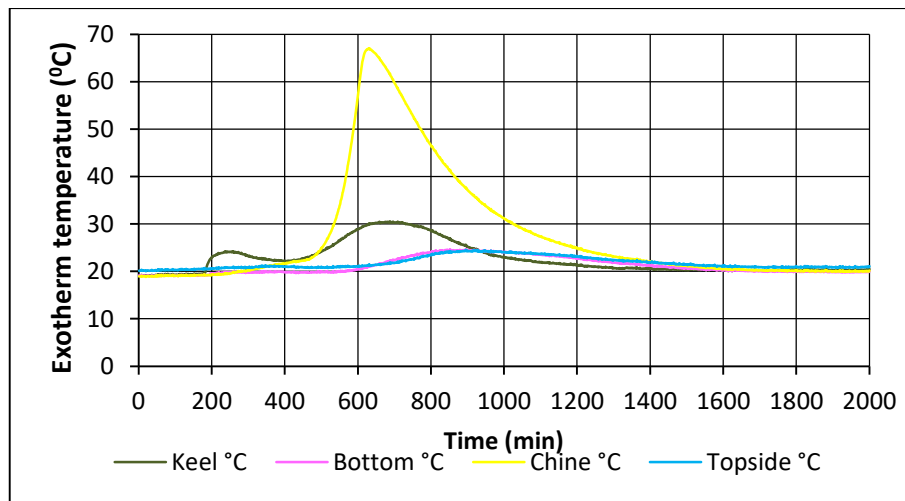


Figure 50: Exothermic cure temperatures for model A3 build 27.

PYI have also carried out cure temperature profiling and shore D hardness investigations on flat tiles. Hardness profiling has shown links to the cure status of the resin where increases in hardness relate to the resin transition from liquid to gel and gel to solid. Thermocouples were again located within the mould tool face and on the outside of the core face of the infused tile. The interesting results, relating to residual stress development are shown in Figure 51, which show that a significant increase in exothermic temperature was recorded for the 8mm tile in comparison to the thinner 4 and 6 mm tiles. The increased cure temperature identifies the effect of higher resin quantities on the exothermic reaction. Due to the variable reinforcement schedule used by PYI in the hulls, a significant variation in cure temperatures between the monolithic and sandwich sections could be expected. This will result in different cure profiles which effect the rate of cure, rate of resin shrinkage and residual stress development.

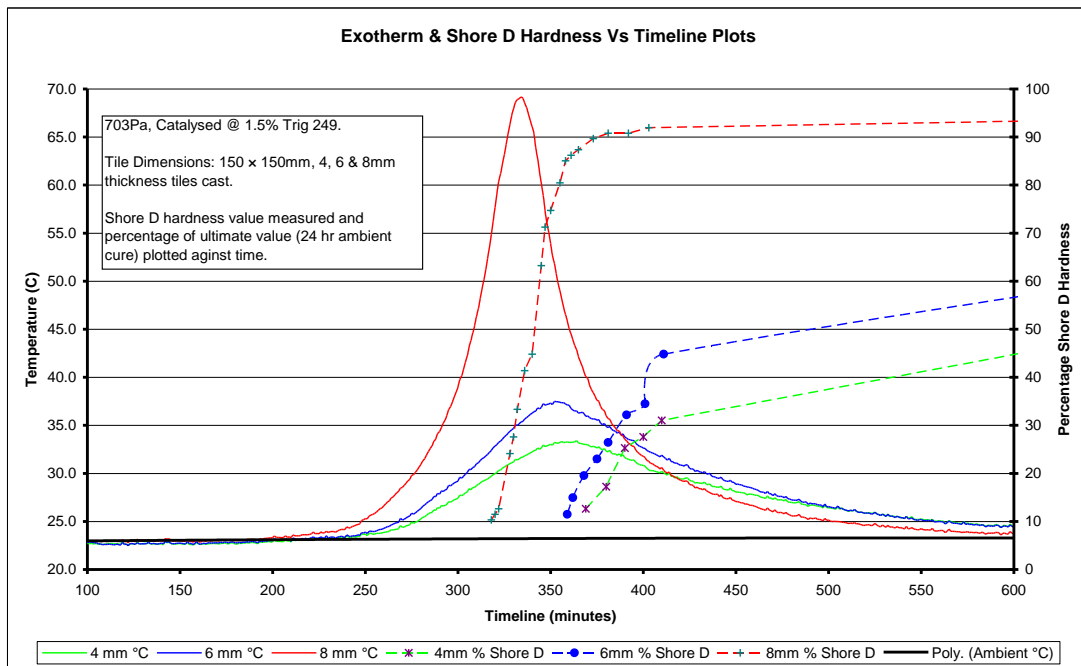


Figure 51: Exotherm and Shore D Hardness curves for three infused tiles with varying thickness (Douglas 2010).

3.2.2.3 Results of the experiments completed by Scott Bader

A critical factor affecting large polyester resin infusions is the effect of resin shrinkage during curing. The dimensional stability of the component is a key deliverable for all of the components produced by PYI. Any imperfections in the surface finish require additional post infusion finishing which delays the production process and adds costs. Scott Bader have therefore concentrated on profiling the cure process of the resin, using test tubes as the mould and a variety of resin masses and thicknesses to investigate the shrinkage, cure progression and the physical state of the resin during cure. The resin system used, a polyester resin, Crystic C703pa, is the same resin used by PYI for the infusion of the hull and deck components. Volumetric shrinkage measurements of the resin were obtained from three experiments, the first using a small 12 mm diameter test tube containing 20 g of resin, the second and third experiments used a larger 18 mm diameter test tube containing 20 g of resin and finally 40 g of resin (Cook 2011). The shrinkage measurements were obtained by recording the height of the resin mass at regular intervals against a 0.5 mm pitch scale attached to each tube.

For the larger 40 g mass, the exotherm temperature was higher than the smaller resin masses, 50°C compared to 23°C in the smaller test tube and 27°C in the larger test tube. The results also showed the resin transition from gel to solid occurring as the temperature rises to its peak, as can be seen in Figure 52. Figure 52 also shows that the peak shrinkage occurs within minutes of

the peak exothermic temperature, 270 vs. 265 minutes in the large test tube with 40 g resin mass.

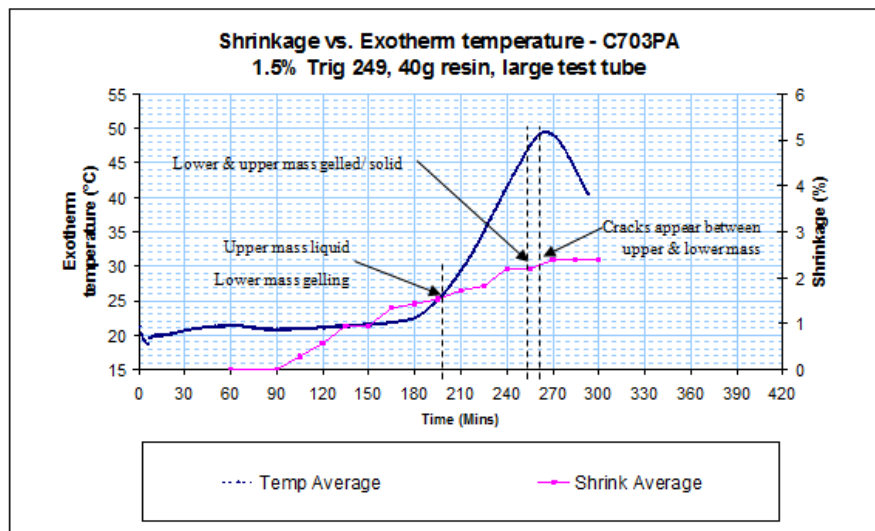


Figure 52: Cure temperature and shrinkage averages for Crystic 703pa large resin tube (Cook 2010).

Scott Bader also found that for smaller resin volumes the resin peak exotherm, shrinkage and solidification did not occur at similar times like the larger resin mass. The smaller resin masses continued to shrink for up to 120 minutes after the peak exotherm, Figure 53. The peak exotherm temperatures were also found to be lower for the smaller resin mass with peak temperature recorded being 27°C. The resin continued to solidify for up to 120 minutes after the catalyst and resin were mixed as can be seen in Figure 53 and Figure 54. The results show that the resin in smaller samples continues to solidify for up to and beyond 7 hours after the catalyst is mixed with the resin, over 3 hours after the larger resin masses have fully solidified.

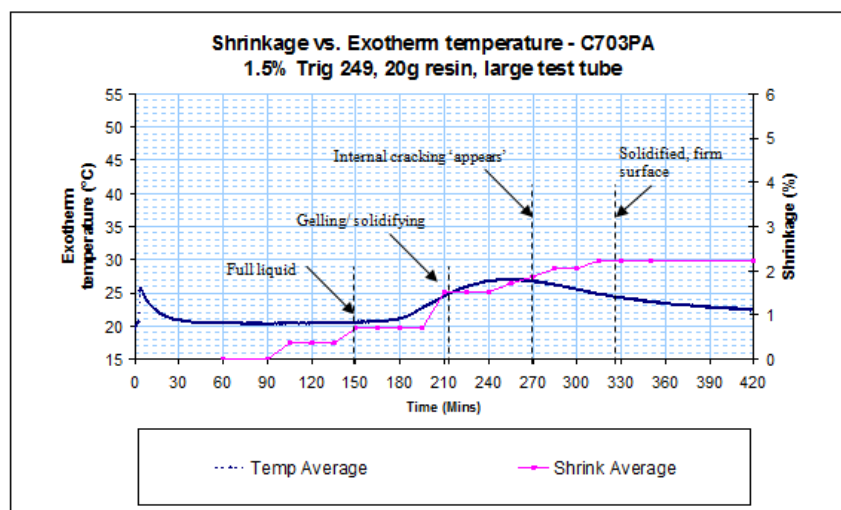


Figure 53: Exotherm and shrinkage for Crystic 703pa – 20 g mass and 12 mm diameter test tube (Cook 2011).

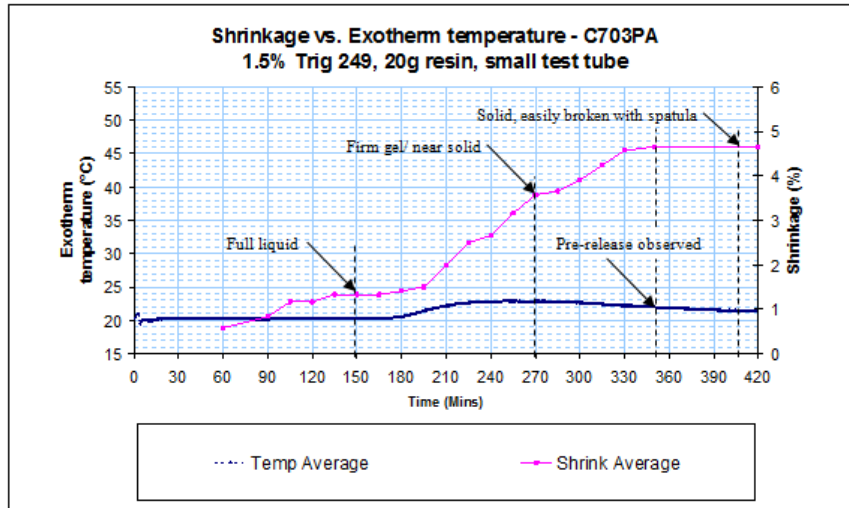


Figure 54: Exotherm and shrinkage for Crystic 703pa – 20 g mass and 18 mm diameter test tube (Cook 2011).

Scott Bader also reported that 35% of the resin samples tested displayed signs of internal tearing and cracking during the latter stages of the curing process near the top surface of the resin, Figure 55. It was found that the upper 10 mm of resin in the test tubes remained in liquid or gel state for a greater length of time than the majority of the resin mass (Cook 2011). The cracking appears to be at a boundary line between the two resin masses, where the discrepancy between the cure stages was hypothesised to have been caused by the cure retarded effects of the thermal soak into the glass tube combined with the heat extraction by the ambient air temperature at the top of the test tube. A difference between the samples containing internal cracking or tearing was recorded where the entire resin mass appeared to release from the test tube walls during the curing process allowing the mass to shrink as a single object.



Figure 55: Cracking and tearing seen in the resin mass post cure (Cook 2010).

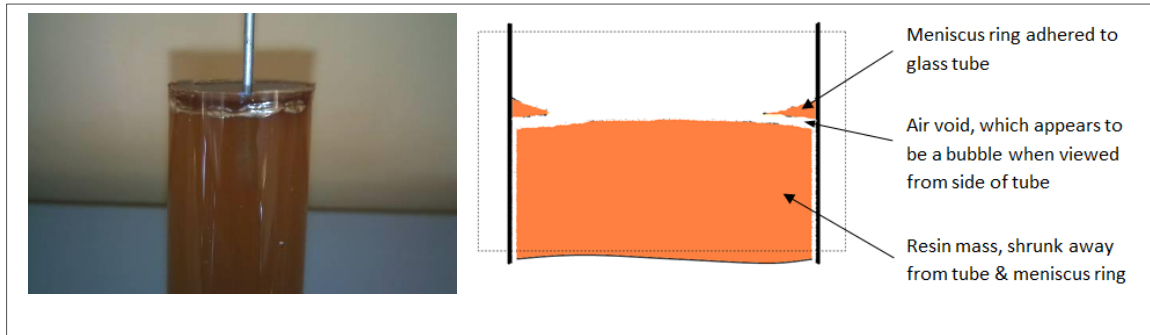


Figure 56: Air bubbles in the top of the resin mass, and details of the upper section of cured resin (Cook 2011).

In addition to the 20 g and 40 g resin masses, Scott Bader tested the exothermic temperature of a 100 g resin mass during ambient cure. It was found that the larger resin mass in an aluminium mould reached a peak temperature of 141.2⁰C, 262 minutes after mixing the resin and catalyst. A peak cure temperature in the chine has been shown in Chapter 2, Figure 20, where a 44.9⁰C difference in temperature between the mould surface and the bag surface was recorded.

The results of the resin cure experiments suggest that sections of laminate with a lower resin mass will reach a lower exotherm temperature and will undergo a significantly different cure schedule to areas of the laminate with higher resin masses. The results shown in Chapter 2 identify the difference between the chine exotherm temperature and the rest of the hull. Due to the complex layup of the fibre reinforcement a varied cure schedule is expected throughout the component which will affect the resin shrinkage rates and transitions from liquid to gel to solid state.

Through thickness cure variations and their effects on the development of residual stress and the resulting material quality degradation and potential stress alleviation mechanisms were discussed in Chapter 2.

Additional testing was then carried out to establish the cause of internal voids in some of the tubes as shown in Figure 56. Cook (2011) concluded that due to the proximity of the voiding to the top of the resin mass, that the voids were caused by tearing as opposed to crack propagation from an external source. The tearing was found to be caused by the top section of the resin mass adhering to the wall of the glass tube during cure. The main body of the resin released from the tube walls, allowing for uniform shrinkage, potentially creating some of the internal cracks found on the chine of hulls released from repaired moulds at PYI. The tape used to repair the mould appears to adhere to the laminate, causing a stress concentration which results in long cracks around the region where the tape has been used.

The experiments which have been reviewed have resulted in a number of unanswered questions where further experimentations and data collection are required to generate conclusive results. In particular the results of the resin cure relationship with resin volumes generates a number of concerns when combined with the changing laminate schedule used by PYI. Experimental investigations need to be carried out to assess if the internal voiding is solely related to percentage shrinkage threshold, or if it is affected by other factors such as mass geometry or exotherm temperature. A greater range of through thickness temperature profiling is needed, followed by samples of those sections being analysed to establish residual stress levels, resin consolidation and the level of internal tearing or voiding.

3.2.3 Joint PYI and Scott Bader Investigations

The areas investigated by Scott Bader and PYI, have resulted in PYI focussing on the implementation of temperature controlled tooling. Temperature controlled moulds allow for a greater degree of control over the cure temperature and the post cure process which PYI implement. However to fully optimise this process additional data is required during the manufacturing process to optimise the use of the temperature controlled moulds. The through thickness temperature variations and the potential variations in the cure stages of the resin at different temperatures highlight the need for a sensory system to measure through thickness temperature profiles accurately and the resin cure state.

The resin tearing which occurred during the resin mass cure experiment could represent the same processes occurring during the hull infusions which are resulting in the matrix dominated failures which result in delamination.

A correlation was reported by PYI between areas of the mould that have been repaired and areas where delamination or tearing has occurred during the infusion and curing process. The repairs are done in a way that changes the surface of the mould. Further investigation may identify if changes to the adhesion between the mould surface and gelcoat are occurring as well as an analysis of temperature variations caused by the change in mould materials. The shrinkage variations that are dependent on resins and volume need to be further assessed. It is also suggested that experimentation is carried out to assess the effects of resin rich regions within the component.

3.3 Industry Process Review Discussion

The assessment of the data provided by PYI has shown that the resin volumes, cure temperatures, size and resin flow rates have been identified as critical aspects impacting

laminate defects in VARI composites. However the lack of full scale production data restricts the ability to fully identify the critical parameters resulting in defects during the VARI. The high level of variance in the recorded surface voids shown in Figure 38 and Figure 39, combined with inconsistent variations in the processing parameters limits the identification of the optimum production procedure. Improved quality and quantity of the manufacturing data would be beneficial in identifying relationships between input variables and the resulting component quality.

The void inspection procedure used by PYI is limited and inadequate to understand the quality of the resulting component. Surface inspections limited to a small area of the hull limit the validity and usefulness of the information presented on the void recording sheets. Improvements could be made to the process by introducing an internal component inspection procedure where the vacuum bag surface of the component is also inspected. Non-destructive testing equipment needs to be reviewed to see if any suitable tools exist which PYI could use regularly to investigate the through thickness part quality of the hulls produced. The core samples provided by PYI will be investigated further in Chapter 4 where the achieved fibre volume fraction and void distribution are discussed.

The resin flow experiments conducted by PYI combined with the variable flow front identified on the full scale infusions suggest that the resin flow front advance will be a contributing factor in the generation of voids and defects. The lab experiments have identified two of the risks associated with using resin distribution techniques such as high flow fabric and core grooves. The effect of the resin accelerating past the additional reinforcement at the monolithic to sandwich regions could be a key factor in causing the defects on the chine. Secondly the converging flow front associated with using core distribution holes introduces voids into the resin.

The inconsistent generation of voids in the forward section of the hull suggest that the increased number of flow obstacles in the aft section of the hull is contributing to the generation of defects. The void frequency schematic showed that there is a link between the surface voids and the areas of the hull which require additional reinforcement. The additional reinforcement effects two primary areas, firstly the permeability which is linked to the resin flow speed and secondly the resin cure characteristics.

The experiments conducted by PYI and Scott Bader have identified that increased resin volumes result in increased exothermic cure temperatures, increasing resin shrinkage. The temperature

measurements undertaken by PYI on the A3 model confirm the lab tests by recording significantly higher cure temperatures in the chine compared with the rest of the component. Scott Bader also showed that the rate at which the resin cures was linked to the resin volume which suggests that the resin in the chine not only cures at a high temperature but also earlier than the resin in sandwich sections of the hull. The impact of the faster cure is that the continuous fibres will be placed under compression in the monolithic sections whilst the sandwich sections where the resin is still in a gel state will be placed in tension. The inconsistent stress state will impact the dimensional stability of the component, an area which PYI are very interested in due to the market they operate in.

The resin test tube curing experiments conducted by Scott Bader identified that as a result of increased exothermic cure temperatures, high levels of volumetric shrinkage can cause resin tearing to occur. The inconsistency across each resin mass raises questions about the possible cause of the resin tearing. Scott Bader suggested that the resin adhered to the wall of the test tube, therefore limiting the ability of the resin to shrink naturally during the curing process, however no difference was reported about the test tubes used for the experiments or the preparation of those test tubes. These results show that even for simple resin curing experiments, inconsistencies in the resin quality exist.

However if each of the factors discussed above were causing the defects to occur the defect levels would be consistent from one infusion to the next using the same mould, reinforcement and resin. This however is not the case based on the information recorded by the quality control procedure at PYI. Similar to the resin curing experiment, the level of information required to identify the cause of the defects are unknown. Additional information is required about the defects and the infusion and curing process to identify developments to the manufacturing process which will be enhanced to improve the quality of the composite components manufactured by PYI.

An investigation into the available sensor networks and computational tools is required to identify the accessible tools available to carry out the required process optimisation. An automated recording network is required to eliminate the inherent variability of relying on manual recording of the production data. Increases in the volume and accuracy of the processing data could then be utilised alongside proven computational tools available to carry out process simulations to optimise the infusion process.

Chapter 4

4 Component Quality Assessment

The previous Chapter discussed the defects recorded through surface visual inspections at PYI. However, to fully understand the nature of the defects which occur during large scale VARI, three-dimensional defect analysis is required. Due to the limitations in relation to completing visual inspection of the voids, a number of outer skin core samples were provided by PYI for through thickness analysis. The laminate samples were all extracted from hull sections where surface defects had been found.

4.1 Outer Skin Void Analysis

Two techniques exist to carry out composite part defect analysis, optical microscopy and micro X-ray computed tomography (μ -CT). Optical microscopy has been used for many decades to provide insight into the micro and macro structure of composite components, mainly concentrating on void content, ply counts and fibre orientation (Hayes & Gammon, 2010). Optical microscopy is restricted by the requirement to remove and segment a sample of the component to be polished to provide through thickness defect analysis. Optical microscopy examines the components in two dimensions, limiting the detail that a void characterisation can achieve. μ -CT is an emerging alternative to optical microscopy, which can provide void distribution characterisation in three dimensions. The spatial distribution of voids is a critical factor when assessing laminate quality and it is important to determine the void distribution as a function of manufacturing technique and the associated processing parameters in order to improve quality (Leonard et al. 2013). μ -CT uses a sequence of X-ray radiographs that are created by a micro focused X-ray source which illuminates the sample onto a planar X-ray detector and magnifies the image whilst the sample rotates around a known central point to reconstruct a three-dimensional reconstruction of the sample. Post processing software synthesises a stack of individual virtual cross section slices to create a volumetric rendering (Bruker, 2014).

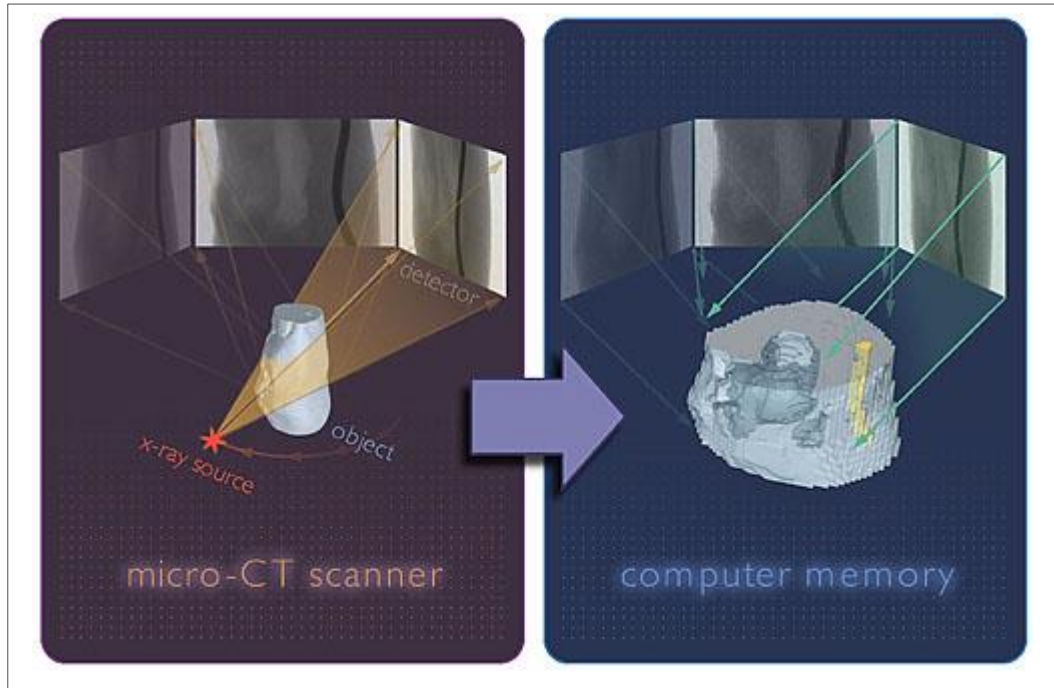


Figure 57: Micro computed tomography x-ray radiographs to three-dimensional volumetric rendering (Bruker, 2014).

The 225/450kV hutch μ -CT scanner located at the University of Southampton was used to create a three-dimensional volume fraction and void analysis of the samples provided by PYI (Mavrogordato 2017). The μ -CT analysed distribution, size and shape of the voids as well as the through thickness location. The samples were extracted from two different infusions; firstly model A3 build 6, the 22.35m fly bridge motor yacht and the Y9 build 8, the 24.10 m fly bridge motor yacht.

4.2 A3_S6_2 Large Void Sample

Sample A3_S6_2 which is shown in Figure 58, has been extracted post cure from the port side close to the chine and air vent. The defect distribution discussed in Chapter 3 identified this area as a common section of hull infusions for voids, delamination and surface imperfections. Quality control inspections identified a high level of discolouration in the gelcoat, suggesting voids and potential delamination in this region. A core sample was extracted using a 60 mm holesaw, which cut through only the outer skin thickness, leaving the inner skin and core intact for repair.

During the core sample extraction, the delamination between the outer reinforcement layers resulted in the gelcoat, skin coat barrier coat and first layer of reinforcement separating from the rest of the core sample. The delamination surface is clearly visible in Figure 58, which will

need to be included in the analysis of the through thickness void density. The complete matrix delamination will affect the through thickness void distribution due to the failure of the matrix.

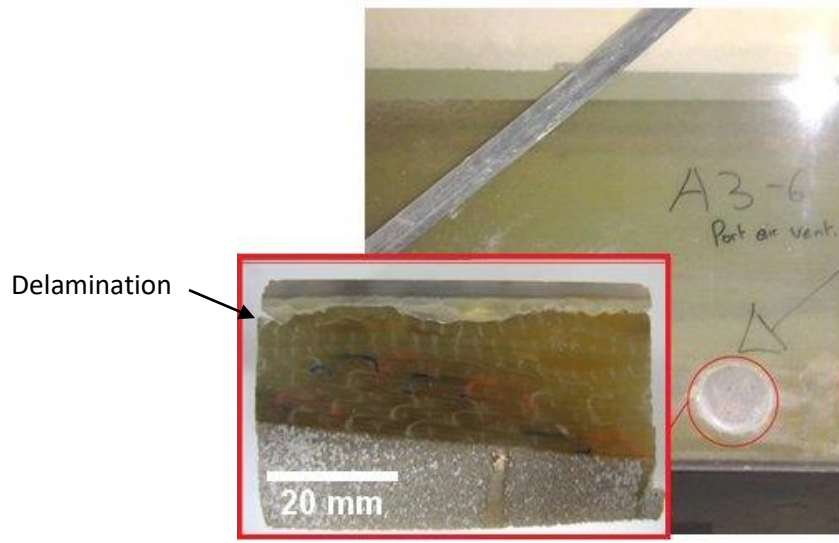


Figure 58: A3_S6_2 extraction location and profile view.

The μ -CT images provided a useful insight into the material microstructures and identified variations in fibre orientation, compaction, matrix, fibre and void volumes. The μ -CT scan results in a volume reconstruction of the scanned item, made up of voxels. Each voxel represents a local attenuation coefficient which represents a local X-ray absorption density. The X-ray attenuation is proportional to the X-rays absorbed or scattered as they pass through the sample which are linked to two primary factors, material composition and density. The different density of the three materials in a composite component, resin, fibre and voids allows for a segmentation process to be conducted to separate the three materials. The grey scale histogram of the volume reconstruction can be used to identify the three material volumes. The greyscale histogram in Figure 59 illustrates three peaks, the value with the highest greyscale value on the x-axis are the fibres, whilst the peak close to 100 represents the resin and the peak closest to zero are the voids.

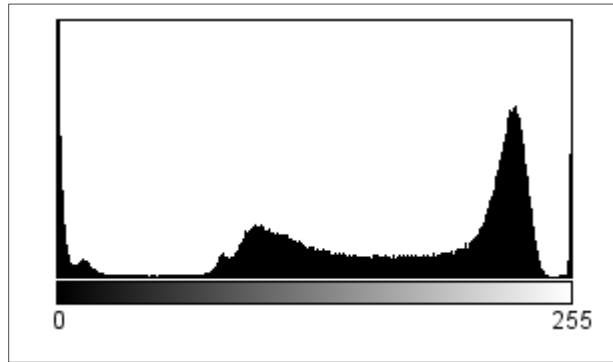


Figure 59: Greyscale histogram of the μ -CT image with the greyscale value on the x-axis

To illustrate how the resin fibre transition regions are represented by the greyscale histogram, Figure 60 shows the grey value on the y-axis along a linear section of a μ -CT image, shown by the orange line. The line starts on a fibre and has a grey value of 230, moving from left to right along the line, the grey value drops to 110 representing the resin volume, before moving back to 230 at the next fibre tow. A void region is clearly visible as the grey value drops to zero at 2.5mm.

These transitions were used to identify the grey scale value which could be selected for the volume segmentation to separate the μ -CT voxels into the constituent parts. The sections of the volume reconstruction with a grey value between the three materials identify the transition regions between fibres, resin and voids, these volumes introduce errors to the segmentation process due to the uncertain boundary between the materials. The uncertainty introduced by the segmentation limits the accuracy of the quantitative analysis, to reduce any errors introduced, the segmentation process is repeated for each volume and the average used.

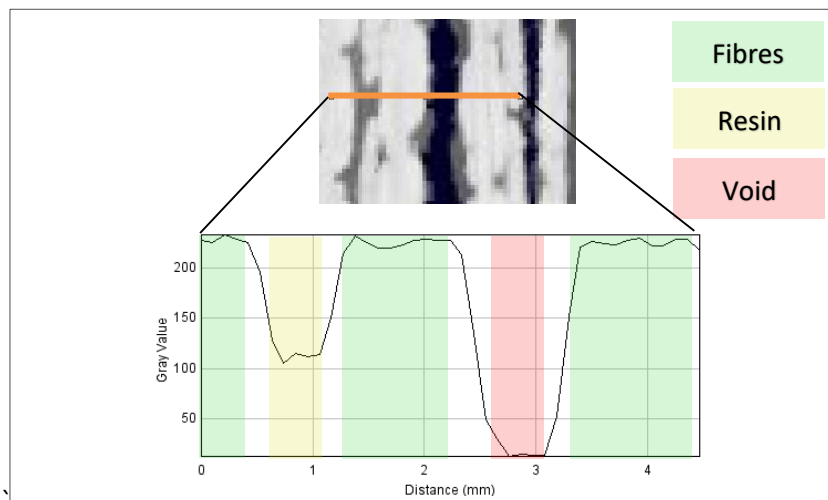


Figure 60: Greys scale transition between fibre, resin and void volume in a μ -CT image.

Sample A3 S6 showed severe discolouration during the surface inspection. Once the μ -CT had been reconstructed and the volumes segmented, the delamination surface could be easily identified and can be seen in red in Figure 61. In addition to the planar delamination near the mould surface, a large void is also clearly visible in the centre of the sample which would have remained undetected without the use of μ -CT scan and reconstruction.

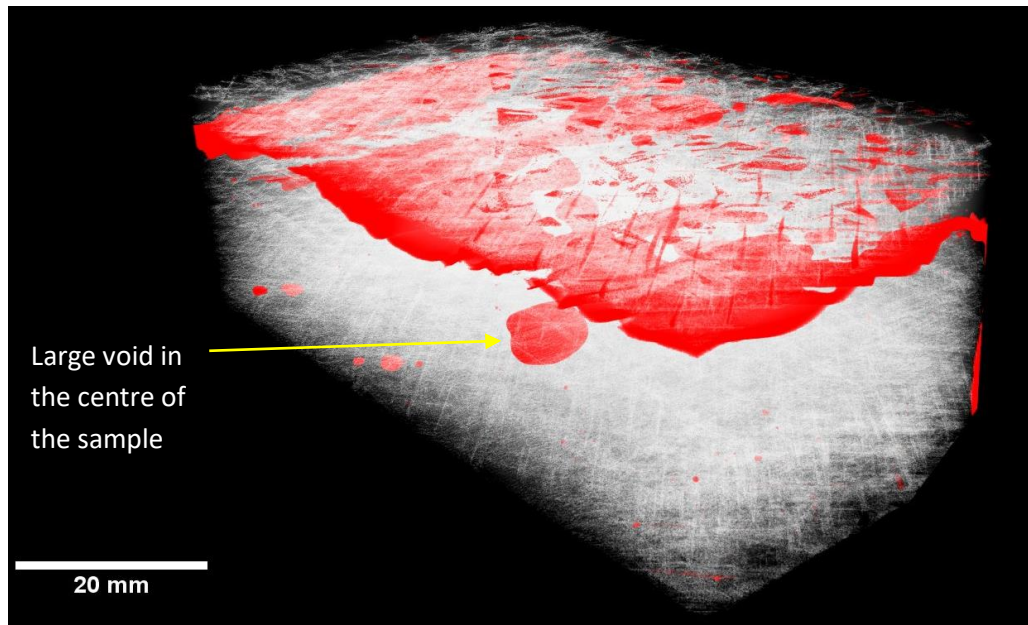


Figure 61: A3_S6_2 Delamination surface in the outer reinforcement of the sample.

Once the sample was removed and sectioned, it was clear that delamination had occurred in the region where a high level of fibre waviness existed, as is visible in Figure 62 and Figure 63. The misalignment of the reinforcement has resulted in multiple pockets between the reinforcement layers which will result in a higher volume of resin between the fibre plies, which in turn leads to a localised increase in cure temperature, as well as volumetric shrinkage and is likely to result in void clustering. Figure 64 shows that both the second and fourth layers of reinforcement have been laid into the mould with wrinkles in the fabric.

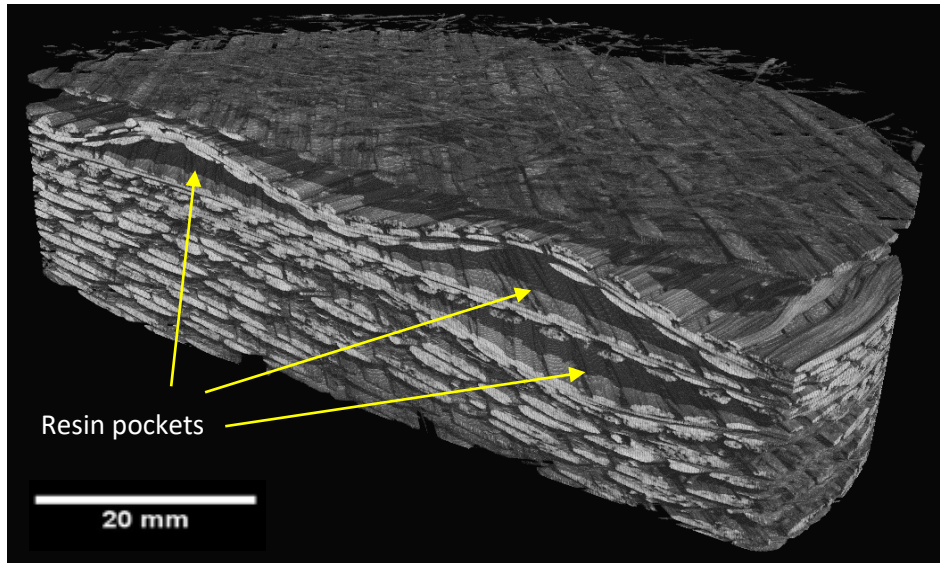


Figure 62: A3_S6_2 Extracted fibres from μ-CT volume.

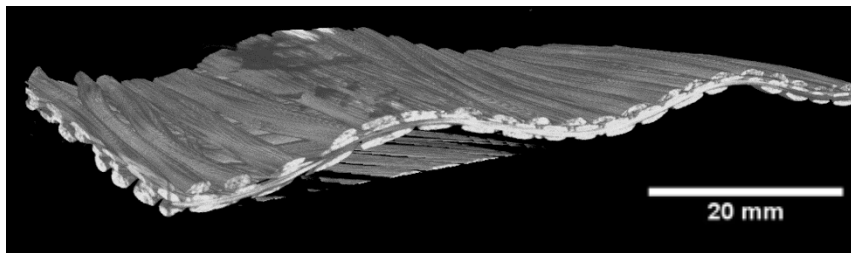


Figure 63: A3_S6_2 Fibre misalignment and waviness in the fabric positioning creating resin pockets.

The void volume extraction identified two distinct void shapes and four separate void clusters through the thickness, with the matrix delamination dominating between the first and second lamina from the mould surface. Starting from the mould surface, the outer surface of the voids appears to consist of elongated voids that are consistent with voids that are created during the infusion process as a result of resin flow front fingering during the infusion. The elongated shape of the voids is caused by the restriction created by the fibre bundles, which form channels for the voids to join together and creates the distinctive plus and minus 45° orientation that is expected from the biaxial fabric used on the outer surface of the layup used by PYI, see Figure 160 in the Appendix D. It is thought that these voids may be caused by a reduced flow front velocity resulting in a converging flow front at the bottom of the chine, as is suggested in Figure 41. As the resin flow front slows due to the converging flow front, the capillary flow will have dominated, saturating the fibre tows but leaving the channels between the fibre tows semi-impregnated.

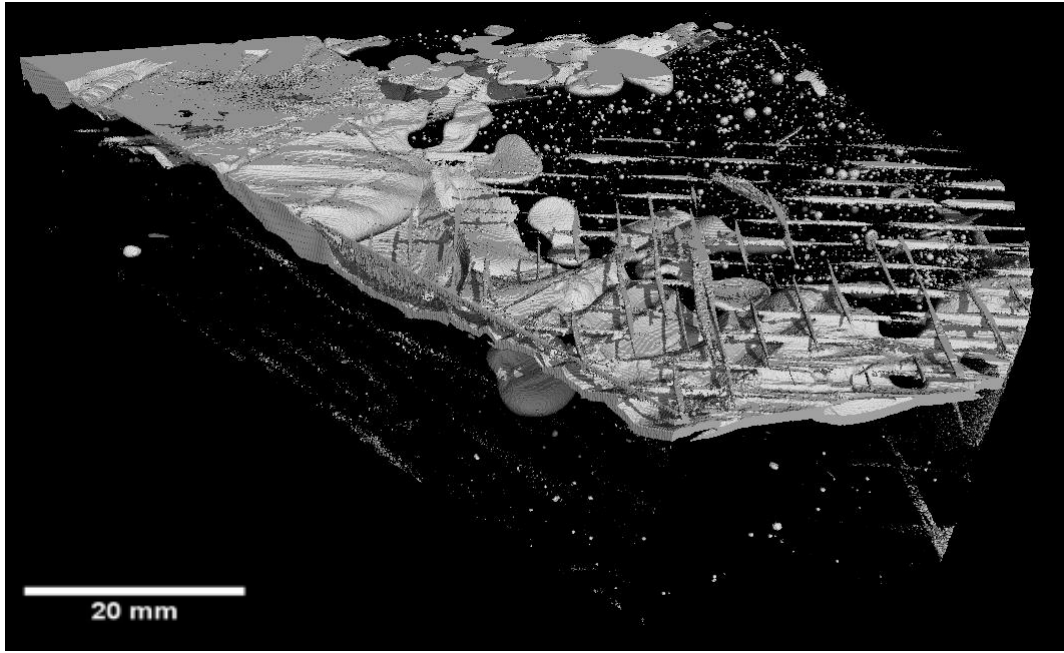


Figure 64: Extracted voids from μ -CT volume.

When the outer layer of elongated voids are extracted, the large area of delamination is clearly visible and follows a path between the outer biaxial layer and the first layer of quad axial fabric which exhibited signs of fibre waviness as seen in Figure 62. Three forms of voids are visible in this surface: delamination, dry spots and spherically shaped microvoids. Firstly the delamination that covered 60% of the sample area appeared to be initiated or be stabilised by the large dry spots highlighted in red in Figure 65. From this central dry spot, fibre-matrix debonding has occurred due to an increase in voids in this region, which is known to reduce the inter laminar shear strength due to a decrease in the adhesion between the matrix and the reinforcement (Gurit 2011). It is likely that before delamination occurred, the large dry spot and the smaller microvoids highlighted in yellow in Figure 65 existed, it is possible that a combination of these voids may have resulted in the delamination which occurred during the resin cure due to the development of residual stresses. Although the delamination is the major structural failure in this sample, the dry spots and the smaller microvoids could be the crack initiators and therefore could have aided the crack propagation throughout this region. These voids need to be eliminated to avoid the development of the delamination regions.

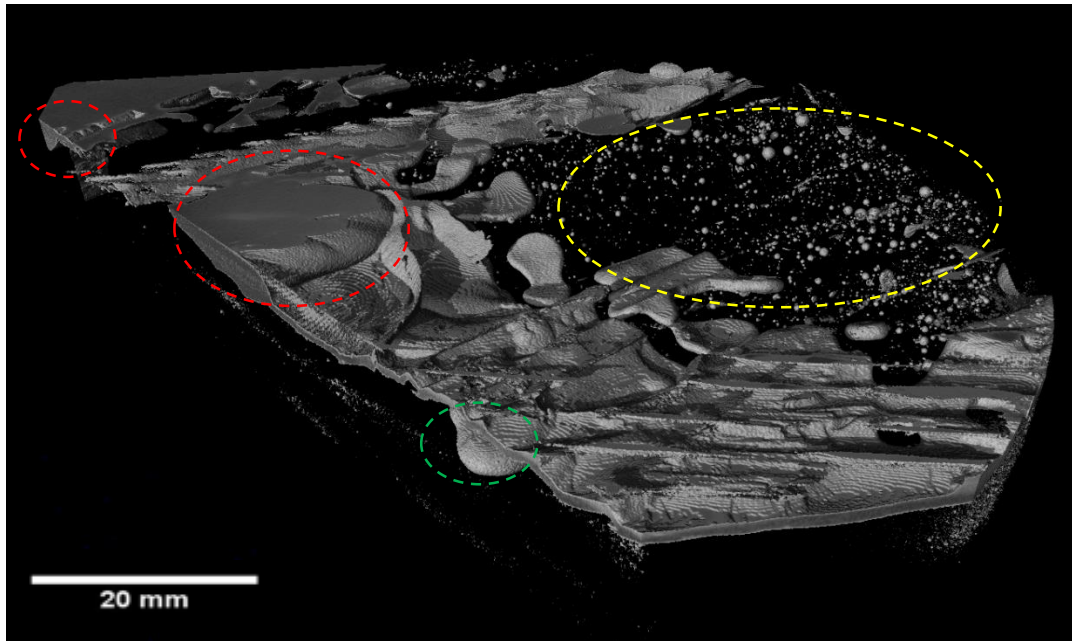


Figure 65: A3_S6_2 Extracted second layer of voids from μ -CT volume.

The area highlighted in green in Figure 65 is another large spherically shaped void, located between 40-50% of the through thickness distance from the mould surface as is shown by the void volume increase in Figure 66. The existence of these voids without the resulting delamination suggests that a combination of both large dry spots and smaller spherical voids are needed to cause the large scale delamination seen in the outer surfaces. This is also suggested by the lack of delamination in the region circled in yellow, which shows that the smaller spherical voids exist without any larger voids. The smaller spherical voids are located in the resin rich region between fibre layers; it is not possible to establish the cause of these voids from the μ -CT image. Possible causes are the resin flow mechanics, cure gas release and outgassing during the infusion. The spherical shape of the voids suggests that the voids have not been influenced by the surrounding fibres which would have resulted in a tubular shape rather than spheres. The maximum size of the spherical voids is 0.2 mm, and their shape suggests that no external restrictions existed during their formation.

The ability to accurately assess volume fractions using the μ -CT images can be restricted by the segmentation process used. A perfect image would have clearly segregated maxima on the greyscale histogram which would represent the scaled absorption for each of the three volumes, voids, resin and fibres, however due to dispersion, noise and partial volume effects, overlap in the grey scale histogram exists (Schell et al. 2007). Previous researchers, who have investigated carbon fibre and epoxy laminates, have added a tracer to the resin to increase the variation between the matrix absorption coefficients. However, it was decided that due to the sole use

of glass fibres and polyester resin the distinction between the absorption coefficients was adequate and that the tracer technique was not necessary.

The software package, AVIZO Fire allows for the volumetric distribution from a greyscale histogram. Figure 66 shows the void volume fraction, through the thickness from the gelcoat surface (0) to the core surface (1), whilst Figure 67 illustrates the fibre and resin volume fractions. Combining the volume fraction in Figure 66 and Figure 67 for the fibres, resin and voids adds to 1, representing the three volumes identified by the segmentation process. The average fibre volume fraction is 52.5 % whilst the void fraction is 1.75 %. The first region, from 0 to 0.2, represents the outer layer of the core sample where the gelcoat, barrier coat and skin coat regions are visible, the second area, between 0.2 and 0.3 from the mould surface is where the delamination has occurred and thirdly from 0.3% onwards the laminate stabilises to form a more consistent volume fraction, where a very low void volume and high fibre volume fraction is demonstrated.

The resin rich region between 10 % and 30 % from the mould surface identifies the volume where the fibre waviness occurred; this is identified by the maxima at 10% where the biaxial fabric is located. The fibre volume fraction of 30 % between these points is a result of the increased resin volume which is caused by the increased interfibre bundle volume and the delamination/void volume. The oscillation in the fibre and matrix volume fraction between 30% and 70% is due to low fibre nesting under the vacuum compaction which results in layers of resin and reinforcement. If a high level of compaction was achieved, a uniform fibre volume fraction should be attained, especially in regions where the fibre type and weight are the same,

the oscillations are therefore a result of increased compaction from the fibre stitching used for NCF and the limitations of infusing under vacuum.

The increased void fraction at 45% from the mould surface is a result of the large void identified in Figure 65, circled in green.

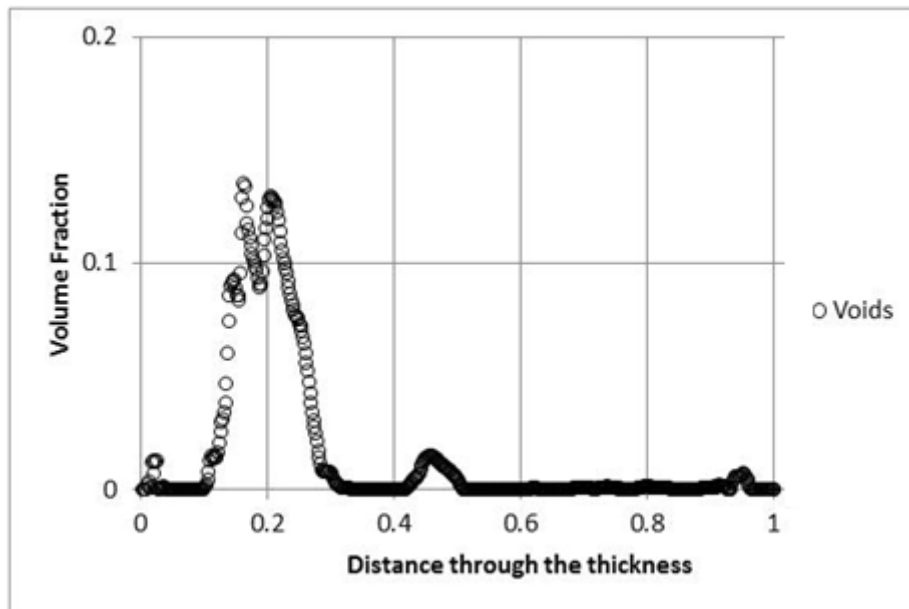


Figure 66: A3_S6_2 through thickness void volume fraction where 0 depicts the mould surface and 1 the core surface.

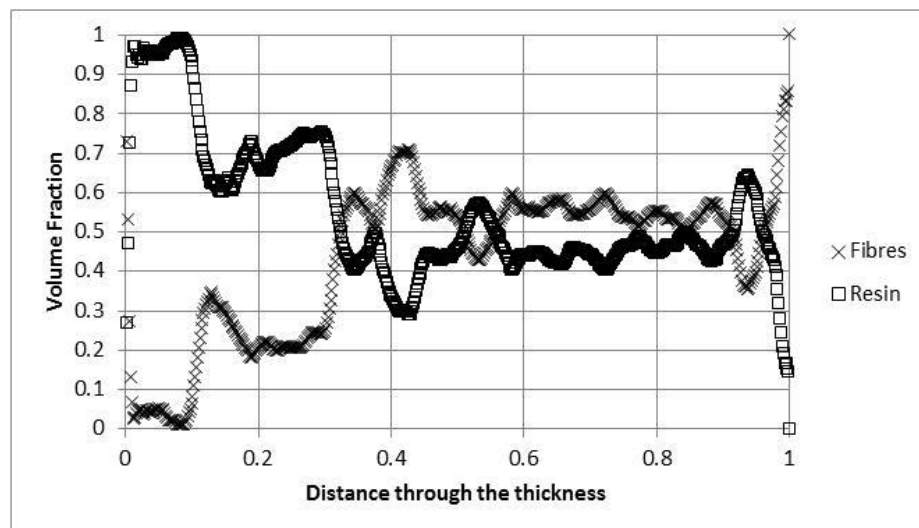


Figure 67 A3_S6_2 through thickness fibre and resin void volume fraction where 0 depicts the mould surface and 1 the core surface.

The high resin volume in the first 10% of the sample from the mould surface identifies the gelcoat, barrier coat and skin coat which are rolled into the mould and cured prior to the dry

fibres and resin infusion. The peak in fibre volume at 11-12% identifies the first layer of reinforcement, the biaxial glass fibre. The resin saturation of the mould surface has been researched and discussed previously, it was found that the flow acceleration along the resin distribution channels in the core material results in the resin impregnating low reinforcement areas leading to a flow front running in the opposite direction back towards the resin flow from the injection point. The two resin flows converge trapping an unsaturated area of reinforcement which reduces the infusion pressure and slows the resin flow progression. The cylindrical voids found in the μ -CT reconstruction support this assessment, their shape and location between the fibre tows, due to the reducing flow front velocity, allowing capillary forces to draw the resin along the fibre tows ahead of the channels between the fibres, as shown in Figure 68. The higher level of voids in the channels between the fibre tows suggests that the lack of complete fibre saturation was a factor influencing the delamination in this sample.

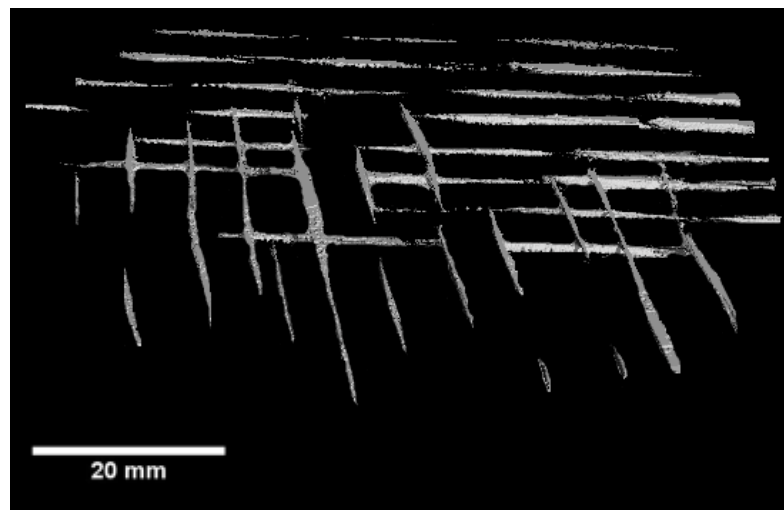


Figure 68: A3_S6_2 cylindrical voids formed between the fibre tows in the first layer of biaxial reinforcement from the mould surface.

The high volume of resin from 10-30% of the distance from the mould surface caused by the fabric wrinkles not only increases the volume of resin and voids, but also the through thickness cure temperature profile. During the curing process, the mould tooling acts as a heat sink, cooling the outer surface of the component, whilst the high resin volume in the first 30% of the sample will result in a higher exothermic cure temperature as was discussed in Chapter 3. The inconsistency of the cure temperature effects the cure schedule as well as the resin shrinkage and therefore the development of residual stresses. The fabric wrinkles add an additional level of inconsistency to these composite components which are already variable in their laminate schedule, resin distribution and cure schedule.

4.3 A3_S6_4 Void Sample

Sample A3_S6_4 shown in Figure 69, has been extracted post cure from the port side close to the chine, on the transom side of the air vent. A very high level of discolouration exists up to 150 mm above the chine for a length of over 500 mm. The 60 mm diameter core sample was extracted from the centre of this region, where a slight change in colour density occurred at the top and bottom of the sample. No damage to the sample was recorded during extraction of the sample.

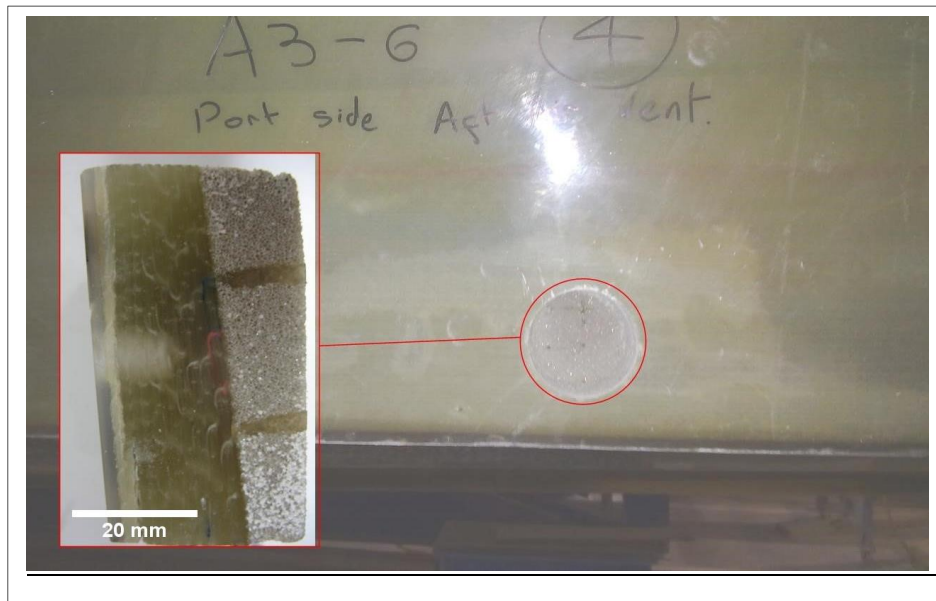


Figure 69: A3_S6_4 extraction location and profile view.

The profile view in Figure 69 shows the location of the delamination region, which has resulted in the discolouration of the laminate. The μ -CT reconstruction in Figure 70 identifies three separate delamination surfaces, circled in red, which overlap each other and are separated by a layer of reinforcement.

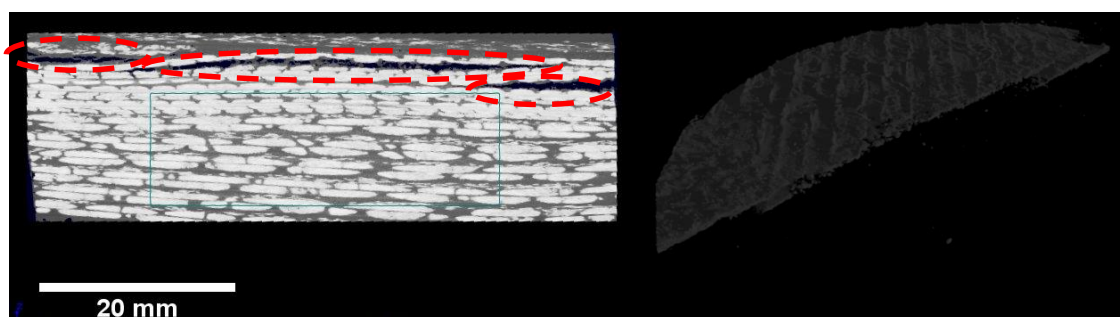


Figure 70: A3_S6_4 through thickness radiograph.

Segmenting the volume reconstruction allows for the three delamination regions to be investigated. Figure 71 shows the three regions in red, with the right hand image showing the fibre arrangement around the delamination. A small amount of fibre misalignment can be seen in Figure 71 which suggests one of the causes for the delamination may be the same as that for sample A3_S6_2, misalignment of the fibres and resultant wrinkles in the reinforcement. In addition to the fibre misalignment, the delamination on the left hand side of the sample circled in red in Figure 70 is located under the end of a lamina. Due to the size of the infusions undertaken at PYI multiple laminas are used for each layer of reinforcement which requires overlaps on each edge to join the reinforcement together. However due to the proximity of this reinforcement edge and the chine, this suggests that the edge of the lamina is a factor in the delamination.

The right hand image in Figure 71 identifies that not only are there small wrinkles in the reinforcement but that the fibre tows are also not aligned correctly, circled in yellow below. Due to a NCF reinforcement being used, the fibre tow misalignment suggests external forces have been applied to the fabric changing the arrangement of the fibres increasing the channels between the fibre tows and changing the architecture of the reinforcement.

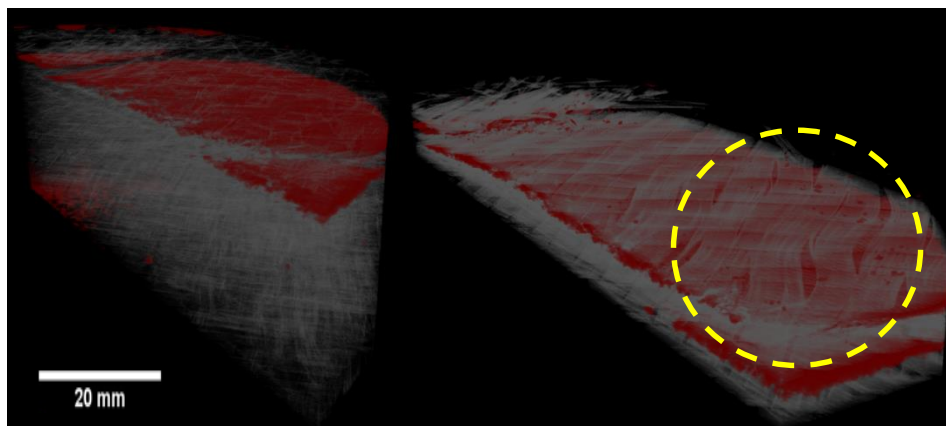


Figure 71: A3_S6_4 delamination regions highlighted in red illustrating the three delamination sections overlapping.

Figure 70 also shows the through thickness variation in the fibre volume fraction, which is caused by different weights and types of reinforcement being used in the layup schedule. Lighter fabrics have been used closer to the mould surface to reduce the possibility of fibre print through to the gelcoat surface. The reduced size of the fibre tows increases the nesting effect and reduces the volume of resin between each lamina.

The through thickness void volume fraction shown in Figure 72 identifies the delamination region in the outer surface. Below the delamination area, the void fraction quickly reduces to a very low level.

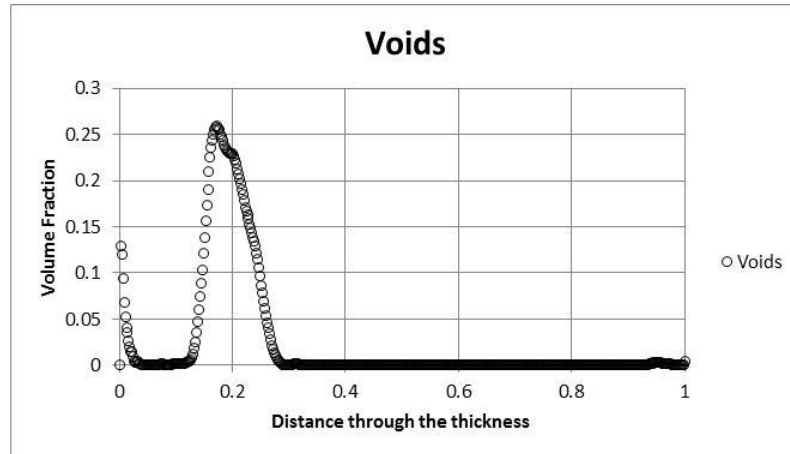


Figure 72: A3_S6_4 through thickness void volume fraction where 0 depicts the mould surface and 1 the core surface.

The fibre volume fraction through the thickness shown in Figure 73, identifies the delamination region at around 10% of the distance from the mould surface. Between 25 % and 50 % of the way through the laminate, the fibre volume fraction is significantly higher than expected at an average of 70%. The increase in fibre volume fraction is attributed to a lower weight reinforcement being used which has resulted in increased levels of fibre nesting and compaction which can be seen in Figure 70. From 50% to 100% the achieved fibre volume fraction of 0.56 meets the design criteria for the hull infusions and is similar to the results found for the previous sample, A3_S6_2.

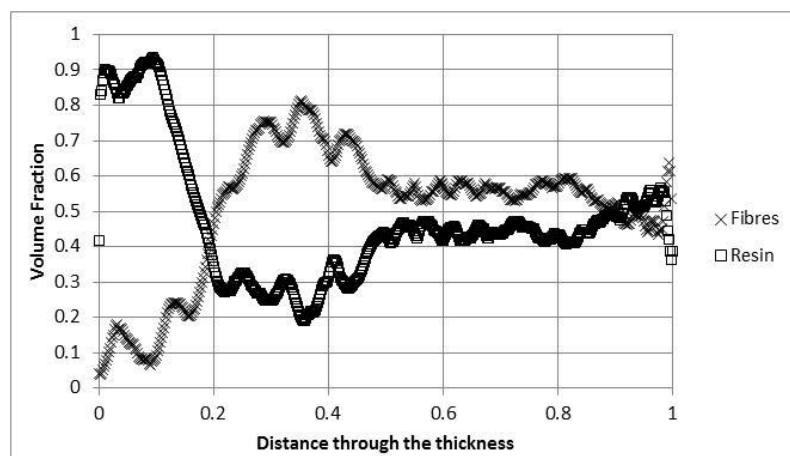


Figure 73: A3_S6_4 through thickness fibre and resin void volume fraction where 0 depicts the mould surface and 1 the core surface.

4.4 Y9_S8_1 Void Sample

Sample Y9-S8_1 shown in Figure 74 was extracted from the port side chine area, on the transom side of the signature windows of the eighth hull produced in the Y9 mould. The lighter area in Figure 74 suggests that a delamination region exists near the surface of the laminate, it extends up to 80 mm above the chine and is 202 mm in length. The core sample was sectioned and the bottom half of the sample was then analysed.

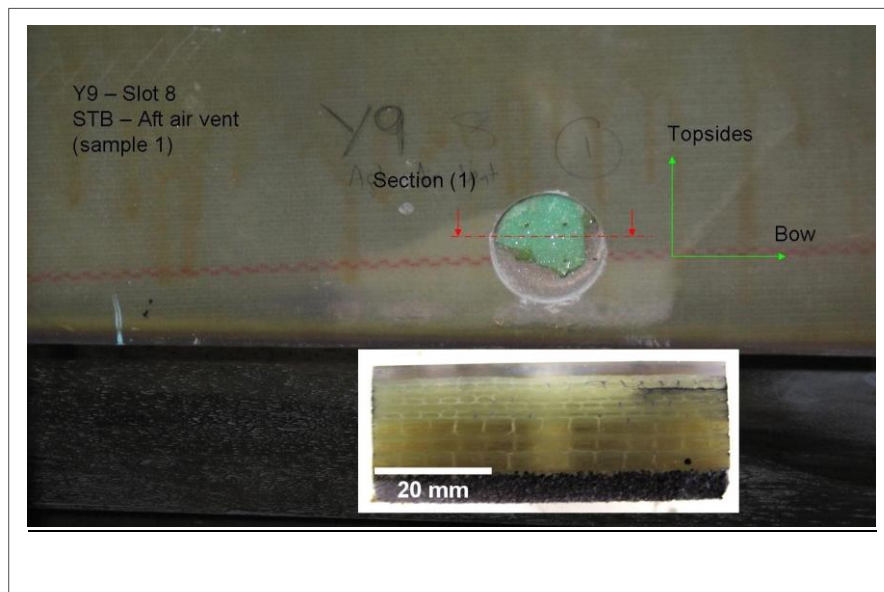


Figure 74: Sample Y9_S8_1 extraction location and profile.

Over the course of the manufacturing life of the Y9 model, the laminate schedule has changed, with the more recent model utilising heavier NCFs to help to reduce the layup time during the manufacturing process. The earlier build numbers, an example of which is being analysed, utilised lighter NCF with a higher number of lamina used, which can be seen in Figure 74; because of this, less emphasis has been placed on the lamina structure and through thickness volume fractions. The area of greater interest exists between the second and third lamina, where a clearly defined area of delamination exists, which is visible from both the profile view in Figure 74 in the top right hand corner and the void volume shown in Figure 75. Figure 75 shows the delamination region between the first and second lamina from the mould surface. The delamination on the corner of the sample is representative of the condition of the laminate across the entirety of the lighter coloured area, as can be seen by the continuation of the delaminated area along the top corner of the void volume. Unlike sample A3_S6_2, where the large voids and high density of smaller voids suggested a cause for the delamination, the delamination volume for sample Y9_S8_1 demonstrates very few smaller voids and no examples of larger voids caused by fibre waviness. This may suggest the sample being analysed

sits at the edge of the delamination region and was caused by voiding in a different area of the defect. The shape of the delamination boundary is also interesting; the delamination follows a curve around a 90° change of direction where the core sample was extracted from. It is not known if any shrinkage occurred at this point or if any repair tape had been used on the mould on this surface.

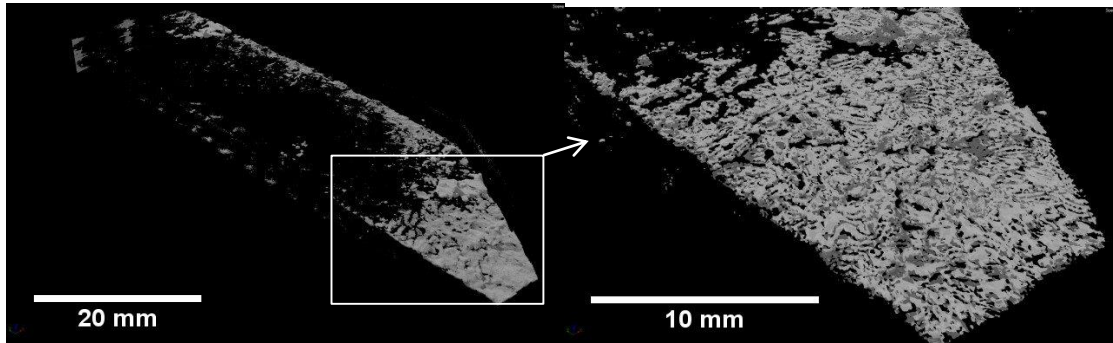


Figure 75: Y9_S8_1 extracted void volume.

In Figure 74 a red stitch line can be seen running parallel to the chine, the red stitching is used at the edge of the lamina and signifies that similarly to the A3_S6_4 sample, a join in the reinforcement exists on the outer surface of the laminate. The join has not been captured by the core sample taken, however the inclusions of a reinforcement join at a location where defects are repeatedly reported as well as the high temperatures experienced during the cure schedule in the chine might impact the location of the defects. At the edge of laminas the fibres are often distorted whilst being handled prior to being laid into the mould which effects the fibre alignments, the edges also create localised flow variations which can increase the void generation and clustering.

The fibre reinforcement used by PYI comes from their supplier in 47 m long rolls with a width of 1.27 m, the reinforcement is laid longitudinally from the stern to the bow of the component, parallel to the chine. It should be possible to design the layup schedule to avoid the reinforcement overlaps occurring at the chine region where the highest cure temperatures and resin shrinkage will occur.

4.5 Microstructural Analysis Discussions

The core samples provided by PYI have been scanned using μ -CT to carry out a three-dimensional defect analysis. A correlation between the surface discolouration and the significant delamination in the outer layers of the core samples has been found. The results have shown the expected void location in the outer 25% of the laminate to exist where

delamination has occurred. Between 25 and 100% of the distance from the mould surface, the void content has been very low, to prove that this was representative of a normal hull section where no surface defects were visible, a core sample could be removed. However due to the time and cost associated with repairing the components post sample removal, this was not possible.

The results of the fibre volume fraction analysis have shown that a 0.55 volume fraction is being achieved, these results match those found by the optical microscope analysis carried out by the University of Plymouth and internal work conducted by PYI.

A number of void forms have been reported in this section, delamination, smooth microvoids or porosity, elongated cylindrically shaped voids and irregular larger defects. The samples which exhibit delamination have shown signs of a high localised porosity and some larger irregularly shaped voids which have been allowed to form due to fibre wrinkles. The combination of localised porosity and larger defects may have worked with the resin shrinkage to cause the delamination between the first and second lamina from the mould surface. The porosity and large defects in each sample will result in a variation in the expected volumetric cure shrinkage and coefficients of thermal expansion (CTE). A relationship may exist between the outer lamina delamination, the CTE of the pre-infusion surface applications (gelcoat, skin coat and barrier coat) and the cure shrinkage of the unsaturated polyester resin which may result in the development of residual stresses at each stage which then lead to delamination during the final resin cure. The elongated cylindrically shaped voids are created by the fibre bundle restriction and are likely caused by the slowing flow front caused by a convergence of the primary flow front from the keel and a return flow front from the top of the top sides. The location of the voids which were identified in Chapter 3 suggest that the defects regularly recorded on the chine are located behind multiple reinforcement points in the preform along the resin flow path. Each area of reinforcement changes the shape and progress of the resin flow front which could be causing the converging flow front discussed in Chapter 3.

4.6 Microstructural Analysis Conclusions

The irregularity of through thickness void distribution and delamination further suggest a combination of factors effecting the creation and resting location of the voids. The features which have been identified with each of the samples are common across the laminate, however the voids are not, suggesting that the physical changes in the reinforcement, fibre waviness and misaligned fibre tows, are not sufficient to cause the delamination. Further investigation is

needed under a controlled environment into each void creation mechanisms to aid the identification of the key factors increasing the volume of voids.

μ -CT has shown to be a useful tool to examine three-dimensional composite structures and defect distributions. μ -CT has shown to be able to detect important features and is the only available non-destructive testing technology which provides the required resolution to accurately identify issues such as fibre misalignment, variations in the resin distribution and porosity on thick glass fibre laminates. The volumetric reconstruction of the core samples extracted from a large infusion have allowed the identification of a number of defects in each sample. The inclusion of fibre waviness and fibre wrinkles in the two samples provided from the A3 infusion identifies an issue with the commercialisation of the VARI process. The teams working to lay the dry fibres into the moulds are working with quad axial heavy NCFs which can be difficult to manipulate to produce the three-dimensional shapes of the hull and deck moulds at PYI. An advantage may be found by using biaxial fabrics in areas of the mould where complex forming shapes exist to minimise the probability of wrinkles and fibre misalignment.

Chapter 5

5 Process Monitoring

Chapters 1 to 4 have identified the requirement to gather additional information and data about the processing parameters affecting VARI component quality. Process monitoring is crucial to identify the optimal processing variables that allow for the material properties to be maximised as well as to allow for the consistent replication of high quality infusions in industry. The surface finish review that was conducted in Chapter 3 identified that the current level of process monitoring at PYI is insufficient to generate conclusive links between variations in the processing parameters, variable surface finish and the number of void areas recorded. The use of additional monitoring techniques is required to investigate in more detail the potential causes of the inconsistent quality so that a strategy can be implemented to limit the variation between infusions. Both cure progression and flow front progression can be monitored to provide information that can then be used to predict dry spots, final material properties and aid in the development of future infusion strategies. A review of the available sensors and monitoring techniques has been completed to identify any suitable sensor arrays which could be implemented to monitor an industrial scale VARI. Cost and the level of intrusiveness into the component were key factors in deciding if the sensors were suitable for implementation in the marine industry.

5.1 Carbon Fibre Conductive Sensors

Previous research discussed in Chapter 3 has shown that using carbon fibre bundles placed in an orthogonal grid or linearly can be used to measure infusion parameters and through life stress analysis. Both electrical and dielectric measurements can be made with carbon fibre sensors, although both also have their restrictions in terms of their ability to provide low cost, accurate measurements. The electric method results in a time and position dependent output due to polarization from the DC voltage, whilst the dielectric method requires complex data acquisition equipment to accurately monitor the process variations. It has been shown that a combination of both processes can be used to carry out low cost, quick embedded process and through life measurements.

5.1.1 Experimental Procedure

Initial experiments were required to validate the results from previous researchers. A simple experimental set-up based around a rectilinear flow experiment using a glass mould to monitor the mould surface flow front progression was set-up using two video cameras. Two quad axial

lamina will be used above and below the carbon fibre bundles, placed 30 mm apart, running parallel to the flow direction. Thermocouples and video cameras were used to validate the results and the thermocouples were used to monitor the resin cure reaction.

A signal generator was used to create 10V AC with a frequency of 1 kHz, the circuit diagram in Figure 76 was used to measure the voltage change across the resistor.

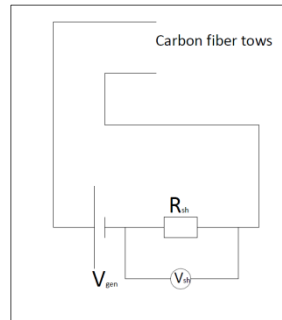


Figure 76: Carbon fibre linear voltage sensor circuit diagram.

The sensor array can be seen in Figure 77, which shows the increase in the gap between the fibre bundles which acts as a calibration section at the beginning of the infusion.

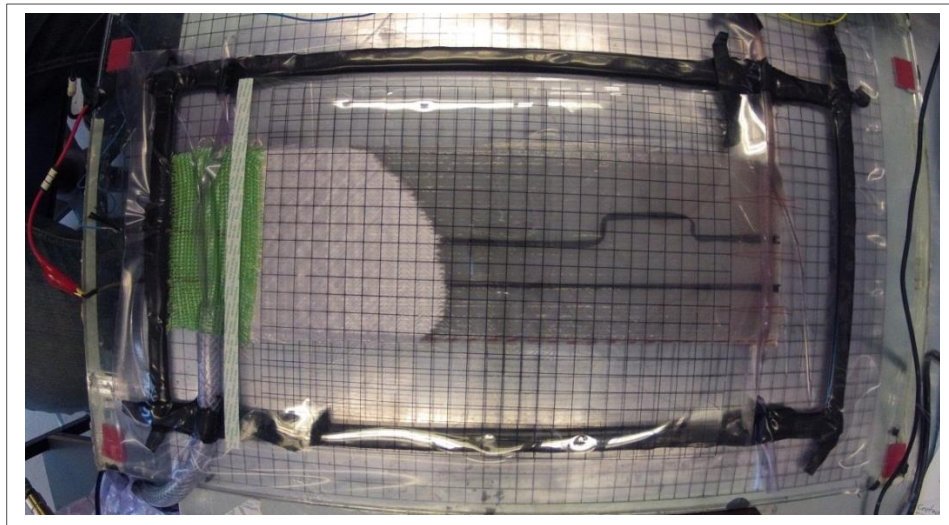


Figure 77: Carbon fibre linear sensor array.

A linear relationship between the voltage and the resin distance would be expected from this experimental set-up. The output voltage changes shown in Figure 78 are not linear and also fail to identify the calibration section used by Thibaudeau (2003).

Due to the carbon fibre tows being passed through the vacuum infusion tape at the edge of the preform, leaks were found at the edge. Although a 50mbar vacuum pressure was maintained during the infusion experiments, the scalability of the sensors to a larger industrial infusion was questioned as PYI expect a vacuum level of below 12mbar during the vacuum leak tests

conducted before each infusion. Considering the size of the preform used during this study and the use of only two carbon fibre tows, the vacuum integrity achieved would be unacceptable for a full industrial infusion. Smaller tows could have been used to reduce the level of leakage, however it would have been likely that the tow would have been required to reduce to a single fibre to reach an acceptable level of vacuum integrity.

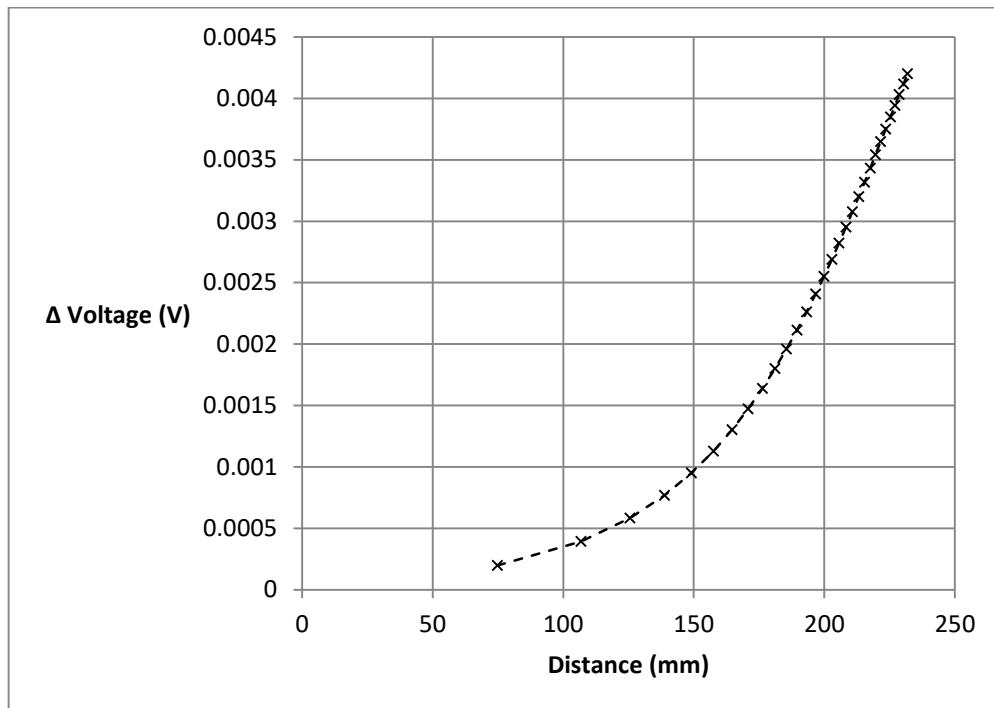


Figure 78: Voltage against distance for the carbon fibre linear voltage sensors.

During the experiment it was found that the sensors could only identify the leading flow front, shielding any unsaturated areas which could potentially mislead the infusion operators if this technique was relied upon to implement the correct infusion strategy. Chapter 1 of this thesis highlighted the variability of the resin flow front due to the use of high flow mesh and grooves in the core materials. If the sensors were used on the topside mould surface the flow front location would be found to jump from the chine to the top of the additional reinforcement 500mm along the infusion path. This could lead to the infusion operator changing the infusion strategy by switching the resin injection points earlier than required leading to increased void volumes.

5.1.2 Discussion

Two considerable drawbacks associated with the carbon fibre linear voltage sensors have been identified, firstly issues with the vacuum integrity of the preform and secondly the inability of the sensors to identify multiple flow front locations. Due to the suggested flow irregularities

identified in Chapter 3, the inability of the carbon fibre sensors to identify dry spots behind the most advanced flow front, limits the data's reliability and could lead to incorrect infusion strategies being implemented. The vacuum integrity in a large scale infusion is critical to guaranteeing complete preform saturation before the resin gelation. The leaks experienced in the lab would only be exaggerated by the additional sensors which would be required to assess the flow and cure characteristics across multiple areas of a large infusion. In addition to the vacuum integrity issues, the author found laying the carbon fibre tows at the correct width into the preform to be a time consuming process. The likely impact on production time would likely restrict its implementation in industry. The results in Chapter 4 highlight the challenges already faced in industry to lay the fibres wrinkle free at the correct orientation. The implementation of the sensors at the correct locations with a continuous width between them would be very difficult to achieve.

The output from the carbon fibre linear voltage sensors has identified the draw backs associated with the sensory system, reducing its usability and possible implementation to a full scale infusion. It has been decided that although considerably more expensive, fibre optic sensors will be used in a full scale hull infusion at PYI as an alternative means of measuring the resin infusion and resin cure characteristics.

5.2 Fibre Optic Flow and Cure Monitoring

5.2.1 Introduction

Fibre optic sensors have gained approval from both the composites research community and industry as a means of monitoring the internal strain development from manufacturing through to the end of life (Nielsen et al., 2013). The ease of integration during the manufacturing process and the minimal influence on the composite component's structural properties has resulted in acceptance from the composites industry. Fibre optics have been embedded in multiple composite structures from wind turbine blades to America's Cup yachts. The advantages presented by a sensor able to monitor local internal strain development and resin flow front progression has resulted in the frequent use of fibre optics in the composite industry.

This study aims to assess the industrial application of FBGs in a large scale VARI at PYI. Chapter 4 identified the failures experienced on multiple infusions at PYI in the layup above the chine region, with the majority of failures being located between the first and second lamina which was closest to the mould surface. Three fibre optics were therefore positioned on the mould surface of one of the hull infusions at PYI. As was discussed in Chapter 2, process induced stresses can result from the manufacture of a thermosetting matrix composite due to the transition from viscous to rubbery and then solid state during cure. These process-induced stresses are known to cause a number of failure mechanisms such as matrix tearing, especially in constrained components (Nielsen et al., 2013). The fibre optics will be positioned near to the mould surface in order to measure the strain developments which could cause the matrix failures identified in Chapter 4. The suitability of fibre optic measurements for use in the marine composite industry will be evaluated, as well as negative effects the fibre optics have on the layup, resin infusion, curing and de-moulding processes on residual stresses during the manufacturing process. The aim is to leave the fibre optics intact post infusions so that PYI can conduct through life strain measurements in the future.

5.2.2 Temperature and Strain Sensitivity

Accurate temperature measurements at the location of the fibre optics are critical to accurately measuring mechanical strain. Temperature has a larger effect on the FBG wavelength than mechanical strain, leading to the requirement for temperature compensation in order to achieve accurate mechanical strain measurements. Strain isolated FBGs exist to measure the temperature within the component during manufacturing. The mechanical strain isolation is achieved by housing the FBG in a protective tube which removes any mechanical strain influence on the FBG measurements. The results from the temperature FBG can then be

deducted from the changing wavelength recorded by the unprotected strain measuring FBG. However, a strain isolated FBG requires a loose tubular housing to isolate the sensor from external strain. The size of outer tubing can be between 2 and 4mm in diameter, significantly larger than the exposed FBG (SmartFibres 2016). A 2 to 4mm diameter tubing could have significant effects on the final composite material properties as well as impacting the resin flow progression and void locations. The temperature FBG was therefore deemed to be too large to be positioned within the composite component. The alternative option was to use a surface measuring device which would impact the accuracy of the mechanical strain measurements during the infusion. Due to the strict limitations on what could be embedded into the component, a surface temperature measurement was chosen to isolate the mechanical strain during the experiment.

The relationship between the changing Bragg wavelength shift ($\Delta\lambda$), temperature (T) and mechanical strain (ϵ) can be found using equation 4.1:

$$\frac{\Delta\lambda}{\lambda_0} = k \cdot \epsilon + \alpha_\delta \cdot \Delta T \quad 4.1$$

where k represents the gauge factor, which can be derived from the photoelastic coefficient p . The photoelastic coefficient of silica optical fibres is commonly quoted as 0.22 which results in a gauge factor of 0.78[pm/ $\mu\epsilon$] (Kreuzer 2015). α_δ represents the changing refractive index which is a constant for the fibre optic used during the study.

$$K = 1-p \quad 4.2$$

The first expressions ($k \cdot \epsilon$) of equation 4.1 describes the strain caused by force ϵ_m and temperature ϵ_T . The second part ($\alpha_\delta \cdot \Delta T$) describes the change in the glass refraction index, n , caused only by temperature.

Separating the mechanical and thermal strain is calculated by using equation 4.3 and equation 4.4, where α_{sp} represents the expansion coefficient of the specimen.

$$\epsilon = \epsilon_m + \epsilon_T \quad 4.3$$

$$\epsilon_T = \alpha_{sp} \cdot \Delta T \quad 4.4$$

The changing FBG wavelength can be separated into an equation combining fixed constants associated with the fibre optic and the changing wavelength. Equation 4.1 can then be rearranged to provide the mechanical strain from the changing wavelength, where a positive shift in wavelength relates to a tensile strain and a negative shift in wavelength relates to compressive strain.

$$\frac{\Delta\lambda}{\lambda_0} = k \cdot (\varepsilon_m + \alpha_{sp} \cdot \Delta T) + \alpha_\delta \cdot \Delta T \quad 4.5$$

$$\varepsilon_m = \left(\frac{\Delta\lambda}{\lambda_0} - \alpha_\delta \cdot \Delta T / K \right) - \alpha_{sp} \cdot \Delta T \quad 4.6$$

5.2.3 Experimental Set-up

The component chosen for this study was a 13m motor yacht hull, V39, constructed using the VARI process in a female mould. The component consists of multiple monolithic and sandwich sections and was produced under normal industrial manufacturing conditions at PYI. This hull was chosen due to it being the smallest in the PYI range, which means that it is manufactured quicker and therefore minimises the failure risks associated with fibre optic measurements. The V39 hull can be produced in four days in comparison to the largest yacht that PYI produce, which could be in the mould for up to three months. Due to the high turnover of this model the effects of processing times and the effects of cure times are of particular interest to PYI as they try to keep up with the level of demand.



Figure 79: Princess Yachts V39.

The composite constituent materials used in this study comprise of the following non-crimp fibre reinforced fabrics from Saertex:

- X-E-612g/m² biaxial
- Q-E-1232g/m² quad axial
- X-S-E- 1109g/m² biaxial and CSM.
- Q-E-986g/m² quad axial
- 1300 g/m² biaxial

The core used was a high density PVC foam core with a thickness of 30mm consisting of resin flow channels cut into the core at a spacing of 40mm on the vacuum bag surface. Through thickness holes were located every 40mm to promote consistent resin flow on both sides of the core. The resin system used was a DCPD based polyester resin, Crystic 703pa, which uses Butanox M50 catalyst mixed 100:1.2 parts by weight, the data sheet can be found in Appendix B. The reinforcement and resin system used in this study were not changed from the standard infusion used for this class of yacht at PYI.

The component consists of a complex layup arrangement which involves multiple monolithic and sandwich sections, with the largest monolithic sections being the keel and the chine. Additional areas such as the propeller shaft stern tubes and the bow thruster, where reinforcing is required, are also monolithic layup. A cross section of the port side of the hull layup at the location of the FBGs can be seen in Figure 80. Substantial reinforcement is applied in the chine and keel area where it is expected the resin flow front will be highly non-uniform as was discussed in Chapter 3.

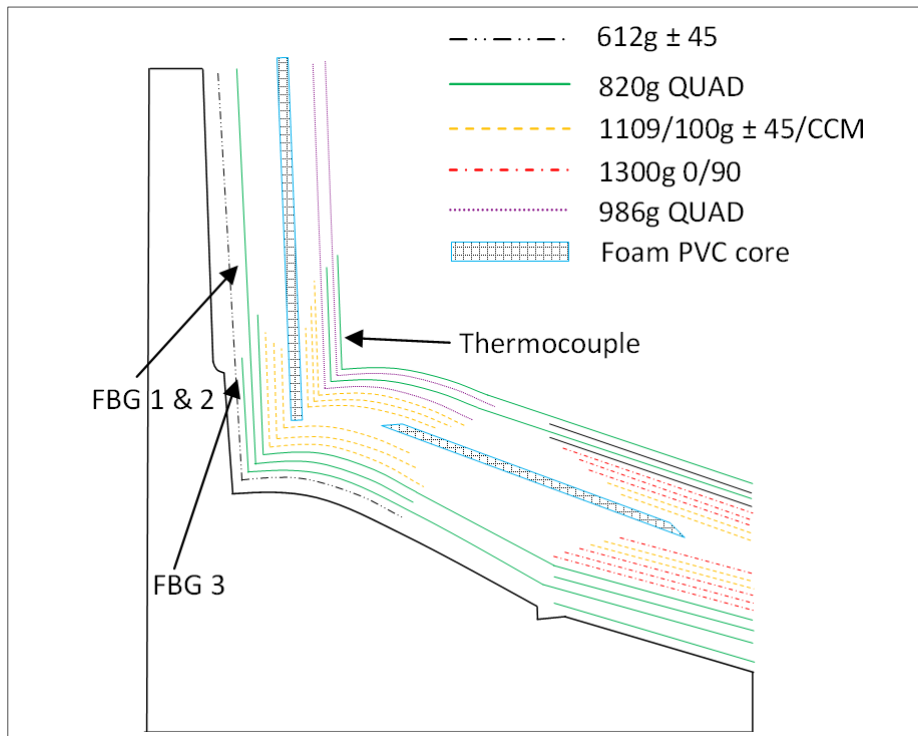


Figure 80: Reinforcement layup schedule.

The tooling used for this study was a vinylester glassfibre female mould. A white gelcoat was specified for this vessel and was applied to the mould above the D.W.L which can be seen in Figure 81. Following the gelcoat, a skin coat and a barrier coat are applied to the mould before the reinforcement specified in Figure 80 is laid into the mould.

During the layup process the placement of the FBGs and the thermocouple sensors were conducted as described below in section 5.2.4. After layup a vacuum leak test was carried out prior to the infusion commencing. An average leak rate of 7.9 mbar/minute was recorded, this is within the normal operating range at PYI and showed that the seal around the fibre optic exiting the vacuum bag was not severely reducing the vacuum integrity. The resin and catalyst were mixed at a temperature of 21°C with an expected gel time of 240 minutes after mixing. A vacuum pressure of 12.6 mbar was recorded before the infusion commenced, with the mould temperature at 19.4°C and the air temperature at 21°C.

Seven injection points running parallel from the stern to the bow were used to create a rectilinear flow front which runs from the keel to the top of the topsides, as is shown in Figure 81. The opening and closing times for each injection point (boost 1, 2 and chine are mirrored on each side of the hull) can be seen in Table 5. The component took 100 minutes to saturate the dry fibres, at which point the inlets were closed and the vacuum outlets were left open for a further 935 minutes whilst the resin cured.

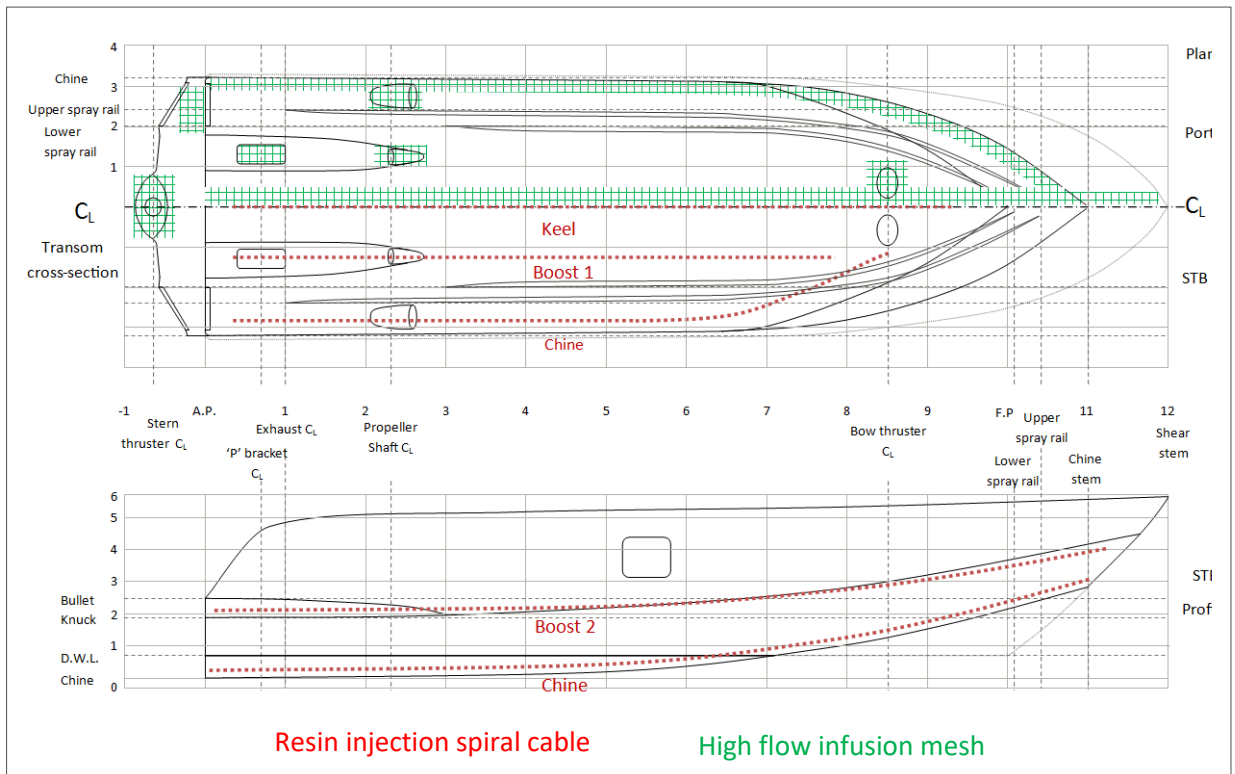


Figure 81 Resin injection and high flow medium locations

Injection point	Opening time	Closing time	Elapsed time (minutes)
Keel	12:45	14:01	76
Boost 1	13:06	14:01	76
Chine	13:24	14:25	100
Boost 2	13:57	14:25	100

Table 5: Resin injection opening and closing times.

During the infusion a non-linear resin flow front was visible from the vacuum bag surface, as shown in Figure 82. The variable fibre layup, core grooves to promote resin flow and any gaps between the core materials resulted in the race tracking effect discussed in Chapter 2 and 3. Figure 82 shows the resin flow front, shown by the yellow dashed line, around the propeller shaft outlet, the keel and initial injection point are visible at the bottom of the image. The stern tube consists of a highly reinforced monolithic area which substantially slows the resin flow front. High flow material is placed on top of this area to promote resin impregnation, however the negative effect of the high flow material can be seen by the non-linear flow front partially caused by higher flow speeds around the high flow material. Multiple areas where unsaturated sections will be fully enclosed by the resin flow front are visible behind the stern tube as well as to the left and right of the stern tube where further reinforcements are placed for the P-bracket

and rudders. The reinforcement interference with the resin flow front progression substantially increases the probability of voids being included in the final component.

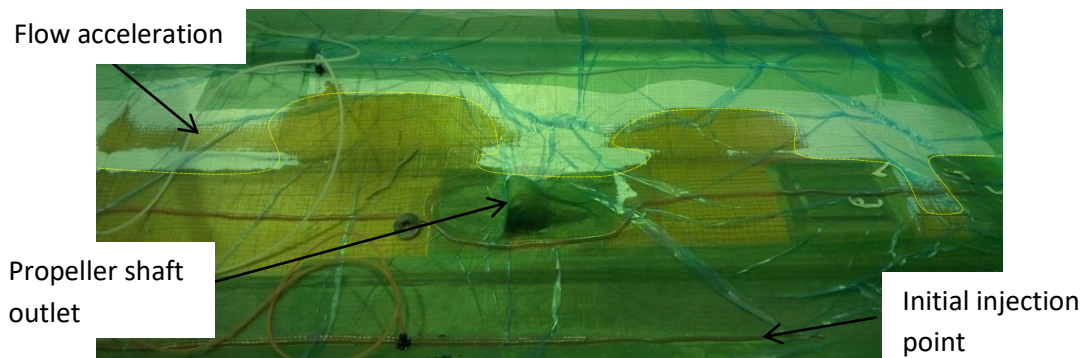


Figure 82: Non-linear resin flow front after passing the propeller stern tubes.

The flow front at the location of the three FBGs can be seen in Figure 83, where the effects of the additional reinforcement in the chine layup have resulted in multiple flow fronts as the resin flowing along the core channels penetrate through the thickness of the reduced reinforcement higher up the topsides. The same flow effects were reported in Chapter 3 and are likely to also occur on the mould surface due to the holes in the core material distributing resin through the thickness of the component.

The flow channels in the core material also result in small converging flow fronts which result in multiple enclosed dry areas behind the resin flow front, as was also discussed in Chapter 3. The inclusion of these flow features, which were also recorded on other infusions, suggested that similar issues were present on this model, as well as the large models manufactured by PYI.

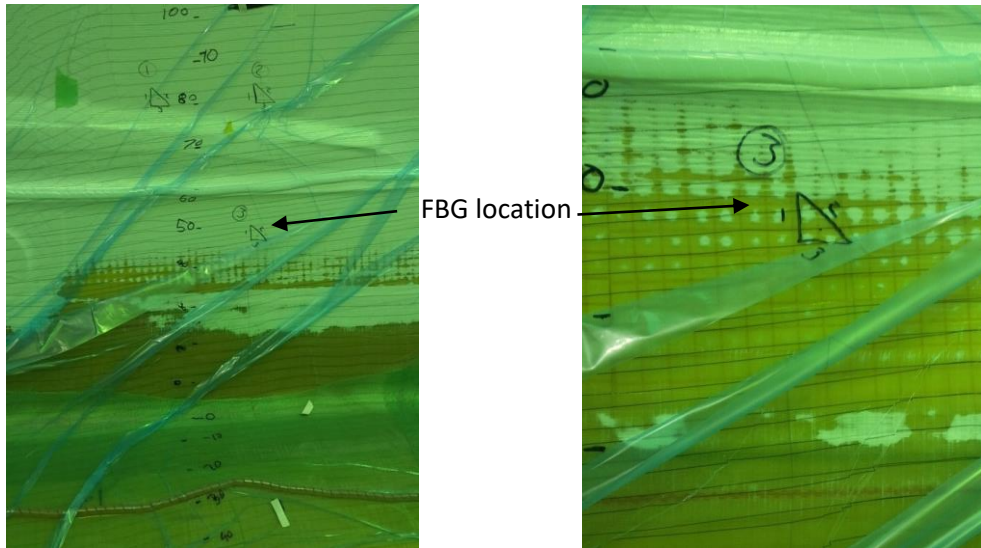


Figure 83: Non-linear resin flow front at the FBG location.

After 100 minutes the resin inlets were closed and visual inspections of the vacuum bag surface identified full saturation of the reinforcement, as is shown in Figure 84. The mould continued to be tested for leaks using audio leak testers to ensure that no dry spots could be created from a bag leak in the 140 minutes between the resin inlets closing and the expected resin gel time. The fibre egress points were also continuously checked for leaks to ensure the fibre optics did not have a negative impact on the final component quality.

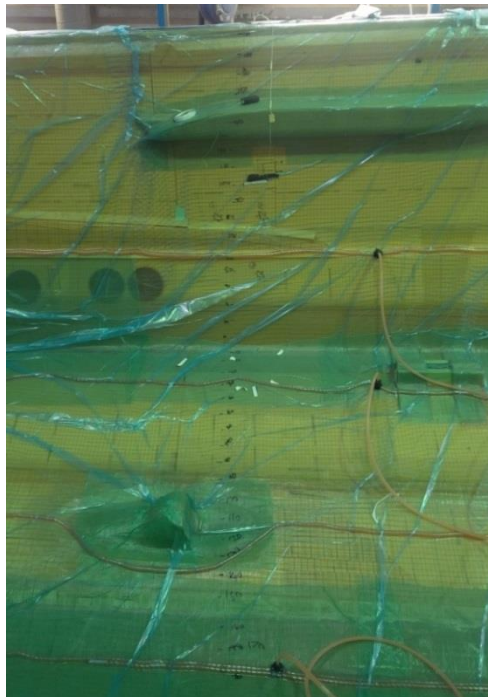


Figure 84: Fully infused component 100 minutes into the infusion process.

5.2.4 FBG and Thermocouple Positioning

The fibre optics were positioned based on the information discussed in the previous Chapters. The results in Chapter 3 identified a high frequency of surface visible voids in the chine, transom, bow thruster and stern tube areas. Each of these areas has significant fibre reinforcement, either due to being in a monolithic layup or in a transition region from monolithic to sandwich layup. The defect assessment conducted in Chapter 3 also identified that the defect analysis had not taken place above the D.W.L. of each hull due to the gelcoat restricting any visual surface defect identification. The surface finish of the topsides is only visually inspected to identify any major residual stress alleviation mechanisms such as distortion of the topsides resulting in a shimmering effect in the gelcoat. The FBGs were chosen to be positioned higher than the D.W.L mark so that an assessment of the manufacturing induced residual stresses could be conducted in an area which has previously been restricted to limited assessments of component quality and therefore assumed to be defect free by PYI. The decision not to put the fibre optics lower towards the chine was also taken to minimise the risk of the fibre optics being damaged whilst the additional reinforcement materials were laid into the mould.

The inter lamina matrix failures identified during the μ -CT scans of the core samples identified failures between the outer reinforcement layer and the first layer of additional reinforcement. The FBGs were therefore located between the first layer of $612\text{g}/\text{m}^2$ biaxial reinforcement and the $820\text{g}/\text{m}^2$ quad axial reinforcement on the topside of the hull, as is shown in Figure 80 and Figure 85. FBG 3 was positioned below the hull knuckle at the top of the area where the additional reinforcement is located above the chine, whilst FBGs 1 and 2 were located 800mm above the chine in the continuous sandwich section between the $612\text{g}/\text{m}^2$ biaxial reinforcement and the $820\text{g}/\text{m}^2$ quad axial reinforcement. These locations would allow the effect of the additional fibre reinforcement to be assessed by comparing the strain development during the infusion and curing process. The separation of the FBGs would also allow the effect on the flow front location of the additional reinforcement to be confirmed using FBG 3 to confirm the flow front delay in the chine.

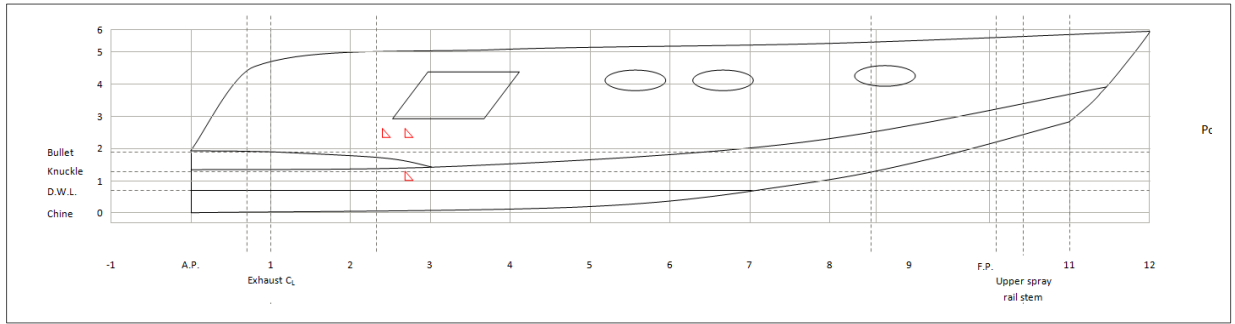


Figure 85: Fibre optic location on the port topside of the hull.

The potential increase in manufacturing time caused by the embedding of the fibre optics has been previously discussed. In order to ensure the FBGs do not delay the layup process and remain in place during the initial layup and the subsequent application of the vacuum and resin infusion, the fibre optics were positioned between two layers of ultra-fine $30\text{g}/\text{m}^2$ CSM strand mat (CSM) glass surface tissue. The FBGs were arranged in a rosette in the centre of the surface tissue in a cut out so that the surface tissue had no effect on the data recorded, as is shown in Figure 86. A spray adhesive was used to bond the two layers of glass surface tissue around the fibre optic, before being used to bond the three FBG rosettes to the glass fibre. Due to the shape of the component all reinforcement was applied using adhesive; the spray adhesive used to position the fibre optics should not have a negative influence on the component infusion or the strain measurements recorded.

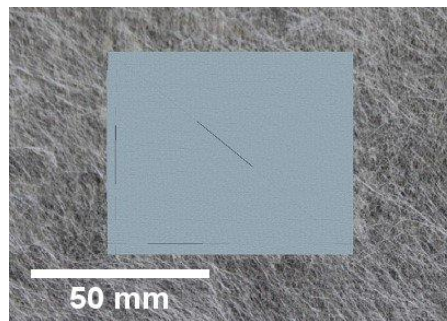


Figure 86: FBG rosette arrangement in the CSM surface tissue.

The FBG rosette was arranged at 0° , 45° and 90° to the resin flow direction, where 0° is defined as the direction of the resin flow from the keel to the chine and then up the topsides to the top of the mould. The 90° FBG measured strain running from the transom of the hull to the bow.

Due to the risks associated with fibre failure at the location of the FBGs and the egress point from the preform, it was decided that three individual fibre optics should be used with three

FBGs on each. The three FBGs had the following static wavelengths 1538, 1548 and 1558nm. The FBGs were located 200mm apart along the fibre optic to allow for a large radius curve to be used to create the rosette to minimise the possibility of the fibre optics failing whilst producing the rosette. The fibre optics used were supplied by SmartFibres and had the properties listed in Table 6. National instruments Optical Sensor Interrogator NI PXIe-4844 was used with a wavelength range of 1510nm to 1590nm.

Outer coating	Polyimide
Strain sensitivity	1.2 pm/ $\mu\epsilon$
Strain resolution	0.4 $\mu\epsilon$
Temperature sensitivity	11 pm/ $^{\circ}\text{C}$
Temperature resolution	0.05 $^{\circ}\text{C}$
FBG length	5mm
Temperature range	-270 to 300 $^{\circ}\text{C}$

Table 6: FBG properties.

Temperature monitoring served two purposes during the investigation; firstly temperature compensation of the FBGs is critical to recording accurate mechanical strain measurements. Secondly the temperature data was used to monitor the exothermic reaction of the resin during the curing process. The temperature measurements were used to ensure the resin cure had been successfully completed before the vacuum bag removal and removal of the component from the mould. Temperature monitoring during processing was conducted using a thermocouple positioned on the vacuum bag between the three FBG rosettes. Due to the manufacturing constraints of an industrial infusion a thermocouple or strain isolated FBG were not permitted within the reinforcement. The effect this may have on the temperature compensation of the strain measurements and the determination of the total mechanical strain within the component will be investigated in the results and analysis section of this Chapter.

Temperature and fibre optic measurements commenced before the vacuum was applied so that any vacuum induced mechanical strain could be monitored as the vacuum compacted the reinforcement into the female mould tooling. Due to the scale, shape and industrial nature of the infusion it was hypothesised that any irregularities within the fibre layup would result in the FBGs being placed in tension before the infusion started.

The infusion progress was monitored visually from the vacuum bag surface, allowing the expected resin arrival time to be used to validate any change in wavelength which could occur

due to changing pressure, fibre optic saturation and temperature differences between the resin and the dry fibre layup.

Temperature measurements continued until the vacuum bag was removed from the component 1243 minutes after the start of the investigation. The difference between the ambient and vacuum bag surface temperature at this point was 5.0°C. Due to the removal of the vacuum bag before the FBG measurements were complete, the final recorded temperature from the vacuum bag surface, 24.1°C, was used for strain temperature compensation.

Post infusion the egress point of the fibre optics became delicate, with the third fibre optic failing during the debuggging process. Fibre optics one and two continued to successfully monitor the changing strain within the component until the removal from the mould.

The final process which was monitored was the removal of the hull from the mould, this was a key phase to monitor as it was expected some of the residual stresses created during the infusion would result in surface defects potentially causing the topsides to spring in. The component was lifted out of the mould between 1243 minutes and 1290 minutes after the start of the investigation. During this final process another fibre optic failed, fibre optic one, whilst the final fibre optic had to be disconnected so that the crane could move the hull onto the next stage of the production process.

Further strain measurements were taken once the component had been moved along the production line, 1394 minutes after the start of the investigation. During the lifting process, the hull is only supported by four lifting points on the bottom on the hull, which results in the topsides being unsupported during this process. The final intact fibre optic was left housed in a protective box mounted on the component so that further measurements could be taken in the future to monitor the change in strain caused by the further manufacturing stages, as well as through life strain variations caused by the aging of the hull and changing environmental conditions.

5.2.5 Results

Figure 87 displays the three recorded FBG wavelengths from fibre optic 2 at 0°, 45° and 90° from the start of the investigation to the final measurement after removal from the mould. The zero timing on the x-axis marks the beginning of the study, after the vacuum bag had been laid but before the vacuum was applied to the preform. The data gap at 1300 minutes represents the time when the component was lifted and removed from the mould before being moved along the production line. Further measurements were taken at 1400 minutes, once the component had been secured in position on a movable cradle. The transverse strain measurements from fibre optic 2 were lost after the component was removed from the mould. During the demoulding process the wavelength at 45° dropped to zero on a number of occasions which identified that an issue had been caused by the demoulding process.

Fibre optics 1 and 3 show very similar wavelength changes throughout the investigation and the wavelengths can be seen in Appendix H, Figure 161 and Figure 163.

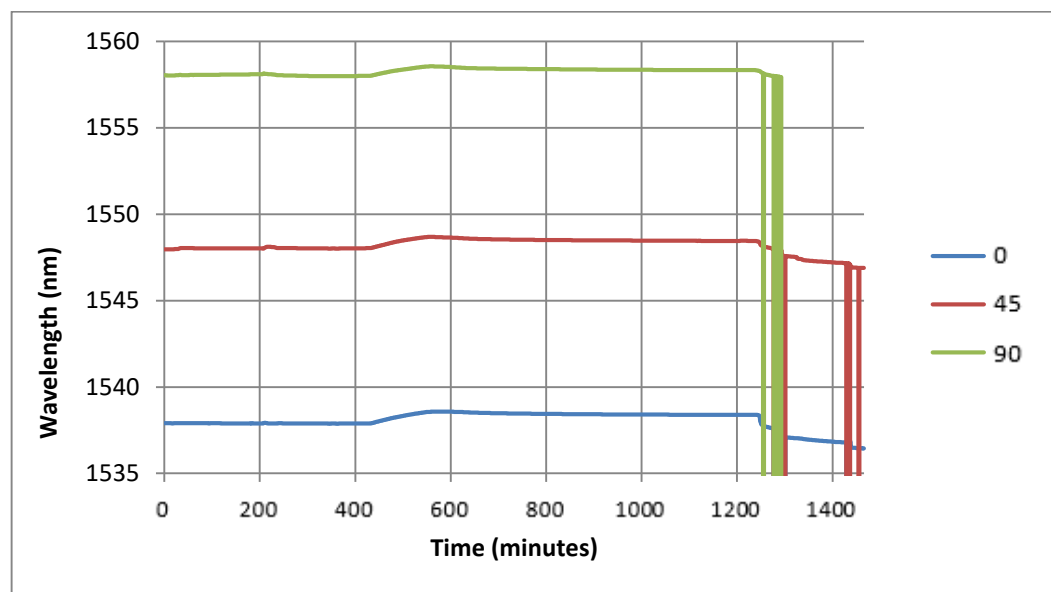


Figure 87: Fibre optic 2 wavelength measurements from vacuum to demoulding.

Figure 88 shows the temperature measurements on the vacuum bag surface throughout the investigations. Once the vacuum bag was removed the temperature measurements were also lost due to the location of the thermocouple on the vacuum bag. In order to estimate the temperature compensation for the final measurements once the component had been removed from the mould, the final temperature measurement was assumed to be fixed.

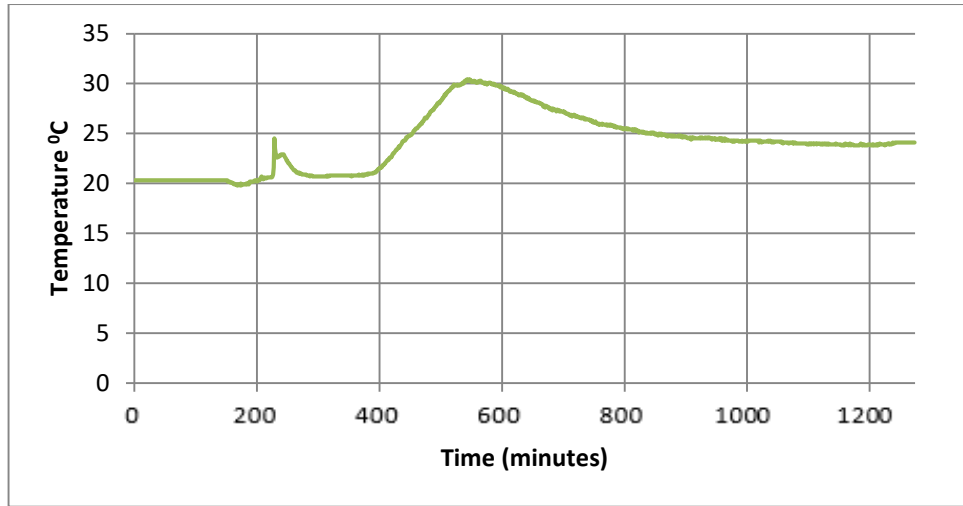


Figure 88 Thermocouple recordings from the vacuum bag surface temperature and the ambient temperature.

Combining the temperature measurements and the FBG wavelengths using Equation 4.6, the wavelength response is converted to mechanical strain.

$$\varepsilon_m = \left(\frac{\Delta\lambda}{\lambda_0} - \alpha_\delta \cdot \Delta T / k \right) - \alpha_{sp} \cdot \Delta T \quad 4.6$$

The following constants were used in Equation 4.6, $\alpha_{sp} = 2.5 \times 10^{-5}/K$, $k=0.78\mu\text{m}/\mu\epsilon$ and $\alpha_\delta = 6 \times 10^{-6}/K$ (SmartFibres, 2016; Kreuzer, 2015)

Figure 89 shows the temperature compensated mechanical strain response from FBG 1 in a longitudinal direction. The changes in temperature and wavelength can also be seen on the graph so that the effect of temperature can be deduced.

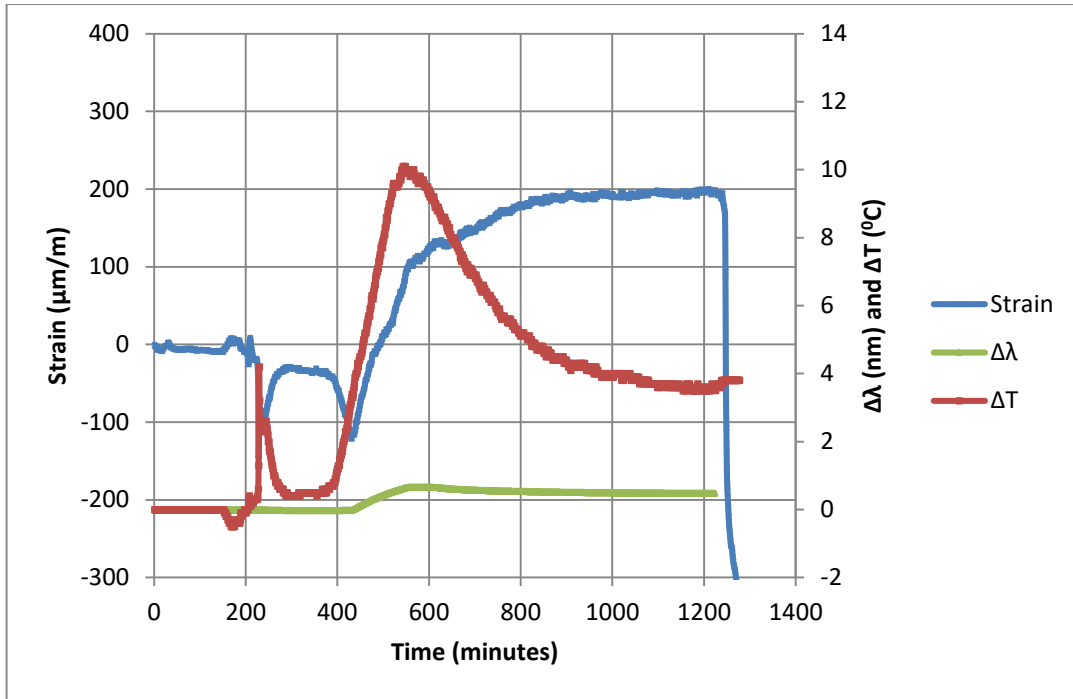


Figure 89: FBG 2 longitudinal strain measurements with change in temperature and change in wavelength from vacuum bag to demoulding.

Table 7 provides reference times for each of the key phases of the VARI process including the demoulding times and the final measurement taken once the component had been removed from the mould and moved along the production line. Each phase will be referred to using the number denoted in Table 7.

	Infusion Stages	Time from process start
1	Vacuum bag laying	0-40 minutes
2	Vacuum applied	41-147 minutes
3	Resin infusion	148-248 minutes
4	Resin cure	249-1243 minutes
6	Vacuum bag removal and demoulding	1230-1290 minutes
7	Component suspended from lifting points	1291-1294 minutes
8	Post demoulding unsupported in the cradle	1391-1529 minutes

Table 7: Reference times for each of the key phases during the production process.

The average strain measurement during each phase of the VARI process have been combined using fibre optics 1 and 2, as is shown in Figure 90, so that the changing strain state can easily be identified.

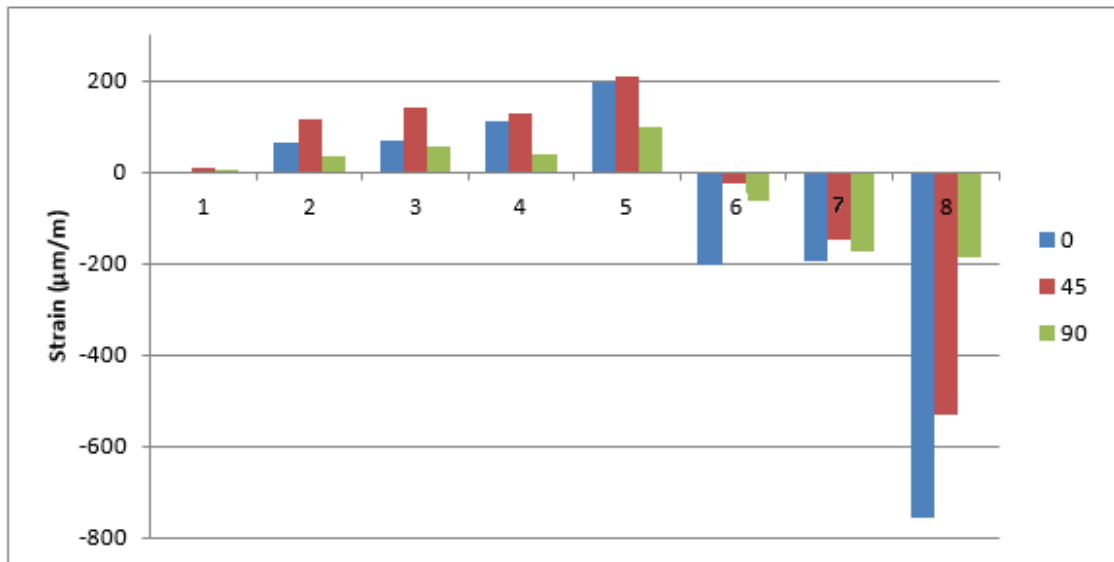


Figure 90: Average mechanical longitudinal, transverse and shear strain from fibre optics one and two.

Fibre optics 1 and 2 showed similar results throughout the study whilst fibre optic 3 recorded a number of failures in measurements throughout the manufacturing process. During the demoulding phase the output from fibre optic 3 was lost completely. Due to the irregularity of the output from fibre optic 3 and the irregular output it was decided that all results from fibre optic 3 would be discarded from the investigation. This unfortunately led to the loss of information collected from the area of the chine where the additional fibre reinforcement is located which should have resulted in a different strain response.

Using the average mechanical strain measurements from fibre optics 1 and 2 (Figure 90) the general tendencies during the resin infusion were as follows:

1. Before the application of the vacuum pressure the FBGs all recorded a small level of tensile strain. The values recorded are minimal and are likely attributed to small movements in the reinforcement or tension applied to the fibre optic whilst weaving the fibre through the core material, reinforcement, peel ply and vacuum bag.
2. During the application of the vacuum pressure, the FBGs recorded an increase in the tensile strain in all three directions. This is likely to be caused by the reinforcement being extended into the corners of the mould shape at the chine, bow and transom.

Some of the waviness in the reinforcement from the layup process will be removed by this process, straightening the fibres, removing wrinkles and inducing tension in the FBG.

3. As the flow front moved past the FBG locations, the strain measurements shifted from a small tensile strain to a small compressive strain. The resin arrival caused an increase in pressure and relaxation of the reinforcement, allowing the tensile strain induced by the vacuum to be removed. Due to the indirect temperature measurement being used, changes in the FBG strain measurement could be down to the temperature compensation not accounting for local changes in temperature as the resin saturates the fibres. Figure 91 shows that there was minimal change in the FBG wavelength before 400 minutes whilst Figure 88 identifies a change in temperature around 200 minutes into the study. The visual monitoring of the resin flow front progress recorded that the resin arrived at the FBG locations at around 193 minutes into the study. Without any substantial change in wavelength the temperature change used for the temperature compensation of the strain measurements may have resulted in a change in mechanical strain which did not exist.

The magnitude of the mechanical strain recorded during stages 1 to 3 are minor in comparison to the strain recorded after cure and demoulding.

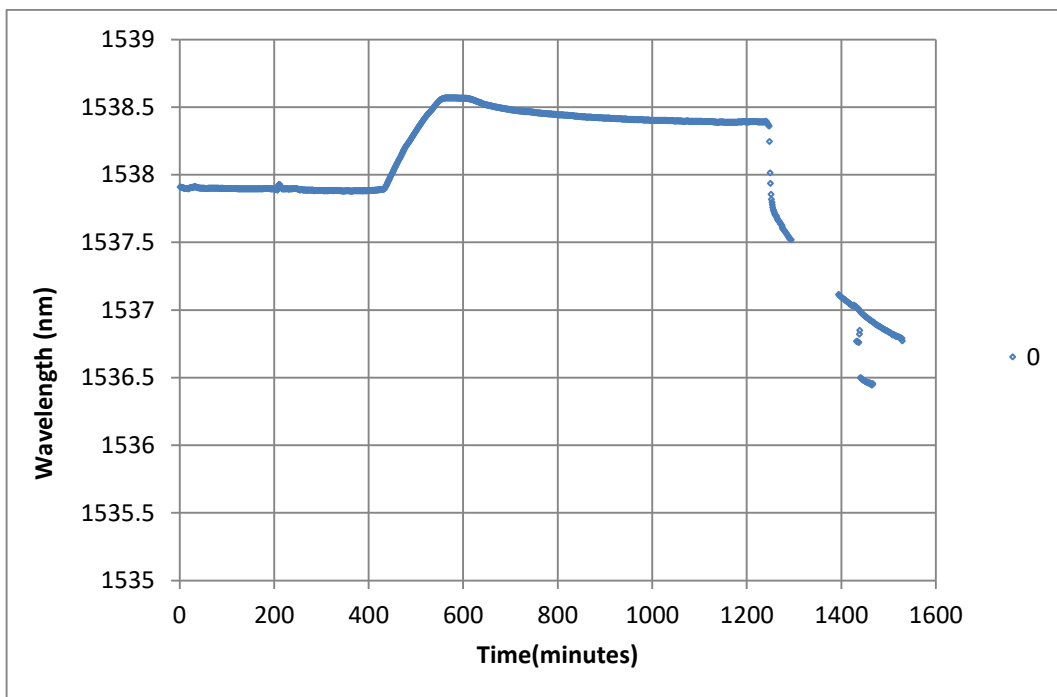


Figure 91: Fibre optic 2 longitudinal FBG wavelength.

The thermocouple detected the start of the exothermic curing process 380 minutes into the study. The strain recordings in all directions initially indicated increasing compression in the reinforcement. As expected the polyester resin shrank during the curing process, with higher volumes of resin expected to shrink by 2% or more during the curing process as discussed in Chapter 1 and 3 and shown in Figure 92.

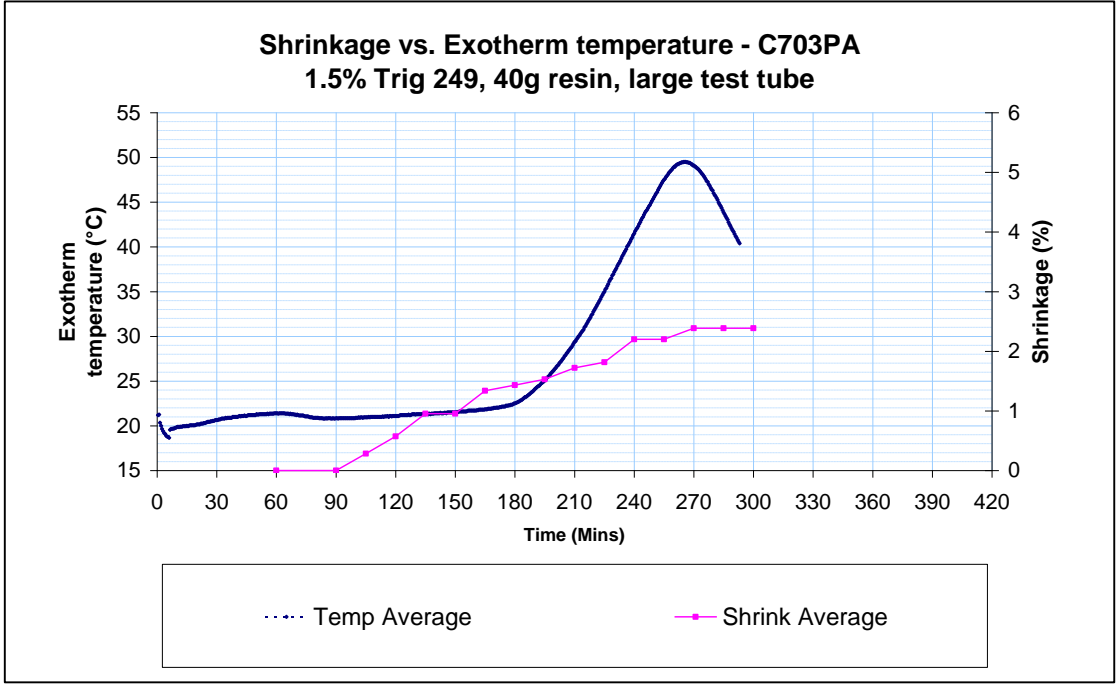


Figure 92: Polyester resin shrinkage and exothermic temperature during cure (Cook, 2011).

400 minutes into the study, peak compressive strains were recorded, approximately 100 minutes before the gel point of the resin. As the exothermic temperature continued to rise the compressive strain measurements reduced and transitioned to tensile strain. The tensile strain measurements in all directions continued to increase beyond the gel point of the resin until the vacuum bag was removed and the resin was assumed to have fully cured and the component was removed from the mould.

Figure 93 shows the measured mechanical strain from fibre optic 2 whilst the vacuum, vacuum bag and component were removed from the mould. The temperature used to isolate the mechanical strain was assumed to be the same as the last recorded temperature on the vacuum bag before removal. It was assumed that the component temperature remained constant over the 50 minutes between debagging and removal from the mould. Upon removal of the vacuum bag the component was allowed to begin releasing from the mould which can be seen by the significant negative strain increment shifting from tensile strain to compressive. The trend continues as the component was lifted from the mould, the negative strain measurements

continued to increase until measurements were stopped so that the component could be moved fully from the mould. The longitudinal strain measurement displayed the largest transformation from tensile to compressive strain.

Mould, laminate interaction appeared to have restrained movement during the infusion and curing, resulting in the tensile strain measurements before debagging. The removal of the vacuum bag constraining the component has resulted in a section of the component releasing from the mould before being lifted. The early release from the mould can be seen in Figure 93 between 1245 and 1255 minutes.

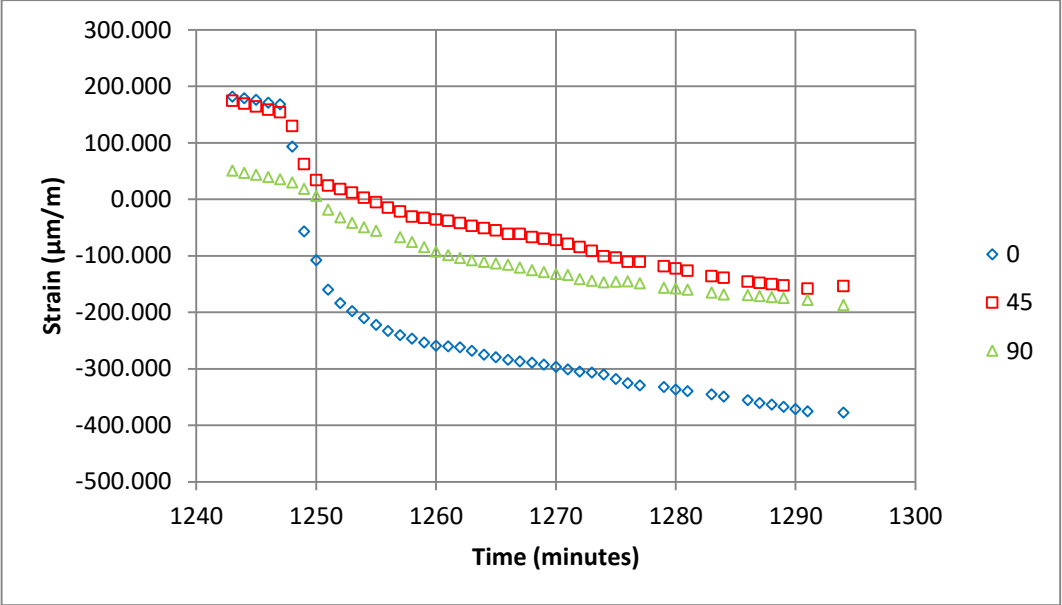


Figure 93: FBG2 Strain measurements during debagging and removal from the mould.

During the removal from the mould the lifting of the component is carried out using fixed points on the bottom of the component near the chine. During this process the topsides are unsupported except for two bracing beams set across the top of the hull. The result of the method used for demoulding is likely to lead to the upper section of the topside sagging outwards, Figure 94, transferring the tensile strain into compressive strain on the mould surface of the component.

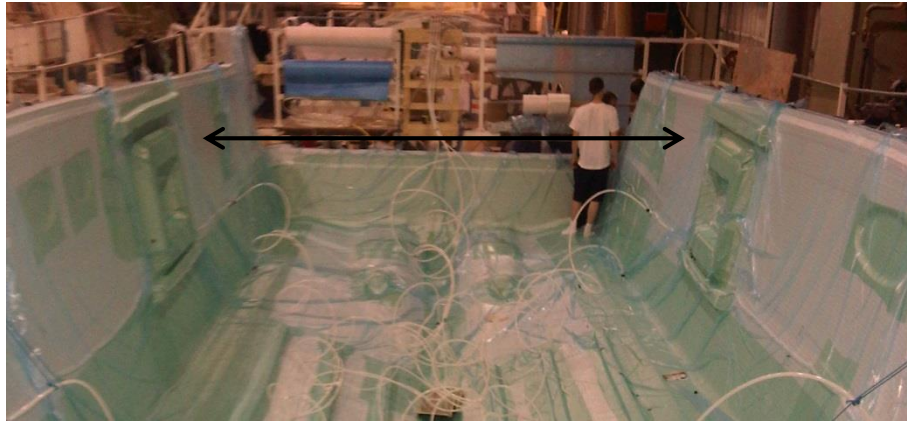


Figure 94: During the demoulding process the component is supported by four lifting points and two reinforcing beams across the top to support the sagging effects on to topsides as shown by the arrows.

Once the component had been moved to the next stage of the production line, the compressive strain measurements had significantly increased from those measured during the lifting process. Figure 95 shows the final strain measurements for fibre optic 2 after the component had been lifted and moved to the next stage of the production process where the component was supported in a cradle under the bottom and keel. Longitudinal strain measurements increased to over $-1000\mu\text{m}/\text{m}$ whilst 45° strain increased from $-150\mu\text{m}/\text{m}$ to $-800\mu\text{m}/\text{m}$, Figure 95. The output from the FBG set at 90° was lost during the demoulding process. These post processing strain increases are likely to be caused by the lack of support to the component before the internal reinforcement is added during the next stage of the manufacturing process.

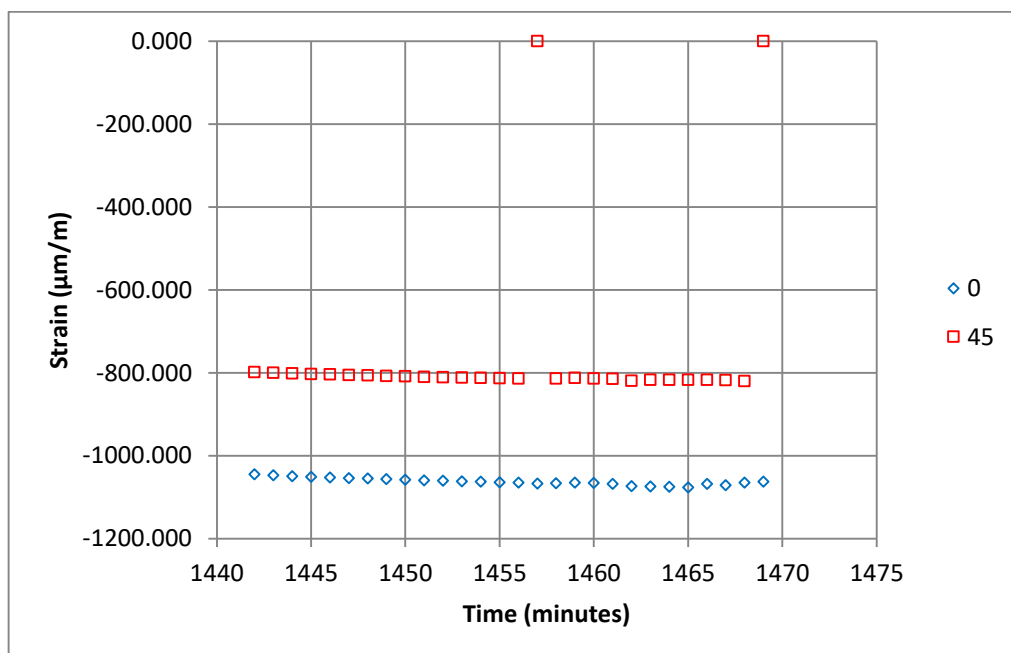


Figure 95: Mechanical strain measurements at fibre optic 2 after being removed from the mould and moved along the production line.

Figure 96 illustrates the mechanical strain measurements from fibre optic 2 in all three directions. Due to the combination of quad axial and biaxial reinforcement used in the component at the location of the fibre optics, it was expected that the strain response would be very similar in all directions. The additional $\pm 45^\circ$ biaxial reinforcement on the outer layer of the component was expected to reduce the strain at 45° in the component. However, the results seen in Figure 96 show that the 0° and 45° strain follow a very similar response during the infusion and curing phases, whilst the transverse strain measuring the strain from the transom to the bow of the hull displayed the lowest mechanical strain.

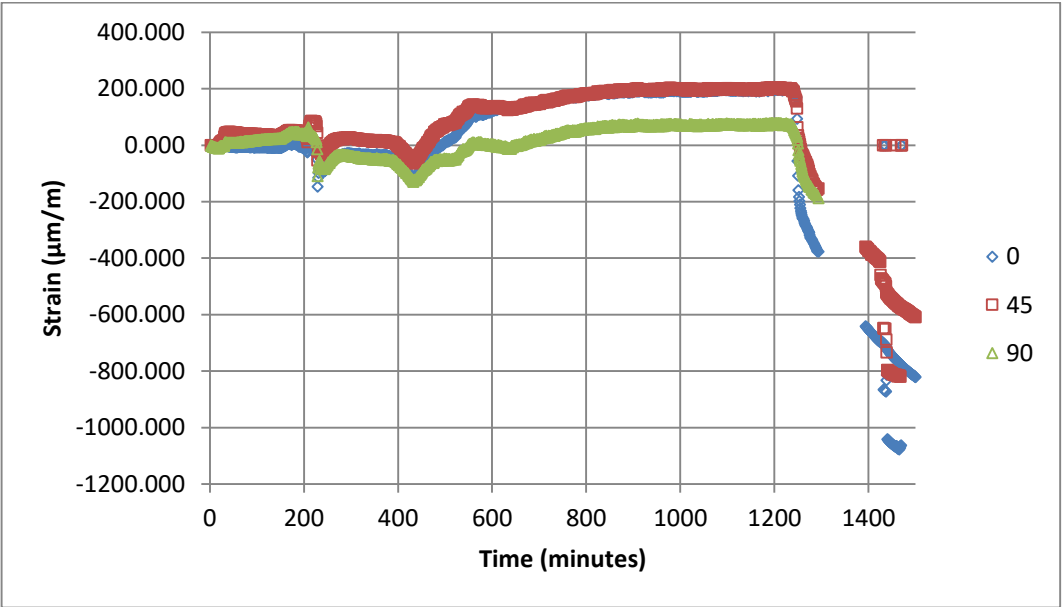


Figure 96: Fibre optic 2 mechanical strain.

5.2.6 Discussion

The results show that in order to accurately detect the resin flow front, local temperature changes need to be accurately monitored. Due to the limitations applied by the industrial nature of this experiment restricting the location of the temperature sensor, detecting the flow front of the fibre optics has not proven to be successful.

During the infusion process, the expected strain measurements were recorded up until the resin began to cure. The localised tensile strain recorded does not follow the expected result of a glass fibre polyester resin composite component due to the expected resin cure shrinkage. The experiments conducted by Scott Bader using the same resin system all resulted in resin shrinkage and it was found that the level of shrinkage directly related to the peak exothermic temperature and resin volume.

Due to the positioning of Fibre optics 1 and 2 above the reinforcement area of the chine, the tensile strain may be affected by the higher level of resin shrinkage in the chine area. The fibre optics were located above the chine in the topside where only two layers of reinforcement existed, as shown in Figure 80. The chine region has significant additional reinforcement due to the transition from a monolithic to sandwich layup. The additional reinforcement results in a significantly higher volume of resin in the chine area which will lead to higher cure temperatures and therefore an increase in cure shrinkage. Temperature measurements conducted by PYI on the bag, core and mould surface of an infusion showed significantly higher exothermic cure temperatures than those recorded during this experiment. The additional volume of resin results in a higher cure temperature which will have led to higher and faster resin shrinkage in the chine region. The result of the shrinkage in the chine is to cause the topsides to be put under tensile load due to the constraints of the fibres at the top of the mould. The transverse strain is also affected by the higher resin shrinkage in the monolithic layups in the transom and bow areas following a similar layup schedule to the chine.

Figure 97 shows a scaled version of the laminate layup and the transitions from sandwich to monolithic sections used in the chine area of the PYI hulls. The transition from the sandwich layup on the bottom of the hull to the monolithic layup before the chine followed by the sandwich topside can clearly be seen. The wedge of core material used to help chamfer the radius at the chine can also be seen to create pockets for excess resin to cluster in.

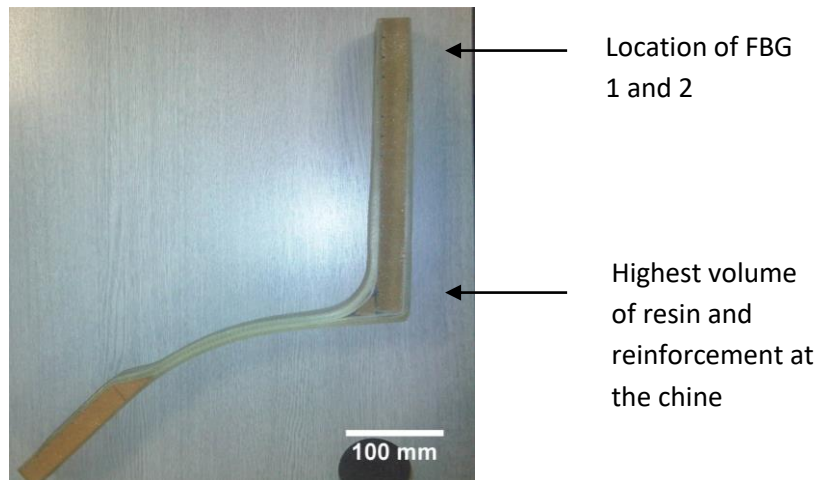


Figure 97: Chine region cross section.

Using the areal weight of the reinforcement and a fibre volume fraction of 55%, the volume of resin in the chine and topside can be estimated and compared. Using the laminate schedule in Figure 80 the areal weight of the reinforcement can be estimated to be 13.938 kg/m^2 in the monolithic section below the chine. Assuming a uniform fibre volume fraction of 55%, the average resin weight can be estimated to be 12.544 kg/m^2 . The areal weight of the reinforcement used on the mould surface of the topside above all of the reinforcing layers is 1.432 kg/m^2 which would lead to an estimated 1.288 kg/m^2 of resin. The volume of resin at the chine is therefore ten times higher than at the location of fibre optics one and two. The work conducted by resin suppliers Scott Bader, which was reviewed in Chapter 3, showed that comparing two resin masses (20 g and 40 g) in 12 mm diameter test tubes resulted in different cure and shrinkage profiles. Although the maximum shrinkage results were comparable, 2.26 % for the 20 g mass and 2.39 % for the 40 g mass, the time to reach the maximum shrinkage was significantly different. The smaller resin mass took an additional 60 minutes to reach the maximum shrinkage level.

A similar level of variation in cure speeds and shrinkage profiles is likely to have occurred during the hull infusion which resulted in the transition from compressive to tensile load on the topside. The chine region is expected to have ten times more resin by mass than the topside area of the hull. The effect of this on the cure characteristics will have been for the resin in the chine to cure at a faster rate and at a higher peak exotherm, as is shown in Figure 98. This will have resulted in the resin shrinking at a higher rate in the chine at an earlier point during the curing process. Leading to the fibres higher up the topside experiencing tensile loads as the resin in the chine transitioned from a gel state to a solid state, before the resin in the topside had developed its mechanical properties.

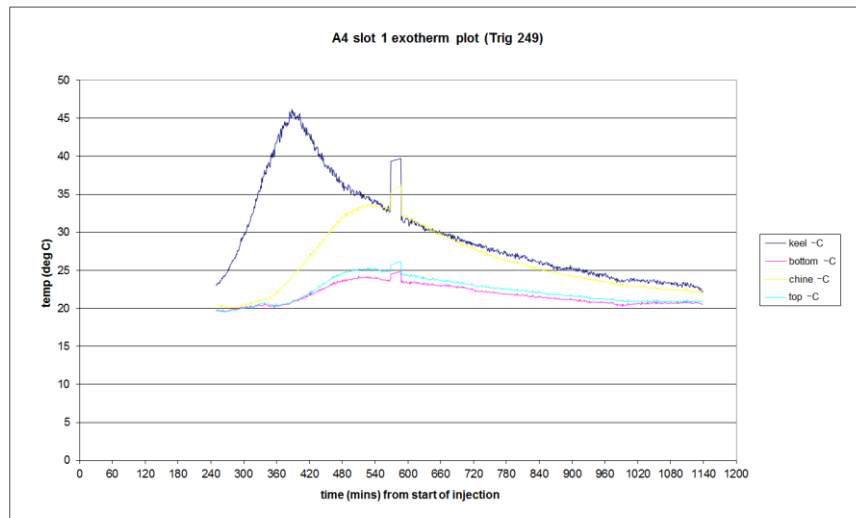


Figure 98 Vacuum bag temperatures recorded at the keel, bottom, chine and topsides on model A4 slot 1.

The voids reviewed in Chapter 4 between the first and second layer of reinforcement could also be related to the variable lamina schedule between the hull bottom, chine and topside regions. Scott Bader reported that the resin adhered to the test tube during cure, which restricted the ability of the resin to shrink during the curing process. The first layer of reinforcement was laid onto the gelcoat, skin coat and barrier coats which are cured before the infusion. The first layer of reinforcement could have adhered to the skin coat, which would restrict the ability of the resin and fibres to shrink away from the mould and pre-release. The result of which could be the matrix failures identified and examined in Chapter 4, leading to the hypothesis that the high volume of resin in the monolithic region of the chine is a contributing factor to the delamination identified on the topside above the chine.

The previous discussion in relation to the effect of the additional reinforcement in the chine region suggests that the reduced transverse strain may have been affected by the location of the fibre optics in relation to the transom and the bow. The transom reinforcement schedule is comparable to the chine region, where the laminate transitions from a sandwich to monolithic layup. The transom shape and laminate schedule are influenced by the requirement to support trim tabs, bathing platforms and stern thrusters which results in a complex reinforcement schedule and a complex mould shape. It is expected that the laminate would behave comparably to the chine region which would result in high levels of strain in the areas near the transom. However, due to the distance between the fibre optic sensors and the transom (approximately three metres), the effect of the resin shrinkage is reduced over a greater distance.

The reduced transverse strain measurement suggests that a relationship between the strain measurements and the proximity to higher resin volumes exists. The transverse strain measurements also showed higher levels of compression during the initial cure stages, which suggests that the transverse fibres are constrained less than the longitudinal and $\mp 45^\circ$ fibre reinforcement.

The strain measurement of $200\mu\text{m}/\text{m}$ before the component was removed from the mould indicates that the tension exerted on the FBG was approximately 0.55MPa based on the Young's modulus of 2754MPa for Crystic 703pa. After demoulding, the compressive force exerted on the FBG was found to be 2.76MPa , where the adhesive and stiffness properties of the resin would have become critical to maintain the reinforcement structure to avoid buckling whilst in compression. The tensile strength of Crystic 703pa is 49MPa , Appendix B Figure 148, following a 24 hour room temperature cure and a 16 hour post cure at 40°C . The strain measurements indicate the resin was under a smaller load than required to cause resin failure. However Barcol hardness tests performed by PYI, shown in Figure 99, show that after one day, the Barcol value is 25B having undergone no post cure. The resin samples which were subject to a post cure, record values of 30B and 40B, this shows that the room temperature cure sample had not fully cured after 24 hours, which means that the material properties used above will not have been achieved. In addition to the reduced material properties after 24 hours, the component in this study was extracted from the mould 14.5 hours after the gel point of the resin, suggesting that the material properties would be further reduced against the ones provided in the material data sheet for Crystic 703pa.

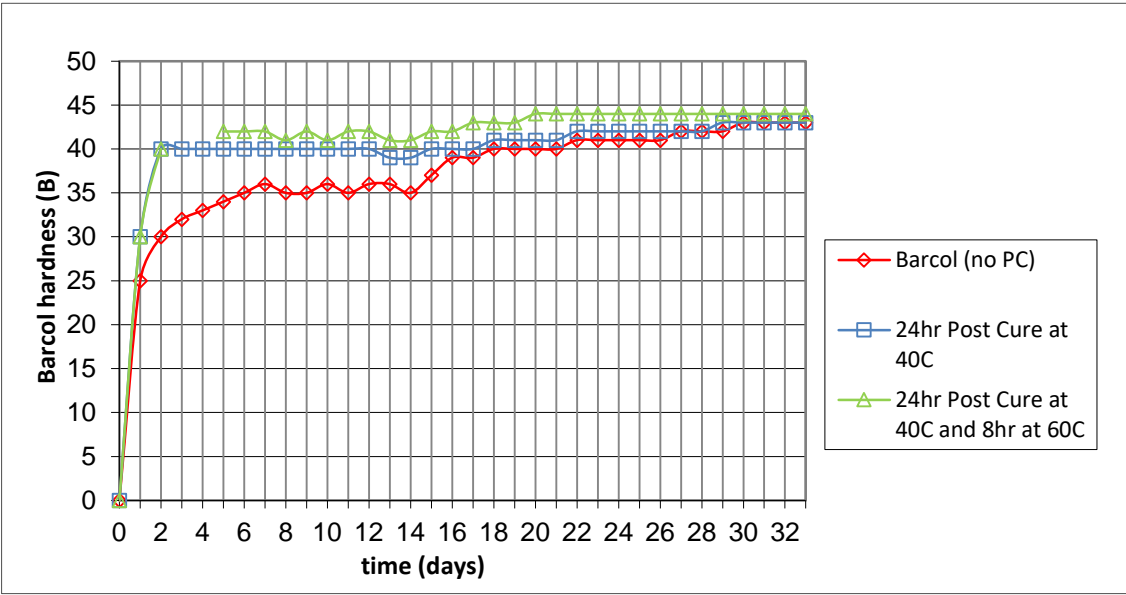


Figure 99: Crystic 703pa Barcol hardness results comparing post cured samples and non-post cured samples.

Scott Bader conducted experiments on unsaturated polyester resins to analyse the benefits of post cure on the resin mechanical properties (Norwood 2001). Resin samples were tested during room temperature cure cycles and at a combination of room temperature and elevated post cure temperature to compare the relationship between cure times and mechanical properties. Figure 100 shows the tensile strength, tensile modulus and cure level during the curing process. Each measurement was taken at a time relating to the gelation point for the resin. The results show that the mechanical properties develop a considerable time after the gelation point of the resin, as well as illustrating that 24 hours after the gelation point of the resin, the resin is only 80% cured and the tensile strength and modulus are continuing to develop.

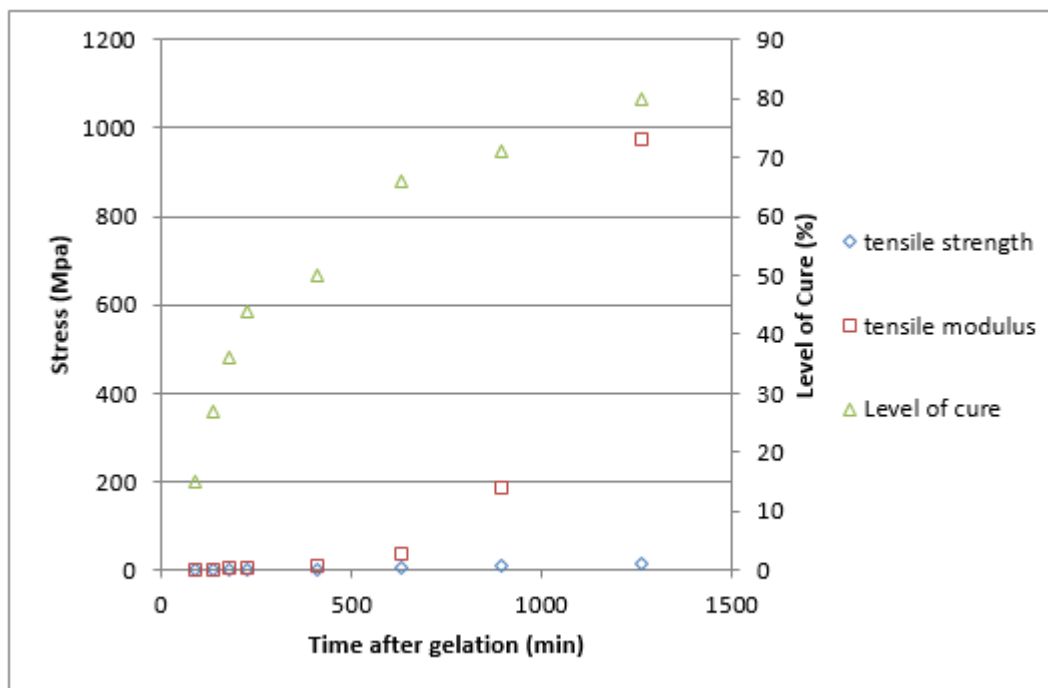


Figure 100: Mechanical property and cure level development in unsaturated polyester resin (Norwood 2001).

Taking the cure and mechanical properties from the results found by Norwood (2001), as well as the strain measurements and the infusion times from the PYI hull infusions a number of topics need to be discussed.

Using the times listed in Table 7, assuming the gel time to be 240 minutes after resin mixing, leads to the component being released from the mould 855 minutes after the approximate gelation time of the resin. The results from the experiment conducted by Scott Bader would suggest that the resin had reached only 68% cure and a fraction of its maximum material properties when the hull is removed from the mould. However, due to the polyester resin tested

by Norwood not being the same Crystic 703pa which is used by PYI or used during this experiment this restricts the author to qualitative comparison. Norwood used a 1:1 maleic acid: isophthalic acid unsaturated polyester resin, whilst Crystic 703pa is a dicyclopentadiene resin.

The strain measurements have shown that due to the topsides not being constrained during the demoulding process, the force applied to the resin and fibres increases. Scott Bader recommends that Crystic 703pa cures for a minimum of 20 hours before being removed from the mould. This increase in stress, coupled with the suggestion that the resin is likely to only be partially cured, will influence the component defects, specifically failures linked to the matrix properties. The relationships between void fraction and reduced material properties were discussed in Chapter 3 where a 1% increase in void fraction has been shown in research to reduce the tensile strength by 3% and the ILSS by 7%. The void fraction in the core sample A3_S6_2 analysed in Chapter 4 peaked at 13% at a location 20% from the mould surface through to the core material. Based on the knowledge that the tensile loads applied at the location of the FBGs are a fraction of the tensile strength of polyester resin, the results suggest that voids are required at the location of the defects to initiate the matrix failures. These results further confirm the earlier hypothesis that a combination of factors is required to cause the defects recorded at PYI, the combination of which are not regularly produced which results in the variability in defects recorded post infusion.

5.3 Conclusions

The results of the strain measurements of a complex large VARI in industrial surroundings has identified a number of issues which will contribute to the defects which were reported in Chapter 4. Due to the expected cure shrinkage of the resin system, the overall stress state post cure was expected to be compressive. The introduction of variable curing rates in the monolithic sections results in the sandwich sections of the component being placed in tension during the curing process. The tensile load in the topsides whilst the resin in this region remains in a gel state reduces the dimensional stability of the reinforcement and the resin. The rapid transition from a thin skin sandwich section to a thick monolithic section is likely to increase the number of delamination failures which were analysed in Chapter 4. The results of these measurements suggest that the laminate schedule in the chine and topsides should be reviewed with respect to the structural requirements to assess if changes can be made to reduce the build-up of resin below the chine. Additional FBG measurements could also be taken on a future infusion to measure the strain changes closer to the chine and in the monolithic section below the chine. The FBGs have been shown to be delicate in an industrial environment, with multiple sensors failing during this study. Positioning FBGs closer to the chine would increase the difficulty of feeding the fibre optic out of the laminate which would increase the probability of failure. However additional data is required to validate the conclusions made, to show that the thicker laminate sections are undergoing a faster cure and result in higher volumetric shrinkage which causes the topsides to be in tension.

The calculated tensile load recorded by the FBGs was significantly lower than the tensile strength of Crystic 703pa which suggests that the stress applied to the component during curing is insufficient to cause the delamination seen in Chapter 4. This result agrees with the findings in Chapter 3, where a high level of inconsistency was reported between infusions. This supports the hypothesis that the delamination and defects found in the chine area of the hull are a result of porosity and the cure characteristics of the component. If the irregular resin distribution and resin shrinkage were the primary causes of failure the delamination would occur consistently from one component to the next. However, the results suggest that additional factors such as porosity, fibre wrinkles or misalignment of the reinforcement are required to cause the matrix dominated failures reported in Chapter 4. Further information is required to investigate the creation and distribution of the defects caused by the changing laminate schedule at PYI. The results of the strain measurements coupled with the findings in Chapters 3 and 4 suggest that a combination of thermal induced shrinkage and resin flow defects exist for delamination to occur.

Comparing the strain development to the cure times reported by Norwood and the Barcol hardness tests completed by PYI, the results suggest that the resin had not fully cured at the point the vacuum bag was removed and the component demoulded. If the resin had fully cured, the strain measured during the demoulding process would have been smaller. The high strain variations recorded during the demoulding process could have a significant impact on the component leading to matrix dominated failures during the demoulding process. The work carried out by Norwood and PYI shows the benefit of post curing polyester resins after an initial room temperature cure. PYI are developing their component post cure capabilities, however at this time, post cure is only on limited moulds and is only being applied to the mould surface of the topsides and at a relatively low temperature of 40°C. Until the post cure process has been optimised and distributed, it is suggested that PYI hold the hulls in the mould for at least 24 hours after the start of the infusion to ensure adequate resin cure before demoulding.

The findings from this Chapter show that improvements could be sought in the lamina schedule used by PYI to reduce the development of residual stresses in the monolithic sections of the component. The findings emphasise the importance of resin defects which work with the thermal induced cure characteristics to cause the component delamination. In order to develop further understanding of the voids created at the chine, experiments need to be conducted to investigate the creation and location of the voids caused by the converging flow front at the chine. The next Chapter will detail the experiments that were created to investigate the creation of the voids in the outer layers of the chine region as well as to investigate the characteristics of the voids.

Chapter 6

6 Flow Front and Void Re-creation Experiment

Chapter 5 has shown that although the lamina schedule used by PYI induces tensile loading in the topsides of the hull, the residual stress levels recorded are not significant enough to cause failure in the matrix without further defects being present. The core sample review in Chapter 4 examined the delamination which had occurred in the heavily reinforced area of the topside above the chine area. The results showed that fibre wrinkles, porosity and larger voids existed around the area where the delamination occurred, suggesting that the existence of the macrovoids impacted the delamination. This Chapter investigates the creation and characterisation of the voids created by a slow resin flow velocity in an area where the laminate transitions from a monolithic to sandwich structure.

6.1 Void Re-creation

The results of the PYI process study and the limitations of computational modelling to accurately simulate and record voids, has identified the need to devise a method to recreate the voids identified in Chapter 4. Previous research has concentrated on post process void analysis and two dimensional real time void creation and mobility (Lundström, Frishfelds & Jakovics, 2010; Pearce, Guild & Summerscales, 1998; Matsuzaki et al., 2013). However, a three-dimensional approach is required to identify and separate the major void causes, so that the required processing alterations for large scale infusions can be identified.

A number of experiments have been created in an attempt to monitor the production and mobility of voids during liquid composite moulding (LCM). Matsuzaki et al. (2013) used a glass mould with dimensions of 200mm x 50mm, a dispersed light was placed below and a microscope above to monitor and record the production of voids due to the fingering process for a single layer of plain weave glass fibre. The experimental set-up allowed for the effect of mechanical entrapment and the effects of the injection pressure and the resin flow velocity on void creation to be assessed. The results showed how the fingering process can be extremely detrimental to final porosity, as is shown in Figure 101.

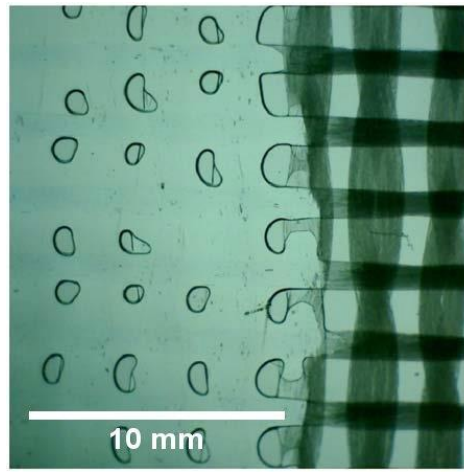


Figure 101: Microscopic image of the flow front and voids observed by the visualisation method during RTM (Matsuzaki et al., 2013).

However no through thickness analysis was possible and the limitations of the experimental set-up restricted the investigations to single lamina, introducing edge effects from both mould surfaces as well as restricting the use of multi axial NCFs.

The author created a similar experiment to the one used by Matsuzaki et al. (2013), using a glass mould, bright light below the mould and a camera positioned above the location of the flow front. Two layers of 1200 g/m² quad axial NCF glass fibre cut to 450 mm in length and 200 mm in width were laid onto the glass mould with the vacuum bag laid directly on top of the fibres. A rectilinear flow front was created and photographs of the resin flow front were taken every second. Figure 102 shows the clearly defined resin flow front, with the saturated fibres behind the resin flow front becoming transparent once impregnated by the resin.

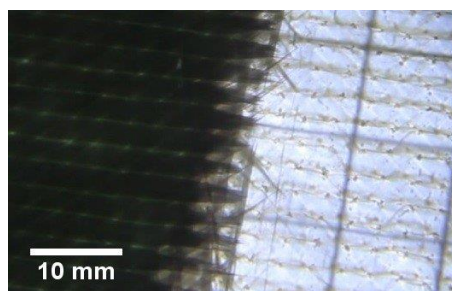


Figure 102: Resin flow front progressing from right to left through two layers of 1200g/m² quad axial glass fibre.

A similar result to Matsuzaki et al. (2013) was achieved through the identification of the irregularity of the flow front and the fingering effect, the video analysis also identified macrovoid movement throughout saturated fibres behind the resin flow front. The images captured highlight one of the issues with NCF caused by the stitches used to hold the

reinforcement together. As the macrovoids flow through the channels between fibres, the stitches acted as obstruction to the void washout, forcing the voids to either get held at the stitch location or move down through the reinforcement to find another path out of the preform.

The images of the resin flow front have been transformed into binary images in Figure 103 so that the irregular shape of the flow front can be visualised. Figure 103 displays the saturated reinforcement in white, with the dry fibres in black, areas where the fingering process have occurred can be seen at multiple locations along the flow front. Image (d) in Figure 103 shows areas behind the resin flow front where dry fibres still exist (circled in yellow), illustrating the risks associated with an irregular flow front.

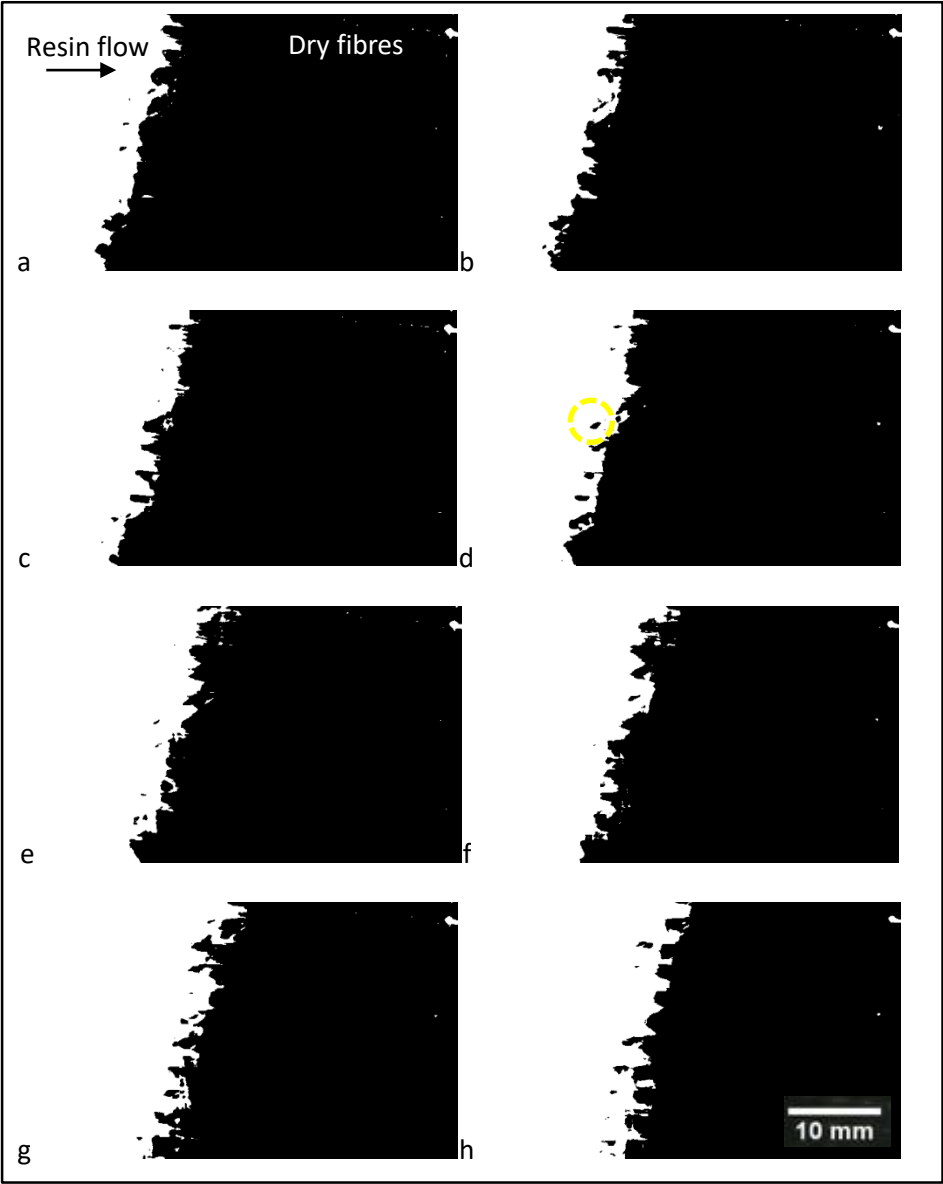


Figure 103: Greyscale image of the flow front at one second intervals from a to h.

Matsuzaki et al. (2013) only used this experimental set-up for void production analysis, though Lundsstrom (2010) used a similar experimental set-up to investigate void collapse during RTM for two layers of CSM. Lundström, Frishfelds & Jakovics (2010) used a smaller mould size than Matsuzaki et al. (2013), measuring 40mm x160mm, with two thin glass moulds to minimise deflection whilst allowing visual monitoring. Instead of relying on mechanical entrapment and the release of volatile curing by products, Lundström Frishfelds & Jakovics (2010) used a degassed resin to infuse the preform whilst artificially injecting bubbles from a syringe to control and monitor the bubble content. The experimental technique used by, Lundström Frishfelds & Jakovics (2010), suffers the same drawbacks as that used by Matsuzaki et al. (2013) due to the limitations on mould size as well as the requirement to use thin preforms. A thicker fibre stack will have an effect on void mobility through the fibre stack, especially due to stitching in NCF forcing voids to disperse in all three axes which cannot be monitored using this method.

Pearce, Guild & Summerscales (1998) used a larger 500 x 500 x 50 mm mould with a single glass surface and an aluminium surface with multiple injection points to investigate the effects of a converging flow front. Post infusion, converging flow points were analysed using an Ultrasound C-scan, allowing qualitative two dimensional void analysis. Pearce, Guild & Summerscales's method has limitations in its ability to separate and identify the cause of the voids, though the results were consistent with previous research which identified an increase in void volume fraction at the point of the converging flow front and a reduction in ILSS as would be expected. The use of multiple injection points allows a multitude of converging flow front shapes, lengths and angles to be investigated, the results of which highlighted the danger of flow fronts converging head on. Stone and Clarke (1975) used an ultrasonic attenuation technique to measure the void content of constant thickness carbon fibre reinforced plastic panels and identified a relationship between void volume fraction and void shape. At low void content (less than 1.5%) the shape of the voids tend to be spherical with a diameter of 5-20 μ m, whereas at high void content, the voids were cylindrical, their length being up to an order of magnitude higher than their diameter. The cylindrical voids were orientated parallel to the fibre axis, their shape caused by the physical restrictions of the fibre bundles, as was seen in the PYI μ -CT analysis in Chapter 4.

Centea and Hubert (2011) devised a method to investigate in 3D the impregnation behaviour of an out of autoclave prepreg carbon epoxy structure utilising μ -CT technology. Partial processing of the laminate to four chosen stages was carried out before it was removed from the oven and quickly cooled to freeze the impregnation process. The samples were then

scanned and the evolution of the impregnation and porosity due to the resin flow was measured. The scans for each of the four stages are shown below in Figure 104.

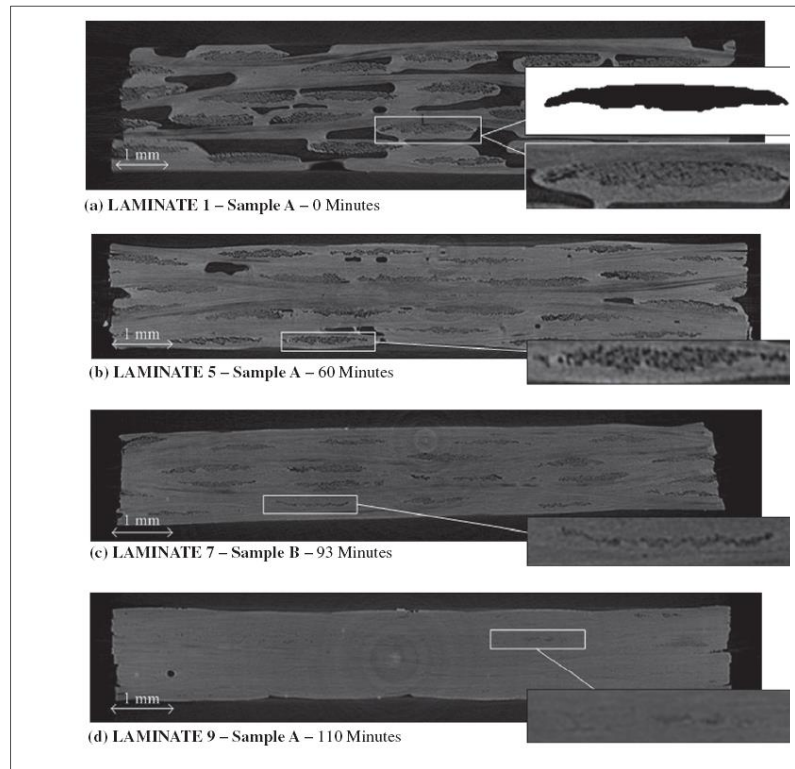


Figure 104: X-ray micrographs of the impregnation process recorded by Centea and Hubert (2011).

The initial analysis was carried out before vacuum or temperature was applied so that the non-compacted natural state of the prepregs could be assessed. The extracts in Figure 104 image (a) show how the visible dry fibre tow area was calculated to quantify impregnation levels. The process was then paused at 60, 93 and 110 minutes, so that the resin flow could be analysed.

They found that the impregnation was highly non-uniform along fibre bundle perimeters as well as between fibre bundles. At 93 minutes it was found that some fibre bundles had fully impregnated whilst others with aligned orientation still required substantial impregnation. A $7\mu\text{m}/\text{pixel}$ resolution was used, allowing for clear identification of the fibre, matrix and voids, though impregnated fibre bundles were rendered invisible. A higher resolution scan at $2\mu\text{m}/\text{pixel}$ was used to identify finer intra-tow details, though this was at the cost of sample size. For each sample, a representative volume of interest was extracted to remove any edge effects from sample extraction and preparation. The results identified the expected trends as vacuum and temperature were applied to the laminate, with the void volume reducing from 7% to 4% after the initial vacuum was applied. The experimental procedure used resulted in a clear and accurate impregnation recording for out of autoclave prepreg materials. The use of prepreg

fibres reduces the number of variable processing parameters, most importantly pressure variations and compaction variations associated with VARI, however the resulting three-dimensional images of the impregnation illustrate a level of detail that to the author's knowledge has never been achieved for LCM process monitoring. A method to control the highly variable processing parameters associated with VARI needs to be deduced so that a similar technique utilising the μ -CT scanner can be used to monitor the VARI.

6.2 Void Re-creation Experiment and μ -CT Analysis

As stated in Chapter 4, μ -CT scanners have proven to be a useful tool for composite part characterisation, detecting a number of critical features (Schilling et al., 2005). The methodology followed by Centea and Hubert cannot be followed for a VARI infusion, however the process of partially infusing samples to analyse the non-uniformity of the resin flow front is possible and will be outlined in the following sections of this Chapter.

6.2.1 Void Re-creation and μ -CT Analysis Objective

This study aims to use μ -CT to investigate the impregnation behaviour of a large complex layup VARI. The proposed steps consist of partially processing the laminate and scanning the samples using the μ -CT scanner so that the resulting data can be used to quantify the evolution of the flow front, voids, compaction and cure.

6.2.2 Experimental Procedure

Due to the level of non-uniformity of the flow front in a large irregular infusion, it was decided that an initial experiment should be carried out to assess the ability to capture a fully cured flow front within a μ -CT scan. Comparable features to an industrial infusion were to be used to cause all of the expected flow anomalies that would not occur on a small lab scale rectilinear flow experiment.

Multiple ply drops, transition regions from monolithic to sandwich structures as well as core grooves and joints were all used to induce converging flow fronts, race tracking and mechanical entrapment. In order to restrict the infusion and ensure that the section of the laminate remained unsaturated, the resin inlet was closed once the visible flow front reached the sandwich section, and the continuing flow was then monitored using a time lapse camera. It is expected that the resin inlet closure whilst maintaining the vacuum level would result in increased inter-fibre bundle voiding due to the dominance of the capillary flow. This has been implemented so that the fibre compaction is maintained whilst the resin cures and to avoid the introduction of voids due to leaks in the vacuum bag. As has been discussed previously it is thought that the areas of the topside near the chine experience a converging flow front as the

resin flows through the core grooves. The result of the converging flow fronts is the loss of vacuum pressure which results in a reduce flow front velocity, similar to the effects of removing the resin inlet. Leaks were minimised to reduce the resin starvation effects and to avoid introducing voids behind the resin flow front before the resin cured.

Limitations in the laboratory restrict the size of the infusion to 1.5m long and 0.5m wide. The resin inlet position was located 0.25m from the end of the laminate to reduce the race tracking effects around the side of the mould. Spiral cable was used to distribute the resin inlet point and create a rectilinear flow and a high flow fabric was used in an attempt to create lead-lag between the vacuum bag and mould surface at the location of the resin inlet Figure 105. This resin inlet arrangement mirrors the set-up used by PYI at the keel of the hull, where the initial resin inlet is located.

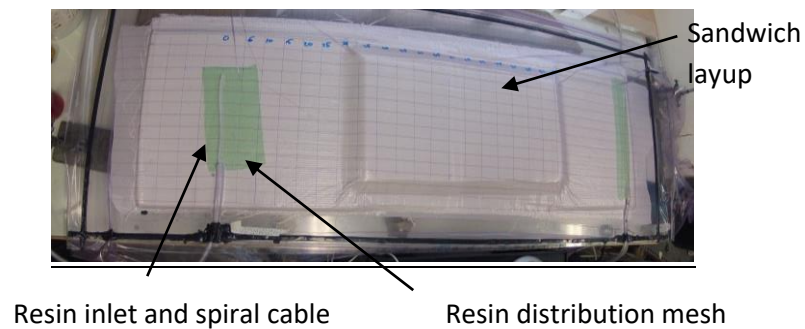


Figure 105: Experimental set-up showing location of the resin inlet and sandwich layup.

The layup schedule used was chosen to be comparable to the layup used on the chine, keel and other areas where additional reinforcement is used at PYI. All core edges were chamfered at 45° to minimise fibre bridging and resin race tracking, the schematic for the chosen layup including the positions of the ply drops and fabric weights are shown in Figure 106. In Figure 106 the lengths (in mm) of each section of the layup are represented under the headers A, B or C. Header A represents the length from the resin inlet end of the mould, the header B represents the gap between the reinforcement where ply drops have been added in and C represents the length of reinforcement after the ply drop. If laid correctly, all lengths under the headers A, B and C add to the mould length of 1500mm. A glass mould was also chosen so that the mould surface flow could be monitored to assess the degree of lead-lag and to identify any variations in flow progression on both sides of the preform at the monolithic sandwich structure interface.

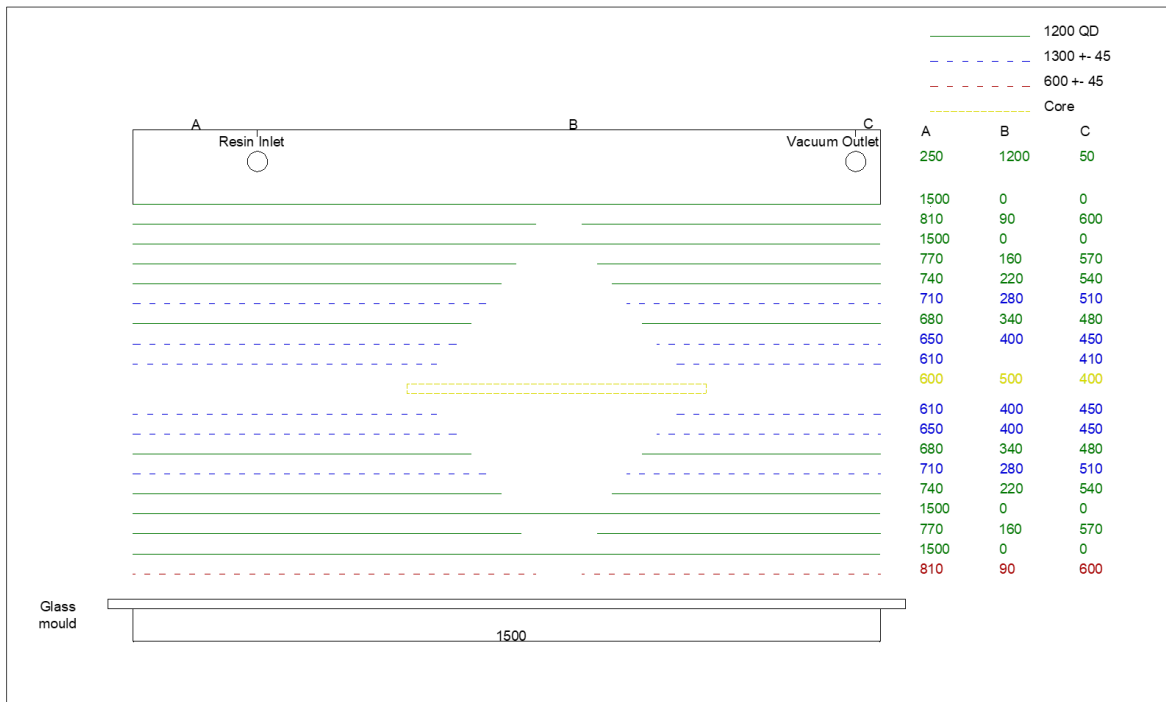


Figure 106: Laminate layup schedule.

A vacuum level of 25mbar was achieved before the infusion took place, the preform was held under vacuum for 60 minutes before the infusion was started. The resin used was the same as that used by PYI for the hull infusions, Crystic 703pa mixed with Butanox M50 catalyst at a ratio of 1.25:100 with an expected resin gel time of 240 minutes, see Appendix B. The core used was the same as discussed in the core groove research discussed in section 3.2.1, a 40mm thick high density foam with channels cut into the foam on the vacuum bag side at a 40mm spacing with holes through every 40mm to promote resin flow through the thickness of the core.

Cameras were used to monitor the resin flow velocity on both the mould and vacuum bag surfaces, the measured resin flow can be seen in Figure 107 and Figure 108. The resin inlet was closed 72 minutes after the start of the infusions process. The resulting reduced flow rate can be seen on both the vacuum bag surface and the mould surface.

The flow rate appeared to be comparatively slow in the monolithic region due to the lack of continuous distribution mesh. The flow rate was also substantially slower than the flow rate recorded by PYI when measuring infusion speeds, as detailed in section 3.2.1, on sandwich panels consisting of four layers of 1200gm² quad axial reinforcement. The flow rate increases at 38 minutes based on the visible location of the resin on the mould surface, this was caused by the resin reaching the core material which allowed for the resin to flow through the core

grooves and to begin impregnating the sandwich section ahead of the monolithic laminate being fully impregnated.

Using equation 2.1 the Capillary number can be calculated using the resin velocity in Figure 107, the resin viscosity of 1.6poise and the surface tension of polyester resin to be 35mN/m, the capillary number can be calculated as being between 8.5×10^{-4} and 9.5×10^{-5} (Wang, Zheng & Zheng 2011). The optimum capillary number to minimise void content was found to be between 1×10^{-3} and 1×10^{-2} which can be seen in Figure 10 (Gourichon, Binetruy & Krawczak, 2006). These results identify that the flow rate achieved during this experiment will result in a high degree of capillary flow and macrovoids.

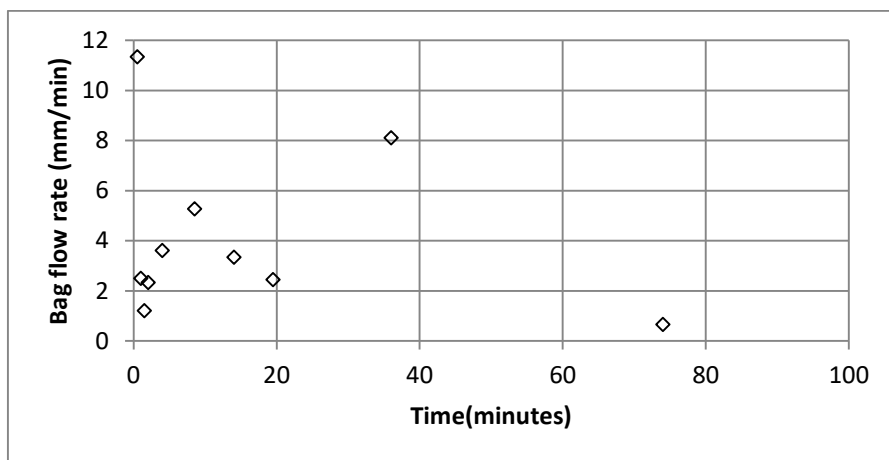


Figure 107: Bag surface flow rate.

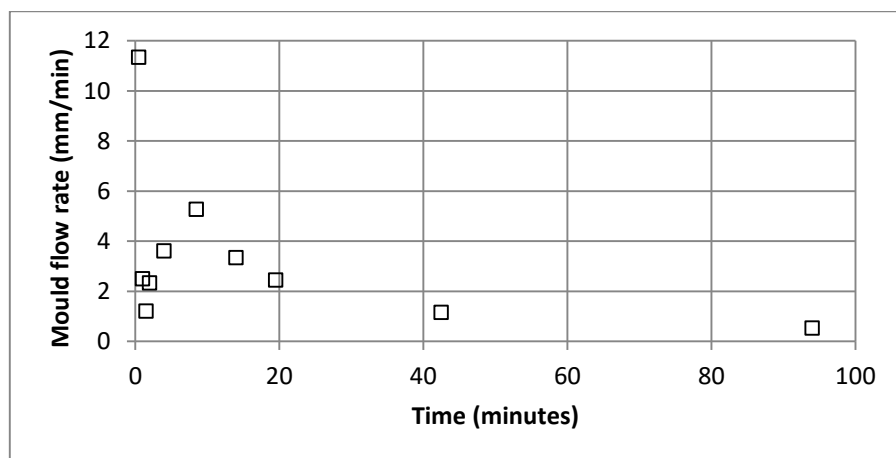


Figure 108: Mould surface flow rate.

Similar effects as those reported in Chapter 3 can be seen in Figure 109, where the core grooves and the lamina ply drops resulted in multiple converging flow fronts in the sandwich section as was expected.

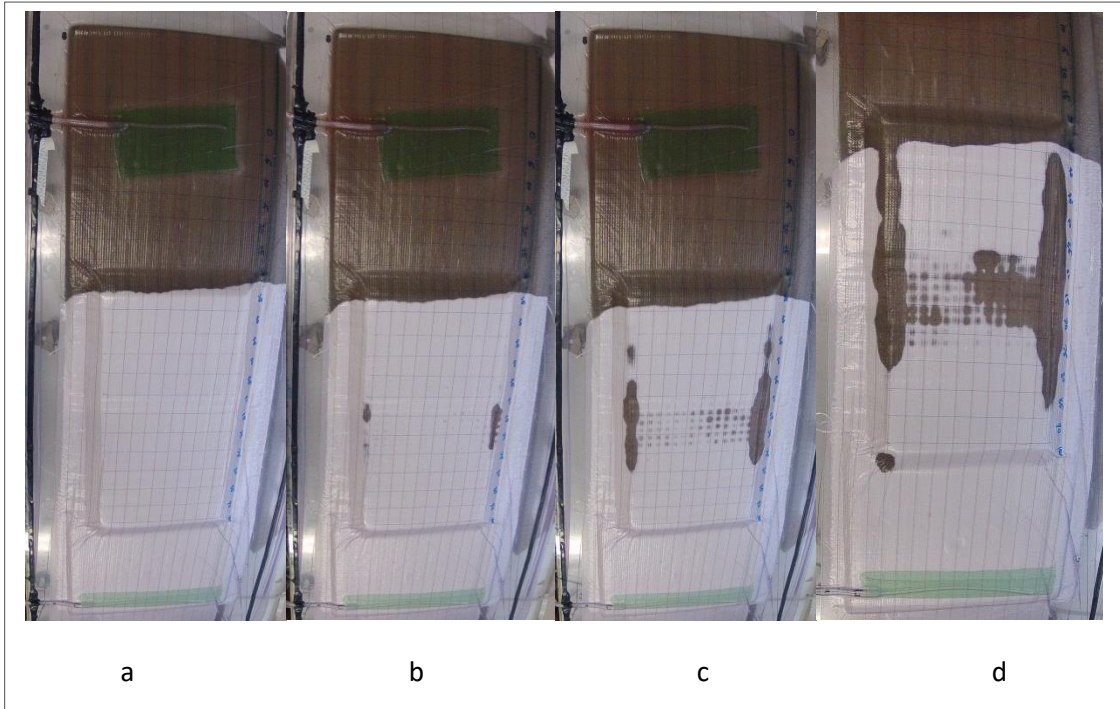


Figure 109: Flow front progression at a) 36:30, b) 46:00, c) 60:00 and d) 72:00 minutes.

Clear race-tracking can be observed either side of the core section, where a small 1.5 mm gap was present between the core and the core chamfer, as shown in Figure 110. The butt joints for the core material used by PYI are likely to cause small gaps between the core sections which will result in similar flow effects to that seen during this experiment. This has been identified by the author especially in curved areas of the hull, where the curvature of the mould cannot be mirrored by the core material which creates gaps. The resulting dry spot circled in yellow in Figure 111 is more exaggerated than the defects reported by PYI, however it is very likely similar effects occur above the chine due to converging flow fronts.

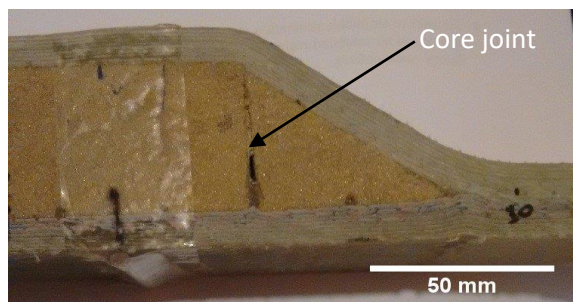


Figure 110: Core butt joint illustrating the gap between the core sections which can impact resin flow.

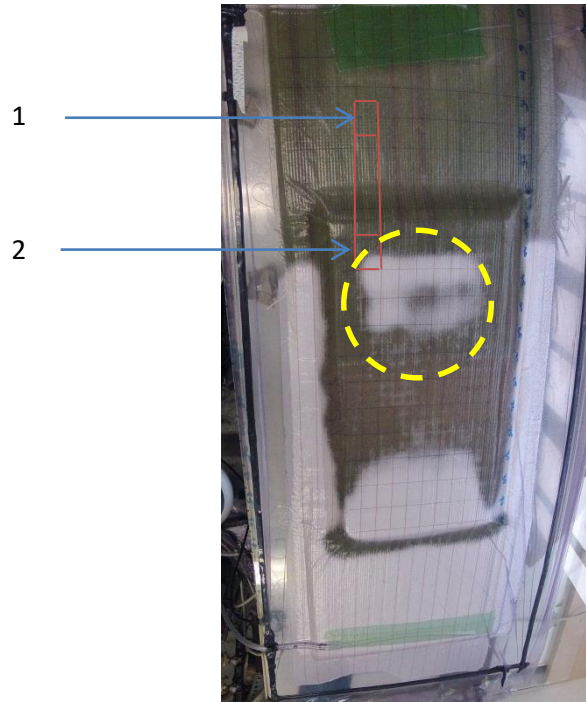


Figure 111: Core sample extraction locations.

Post infusion, locations along the flow path were chosen for more detailed analysis. Firstly, a section in the monolithic region was chosen as a comparative point to assess the quality of the infusion behind the flow front and to measure the extent that resin starvation had occurred. The second region chosen includes the flow front on the fully enclosed dry spot circled in yellow in Figure 111. The forward flow front was chosen due to the higher level of impregnation behind the flow front and the increased fibre thickness over the return flow front region. The extracted section from the sample can be seen in Figure 112, with the location of the extracted sections shown in red in Figure 111.



Figure 112: Extracted section of the component to be assessed.

6.2.3 μ -CT Analysis

The extracted sections were scanned using the 225/450kV hutch μ -CT scanner located at the University of Southampton, the μ -CT scanner settings can be found in Appendix F. Section two, located at the start of the sandwich section was reconstructed and analysed first, followed by section one, the monolithic section.

A similar process to that used in Chapter 4 for segmenting the different materials based on their density was used to identify the resin, fibres, core material and voids in the component. To aid the identification of each material, separate colours were assigned to the resin, fibres and voids, red, grey and green respectively, these were used to help identify and separate each of the volumes.

The results can be seen in Figure 113, where it is possible to identify the through thickness resin channels in the core. It is also possible to see areas of the resin distribution holes which contain voids, this identifies that these areas have not been fully saturated by the resin flow front.

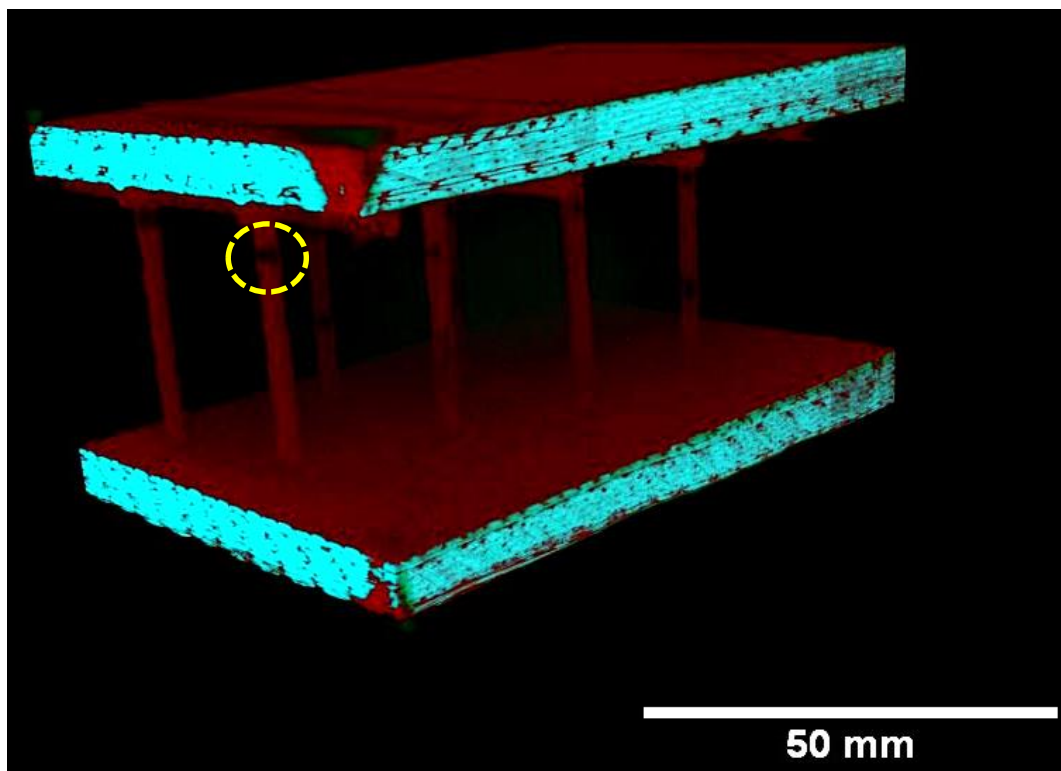


Figure 113: Section 2 of the extracted samples top and bottom laminates including core resin distribution channels.

Once the component had been lifted from the mould, it could be seen that the location of the core grooves on the mould surface had helped to fully saturate the mould surface whilst the bag surface was only partially impregnated with resin. It was therefore decided that the vacuum

bag surface should be focussed upon to analyse the flow front, void distribution and through thickness resin distribution.

The extracted and segmented bag surface laminate can be seen in Figure 114, where the top surface represents the core surface and the unseen bottom surface represents the vacuum bag surface.

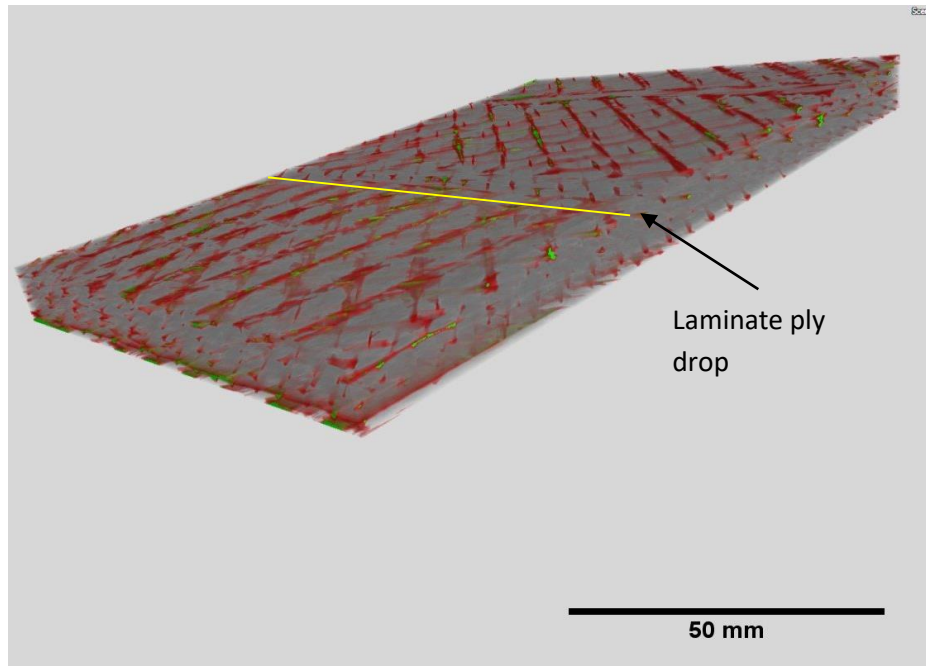


Figure 114: Vacuum bag surface laminate extraction.

The first ply drop on the core surface is visible half way along, allowing for a more exact location of the flow front to be recorded. The resin, void and fibre volume appears to show an even distribution of resin and voids across the entire top surface. A higher volume of green void volumes is visible at the end of the laminate, whilst on the top surface very few void volumes are clearly visible. However further extraction of the fibre volume allows for the true void and resin distribution to be examined.

Figure 115 shows an increase in voids in the same direction as the resin flow, with the highest number of voids at the point of the dry fibres at the flow front. The resin distribution though appears relatively uniform across the scan volume, with visible resin channels running between the 0° , $\pm 45^{\circ}$ and 90° fibre bundles. Further removal of the resin volume was required to clearly identify and examine the void distribution.

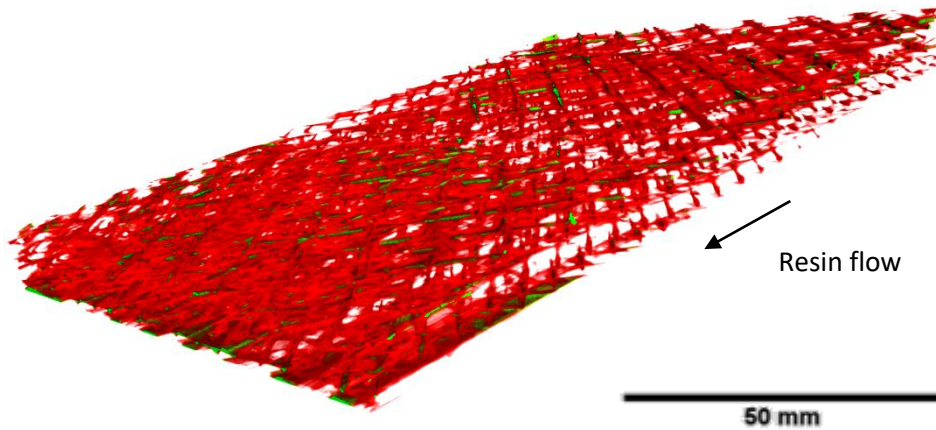


Figure 115: Resin and void extraction from the bag surface laminate.

Figure 116 allows the sole examination of the void distribution through thickness and along the advancing flow front. An increase in voids can be seen in the bottom left corner of Figure 116 where large elongated cylindrical voids located between the first and second fibre lamina positioned between the 0° fibres at the surface visible flow front. Through the thickness, a higher proportion of channel voids between the $\pm 45^\circ$ fibres exist. The intersection between the fibres creates the largest volume for the bubbles to become entrapped, the increased volume of voids forming at an intersection point suggests that a relationship between the stitch point and bubble entrapment may exist, however the stitch lines are not visible at the scan resolution used. The flow front images shown in Figure 103 identified a delay in void flow rate whilst passing a stitch point in the fabric. A higher surface tension or the requirement for an increased force to move from a larger volume to the constricted channel may be the cause of this delay.

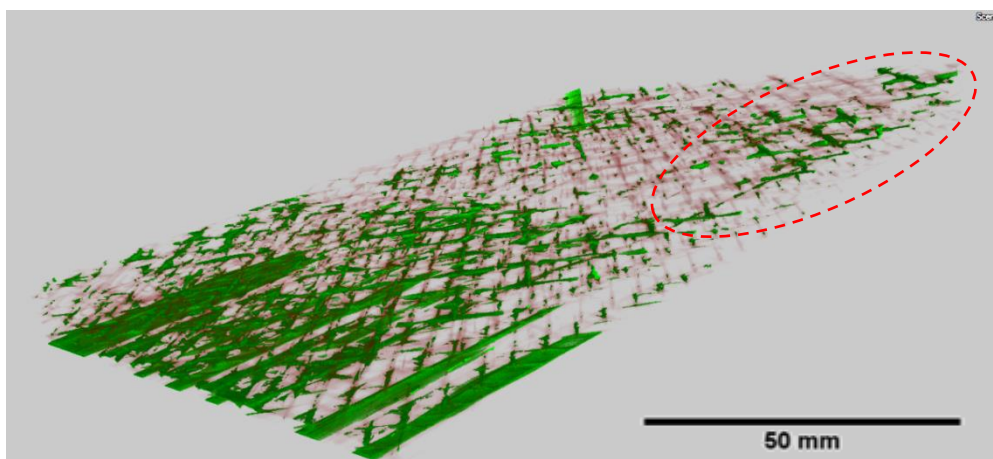


Figure 116: Void extraction from the bag surface laminate.

Circled in the top right hand corner in red are the macrovoids in the channel between the fibre bundles behind the flow front. Located between the $\pm 45^\circ$ fibres in the multi-axial fabric, a notable increase in density of channel voids can be seen in this orientation in comparison to the 90° and 0° fibres. Due to the dominance of the radial flow generated from the through thickness distribution core channels, the flow front in this region may contribute to this effect; however without a real time analysis further conclusions cannot be formed. Also of interest is the through thickness location of these voids, unusually located near the core surface where the through thickness flow will have originated from, a possible cause may be associated with a higher flow rate at the fibre-core material interface where the lack of fibre nesting may increase the permeability at the fibres.

To further assess the large elongated cylindrical voids on the bag surface, the outer two lamina were extracted from the μ -CT image and can be seen in Figure 117.

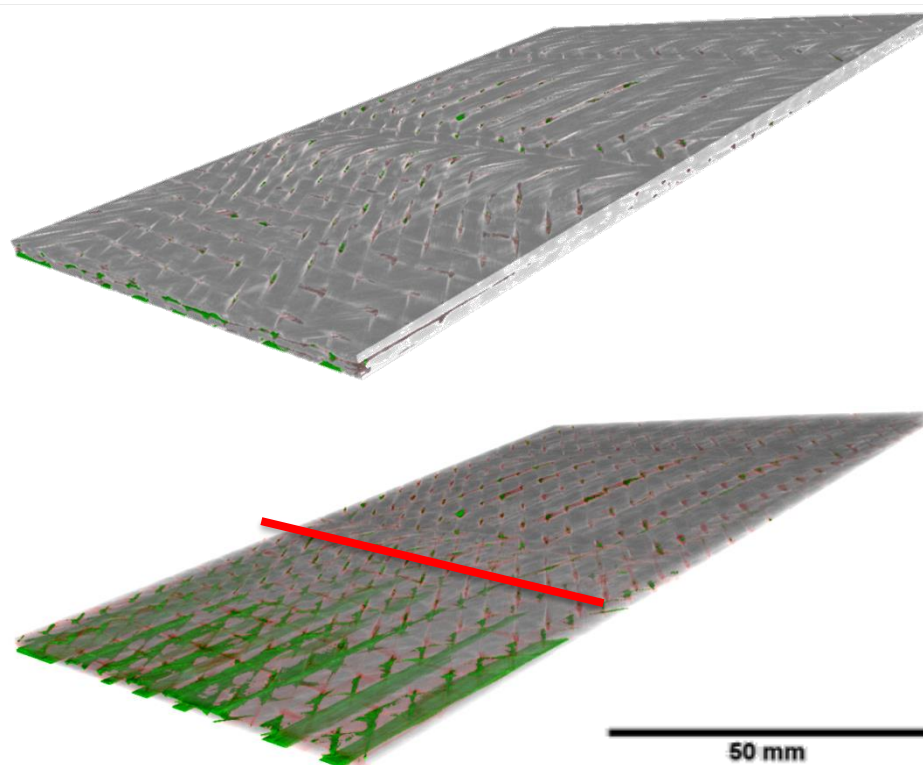


Figure 117: The first two lamina on the vacuum bag surface.

The location of the elongated voids are in front of the visible flow front on the vacuum bag surface shown by the red line in Figure 117, with the outer layer voids representing the dry spots between the 0° fibres on the bag surface which can be seen in Figure 118 where the 0° fibres are semi-saturated by the resin, whilst the channels between the fibres are visibly unsaturated.

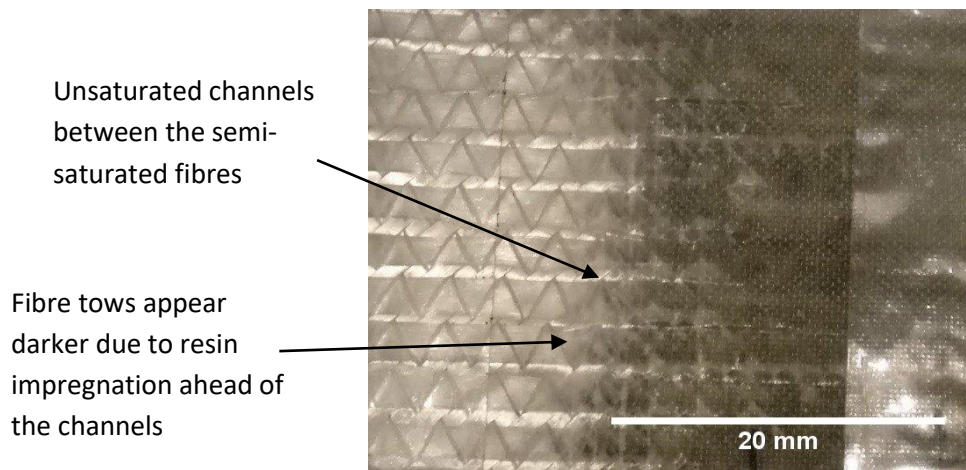


Figure 118: Vacuum bag surface flow front with the capillary flow dominance visible through the fibre saturation whilst the channel between the fibres are clearly unsaturated.

The first layer of voids between the first and second lamina follow a similar pattern to the outer surface. The faint volumes in red represent the resin volume in this region, suggesting a considerable flow front delay on the vacuum bag surface. A magnification of a singular void and resin volume identifies that a clear wicking process is occurring as the resin is drawn from the impregnated fibres into the inter-fibre channels as is shown in Figure 119. This suggests a reduced flow front advancing speed, which follows the suggested hypothesis of it being caused by the continually reducing flow front speed as the resin inlet is closed. Further examination of other microvoids identified similar characteristics where the resin has fully or partially enclosed the void volume. Once the voids are fully enclosed, the existence of the void is guaranteed due to the reduction in vacuum pressure post encapsulation, the mobility of the void is not restricted, however unless the voids are successfully washed out of the fibres, the void will remain in the laminate through to cure.

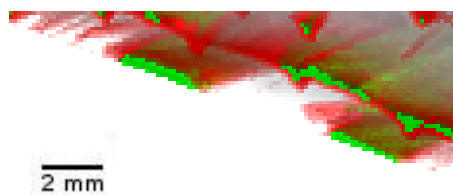


Figure 119: Individual fibre, resin and void volumes at the resin flow front.

The results from section two of the extracted sample have successfully recreated the voids which are expected in areas where the resin flow velocity is below the optimum leading to capillary dominated flow. The shape and distribution of the voids show similarities to the voids recorded from the core sample extraction from the A3 infusions at PYI. The monolithic section

of the infusions will now be investigated to assess the impact of closing the resin inlet and to investigate the voids which have resulted from any leaks in the preform.

Section one, from the monolithic laminate, was removed to assess the shape and location of the voids which had been generated through leaks in the preform after the resin inlet was closed. The sample location can be seen in Figure 111 and is located between 0.2 m and 0.25 m from the resin inlet. The effects of resin starvation and the quality of the infusion were investigated to compare the shape of the voids in a region which was not affected by a partial infusion.

Figure 120 illustrates the vacuum bag surface of the section and shows that a low level of porosity was visible between the fibre bundles, but no major defects could be seen on the surface.

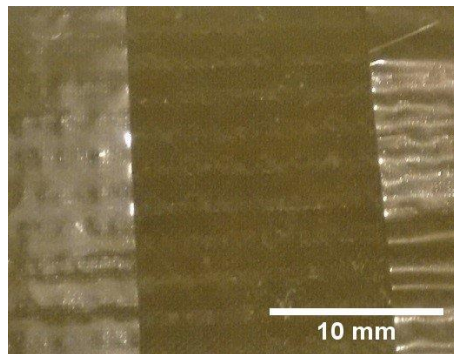


Figure 120: Vacuum bag surface photograph of section one post infusion displaying a low level of porosity between fibre bundles.

The volume reconstruction was segmented in the same way as section two, so that the fibres are displayed in grey, the resin in red and the voids in green. A high level of resin saturation can be seen by the even resin distribution, with very few voids visible on the surface of the component. Through the thickness of the component, a number of green voids can be seen between some of the fibre bundles.

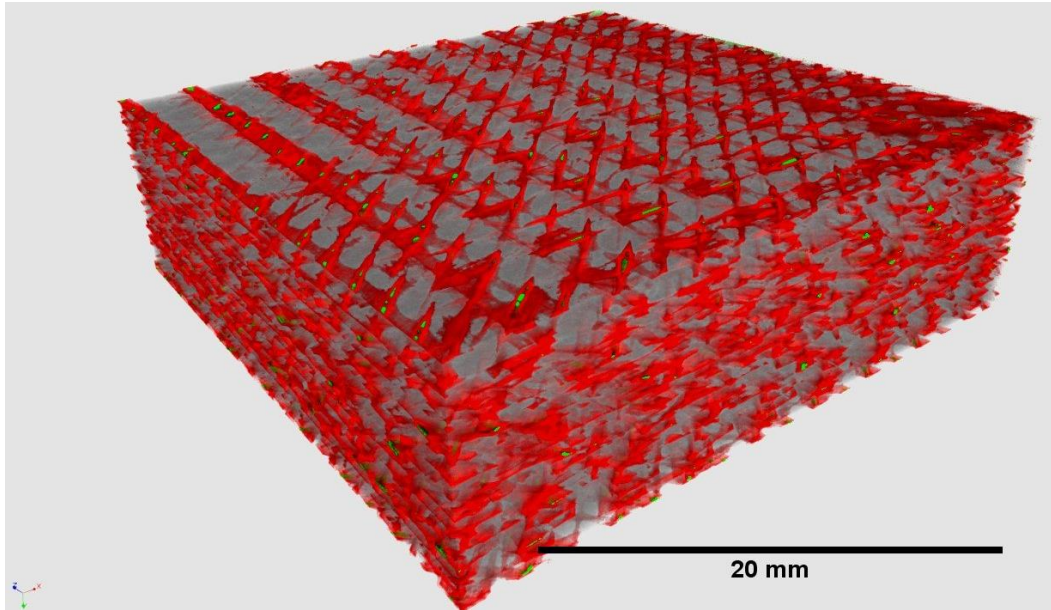


Figure 121: Section one of the resin flow experiment, volumetric reconstruction of the resin, fibres and voids.

One of the voids visible from the surface was identified and the fibre, resin and void volumes were extracted from the larger volume reconstruction. The location within the inter fibre bundle channel identified a fully resin enclosed void with no fibre/ void contact areas. The basic void structure is of a cylinder with additional volumes where the void has spread into the next layer of the NCF fibres. The void dimensions are 1.7 mm in length and have an average diameter of 0.61mm, with an irregular surface geometry. The location of the void between the fibre bundles, with no contact points to the fibre bundles suggest that the void has been created either through the generation of gases during the curing process or the introduction of voids through a leak in the preform.

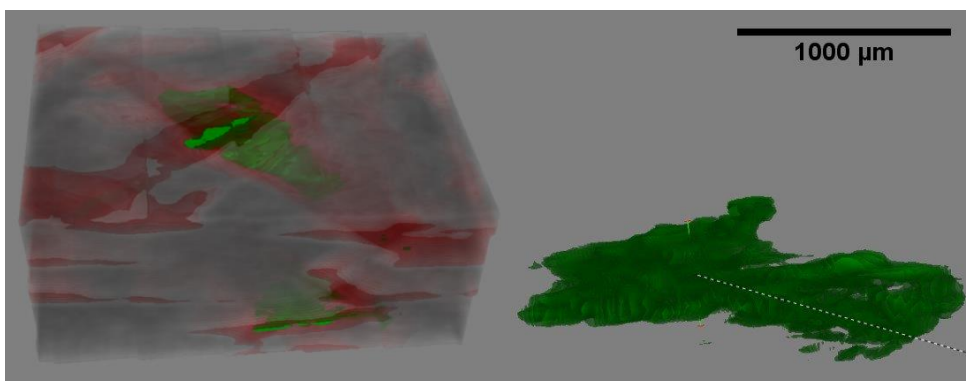


Figure 122: Section one μ -CT analysis of entire section, extracted void location and extracted void.

One of the experiments used to recreate Matsuzaki's (2013) approach to monitoring voids in the VARI process resulted in the investigation of bubbles drawn in through a leak during an

infusion. A simple infusion using two layers of quad axial NCF was set-up with a small leak in the vacuum bag. Figure 123 shows the bubbles filling the preform from the right, with the extracted area showing the voids flowing through the channels between the fibre bundles. Monitoring the void movement through the saturated lamina behind the flow front showed that the stitching holding together the NCF effected the void washout which caused the bubbles to flow through the thickness of the laminate at regular intervals as a stitch was encountered.

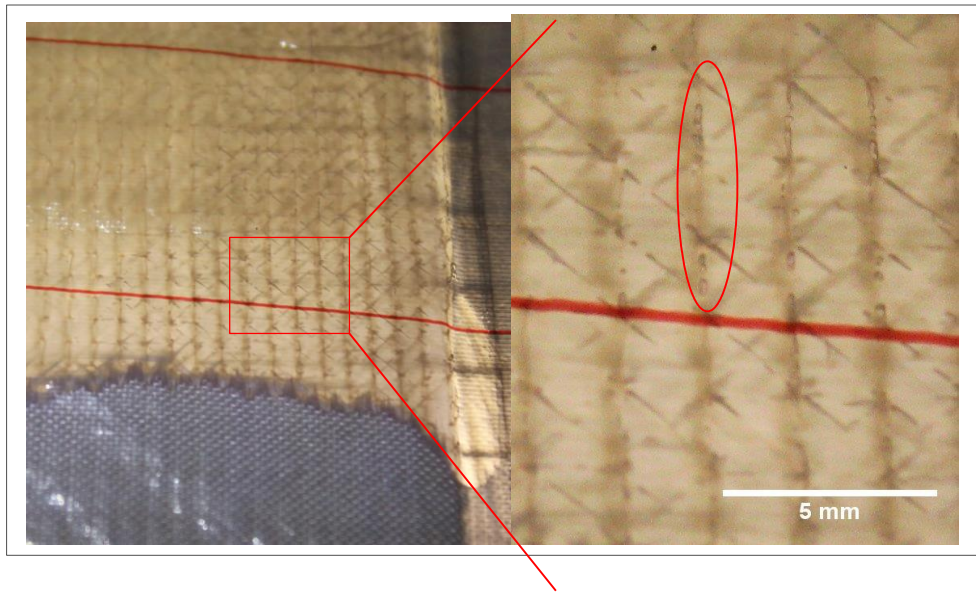


Figure 123: Bubbles drawn into a resin infusion behind the flow front caused by a leak, the voids visible in the right hand image fill the channels between the fibre bundles in the 0° , -45° and $+45^{\circ}$ directions.

The author believes that the location of the voids shown in Figure 122 illustrates a cluster of voids caused by leaks which has allowed bubbles to be drawn into the preform as is illustrated in Figure 123. Leaks in the VARI conducted by PYI are inevitable due to the scale and geometry of the infusions. The voids recorded in this section are therefore likely to represent voids which exist in the components produced by PYI which are never reported due to the lack of non-destructive testing (NDT) of the laminate quality.

6.2.4 Discussion

The results from the μ -CT scans have identified a number of voids behind and in front of the vacuum bag surface visible flow front. The capillary flow is of interest especially due to the full enclosure of the dry section on the vacuum bag surface. There is evidence to suggest that fibre layup and flow irregularities result in fully enclosed dry patches in and around the chine region of the hull infusions at PYI. It is therefore not unreasonable to make the hypothesis that the flow phenomena seen in this lab infusion could be replicating the full scale infusions and therefore one of the causes of the defects recorded by PYI.

The through thickness resin distribution and the location of the voids created by mechanical entrapment on the vacuum bag surface identifies the influence of the resin flow through the core material. The use of the core distribution grooves leads to the resin flow originating from the core material for both the top and bottom laminates of the sandwich sections. This effects the resin infusion strategy which is reliant on the location of the resin on the vacuum bag surface. This experiment has shown that a considerable difference between the location of the mould flow front, core flow front and vacuum bag surface flow front can exist. These results agree with the findings in Chapter 3 where the risks of the irregular flow front were first discussed.

The experiment has highlighted the importance of the positioning of the core distribution grooves as a key resin flow feature. Due to the core grooves being located on the mould surface of the experiment, the mould surface achieved a higher degree of fibre saturation than the vacuum bag surface. The infusions at PYI position the core grooves on the vacuum bag surface to avoid any reduction in surface finish on the outer skin. This suggests that the dry sections above the chine at PYI are partially caused by the core grooves being located on the vacuum bag surface. Rotating the core so that the core grooves were on the mould surface would aid resin distribution on the mould surface and switch the converging flow front and resultant dry areas to the vacuum bag surface which would be visible to the laminating team. Transferring the dry area to the visible surface would allow the laminating team to take proactive action to saturate the fibre before the resin cures rather than having to repair the post cured section.

The experimental set-up involved partial processing of the composite component which coupled with the three-dimensional μ -CT analysis has allowed a unique insight into the creation and shape of voids on a partially infused component. The features used to generate the defects are unrealistic on a full scale infusion. Firstly, the introduction of lamina ply drops every 50 mm will have changed the fibre permeability, compaction and nesting of the laminate. Secondly the transition from monolithic to sandwich and back to monolithic within 1.25 m of the resin inlet will have affected the resin flow progress through the preform. Finally, the use of distribution mesh, core grooves and core distribution holes were arranged differently to the layup used by PYI. The resin distribution mesh was only added to a small section of the monolithic section, and the core grooves were positioned on the mould surface. The lamina schedule was used because the author wanted to avoid the artificial injection of voids, in order to allow the preform architecture to generate the voids, thereby replicating the larger infusions at PYI. The approach succeeded in creating an irregular flow front, mechanical entrapment, leaks in the preform and the lead-lag between the mould and vacuum bag surfaces. Further experiments could be

conducted where each feature affecting the resin flow could be tested individually. An experiment could be set-up where four radial resin injection points are tested to replicate the infusion pattern created by the distribution channels through the core material. The location where the flow fronts converge could then be extracted post cure to assess the void pattern and distribution which would test the link between core distribution holes and voids, as was discussed in Chapter 3 and can be seen in Figure 44.

The approach taken to partially process the component by closing the resin inlet before the infusion completed, resulted in an unexpected level of resin progression after the inlet was closed and the resin cured. Figure 124 shows the resin position at 72 minutes, when the resin inlet was closed, and the resin location post cure. The level of fibre saturation in the sandwich section increased substantially between the two images, showing that the resin continued to flow for a considerable time after the inlet closed. This will have been affected by any leaks in the vacuum bag and the vacuum infusion tape joins to the mould surface, however leaks are expected during a VARI. The continued resin flow resulted in saturation of all but the outer two layers of reinforcement. It had been expected that when the flow inlet was closed, an entire section of the laminate would be dry so that a through thickness assessment of the flow front could be made. However the partial infusion of the reinforcement has added an additional similarity to the defects found at PYI, where the result in Chapter 4 identified the defects locations to be in the outer reinforcement layers, not through the thickness to the core.

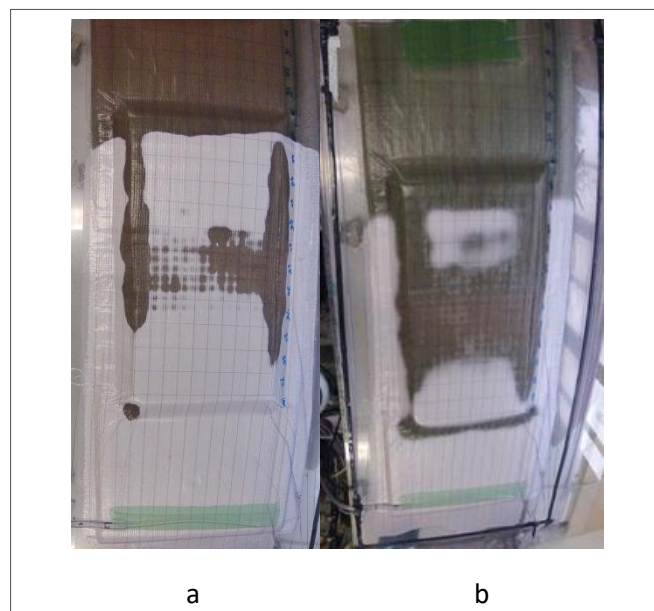


Figure 124: Resin flow front location at a) 72 minutes when the resin inlet was closed and b) once the resin had cured.

Due to the capillary flow between when the resin inlet was closed and when the resin cured, the flow front reconstruction has enabled the visualisation of the resin flow out of the fibre tows into the channels seen in Figure 119. The visualisation of this process helped to identify the fact that a low resin velocity results in a low capillary number and therefore the creation of macrovoids. The shape of the voids that are circled in Figure 116 show similarities to those found in Figure 64 where elongated voids were found on the outer layer of reinforcement of one of the PYI core samples. This is further evidence that the experimental replication of the voids in the outer layer of the laminate have been created in a similar way to the defects recorded at PYI. This also suggests that a converging flow front does exist on the mould surface above the chine of the hull infusions at PYI, partially explaining the higher level of porosity recorded in this area.

The requirement to allow the resin to cure before being able to scan the component also adds additional complexity and variability to the experiment. The ability to control or remove the curing process to eliminate the generation of additional voids through the release of VOCs would increase the repeatability of the experiment. The requirement to cure the component before the void analysis takes place also limits the ability to monitor the resin flow front and voids at different stages of the process. Ideally the component would have been partially processed to different points, similar to the approach taken by Centea and Hubert (2011), this would allow for the development of the flow front and void mechanisms to be monitored throughout the process. The approach used by Centea and Hubert involved cooling the preform by removing the component from the oven used to process prepreg composites. In order to remove the curing process, non-catalysed resin could be used and cooled rapidly once the infusion reached the desired point for further analysis. Cooling polyester resin by 11°C doubles the viscosity of the resin, this could allow for the resin infusion to be slowed enough to capture the features without curing the resin. The exponential relationship between temperature and the viscosity of polyester resin means that a further 7°C cooling would double the viscosity again. The size of the experiment required to introduce the variable laminate schedule and irregular flow front would require the cooling of the sample to be done in-situ. A smaller experiment would need to be created which would be moved in its entirety to the prepreg laminate freezer whilst the vacuum is maintained, this would remove the mechanical entrapment and irregular flow front from the experiment.

6.2.5 Conclusions

The void re-creation experiment has successfully captured a partially infused section of a complex laminate structure. The process used to create the unsaturated section of the

component utilised features in the laminate layup which exist on the infusions undertaken by PYI, reducing the requirement to artificially generate the defects. The partial processing on the component resulted in a high level of capillary flow between the point when the resin inlet was closed and the resin cured. This allowed for the resin flow front speed to drop to ensure that capillary flow dominated at the flow front which resulted in macrovoiding and the visualisation of the resin flow from the fibre tows into the unsaturated channels. The experiment has captured the resin wicking out of the fibre bundles into the dry channels, however the resolution achieved by Centea and Huber (2011) has not been replicated due to the size of the sample being scanned and reconstructed.

The experiment identified the relationship between the location of the core grooves and the level of defects. The additional resin distribution on the side of the core with the distribution channels resulted in the complete saturation of the reinforcement on this surface. The reinforcement on the opposite side of the core suffered from a lack of resin flow which resulted in the large dry section of reinforcement. These results suggest that PYI should investigate a way of adding resin distribution channels to both sides of the core material to reduce the level of variation between the flow locations on the mould versus the vacuum bag side of the core.

The approach to analysing the resin flow front has resulted in the review of the flow front at only one stage on the infusion under very specific conditions where capillary flow dominates and the component has fully cured. To gain further understanding of the resin flow, void creation and movement, the flow front at varying stages of the infusion needs to be captured. This could be carried out by partially processing the same layup to multiple stages, closing the resin inlet at different times and allowing the resin to cure or by recording the flow front during the infusion before the resin cures. The partial processing of different samples would require an increased level of control over the variability of the infusion to ensure that the comparison of the flow at different states were comparable. This could be difficult to achieve with a large complex VARI component. An in-situ μ -CT investigation should be examined to explore the possibilities of pausing the resin infusion for long enough for the scans to be completed before the next stage of the infusion takes place.

6.3 In-situ μ -CT Flow Analysis

The results of the void re-creation and μ -CT analysis have identified the benefits of utilising the three-dimensional characterisation possibilities of μ -CT scanners to review voids at the resin flow front. The restrictions applied by the partial processing of the infusions restrict the review to only one stage of the process. An in-situ experiment within the μ -CT scanner at the University

of Southampton would allow multiple stages in the infusion process to be reviewed. This section reviews an experimental set-up to allow for a three-dimensional characterisation of the VARI process.

Partial processing has been used to perform initial studies into similar techniques described by Centea and Hubert (2011) for out of autoclave prepreg infusions to the more complicated VARI. The results identify the need to remove the effects of allowing the resin to cure and to increase the controllability of the resin flow front to remove the effect of additional capillary resin flow. An in-situ experiment is required to partially process the component whilst minimising the impact on the processing parameters. The effects of the experimental set-up on any processing parameters will need to be monitored and the effects quantified in order to validate the reliability of the experimental results.

This experimental solution provides a unique three-dimensional resin flow and dynamic void analysis allowing for the development of the understanding of the micro-structural process involved with fibre saturation, void creation and mobility during a VARI infusion.

6.3.1 In-situ μ -CT Flow Experiment Objectives

The objective of this study is to record the dynamic impregnation behaviour of the resin and gases associated with VARI, and to document the development and movement of voids as well as fibre saturation and the dual scale flow phenomena.

6.3.2 Vacuum Assisted Resin Infusion Partial Processing

The limitations associated with μ -CT scanning times require the infusion process to be paused so that the hundreds of angular views required to generate the three-dimensional reconstruction can be taken. The review of μ -CT techniques in Chapter 2 identifies the relationship between scan resolutions, material density and scan times. In order to achieve the desired resolution to monitor the macro and micro level flow, the relationship between scan times and resolution needs to be optimised to minimise the resin flow caused by capillary action during the scans.

The process of allowing the sample to cure whilst partially impregnated resulted in a capillary dominated flow at the flow front due to the vacuum pressure being maintained during the curing process. A method to maintain compaction whilst restricting the resin impregnation is needed to examine the microstructural evolution of the flow front as well as a preform shape to maximise μ -CT resolution and contrast.

Centea and Hubert (2011) used μ -CT techniques to monitor the resin flow properties in and out of autoclave prepreg infusion. They used an oven and freezer to partially process the prepreg samples before removing a smaller section of the component in order to reduce the material density being scanned and therefore increase resolution and decrease scan times. The samples were processed at 25°C for 60 minutes before the temperature was increased to 85°C for a further 180 minutes. Samples were partially processed to the times listed in Table 8 before being placed in the freezer to minimise additional resin impregnation.

Laminate	1	2	3	4	5	6	7	8	9	10
Time (min)	0	15	30	45	60	80	93	104	110	180

Table 8: Partially processed laminate and their total processing times (Centea and Hubert 2011).

Centea and Hubert (2011) successfully identified and recorded the impregnation and void reduction processes at these ten stages, identifying the gas evacuation pathways for a monolithic four layer biaxial carbon epoxy layup (Figure 125). The process of re-freezing the partially impregnated laminate not only allows for longer scan times but also allows smaller volumes to be extracted from the sample to increase the attainable resolution from the μ -CT scan. The reduction in sample volume reduces the risk of higher temperatures in the μ -CT scanner decreasing the resin viscosity and affecting the impregnation by reducing scan times. The increased process control achieved by Centea and Hubert is gained through the utilisation of the oven to manage the resin viscosity and impregnation rate.

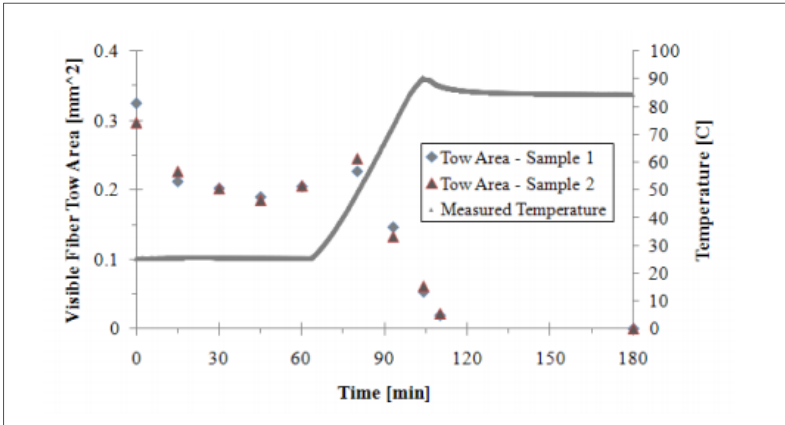


Figure 125: Visible fibre tow area and cure cycle temperature with processing time (Centea & Hubert, 2011).

The methodology of reducing the resin temperature to pause the infusion process is limited in the application of a VARI process. The vacuum pressure on the component would need to be maintained during the cooling process, changing the resin viscosity which would affect the dual scale flow of the resin. The changing viscosity and temperature would affect the dual scale flow

and therefore not reproduce a standard infusion. This methodology was therefore deemed unusable for the VARI process; instead the infusion process would need to be carried out within the μ -CT scanner and the resin impregnation paused to allow for the μ -CT scans to occur.

μ -CT scan resolutions are not only affected by the size of the sample being scanned but also the shape. An object which has a 1:1 aspect ratio minimises the required scan time due to the greater thickness of any of the scanned points being the limiting factor to the resolution and required scan time. It is therefore necessary to devise a preform shape that would minimise the required time taken to achieve the required resolution and contrast, whilst achieving a rectilinear flow progression. Due to the 360° rotation of the object being scanned and the fixed X-ray strength for the full rotation, a 1:1 aspect ratio in the x-y axis provides the optimal preform shape for scanning. Any reductions in unnecessary material also reduce the required scan times due to the contrast and resolution being reliant on different attenuations of the X-ray, which are proportional to the material density and atomic number (Djukic et al., 2013). A cylindrical mould tool would meet the required 1:1 aspect ratio to optimise the μ -CT scan times, whilst also allowing for a rectilinear flow to be created. To meet these requirements a thin section cylindrical tube mould was used to provide the desired aspect ratio, minimal material density and the opportunity to create a rectilinear flow front.

In order to achieve a comparable rectilinear flow experiment, the mould diameter was chosen to be 60 mm providing a fibre width of 160 mm which is comparable to the permeability experiments conducted by Arbter et al. (2011). The mould used was an Acrylic extrude tube, with an outer diameter of 60 mm and an inner diameter of 54 mm.

The infusions conducted at PYI and the infusion completed earlier in this Chapter identified the risks of variable permeability around a preform. Laboratory scale permeability experiments often suffer from race tracking effects down the side of the relatively small moulds which alters the flow front shape and flow rate. The use of a cylindrical mould could remove any edge effects, by wrapping the fibres continuously around the mould. This was initially tested, however, the results found that a continuous lamina wrap around the mould resulted in a high level of wrinkling, as is shown in Figure 126. The required compaction on the continuous wrap was unattainable and difficult to repeat to remove these wrinkles, it was therefore decided that a discontinuous layup would be used to allow the reinforcement to move under vacuum and the edge effects would be monitored during the infusions.

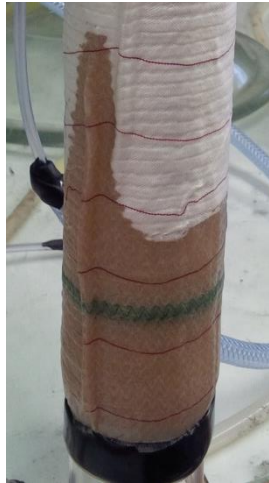


Figure 126: Cylindrical infusion mould showing the effects of using a continuous lamina wrap.

To evenly distribute the resin, spiral cable would be wrapped around the base of the cylindrical mould on top of the dry fibres. Spiral cable would also be laid at the top of the mould to create an even vacuum distribution. The proposed experimental set-up can be seen in Figure 127.

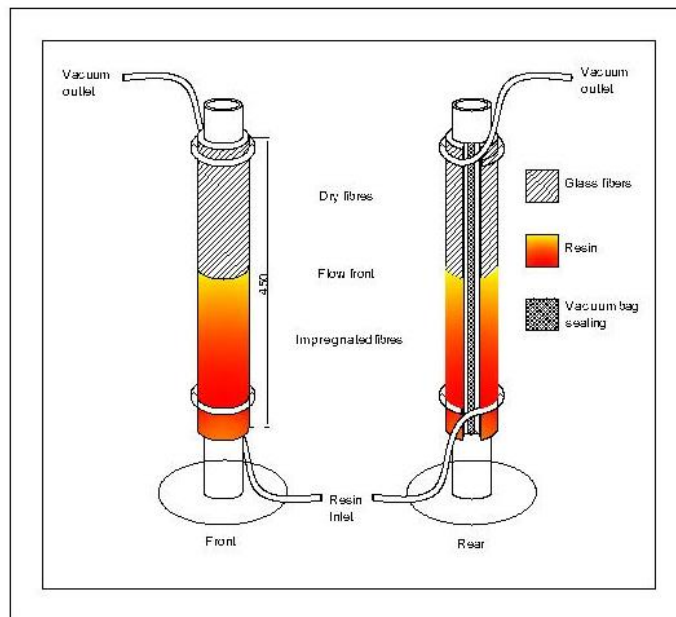


Figure 127: μ -CT in-situ VARI experimental set-up.

A number of variables needed to be controlled to ensure the resin impregnation scans represented a normal VARI impregnation. To pause the resin progression the resin inlet and the vacuum source would need to be closed. This would result in variations in preform thickness and fibre resin consolidation as well as an increased level of capillary flow as was seen earlier in the Chapter. Centea and Hubert (2011) reports removing the vacuum source during the

experiments which suggests expansion of the laminate may have taken place due to vacuum bag leaks or valve leaks, it is unlikely that the preform and the vacuum attachment point were 100% leak free. For the complex VARI set-up being used for this experiment, it is known that the vacuum valves and the vacuum membrane being used will not hold a full vacuum for the required scan time. It was therefore decided that the preform thickness would need to be controlled whilst the vacuum is removed and the sample was being scanned.

A technique used to build composite tubing which utilises shrink wrap tape to seal and apply compaction to the laminate subsequent to wet layup was tested. This technique was trialled over the top of the vacuum bag on the cylindrical mould whilst held under vacuum. The tape was wrapped around the entire preform from injection point to vacuum outlet. Maintaining vacuum pressure, a heat gun is used to shrink the tape tightly around the component. The shrink wrap tape demonstrated the ability to apply an even compaction across the laminate, however the laminate thickness variation expected with a VARI would be restricted. The effect of the fibre compaction needs to be tested against an unrestricted VARI preform to assess the change in permeability and therefore resin flow velocity.

Applying the shrink wrap tape around a normal vacuum bag created wrinkles and an uneven vacuum bag surface around the dry fibres. Similar to the fibre wrinkles seen in Chapter 4, wrinkles in the vacuum bag will change the permeability and can create flow front irregularities. The wrinkles can also cause localised variations in fibre compaction which will alter the resin flow rate.

In order to create an even pressure around the fibres, an elastic vacuum membrane which would leave a smooth surface finish for the shrink wrap tape to be applied to whilst under vacuum needed to be found. The vacuum membrane would need to be continuous with no seam running along the surface of the fibres. Latex has been used as a versatile mould material and is used as bladder material in composite mouldings. Initial tests showed positive results, with a smooth vacuum bag surface achieved.

In order to examine the effects of the alterations to a standard permeability analysis, three experiments were conducted in parallel to examine the impregnation rates of a standard flat plate infusion, a VARI on a vertically mounted cylinder and a shrink wrapped vertically mounted cylinder infusion. The experiment would allow the quantification of any variables introduced by the alterations to the standard VARI laboratory experiment.

The experimental set-up comparing the vertical flat plate and vertical cylindrical mould can be seen in Figure 128. The laminas were all cut to the same dimensions, 450 mm in length and 180 mm in width. The resin inlet and outlets were arranged at the same location for the three infusions, with the resin inlet source for all three experiments coming from the same resin mixing pot. The vacuum outlets were also linked to the same vacuum pump so that the same vacuum pressure would be applied to the three preforms.



Figure 128: Vertical cylinder VARI trials against a flat rectilinear permeability experiment.

The flow front locations were recorded at 50 mm intervals during the infusion for each of the three experiments. The results are shown in Figure 129, where the similarity in resin flow location between the three preforms can be seen. Although small variations in impregnation velocity were seen, the similarities between the three set-ups suggest that the effects of limiting the compaction variations have had a small effect. The permeability benchmarking study discussed in the literature review has shown the high variance that can be recorded using permeability experiments for the VARI process. The second permeability benchmark study resulted in a reduction in the variations recorded in permeability experiments to 25%, suggesting a comparable level of variance to this study. It was therefore decided that the effect of the shrink wrap tape on the resin flow velocity could be ignored for this experiment, and an

assumption made that any variations during the infusion are in line with the variations which are normally experienced when conducting permeability tests and infusion industrial VARIs.

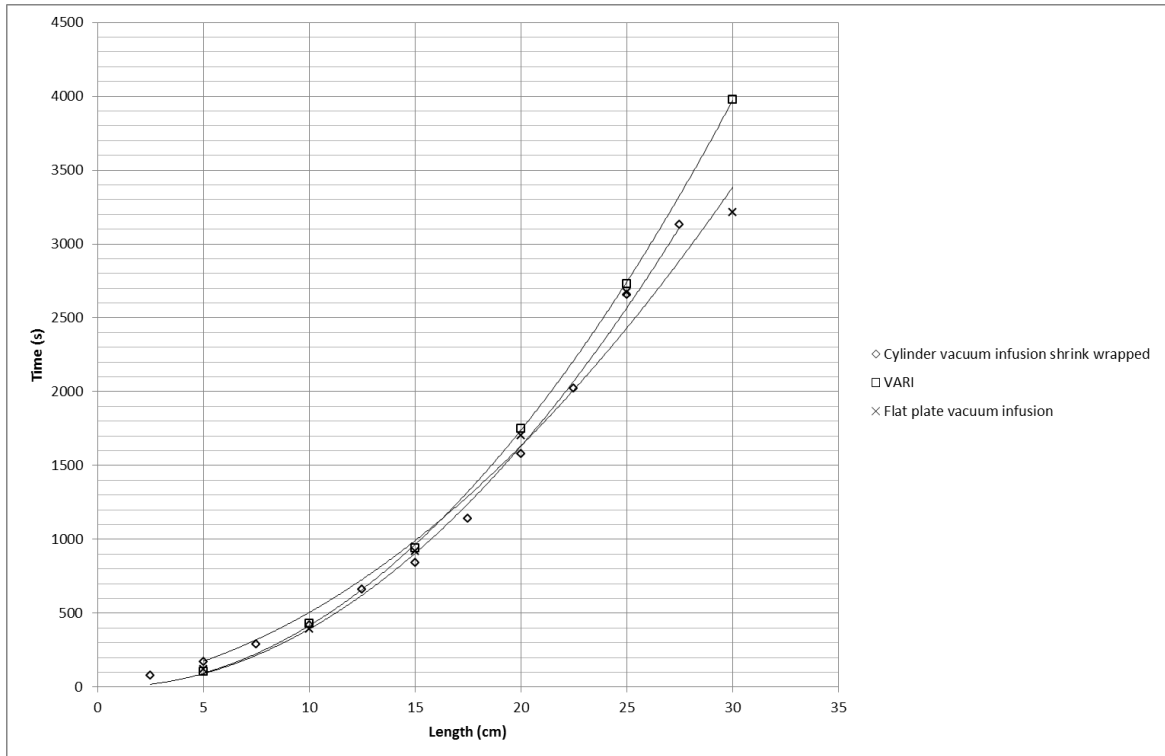


Figure 129: VARI, flat plate and shrink wrapped infusion times.

The experimental set-up within the μ -CT scanner can be seen in Figure 130. The vacuum outlet hose was fed back through the centre of the mould so that the inlet and outlet tubes were located together at the foot of the μ -CT scanner. The inlet and outlet hoses were also led outside of the scanner so that control of the vacuum pressure and resin inlet could be adjusted at all times even when the μ -CT was active and the doors were locked.

The fabric used for this experiment was the same Q-E 1232 g/m² quad axial NCF, provided by Saertex and used by PYI. Laminas were cut at 180 mm by 450 mm for the first layer with an increased width of 6mm added for each layer to account for the increasing diameter. The cylindrical moulds were then mounted on the stand at the foot of the scanner so that a full 360° rotation could be achieved without any restrictions. In order to locate the desired scan locations, a physical marker is required on the sample, elastic bands were located around the outside of the shrink wrap tape at 50 mm intervals to allow for identification of the chosen scan points at 150, 200 and 250 mm, Figure 131. The field of view for each scan was set at ± 50 mm for the chosen scan location to allow for an irregular flow front as well as to allow for any through thickness flow front variations to be captured.

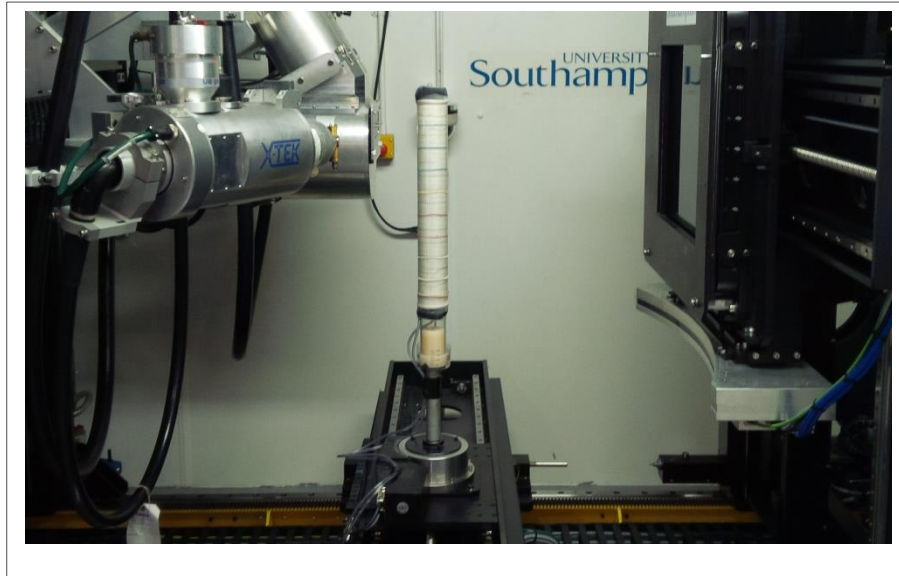


Figure 130: μ -CT in-situ VARI experiment.

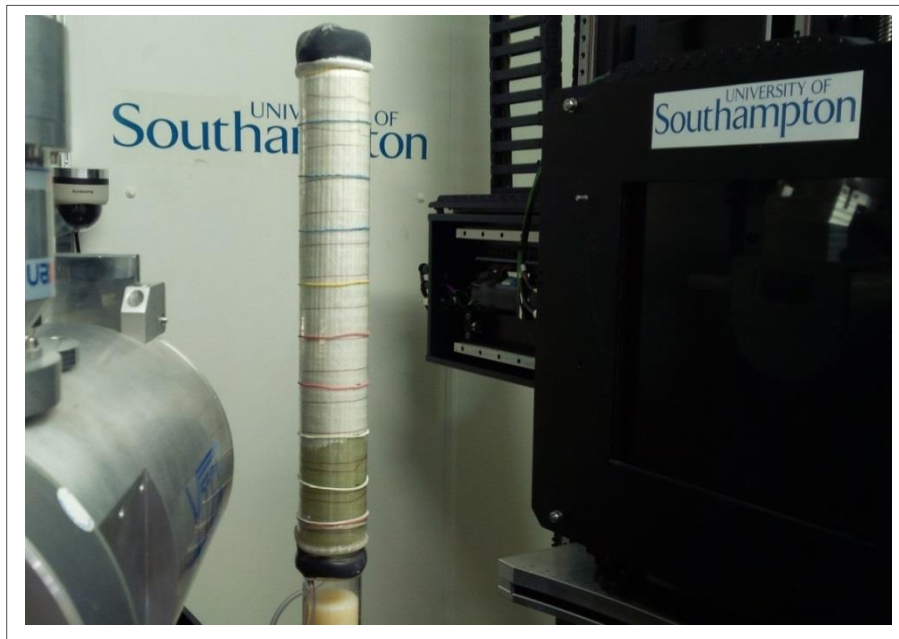


Figure 131: μ -CT in-situ VARI experiment elastic band locations.

The first run of the in-situ experiment was carried out to establish the contrast levels achievable and to assess the suitability of the chosen experimental set-up. The designed mounting platform, mould and inlet/outlet design were all tested to ensure no restriction to movements or mould movement existed before the trial could start. All processing variables were kept the same as those used during the trial runs. The resin system used was consistent with previous experiments, where Crystic C703pa resin was mixed with Butanox M50 catalyst at a ratio of

1.25:100. A gel time of 240 minutes was selected to provide enough time to conduct three scans of the sample before the resin gels.

The achieved resin progression is shown in Figure 132, where it can be seen the progression was considerably slower than achieved in the trial runs.

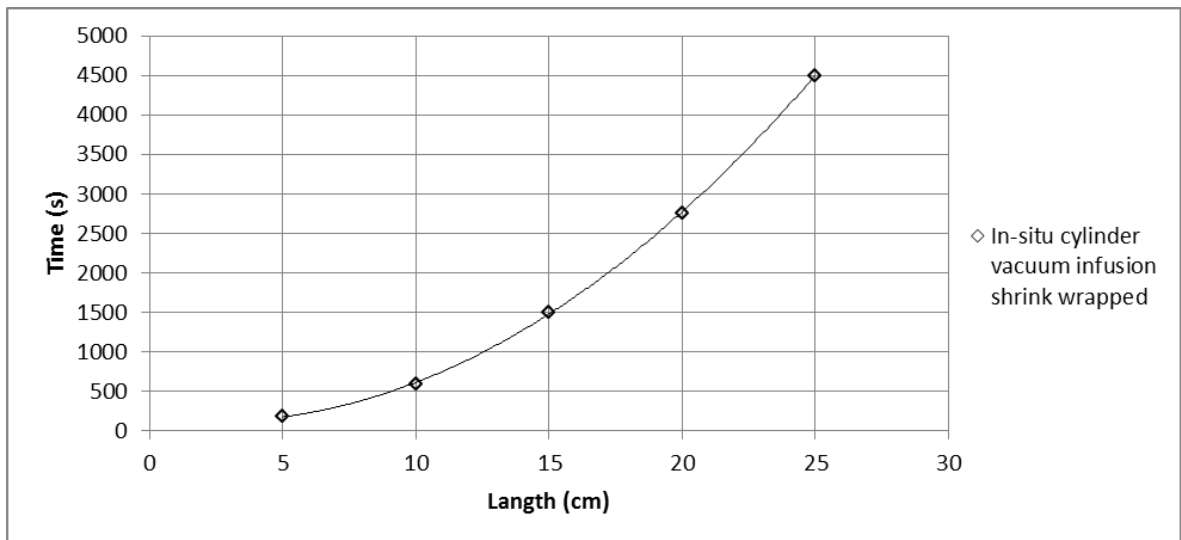


Figure 132: In-situ μ -CT experiment speed.

The infusion rate during the scans was significantly lower than previous experiments with identical set-ups. No leaks were revealed at any point in the system with an absolute pressure of 30 mbar maintained at the vacuum pump. Due to the slowed infusion rate the resin reached its gel point before the third scan could be completed, limiting the analysis that could be conducted on the first sample.

The mould set-up including base mounting, inlet and outlet tubes all worked successfully to allow a full 360° stable rotation whilst allowing the vacuum pump and resin inlet to be controlled from outside the μ -CT room. The initial scans allowed for a review of the effects that wrapping the laminate around the mould had on inter tow packing, fibre compaction and resin and gas evacuation channels.

The latex vacuum bag achieved the results required of the elastic membrane; however a vulnerability to tearing was found during the experimental set-up. It was decided that due to the cost of time in the μ -CT scanner, the risks associated with the vacuum bag failing during one of the scans was too high and a replacement needed to be investigated.

To rectify the durability issues experienced with the latex vacuum bag, a heat shrink tube, similar to the shrink wrap tape was chosen as a replacement vacuum bag. A 76 mm diameter

polyolefin tube with a shrink ratio of 2:1 and a wall thickness of 0.7-1.46 mm depending on degree of shrinkage was chosen. The tube was positioned over the reinforcement and mould before heat of 80°C was applied to the bag using a heat gun causing the plastic to shrink around the reinforcement and mould, as can be seen in Figure 133. Shrink wrap tape was also applied to ensure the fibre volume fraction and consolidation was maintained during the vacuum shut-off stage.

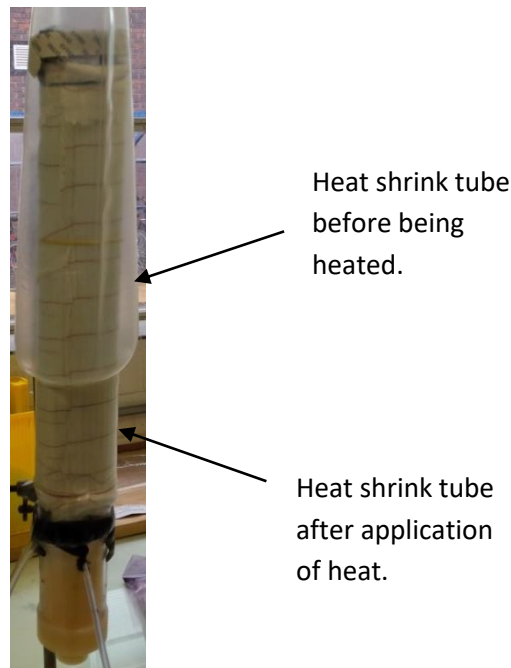


Figure 133: Heat shrink vacuum bag application to the cylindrical mould for the μ -CT experiment.

The laminate schedule can be seen in Figure 134, which shows that six layers of the Q-E 1232 g/m^2 , the material datasheet can be seen in Appendix B, were wrapped around the cylindrical mould. Six layers of reinforcement were chosen to remove the boundary condition effects of the mould and vacuum bag on the top and bottom lamina. The four layers of reinforcement left would then provide the ability to monitor through thickness flow front progress and the interaction between the reinforcing layers.

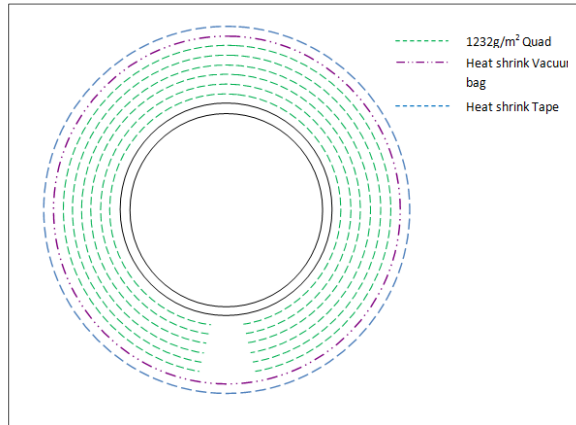


Figure 134: In-situ μ -CT laminate schedule.

Due to the time restrictions of the resin curing during the experiment, it was decided that the catalyst should not be mixed with the resin for this experiment. The viscosity of Crystic 703pa catalysed by Butanox M50 is 1.583 poise, whilst the viscosity of non-catalysed Crystic 703pa is 1.6 poise. The difference of 1% change in viscosity is within the viscosity changes expected under normal industrial infusions and was therefore accepted as a deviation from the normal infusion process.

During the first in-situ infusions the field of view was moved as the flow front progressed through the dry fibres. This meant that had all three planned scan locations been reached, a comparison between the resin saturation at each point would not be possible. It was therefore decided that a fixed field of view should be used which would allow cross sections to be taken at each location to compare the level of resin saturation as the resin flow front progressed.

Five scans were taken of the sample as the surface flow front arrived at the 150, 170, 190, 210 and 230 mm points away from the resin inlet location. Each scan was set to one hour and the field of view was maintained for each scan, with the scan area from 150 to 200 mm from the injection point.

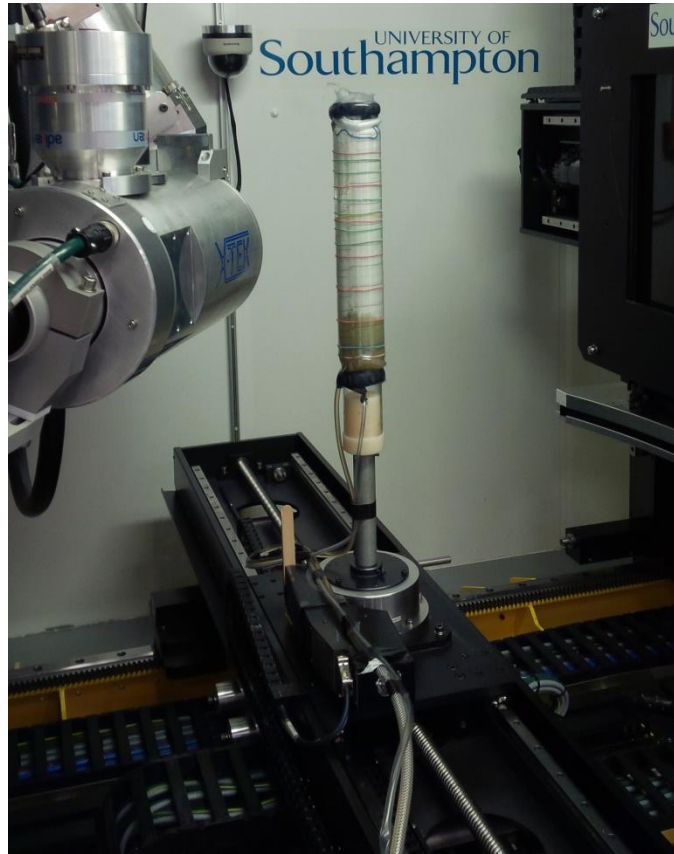


Figure 135: In-situ μ -CT Resin infusion experiment.

6.3.3 Results

Figure 136 shows the three-dimensional reconstruction of the glass fibres wrapped around the cylindrical mould. The reconstruction shows that no significant wrinkles were present in the fibres at the scan location. The cross section of the reinforcement also shows that a high level of compaction had been achieved using the shrink wrap tape, and the removal of the vacuum pressure during scans had not resulted in an expansion of the reinforcing fibres.

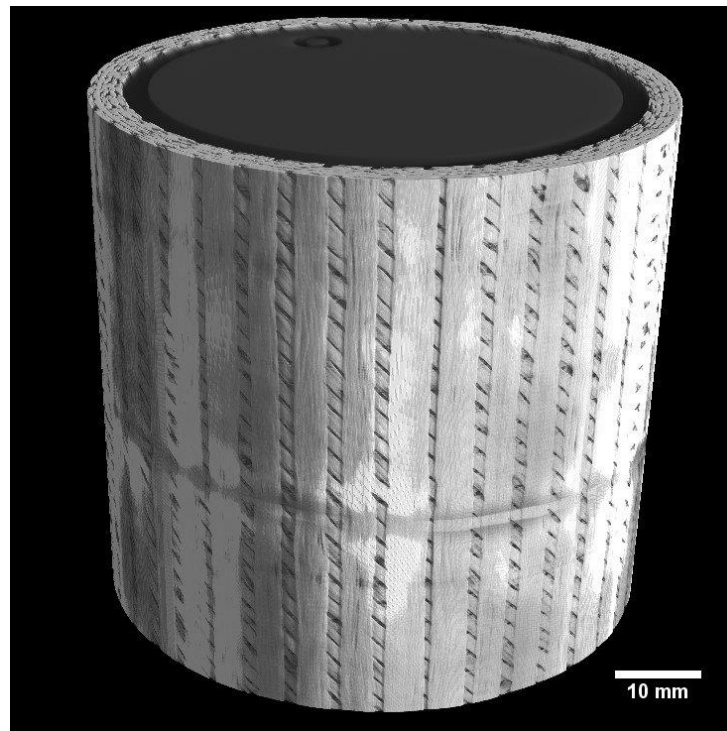


Figure 136: In-situ μ -CT scan of the dry fibre pre-impregnation.

In order to evaluate if the resin flow front could be detected from the μ -CT images, a polar transformation of the reconstruction was carried out. Adjusting the grey scale histogram to enhance the contrast between the different material densities meant that the resin flow front could be visualised as can be seen in Figure 137. The image in the top right of Figure 137 shows that even without the manipulation of the image contrast, the resin flow front is still visible. Figure 137 shows the resin flow front from the third scan taken when the vacuum bag surface resin flow front was positioned at 190 mm from the resin inlet, approximately half way along the μ -CT scanner field of view.

The section circled in blue identifies the join in the reinforcing fibres, the resin flow front either side of this join can be seen to be ahead of the rest of the resin flow front. This signifies that a race tracking effect had occurred down the fibre join, improvements could be made to the

experimental set-up to remove these effects by adding vacuum infusion tape between the reinforcement, creating a sealed edge between the reinforcement.

The dashed red line has been drawn over the resin flow front to help visualise the shape of the flow front, the position of the flow front is higher up the image than expected due to the surface flow front being at 190 mm, 40% of the way up the field of view of the scans which is shown by the green line across the reconstruction. The resin position ahead of the expected location is the result of the capillary effect during the 60 minute scan times.

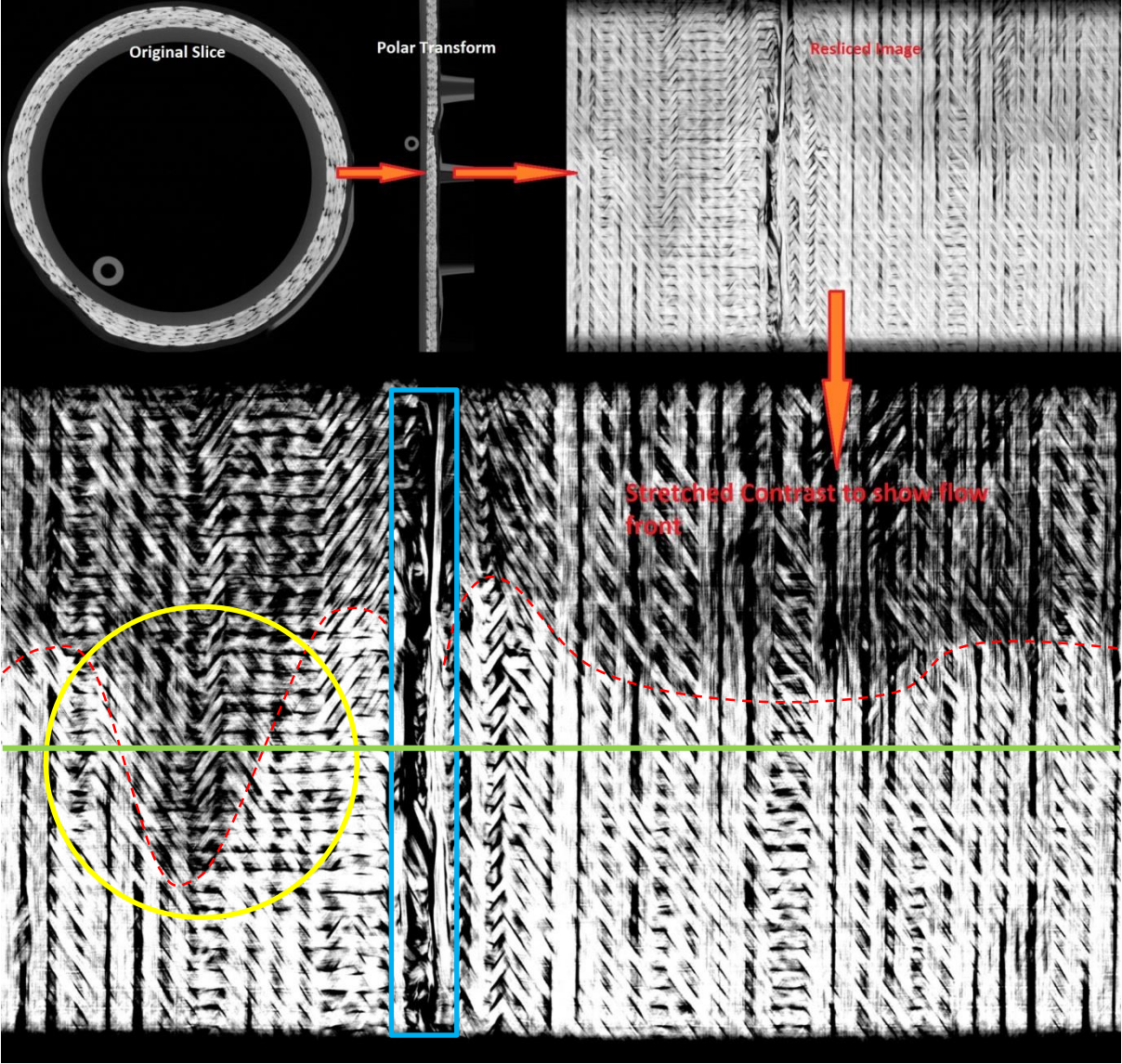


Figure 137: Scan 3 with the resin flow front at 190 mm, polar transformation of the volumetric reconstruction of the in-situ μ -CT resin flow front experiment allowing for the identification of the resin flow front.

The yellow circle in Figure 137 identifies an area of the flow front delayed behind the expected location but also the average flow front location. Figure 138 shows an image of the resin flow front during the in-situ experiment displaying a small variation from the expected rectilinear flow front shape, however the delay circled in Figure 137 cannot be seen as the image was taken from the opposite side of the infusion.



Figure 138: Resin flow front during the in-situ μ -CT resin infusion experiment.

The polar transformation was then conducted on scans one to five, allowing the creation of the scans as the resin flow front reached 150, 170, 190, 210 and 230 mm. Figure 139 shows that all five scans detected the resin flow front as it progressed up the vertical infusion. The resin flow front locations during scans four and five show that the majority of the fibres in the field of view appear to be behind the flow front which further confirms the expectation that capillary forces continue to draw the resin up the fibres during the scanning times.

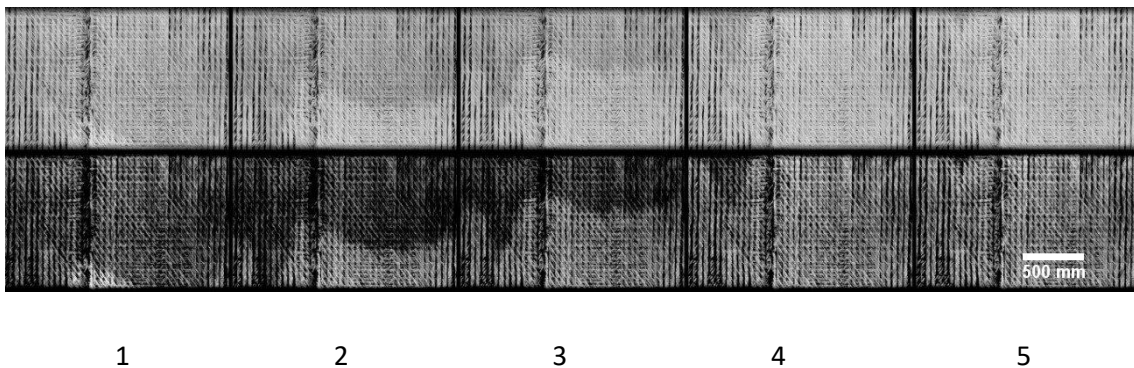


Figure 139: Polar transformation of the resin flow front location for scans one to five from left to right.

To investigate the through thickness resin saturations, cross sections of the preform were taken and analysed further. Through manipulation of the grayscale histogram, voids and other areas with low attenuation are shown as black, whilst the glass fibres are shown as grey and the resin is shown as the brightest material as has been done for the polar transformed sections. The level of resin saturation at each stage of the impregnation was quantified by measuring the visible dry channel areas from each sample and the resin area within the channels. A

representative area was chosen from each cross section, removing any edge effects, mould or consumable materials that might have affected the results. The resin saturation was measured using manual selection and thresholding. A large level of variation was recorded between each sample due to the challenges of segmenting semi-impregnated fibre tows and resin using manual thresholding.

Figure 140 shows the cross sections at 170 mm from the first, third and fifth scans taken when the resin flow front was visible at 150 mm, 190 mm and 230 mm. The cross section at 170 mm, with the surface flow front located at 150 mm illustrates the initial, substantially unsaturated, compacted dry fibre stack with clearly defined resin pockets located in the larger volume channels. Resin saturation in the region of 12-13% was recorded at this location, identifying either a small amount of flow acceleration in front of the surface flow front or capillary flow during the hour long μ -CT scan. The resin is focused in the centre of the laminate, predominately in larger flow channels between the six laminas. Resin contact with the fibres suggests macrovoid creation due to capillary flow domination resulting in resin wicking from the fibre bundles as a result of the slow resin flow front. It was expected that macrovoiding would dominate due to the mechanisms being used to pause the flow front. Whilst macrovoiding is easily identifiable with the μ -CT scan resolution of $43\mu\text{m}$, any detailed microvoid and saturation analysis is not possible, substantially longer scan times and smaller samples would be required.

Further fibre impregnation is visible after the surface flow front has progressed to 190 mm and the cross section is now behind the flow front and assumed to be fully impregnated. Resin saturation of between 34-35% has been achieved. A clear semi-saturated flow front region is identified with a lower volume of resin recorded than was expected at a point behind the flow front. Larger resin volumes are clustered in the larger channels between the fibre tows as can be seen in the top cross section. Clearly defined resin volume on the vacuum bag surface confirms the location behind the flow front. Capillary flow continues to dominate, with void areas being encapsulated by the resin volume.

The final scan is taken once the surface flow front has progressed 60 mm past the cross section location. Resin saturation of 71% has been recorded, identifying a lower level of saturation than might be expected and identifying variations in saturation behind the visible flow front. The larger flow channel that dominated resin flow in the first and third scans demonstrates an increased level of saturation compared to the narrower channels and areas closer to the mould surface. All macrovoids are fully encapsulated by resin wicking from the fibre tows, further suggesting the domination of capillary flow during the infusion.

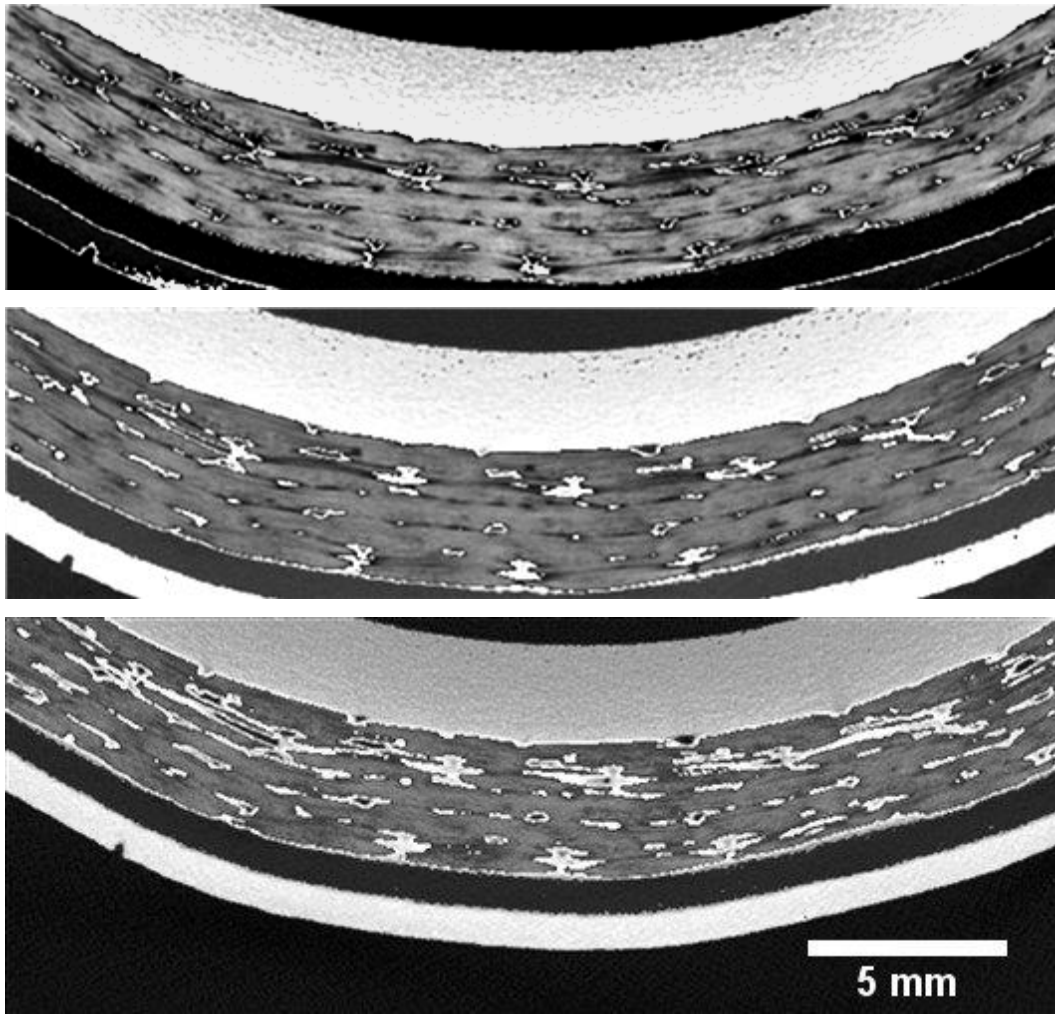


Figure 140: μ -CT cross sections at 170 mm from the injection point when the resin flow front is at 150 mm (top) 190 mm (middle) and 230 mm (bottom).

Figure 141 to Figure 143 show the cross sections of the preform at 190, 210 and 230 mm from the injection points during scans one, three and five. Each of the images show that a lower level of resin is visible during the first scan when the visible resin flow front was at 150 mm. During scan three the volume of resin appears to increase at a similar rate across all three cross sections, with the final images at each cross section showing the highest level of channel saturation which was to be expected with the surface flow front now ahead of all cross sections.

The cross sectional images all show the challenges with trying to segment the grey scale histogram into different material volumes with the resolution achieved for each of the μ -CT scans. The results also show the level of capillary flow which has occurred during the scan times.

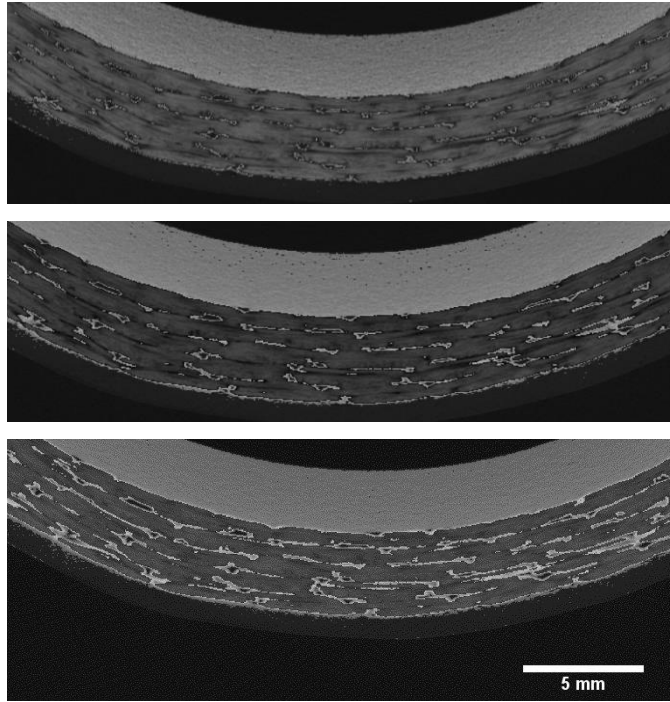


Figure 141: μ -CT cross sections at 190 mm from the injection point when the resin flow front is at 150 mm (top) 190 mm (middle) and 230 mm (bottom).

Figure 142 identifies an unexpected level of resin saturation in the middle image, which suggests capillary flow has impacted the level of saturation.

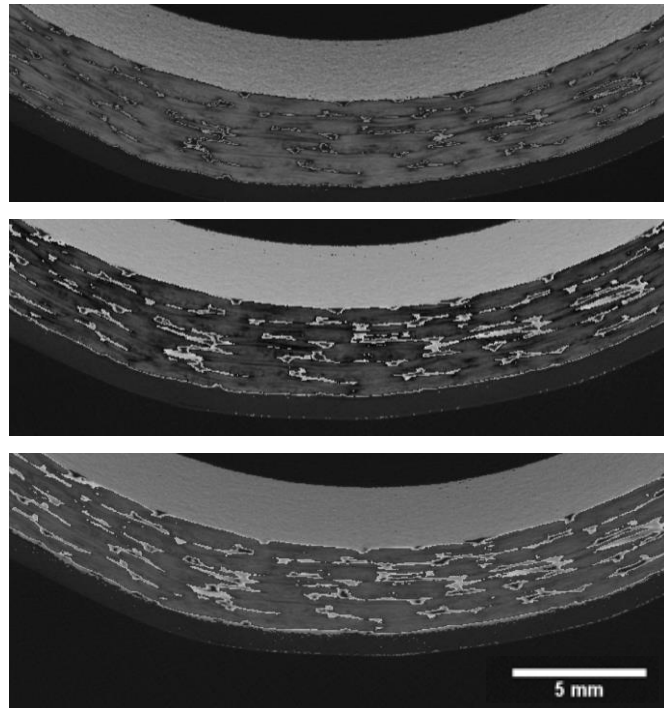


Figure 142: μ -CT cross sections at 210 mm from the injection point when the resin flow front is at 150 mm (top) 190 mm (middle) and 230 mm (bottom).

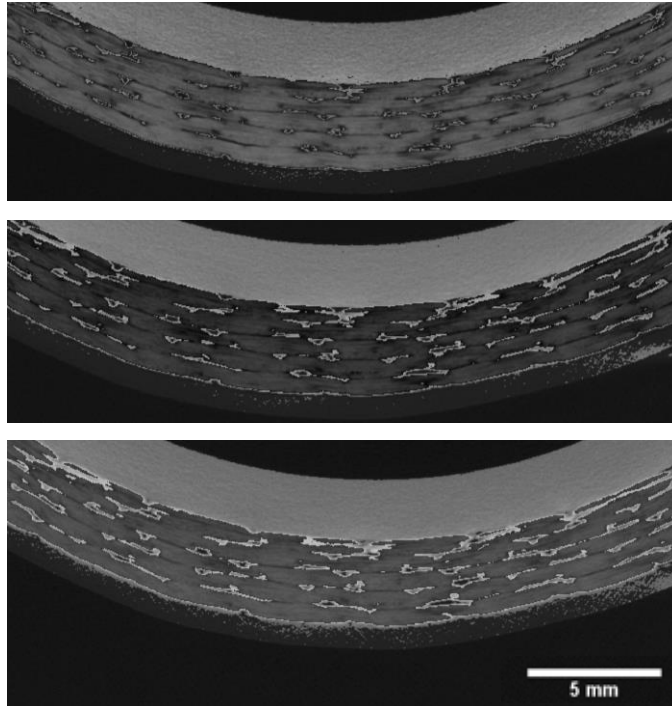


Figure 143: μ -CT cross sections at 230 mm from the injection point when the resin flow front is at 150 mm (top) 190 mm (middle) and 230 mm (bottom).

Figure 144 illustrates the level of saturation at each of the four cross sections from scans one, three and five. The results identify a number of unusual results from the investigation. Using the first scan as an example, it would be expected that the level of resin saturation, 80 mm ahead of the visual resin flow front would not be as high as 12.5%. Neither would it be expected that the four cross sections analysed would all identify comparable levels of resin impregnation at each scan location. The resin saturation levels for each scan would be expected to increase at a similar rate, with the gradient being comparable, but the percentage saturation being lower, the further from the injection point each cross section is.

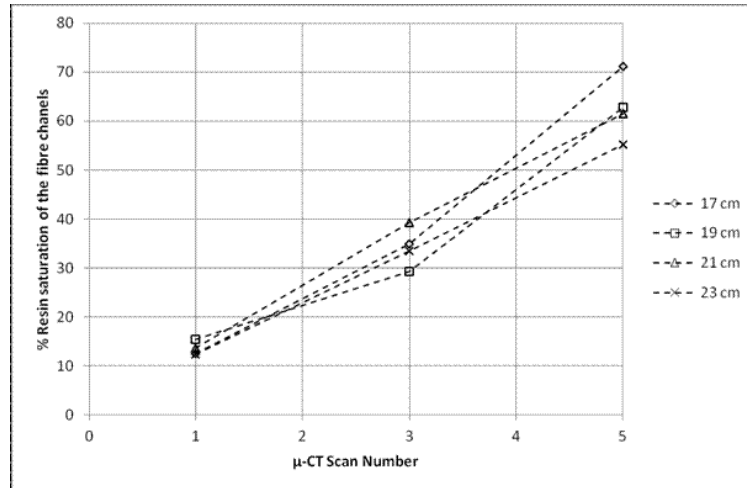


Figure 144: Percentage saturation of the laminate at each of the four cross sections from scans one, three and five.

After analysing the results from the second in-situ μ -CT VARI, it was decided that increased scan lengths and reduced material volume may help to increase the resolution of the flow front. A third experiment was set-up following the same procedures as the second experiment, except for three changes. Firstly the laminate schedule was changed to reduce the density of the materials being scanned. Four layers of reinforcement were removed from the preform, so that two layers of quad axial glass fibre were used. Secondly the number of scans attempted were also reduced to one with the scan times increased to 120 minutes. Finally the join between the lamina was filled with vacuum infusion tape to limit the resin flow accelerations through the gaps between the reinforcement.

The vacuum infusion tape seal at the fabric joint successfully avoided any race tracking in this region. The reconstruction of the experiment can be seen in Figure 145, where the cross section shows a small amount of resin located between the fibre bundles.

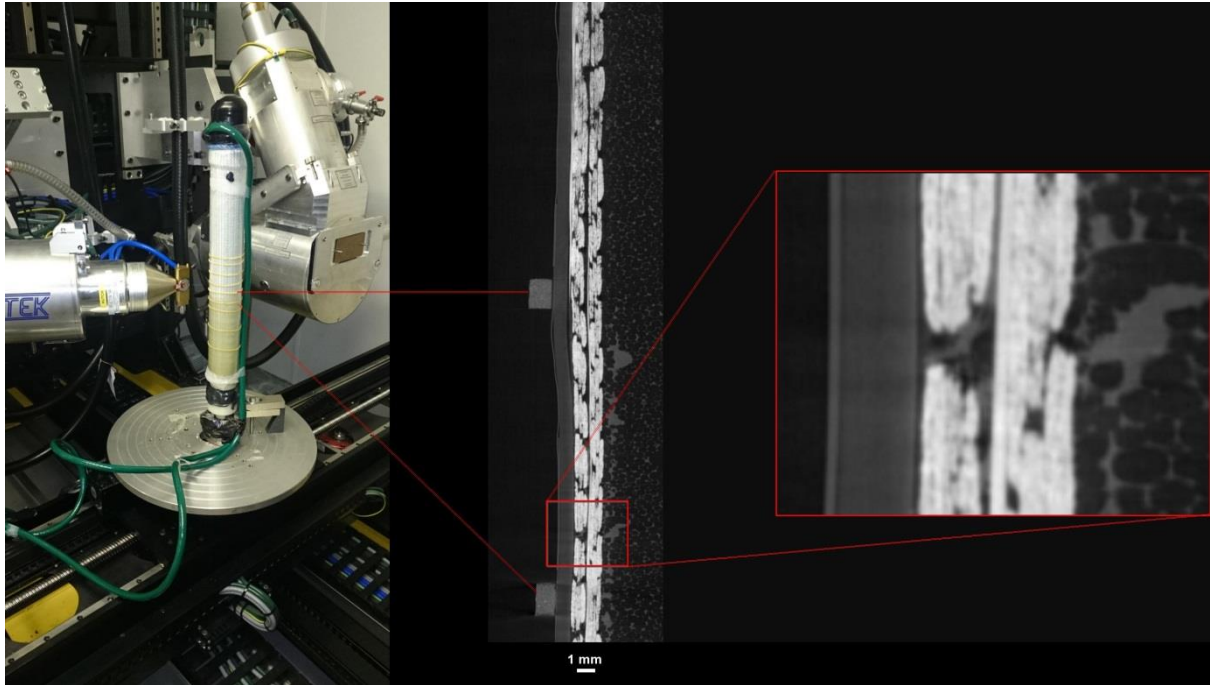


Figure 145: Third in-situ μ -CT VARI experiment conducted using two layers of reinforcement.

6.3.4 Discussion

Three VARIs have been conducted within the μ -CT scanner at the University of Southampton to test the ability of the μ -CT scanner to capture the dynamic process of resin infusing dry fibres under vacuum. The three experiments have each shown developments on the original concepts as the challenges associated with the VARI process and the procedure to capture μ -CT images have been tackled. The requirements for this experiment have been driven by the uncertainties relating to the development of voids in large thick VARI composites and the mobility of these voids once they have been created. Understanding the level of porosity is a critical element to the construction of high quality composite components in industrial applications where conservative design philosophies still exist.

The first experiment was conducted to test the initial concept of the experiment. The results from the first scan identified two areas which required improvements if the experiment was to capture the resin flow front. Firstly the field of view for each scan was maintained at the same location so that the volumetric reconstruction would represent the same preform volume with variable levels of resin saturation. This was important as it allowed the resin saturation at the same location to be compared at different points during the infusion process. If the experiment were to be taken forwards to assess the cure characteristics of the sample, the same field of view would allow for void movement, generation and shape distortions to be monitored as well as the volumetric changes to that resin during the curing process. Secondly it was found during the first experiment that the resin began to transition from liquid to gel before the third scan could be completed. It was decided that the effect of removing the catalyst would be minimal (<1 %) on the resin viscosity which would allow longer scan times, 60 minutes, to be completed with the resin at different locations without any time restrictions resulting from the resin cure.

The second experiment resulted in five scans being conducted as the surface flow front progressed at 20 mm steps. The scans were analysed in two stages, firstly a polar transformation of the cylindrical infusion was carried out to identify the resin flow front as if a normal flat plate rectilinear flow experiment had been conducted. The second stage of the analysis was to extract cross sections of the component at four locations so that the degree of resin saturation could be compared as the flow front progressed. The scan times and material density meant that the analysis was restricted to a macroscale analysis which resulted in the exclusion of any insight into the resin flow within the fibre tows.

The results from the five scans have been combined after the polar transformation has been completed, which allowed for the detection and visualisation of the resin flow front for each of

the five scans. The results show the resin flow front moves through the preform at a higher rate than was recorded on the vacuum bag surface. This is shown by the almost complete saturation of the preform during scan four when the resin flow front was expected to be 40 mm below the top of the field of view. These results suggest that although the vacuum outlet had been closed during the scans, a considerable level of capillary flow had occurred during the 60 minutes required for each of the five scans.

Further research into the effect of capillary forces was conducted to explain the results found during the second experiment. An additional review of the literature found that Morgan (2015) ran fabric dip tests for glass fibre and carbon fibre biaxial fabrics using oil mixed with fluorescent dyes to visualise the capillary effect which can be seen in Figure 146. The results for the biaxial glass fibre lamina showed that over 40 minutes the resin impregnated up to 50 mm above the resin pool.

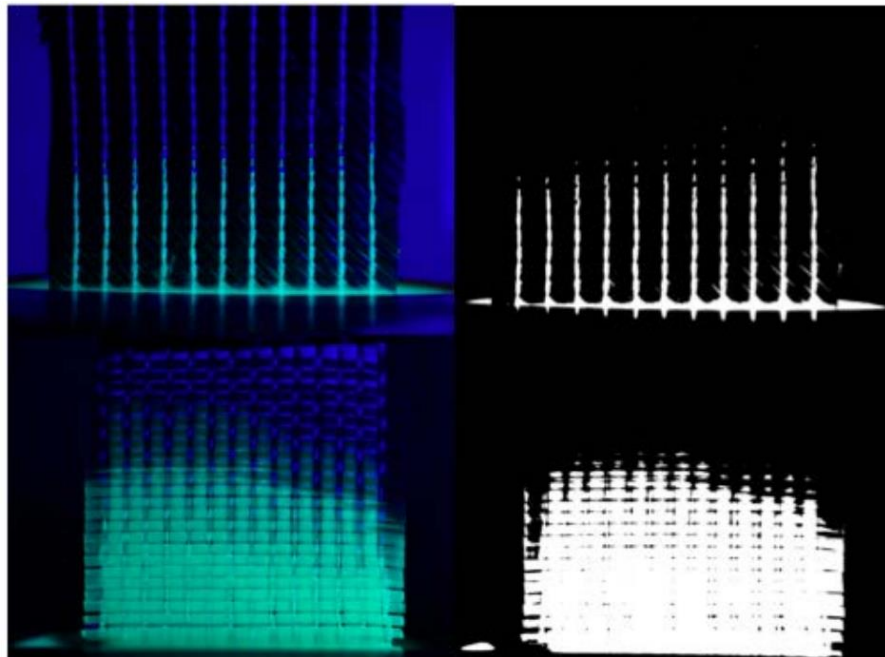


Figure 146: Capillary flow original and binary images of the resin flow front progression under capillary pressure alone (Morgan 2015).

Morgan's results suggest that during scan one, which took 60 minutes, the capillary forces on the resin could have drawn the resin 50 mm up the fibres to a position ahead of the flow front seen on the vacuum bag surface. The resulting flow front within the fibre bundles would have therefore been at 190 mm from the resin inlet not 150 mm at the beginning of the scans. This results in the resin flow front being further progressed than expected when the second stage of the infusion was started, increasing the resin flow front further ahead of the expected position.

These results suggest that the resin saturation shown in Figure 144 is being influenced by the resin capillary flow, which leads to all of the cross sections being behind the resin flow front except for scan one, where the field of view meant that the cross section at 230 mm was 40 mm ahead of the flow front location. Due to the thickness of the preform being used, the capillary flow effect was not visible to the author through the peel ply placed on the outer surface of the reinforcement during the experiment. The result of the capillary flow may have resulted in the resin flow front location within the fibre bundles being outside of the μ -CT scanners field of view by scan three where the surface flow front was located at 190 mm.

The cross sections each identified that the resin location within the channels between the fibre bundles are located closest to the edge of the fibres. Figure 147 shows a zoom in section of the cross section at 190 mm taken from scan five, where the preform should have been fully saturated behind the resin flow front. The zoomed in sections show that the resin within the channels is located next to the fibre bundles with the void being located in the centre of the fibre bundles. This supports the argument that the capillary flow effects are leading the resin impregnation. Figure 147 shows an example of the results of mechanical entrapment which was discussed in the literature view and shown in Figure 8. The void displayed in Figure 147 has been created in the same way as the surface voids reported in the previous experiment in this Chapter, as well as the voids which are reported on the mould surface of the hull infusions at PYI.

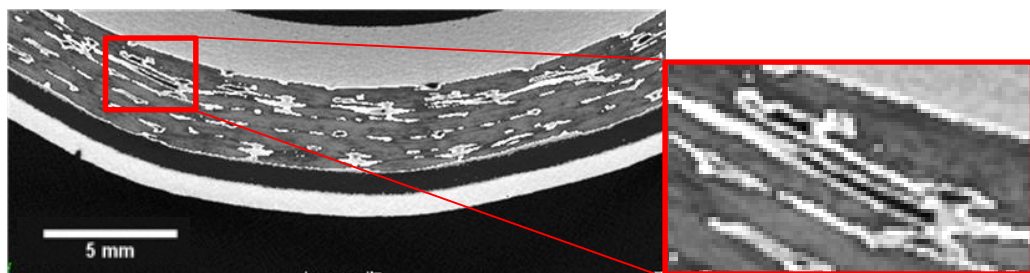


Figure 147: In-situ μ -CT cross section identifying the resin distribution with the channels between the fibre bundles identifying voids fully surrounded by resin.

6.4 Conclusions

This study investigated the resin impregnation of dry fibres during a VARI using μ -CT. An in-situ infusion was carried out and paused at known locations to allow for the saturation development to be monitored and analysed. The process used to allow for partial processing of the laminate resulted in resin flow due to capillary forces whilst the 60 minute scans were undertaken. Due to the material size and density as well as the limited scan times, the micro level flow has not been successfully captured. The process successfully identified and visualised the macro scale resin flow through the dry fibres, however changes to the experimental set-up are required to reduce the level of capillary flow during the scanning time.

The saturation development in front and behind the surface flow front has allowed the identification of non-uniformities in the three-dimensional resin flow front during a resin infusion. The dangers associated with slow resin impregnation speeds have also been emphasised by the method used to scan the impregnation and the resulting capillary flow. The accuracy of experiments and industrial applications relying on observations on the surface flow front to monitor the level of impregnation are also shown to lack consistent reliability, as a considerably non-uniform lead/ lag relationship has been identified. The resulting voids captured within the channels located between the fibre bundles were clearly identified. These voids could then be compared to those identified in Chapter 4 during the μ -CT analysis of the core samples provided by PYI.

Two changes to the experimental procedure have been suggested in order to gain greater control of the capillary flow during the CT scan times. Firstly the cooling of the entire preform at the time when the scan is to be undertaken would allow the viscosity to be significantly changed, restricting the mobility of the resin. The second suggestion is to mix the resin with a radioactive tracer to increase the contrast between the resin, fibres and voids. Tracers are sometimes used for μ -CT experiments with carbon fibre epoxy composites due to the issues relating to segregating the two materials. The tracer would not reduce the capillary flow however the increased contrast between the resin and reinforcement would allow the same scan resolution to be achieved in a shorter scan time. The scan times would need to be reduced to a level where the capillary flow was no longer significantly affected the accuracy of the flow monitoring.

Chapter 7

7 Discussion

As outlined in the introduction, this project aimed to identify the key processing parameters linked to the formation of defects in large scale VARI, and to create guidelines for industry. To achieve the former, a review of the available processing information from PYI, core sample void characterisations, fibre optic strain measurements and μ -CT resin flow experiments has been undertaken.

The review of the commercial context of this research was undertaken to help identify the best research plan to provide the necessary information to reduce the defects created in large scale VARIs at PYI. The process review in Chapter 3 was used to identify relationships between the variable infusion input parameters and the defects recorded. The results were found to show very low levels of consistency from one infusion to the next, with basic principles such as the resin viscosity and temperature not following the expected relationship across the entire dataset. The manufacturing data collected by PYI is reliant on the laminating team to record key information. The results from this review show that the information being collected is not sufficiently accurate to provide actionable information to PYI or this research. Additional processing information is required to consistently record the key processing parameters during the infusion process.

A review of the defect locations recorded by PYI quality control personnel was used to identify the consistency in the location and coverage from one infusion to the next. The void areas recorded identified an inverse relationship between manufacturing number and void area, which shows that the infusion process has improved with increased numbers of infusions leading to a reduction in void area. The locations of the defects were collated so that the frequency of the defects at specific locations could be assessed. The results showed that a relationship exists between the location of the defects and the features in the hulls which require additional reinforcement. The number of voids recorded around the chine, stern tubes, exhaust outlets, transom and bow thrusters identifies a relationship between the defects and areas of the component where the layup transitions from monolithic to sandwich layup. These transition regions create complex regions for the resin to infuse, whilst also increasing the resin volume leading to higher resin cure temperatures and increased resin cure shrinkage. However, the inconsistency of the defects from one infusion to the next showed that the laminate schedule is not the sole cause of these defects.

The review of the defect recording process identified two areas which require enhancements if PYI want to collect the necessary data to improve the infusion process. Firstly, the procedure followed by the quality control engineers allowed for a high degree of subjectivity and interpretation which reduces the quality of the defect information being recorded. To improve the procedure used to collect the defect information, the author generated a new defect recording sheet which provided additional information with respect to the locations and defect types being recorded, Appendix C. Secondly, only a very small fraction of the entire component is visually inspected post infusion. The procedure followed by the quality control engineers restricts the inspection process to surface visible defects on the mould surface of the infusion and on sections of the component where a gelcoat has not been applied. This results in large sections of the hull form not being reviewed post infusion, potentially hiding any structural defects that might exist.

In addition to the infusion parameters and the defect recording process at PYI, the environmental conditions under which the infusions are completed was also reviewed. The information recorded by PYI shows that the environmental conditions are variable depending on the season and are often outside of the optimal conditions in which you would undertake a complex infusion process. This effects the resin viscosity due to the ambient temperature during the infusion as well as the curing temperature, which impacts the development of the materials mechanical properties. PYI are developing their process to implement temperature controlled mouldings and regulate the resin temperature pre-infusion to minimise the negative effect the variable environmental conditions have on the infusion.

Having identified a correlation between defects and the areas of the hull where additional reinforcement and transitions from monolithic to sandwich layup exist, the layup in these areas and the effect that the layup had on resin flow and cure was investigated. The structural requirement at the chine, bow thrusters, exhaust outlets, transom and propeller shafts, dictate that a monolithic layup is used. These transitions in the layup alter the permeability and cure characteristics of the laminate due to the difference in resin volume. Whilst observing the VARI at PYI it was visible from the vacuum bag surface that the high permeability sections of the preform restrict the ability to create a consistent resin flow front with visible areas of the flow front accelerating once the core section has been reached. Isolated monolithic sections such as the bow thrusters often result in dry sections of the laminate becoming fully enclosed by the resin flow front. Previous research has shown that this increases the number of defects due to the reduction in vacuum pressure as the evacuation path disappears resulting in reduced flow

speeds. These reduced resin flow speeds are proven to result in increased macrovoids due to capillary flow which can be shown by a lower capillary number, Figure 10. The capillary number achieved during the resin infusion for the μ -CT flow front analysis was a factor of 10 below the recommended minimum value to optimise and infusion for the least possible voids. The capillary number further decreased before the resin cured, with the final capillary number being 1.8×10^{-5} whilst the minimum recommended capillary number is 1×10^{-3} (Gourichon, Binetruy & Krawczak, 2006). Converging flow fronts have also been shown to increase void creation in previous research, as well as decreasing the probability of void washout once the voids have been created at the flow front. The capillary number void optimisation research has suggested an optimum processing window to reduce voids with a resin flow velocity of between 0.002m/s and 0.0002m/s based on the viscosity of Crystic 703pa at 25°C. It is however of the author's opinion that when attempting to infuse a large component using mixed reinforcement and variable laminate schedules, an optimum speed for the entire resin infusion cannot be achieved. The resin velocity on a sandwich section of the hull has been recorded at approximately 0.0025-0.003m/s during the PYI process review, whilst the resin velocity in the monolithic areas will reduce to below 0.0001m/s depending on the permeability and vacuum pressure which was seen during the infusion for the μ -CT flow front analysis. In addition to the challenges relating to optimising the infusion speed, the increased number of resin flow defects located in areas where the resin volumes are high will increase the cure temperature and therefore cure shrinkage, resulting in higher levels of residual stress development in these areas.

The resin flow experiments conducted by PYI also demonstrated the flow accelerations caused by the core grooves and high flow infusion mesh. The test infusions which replicated the laminate schedule in the chine demonstrates the risk of converging flow fronts on the mould surface where the resulting laminate had surface visible defects on the mould surface after the infusion was completed. Converging flow fronts result in voids being encapsulated, which reduces the chances of the voids being washed out of the component. The infusion completed for the μ -CT flow front analysis identified the inverse relationship between the positioning of the core grooves and the resulting converging flow front. During the infusion the core grooves were placed on the mould surface, which resulted in the converging flow front being created on the vacuum bag surface, whilst PYI position the core grooves on the vacuum bag surface to avoid any reduction in surface quality on the customer facing mould surface. Due to the challenges associated with identifying the mould surface flow front, PYI could investigate alternative core groove patterns and their effect on the surface finish in order to place the core grooves on the mould side of the sandwich layup. This would allow the laminating team to

visually monitor the converging flow front which would be on the vacuum bag surface, where the chine resin inlet is located. The infusion strategy could then be amended to ensure the dhine area receives the required resin flow rate.

These results show that the resin flow strategy implemented by PYI has not been optimised to minimise the creation of defects. The resin flow strategy has been based around reducing the risks of the infusion being incomplete before the resin begins to gel. Alterations to the positioning of the resin flow enhancing materials could be made to reduce the probability of converging flow fronts and resulting slow resin velocity. To aid the investigation of the resulting voids from the converging flow fronts, samples were analysed from above the chine where delamination could be seen from the surface of the laminate.

The information from PYI resulted in three core samples being analysed using μ -CT techniques to assess the three-dimensional fibre, resin and void distributions. The results showed that although all three core samples were extracted due to delamination being visible from the component surface, additional porosity and macrovoids were present in the same location as the delamination. Due to the size restrictions placed on the samples removed from the hull, only a small section of the component could be assessed. This limited the opportunity to assess the edges of the delamination section and the distribution of voids across a wider section of the hull. The review demonstrated the benefits and weaknesses of the μ -CT process. The ability to reconstruct three-dimensional volumetric representations of the fibres, resin and voids is to the author's knowledge unmatched by any other non-destructive testing process for composite materials. The μ -CT reconstruction enabled the identification of minor fibre misalignment which would otherwise have not been visible and allowed voids to be detected down to the macro scale. The resolution of the images is however one of the challenges faced whilst working with large composite structures. Due to the relationship between X-ray intensity, material density, scan time and image resolution, generating images which can capture micro scale voids within the fibre tows can be difficult. Precise identification of the location which requires scanning is needed so that the material density can be minimised before scanning.

The three samples scanned did identify a consistent through thickness void distribution with the majority of the voids located in the first quarter of the sample from the mould surface. The consistency of the through thickness void locations links to the resin flow experiments conducted by PYI and the author, and suggests that the mould surface in this region is the last part of the laminate to be impregnated. The void distribution identified that the void fraction peaks at 12% and 26% for the two samples scanned from the A3_S6 infusion. Both void peaks

were located 20% of the distance from the mould surface to the core material. A second void peak can be seen in the A3_S6_2 sample, approximately 45-50% of the distance from the mould surface. This second void did not result in the same matrix failure as the voids closer to the mould surface, which suggests that although the void fraction increased to over 2.5%, the resin material properties were sufficiently high despite the voids or that the loads at this location were low enough that the resin did not delaminate. Previous research has suggested that an increase in void fraction of 1% results in a decrease in resin tensile strength of 3% and a reduction of ILSS of 7%. An understanding of the loads that the laminate is under during the infusion and cure cycle is needed to understand how important the void fraction is in this region of the laminate.

Due to the inconsistent recording of defects on the chine, the author decided that an additional factor must be influencing the defects in this area. The thermal contraction of polyester resin is well documented in literature and has been comprehensively tested by resin suppliers. Literature suggests that the level of resin shrinkage can vary from 2% to 12% dependent on the resin system used and the exothermic temperature achieved during the curing process. The result of the resin shrinking is to create residual stresses in the component which, if large enough, result in defects or stress releasing mechanisms. Due to the limited availability of strain recordings on large scale VARIs in the public domain, FBGs were used to record the developing strain in the component during the infusion and curing process.

FBGs are a proven technique in the composite industry, however, the author found the sensors to be very delicate and poorly suited to a commercial production environment. The first attempt to embed the FBGs into the hull at PYI resulted in all of the fibre optics breaking before the preform had been fully laid up. The second experiment resulted in two of the three fibre optics collecting data up until the component was removed from the mould. The final measurements taken showed that only two of the original nine FBGs were intact and operating as expected. Due to the requirement to monitor temperature separately and to handle the fibre optics in a controlled environment, the fibre optic sensors may be more appropriate to be laminated within the mould tooling where more time is available to embed them during the mould manufacturing process. Alternatively the FBGs could be positioned within the core, where a section of the core could be removed and replaced with a strain isolated fibre optic to accurately monitor temperature next to the FBGs measuring mechanical strain. This would also allow the temperature measurement to be located next to the FBG sensors for accurate temperature compensation.

The fibre optic measurements were more successful at measuring the strain changes without compromising the vacuum integrity of the component. The process of embedding the sensors in industry proved to be a challenge as it required additional production time with the fibres being monitored through the layup process to avoid them inadvertently being damaged by one of the laminating team. The results of the strain measurements showed an unexpected trend when the fibres were placed under tension soon after the curing process began. The expected result was for the polyester resin shrinkage to result in all areas of the preform being placed in compression during the resin cure. However, this was not the case, the resulting tensile load identified an additional problem with the lamina schedule used by PYI, not only do the monolithic transitions to sandwich sections alter the resin flow front creating voids near the chine, but the increased resin volume below the chine also changes the stress distribution around the hull. Ten times more resin is located in the monolithic section below the chine which has been found to cure at a 50°C higher exothermic temperature as well as at a faster cure rate resulting in higher volumetric cure shrinkage. The combination of voids generated by the irregular flow front and the tensile load applied to the lower topside areas near the chine may be the combination which results in the delamination recorded on the chine area. Due to the complexity and risks of breaking the fibre optics, the FBGs were located at the top of the chine areas to reduce the number of reinforcement layers the fibres had to be passed through to exit the laminate. Additional FBGs are required to be located below and above the chine to map the loads around the monolithic and sandwich sections of the laminate.

After the estimate gel time of the resin, four hours after mixing in the catalyst, the laminate was cured for 14.5hrs before the laminating team began removing the vacuum and lifting the laminate out of the mould. The strain measurements during the demoulding process identified a transition from tensile to compressive loads on the topsides of the hull. The compressive loads were up to four times higher than the tensile loads recorded during the resin cure, identifying the demoulding process as a cause of higher loads than the curing process alone. During the demoulding process the topsides of the hull are only supported by two supporting arms placed across the top of the component. Four lifting points are laminated into the hull post infusion to remove the laminate from the mould. The lifting points and the supporting arms result in the topsides sagging outwards during the demoulding process, which resulted in the compressive loads recorded. Laminates are dependent on the matrix properties whilst under compressive loads which means that the topsides during the demoulding process are reliant on the matrix properties. The resin in this region are known to contain macrovoids due to the slow resin flow velocity. Research into the mechanical properties and cure characteristics of polyester resins

have shown that the resin will have only partially cured under a room temperature cure cycle 14.5hrs after the resin gel time. The strain measurements during the demoulding process are a fraction of the failure properties of the polyester resin. However, the resin supplier recommends a minimum room temperature cure of 24hrs which suggests that the resin properties at 14.5hrs will be inferior to those stated on the material datasheet. In addition to the partial curing, the resin flow experiments have shown that there is a high probability of voids in this area, further reducing the mechanical properties of the resin. PYI are introducing temperature controlled moulds to introduce a 40°C post cure, however it is still recommended that PYI leave the laminate in the mould for a minimum of 24hrs after the end of the infusion.

To further understand the development of voids at the flow front two experimental set-ups were devised to utilise the three-dimensional analysis opportunities created by μ -CT. The first experimental set-up used all of the irregular lamina layups which are used at PYI to create an irregular flow front in an attempt to create converging flow front and lead-lag effects. The set-up was successful in creating the irregular flow front, however the technique to pause the flow front did not have the desired effect. The resin inlet closure was meant to hold the resin flow front at a fixed location, however due to the vacuum source remaining open to maintain fibre compaction, the flow front continued to advance. High capillary flow resulted in an irregular flow front where fibre tow saturation dominated the flow front with dry fibre channels located behind the flow front. The three-dimensional reconstruction highlighted the ability of μ -CT to analyse void, resin and fibre distributions. The results showed that although the vacuum bag surface appears to be unsaturated, all bar the outer two layers of reinforcement were partially infused. The flow front volumetric reconstruction allowed for the identification of the resin wicking from the fibres creating long tubular voids in the channels between the fibre tows. The shape and distribution of the voids behind the flow front was similar to those recorded on the A3_S6_2 void analyses sample provided by PYI. This further supports the argument that the outer two layers of reinforcement at the chine are not only subjected to tensile loads during curing, but they are the last areas to be impregnated by resin in this region. Literature supports the idea that sections of a VARI where a dry area becomes fully enclosed will result in an increased level of voids in this area. The resin infusion also helped to identify the inverse relationship between the location of the core channels and the converging flow fronts. The core material not only has channels to promote resin flow, but holes are also located every 40mm to help feed resin to the opposite side of the core. The holes are not sufficiently distributing the resin which means that the resin flow front on either surface is irregular which results in the converging flow front.

The results from flow front characterisation have not allowed the level of detailed analysis required to isolate the causes of the voids in these large complex infusions. A second experiment was designed to conduct the resin flow experiment inside of the μ -CT scanner at the University of Southampton. To the author's knowledge this had never been attempted before, leading to these experiments being used as a proof of concept, with each infusion developing the experimental procedure further. The same resin system and reinforcement used by PYI were used during the in-situ experiment.

The results from the in-situ experiment have shown that by using a one hour scan time and six layers of 450 mm by 160 mm quad axial NCF the resin flow front could be detected and its progress through the preform could be monitored. The experiment similarly to the large test infusion resulted in a degree of capillary flow which meant that some resin had been drawn through the fibre bundles ahead of the surface visible flow front. It was expected that the capillary effect would have drawn the resin up to 50 mm up the fibre bundles ahead of the flow front during the 60 minute scan times based on results from research by Morgan (2015). The impact of the capillary flow led to the creation of voids caused by the mechanical entrapment process which is expected when an infusion is conducted at a non-optimised capillary number, due to high or low resin flow velocities. The cross sections of the μ -CT volumetric reconstruction identified the resin flow wicking from the fibre tows into the channels between the fibre bundles mirroring the results from the previous μ -CT scan of the cured resin flow front. The reconstruction of this effect can be used to further expand the knowledge about the voids created by low resin flow speeds in VARI components.

The experiment has successfully shown that an in-situ VARI can be monitored using μ -CT techniques. Further developments to the experimental approach are required to increase the resolution of the scans so that the resin flow architecture can be examined at a micro scale rather than macro scale. Two areas of improvements could be focused upon, firstly the use of cooling to increase the viscosity of the resin at the point where the process needs to be paused. The second is to inject a radioactive tracer into the resin; this has no impact on the ability to restrict the capillary flow, but the additional contrast between resin and the fibre bundles may mean that the scan times can be reduced so that the resin is more controllable. With the increased use of computational modelling and CFD resin flow analysis, the requirement for an accurate three-dimensional resin flow analysis tool has never been greater.

In addition to monitoring the resin infusion process, the experiment would also allow for the volumetric shrinkage of the polyester resin and the effect curing has on voids to be monitored.

Using a smaller experimental set-up to reduce scan times, repeat μ -CT scans could be taken throughout the 24hrs required to fully cure Crystic 703pa. The volume and void distribution could be analysed for each scan to create a timeline of the volumetric shrinkage. Alterations to the experiment could be included by heating the sample to recreate the shrinkage experienced in the chine where the peak cure temperature is 100°C.

Combining the resin flow, void characterisation and fibre optic measurements together, three areas have been identified as the primary causes of the failures experienced by PYI in the chine area of the VARI hull components. Firstly, the flow strategy used by PYI includes the use of a resin distribution mesh and core grooves in the high density foam are effecting the saturation of the fibres on the mould face of the preform by introducing converging flow fronts. The resin flow experiments have each resulted in capillary flow dominating within the fibre tows which have resulted in voids comparable to the elongated tubular shaped voids from core sample A3_S6_2. Secondly, the outer lamina in the topsides is also effected by the resin shrinkage which occurs in the monolithic section below the chine. The transition from a thick monolithic layup to a thick sandwich section at the location of a 90° radius changes the resin cure characteristics and the resin shrinkage characteristics. The influence of the mould shape also increases the probability of the laminating team laying the fibres poorly into the mould tools. All three core samples analysed in Chapter 4 showed varying degrees of wrinkles, fibre waviness and distortions. The use of thick, multilayer NCF, impacts the drapability of the fibres in a location where a change in lamina schedule and mould shape exist. It is possible to identify that an irregular level of fibre saturation coupled with an irregular cure schedule exists in sections of the component which are positioned close to each other. The additional complexity of the three-dimensional mould shape and the probability of human error in the fibre layup process adds another layer of complexity and unevenness to the curing process, all of which combine together to cause the delamination failures reported by PYI. Thirdly the removal of the component before the resin has fully cured introduced compressive loads in the outer layer of the laminate. Laminates under compression are dependent on the matrix properties to maintain the fibre arrangement. The increase in voids from the resin flow, increased probability of wrinkles in the reinforcements and compressive loads combine to cause the delamination which was seen in core samples analysed in this research.

Chapter 8

8 Conclusions and Future Work

8.1 Conclusions

A fourfold approach has been taken to investigate and improve the level of understanding relating to the production of voids during large scale commercial VARI and resin curing.

1. An industry process review identified the degree of variability in the number of defects created during the commercial application of large scale VARIs.
2. μ -CT void characterisation of three samples extracted from two hulls at PYI where delamination had been reported on the surface of the component.
3. FBG fibre optic measurements of the cure induced residual stress during the thermal shrinkage of an unsaturated polyester resin.
4. A μ -CT resin flow front analysis was completed to identify the risks and challenges associated with a slow advancing speed during a VARI.

To improve and extend the knowledge relating to the challenges associated with large scale resin infusions, an experimental approach was taken. All four investigations have contributed to the advice to be given to the industry sponsor of this project, PYI.

1. The lamina schedule in the chine area of the hull requires a review with the structural designer of the hull to identify if the monolithic to sandwich transition on the chine can be adjusted to reduce the build-up of residual stresses during the resin curing process. The effect of combining the thick monolithic sections of the laminate with a transition to sandwich layup at the same location as a 90⁰ mould curve all contribute to the build-up of resin in this area. The increased resin volume increases the exothermic cure temperature and the resulting resin cure shrinkage and build-up of residual stress which the author believes is one of the causes of the delamination in the chine region.
2. The resin infusion strategy at PYI has been optimised to guarantee that the preform is fully saturated before the resin begins to gel 240 minutes after the resin is mixed with the catalyst. PYI have therefore concentrated on improving the permeability of the preform in order to minimise infusion times, which allows them to infuse vessels up to 40m in length within the 240 minute infusion window. The result of the methods used to reduce the infusion times of the components are also directly linked to the voids which are being identified on the chine. In combination with the residual stress build up during the resin curing process and the voids

trapped by the converging flow front near the chine, structural weaknesses are being created in this area. A review of the resin flow mechanisms used at the chine and topsides needs to be conducted to reduce the extent that the resin accelerates up the topside on the vacuum bag side of the core ahead of the surface flow front on the mould flow front. A review should also be performed on the ability to rotate the core material so that the resin distribution grooves are positioned on the mould surface not the vacuum bag surface.

3. PYI are driven by commercial targets to reduce the manufacturing time of all of their components. It is the author's view that this is resulting in the demoulding of some of the hulls before the resin has reached an adequate cure point to provide the structural support whilst the hull is lifted and continues to be manufactured whilst supported from the keel only. A longer cure schedule should be implemented alongside the heated tooling program which PYI are undertaking to ensure that the material properties are maximised before the vacuum bag is removed from the component. The combination of voids caused by the irregular resin flow pattern and the removal of the hull before the resin has fully cured is inducing high compressive loads on the outer layer of the reinforcement which are reliant on the resin properties to maintain the structure of the reinforcement.
4. The final area where PYI are reducing manufacturing times is through the use of heavier NCF multiaxial glass fibre. The three core samples provided to the author to conduct the void characterisation all showed signs of fabric wrinkles or fibre misalignment. As the fibres increase in weight so do the challenges associated with draping the reinforcement over the complex three-dimensional mould shape. The additional cost of these defects needs to be reviewed against the cost savings of the heavier reinforcements. A combination of heavier reinforcement on the topside and hull bottom may be combined with lighter reinforcement around the more complex mould shapes.

The contribution of this research towards the characterisation of voids in large scale VARI composite components has been the creation of an experiment which can capture the resin flow progress through the preform at a macro scale. The experiment has successfully captured the flow behaviour associated with mechanical entrapment when a very slow flow front velocity is experienced.

Further development of this experimental approach is required to continue the improvements which have been experienced during the first three iterations of the experimental design. Areas to develop the procedure have been suggested by the author which should allow improvements in the resolution of the resin flow front capture and the ability to restrict the level of capillary flow during the scanning times.

8.2 Further Work

The use of μ -CT to characterise the resin flow front in a VARI has provided a degree of detail which was not previously available to the composite industry. The flow front and void recreation infusion replicated a typical industrial infusion at PYI and resulted in converging flow fronts on the sandwich section of the component which allowed for a single section of the flow front to be scanned as part of this research. This provided an insight into the effects of very slow resin flow on fibre tow saturation and the resultant failure to infuse the entire preform. Utilising the unique insight that μ -CT scans provide could be used to analyse additional samples of partially processed sections of a VARI. Repeating the process used in this research to configure an infusion to include multiple flow features to ensure converging flow fronts and race tracking are created to generate a range of defects. Sections of the flow fronts and areas demonstrating signs of high porosity could be scanned to provide an insight into the resin, fibre and void distribution. This process could be used to further validate existing research into the optimisation of the capillary number at different resin flow speeds. A small section of each sample could be scanned at a very high resolution to investigate the degree of micro and macrovoids.

The in-situ μ -CT experiment has shown positive initial results however an increased resolution is required to investigate the micro flows and microvoiding occurring during the VARI process. Two approaches could be applied to develop the process further either involving cooling the component or the injection of a radioactive tracer into the resin. Due to the exponential relationship between temperature and viscosity, a 20°C reduction in the resin temperature could result in the viscosity increasing by 240%. This would help to limit the resin flow effects during scanning and would require a non-catalysed resin to be used. The application of a radioactive tracer to the resin would not help to control the capillary effects during the scans, however the tracer would increase the contrast between the fibres, resin and voids. This would allow for the scan time to be reduced whilst also improving the definition of the resin and void volumes. Assuming that the resin flow front definition can be improved, the experimental set-up could be further altered to represent a sandwich laminate infusion by replacing the cylindrical mould with a high density foam core. The use of the core material as the mould would allow for research into the effect the fibre core material boundary has on the flow characteristics. The core material could also be used to replicate the core distribution channels at PYI which are used to help promote resin flow and were shown in Chapter 5 to contribute to the converging flow front on the opposite side of the core to the channels. The experiment set-up in this research is based around a rectilinear flow front, however it has been shown that the

resin flow on large scale infusions is altered by resin infusion mesh, core channels and race tracking around edges and channels in the laminate. The resin inlet locations could be adjusted to generate converging flow fronts to investigate the void washout at the flow front boundary.

An additional output from the in-situ μ -CT flow experiment are the three-dimensional reconstructions of the fibres before and after infusions, including variations in compaction. Using the segmentation process to identify the volumes between the fibre tows allows for the extraction of the resin flow channels. High resolution scans of single fibre tows could also be performed to provide the same information for the capillary flow within the fibres. Using these reconstructions, resin flow simulations can be performed using CFD to model the dual scale resin flow during a VARI.

The FBG strain measurements at PYI provided an insight into the effects of the manufacturing process followed in an industry setting. The collection of additional strain measurements at and around the chine section as well as other reinforced areas would help to develop an understanding of the variable cure rate on a large composite structure and the implications of inconsistent shrinkage profiles. FBG sensors have shown to be an acceptable sensor to embed into an industrial laminate, however the sensors proved to be very sensitive to the external environment with only one sensor surviving the manufacturing process.

9 References

- Abrams, F., Advani, S.G., Astrom, B.T., Calado, V.M.A., Campell, F.C., Cohen, D., Dave, R.S., Gebart, B.R., Joseph, B., Kardos, J.L., Khomami, B., Kim, S.C., Kranbuehl, D.E., Kruse, R.L., Li, M-C., Loos, A.C., Mallow, A.R., Mantell, S.C., Miller, A.K., Park, J.W., Strombeck, L.A., Thomas, M.M., Udipi, K. & White, S.R. (2000) *Processing of Composites* R. S. Dave & A. C. Loos. (eds.), Hander/ Gardner Publications.
- Adams, D. (2011) Composite in Cars. *2011 Research Report College of Engineering University of UTAH*. [online] University of UTAH, p.15. Available at: http://www.coe.utah.edu/research_report_2011 [Accessed 16 Sep. 2017].
- Ahlorn, H. (2009) *Characterization of Binder Application on Carbon Fibre Non-Crimp Fabric: Permeability and flow modelling*. PhD thesis, University of Stuttgart.
- Aktas, A., Boyd, S.W. & Sheno, R.A. (2012a) Measurement of Permeability and Cure Using Thermocouples in the Vacuum Assisted Resin Infusion Process to Aid Simulation. In *15th European Conference on Composite Materials*. Venice, pp. 24–28.
- Aktas, A., Boyd, S.W. & Sheno, R.A. (2012b) Monitoring and Simulation of the Vacuum Infusion Process. In *19th International Conference on Composite Materials*. Montreal, pp. 4913.
- Antonucci, J.M., Regnault, W.F. & Skrtic, D. (2010) Polymerization Shrinkage and Stress Development in Amorphous Calcium Phosphate/Urethane Dimethacrylate Polymeric Composites. *Journal of Composite Materials*, 44(3), 355.
- Aranda, S., Klunker, F., Gabber, H., Ziegmann, G. (2009) Void Content and Void Formation Mechanisms in Resin Infusion Process. In *SAMPE Europe*. Paris.
- Arbter, R., Beraud, J.M., Binetruy, C., Bizet, L., Breard, J., Comas-Cordona, S., Demaria, C., Endruweit, A., Ermanni, R., Gommer, F., Hasanovic, S., Henrat, P., Klunker, F., Laine, B., Lavanchy, S., Lomav, S.V., Long, A., Michaud, V., Morren, G., Ruiz, E., Sol, H., Tronchu, F., Verleye, B., Wietgreffe, M., Wu, W. & Ziegmann, G. (2011) Experimental Determination of the Permeability of Textiles: a Benchmark Exercise. *Composites Part A: Applied Science and Manufacturing*, 42(9), pp.1157–1168.

- Beard, J., Saouab, A. & Bouquet, G. (2003) Numerical Simulation of Void Formation in LCM. *Composites Part A: Applied Science and Manufacturing*, 34(6), p.517.
- Blest, D.C., Duffy, B.R. & McKee, S. & Zulkifle, A.K. (1999) Curing Simulation of Thermoset Composites. *Composites Part A: Applied Science and Manufacturing*, 30(6), pp.1289– 1309.
- Bruker, 2014. Bruker. Available at: <http://www.bruker.com/industries.html> [Accessed March 17, 2014].
- Boerckel, J.D., Mason, D.E., McDermott, A.M. & Alsberg, E. (2014) Microcomputed tomography: approaches and application in bioengineering. *Stem Cell Research & Therapy*, 5(6), p. 144.
- Bogetti, T.A. & Gillespie, J.W. (1989) Process-Induced Stress and Deformation in Thick-Section Thermosetting Composites. *Journal of Composite Materials*, 26(5), pp.626-660.
- Bowles, K.J. & Frimpong, S. (1992) Void Effects on the Interlaminar Shear Strength of Unidirectional Graphite Fibre-Reinforced Composites. *Journal of Composite Materials*, 26(10), pp.1487–1509.
- Cantatore, A. and Muller, P. (2011) Introduction to computed tomography. Kgs. Lyngby: DTU Mechanical Engineering. Available at: http://orbit.dtu.dk/files/51297792/Introduction_to_CT.pdf [Accessed 31 Oct. 2016].
- Cao, X. & Lee, L.J. (2003) Control of shrinkage and residual styrene of unsaturated polyester resins cured at low temperatures: I. Effect of curing agents. *Polymer*, 44(6), pp.1893–1902.
- Centea, T. & Hubert, P. (2011) Measuring the impregnation of an out-of-autoclave prepreg by micro-CT. *Composites Science and Technology*, 71(5), pp.593–599.
- Convergent Manufacturing Technologies (2010), *Manufacturing Process*, Available at <http://www.convergent.ca/solutions/manufacturing-processes> [Accessed December 15, 2010]

- Cook, L. (2010) *Princess Infusion Investigation C703PA and VE679-03PA*. Scott Bader Co Ltd. Report number: 1.
- Cook, L. (2011) *Princess Infusion Investigation C703PA and VE679-03PA*. Scott Bader Co Ltd. Report number: 2.
- Correia, N.A.C.M. (2004) *Analysis of the Vacuum Infusion Moulding Process*. PhD thesis, University of Nottingham.
- Cripps, D. (2017) Polyester Resins. [online] Netcomposites.com. Available at: <https://netcomposites.com/guide-tools/guide/resin-systems/polyester-resins/> [Accessed 2 Sep. 2017].
- Djukic, L.P., Pearce, G.M., Herszberg, I., Bannister, M.K. & Mollenhauer, D.H. (2013) Contrast Enhancement of Micro CT Scans to Aid 3D Modelling of Carbon Fibre Fabric Composites. *Applied Composite Materials*, 20, pp 1215-1230.
- Dong, C. (2011) Model Development for the Formation of Resin-Rich Zones in Composites Processing. *Composites Part A: Applied Science and Manufacturing*, 42, pp.419–424.
- Douglas, S. (2010) *Through Thickness Cure Profiles*. Princess Yachts International Plc.
- Douglas, S. (2011) *Resin Cure Characteristics*. Princess Yachts International Plc.
- Doyle, C., Martin, A., Liu, T., Wu, M., Hayes, S., Crosby, P.A., Powell, G.R. & Brooks, D. (1998) A Multi-Purpose Optical Fibre Sensor Design for Fiber Reinforced Composite Materials. *Smart Materials and Structures*, 7, pp.145–158.
- Dunkers, J.P., Lenhart, J.L., Kueh, S.R., Van-Zanten, J.H., Advani, S.G. & Parnas, R.S. (2001) Fibre Optic Flow and Cure Sensing Liquid Composite Moulding. *Optical Laser Engineering*, 35(2), pp.91–104.
- Edgren, F. (2006) *Physically Based Engineering Models for NCF Composites*. PhD thesis, Department of Aeronautical and Vehicle Engineering, School of Engineering Sciences, Stockholm.

- ESI. (2011) Infusion Process Simulation for Large and Complex Components with PAM-RTM. Available at: https://www.esi-group.com/sites/default/files/resource/brochure_flyer/1516/gro10.20a_flyer_pam-rtm_lowres.pdf [Accessed October 29, 2017].
- Fink, B.K., Mathur, R., Heider, D., Hoffman, C., Gillespie, J.W. & Advani, S.G. (2001) Experimental Validation of a Closed-Form Fluid Flow Model for Vacuum-Assisted-Resin-Transfer Moulding. *Army Research Laboratory*.
- Fink, B.K., Roderic, D.C. & Gillespie, J.W. (1999) Development of a Distributed Direct Current Sensor System for Intelligent Resin Transfer Moulding. *Army Research Laboratory*.
- Gardiner, G. (2014) Pushing the Limits of Infusion. [Blog] *Composite World*. Available at <https://www.compositesworld.com/blog/post/pushing-the-limits-of-infusion> [Accessed 30 Sep. 2015].
- George, A. (2011) *Optimization of Resin Processing for Composite Materials: Simulation and Characterization Strategies*. PhD thesis, University of Stuttgart.
- Ghiorse, S.R. (1993) Effect of Void Content on Mechanical Properties of Carbon/Epoxy Laminates. *SAMPE Quarterly*, 24(2), pp.54–59.
- Gourichon, B., Binetruy, C. & Krawczak, P. (2006) Experimental Investigation of High Fiber Tow Count Fabric Unsaturation During RTM. *Composites Science and Technology*, 66(7-8), pp.976-982.
- Greene, E. (1999) *Marine Composites*. 2nd ed. Annapolis: Eric Greene Associates Inc, pp.1.
- Groh, R. (2016) Composite Manufacturing – Autoclave Variability. Available at: www.aerospaceengineeringblog.com [Accessed October 18, 2016].
- Guo, Z.-S., Liu, L., Zhang, B-M., Du, S. (2009) Critical Void Content for Themoset Composite Laminates. *Journal of Composite Materials*, 43(17), pp.1775-1790.
- Gurit, S. (2011) *Infusion Products for Marine*,

- Hattabi, M., Echaabi, J., Benalah, M.O., Breard, J. & Saouab, A. (2005) Flow Analysis During On-Line and Radial Injection in Permeability Measurements. *Reinforced Plastics and Composites*, 24(18), pp.1909–1920.
- Hegg, M.C. (2004) *Monitoring of Resin Transfer Moulding Processes with Distributed Dielectric Sensors*. University of Washington.
- Hexcel. (2011) Advanced Fibre-reinforced Matrix Products for Direct Processes. Available at: [www.hexcel.com/Resources/DataSheets/Brochure-Data-Sheets/Advanced Fibre-Reinforced Matrix Products for Direct Processes.pdf](http://www.hexcel.com/Resources/DataSheets/Brochure-Data-Sheets/Advanced-Fibre-Reinforced-Matrix-Products-for-Direct-Processes.pdf) [Accessed September 25, 2012].
- Hayes, B.S. & Gammon, L.M. (2010) *Optical Microscopy of Fiber-Reinforced Composites*. Ohio, ASM International.
- HSE. (2003) Assessing and controlling styrene levels during contact moulding of fibre-reinforced plastics (FRP) products. *Plastics processing sheet 14*, (14), p.4.
- Jensen, D.K. (2003) Experimental Investigation of Fibre Preform Resin Infiltration in Vacuum Assisted Process, *11th European Conference on Composite materials*, Rhodes, Greece.
- Johnston, A.A. (1997) *An Integrated Model of the Development of Process-induced Deformation in Autoclave Processing of Composite Structures*. PhD thesis, University of New Brunswick.
- Judd, N.C.W. & Wright, W.W. (1978) Voids and Their Effects on Mechanical Properties of Composites- An Appraisal. *SAMPE Journal*, 14(1), pp.10–14.
- Ketcham, R. (2016). *X-ray Computed Tomography (CT)*. Available at: http://serc.carleton.edu/research_education/geochemsheets/techniques/CT.html [Accessed 3 Oct. 2016].
- Khoun, L., Chaudhuri, R.I. & Hubert, P. (2011) Effect of low-profile additives on thermo-mechanical properties of glass fiber-reinforced unsaturated polyester composites. *Journal of Reinforced Plastics and Composites*, 30(9), pp.815–823.

- Kim, Y.K. & Daniel, I.M. (2002) Cure Cycle Effect on Composite Structures Manufactured by Resin Transfer Molding. *Journal of Composite Materials*, 36(14), pp.1725–1743.
- Koorevaar, A. (2002) Simulation of Liquid Injection Moulding. In *SAMPE Europe*. Available at: www.polyworx.com/doc/sampe2002.asp.
- Kranbuehl, D.E., Kingsley, P., Hart, S., Hasko, G., Dexter, B. & Loos, A.C. (1994) In-situ Sensors for Monitoring and Intelligent Control of the Resin Transfer Moulding Process. *Polymer Composites*, 15, pp.299–305.
- Kreuzer, M. (2015). *Strain Measurement with Fibre Bragg Grating Sensors*. [online] Darmstadt: Mircon Optics. Available at; www.micronoptics.com/downloads/strain-measurement-with-fibre-bragg-grating-sensors-3/ [Accessed 21 Oct. 2017]
- Kuentzer, N., Simacek, P. & Advani, G. (2007) Correlation of void distribution to VARTM manufacturing techniques. *Composites Part A: applied science and manufacturing* 38.3 (2007): 802- 813.
- Lai, L., Carman, G., Chiou, S., Kukuchek, P. & Echternach, D. (1995) Processing Monitoring of Carbon/Phenolic Composites Using Smart Sensors. *Smart Materials and Structures*, 5, pp.8–125.
- Leclerc, J.S. & Ruiz, E. (2008) Porosity Reduction Using Optimized Flow Velocity in Resin Transfer Molding. *Composites Part A: Applied Science and Manufacturing*, 39(12), pp.1859–1868.
- Lee, D.H., Lee, W. II & Kang, M.K. (2006) Analysis and Minimization of Void Formation During Resin Transfer Molding Process. *Composite Science Technology*, 66(16), pp.3281–3289.
- Lehmann, E.L. & D’Abrera, H.J.M. (2006) *Nonparametrics: Statistical Methods Based on Ranks*, Springer.
- Leng, J.S. & Asundi, A. (2002) Real-time Cure Monitoring of Smart Composite Materials Using Extrinsic Fabry-Perot Interferometer and Fibre Bragg Grating Sensors. *Smart Materials and Structures*, 11, pp.249–255.

- Léonard, F., Stein, J., Wilkinson, A. & Withers, P.J. (2013) 3D Characterisation of Void Distribution in Resin Film Infused Composites. *Conference on industrial Computed Tomography*, pp.69–76.
- Li, M.A., Wang, A.A., Gu, Y.A., Zhang, Z.A., Li, Y.A., & Potter, K.A. (2010) Dynamic Capillary Impact on Longitudinal Micro-flow in Vacuum Assisted Impregnation and the Unsaturated Permeability of Inner Fiber Tows. *Composites Science Technology* 70 pp.1628-1636.
- Lims, S.T. & Lee, W. (2000) Analysis of the Three-dimensional Resin Transfer Mould Filling Process. *Composite Science Technology*, 60, pp.961–975.
- Lodeiro, M.J. & Mulligan, D.R. (2005) *Cure Monitoring Techniques for Polymer Composites, Adhesives and Coatings*. Engineering and Process Control Division, National Physical Laboratory.
- Loos, A.C. & Springer, G.S. (1982) Curing of Epoxy Matrix Composites. *Journal of Composite Materials*, 17, pp.135–169.
- Lundström, T., Frishfelds, V. & Jakovics, A. (2010) Bubble formation and motion in non-crimp fabrics with perturbed bundle geometry. *Composites Part A: Applied Science and Manufacturing*, 41(1), pp.83–92.
- March, G. (2010) *Airbus A350XWB update – Materials Today*. [online] Materials Today. Available at: <https://www.materialstoday.com/composite-applications/features/airbus-a350-xwb-update/> [Accessed 16 Dec. 2010].
- Martin, R.E. & Gyekenyesi, A.L. (2005) *Flaw Detection for Composite Materials Improved by Advanced Thermal Imaging Reconstruction Techniques*. NASA
- Matsuzaki, R., Seto, D., Todoroki, A. & Mizutani, Y. (2013) In-situ void content measurements during resin transfer molding. *Advanced Composite Materials*, 22(4), pp.239–254.

- Mavrogordato, M. (2017) *The μ -VIS centre*. Engineering and the Environment, University of Southampton. Available at:
<https://www.southampton.ac.uk/muvis/about/equipment.page> [Accessed 5 Oct. 2017].
- Maxwell, A.S., Broughton, W., Lodeiro, M. & Shaw, R. (2009) *Measurement of Residual Stresses Strains in Carbon Fibre Composites*. National Physical Laboratory.
- Mazumdar, S.K. (2002) *Composite Manufacturing: Materials, product, and process engineering*, CRC Press, Taylor & Francis Group.
- Morgan, M. (2015) Characterizing the Effects of Capillary Flow During Liquid Composite Molding. PhD Thesis. Brigham Young University.
- Morrison, C.E. & Bader, M.G. (1989) Computer Modelling of Resin Flow During Laminate Cure. *Composites*, 20(1), pp.9–13.
- NASA. (1996) *New Inspection System Uses Heat to Detect Flaws*. Available at:
<http://www.nasa.gov/centers/langley/news/factsheets/Thermal.html> [Accessed September 21, 2012].
- National Instruments. (2016) *FBG Optical Sensing: A new Alternative for Challenging Strain Measurements- National Instruments* [online] Available at: www.ni.com/white-paper/12338/en/ [Accessed 21 Oct 2017].
- Ngo, N.D. & Tamma, K.K. (2001) Non-isothermal 2-D Flow/3-D Thermal Developments Encompassing Process Modelling of Composites: Flow/Thermal/Cure Formulations and Validations. *International Journal for Numerical Methods in Engineering*, 50(7), pp.1559–1585. Available at: <http://doi.wiley.com/10.1002/nme.85>.
- Nielsen, M.W., Schmidt, J. W., Hogh, J. H., Waldbjorn, J. P., Hattel, J. H., Andersen, T. L. (2013) Life cycle strain monitoring in glass fibre reinforced polymer laminates using embedded fibre Bragg grating sensors from manufacturing to failure. *Journal of Composite Materials*. 48(3), pp.365-381.

- Nixon, J.A. (2000) *Integrated Design and Manufacture Using Fibre-Reinforced Polymeric Composites* M. J. Owen, V. Middleton, & I. A. Jones, eds., Cambridge: Woodhead Publishing.
- Norwood, L.S. (2001) Glass Reinforced Plastics- Performance with Post Cures. *South African Conference University of the Witwatersrand RP/Composites Facility/ SASOL Polymers/ PCISA Conference*
- Pantelalis, N.G. (2003) Optimized Cure Cycles for Resin Transfer Moulding. *Composite Science Technology*, 63, pp.249–263.
- Pantelis, N. & Maistros, G. (2006) Process Monitoring for Liquid Composite Moulding Using Durable Sensors. In *Proceedings of the 27th Risoe International Symposium on Material Science*. pp. 279–285.
- Park, C.H. & Lee, W. I. (2011) Modelling Void Formation and Unsaturated Flow in Liquid Composite Molding Process: A Survey and Review. *Journal of Reinforced Plastics and Composites*, 30(11), pp.957-977.
- Park, H.C. & Lee, S.W. (2001) Cure Simulation of Thick Composite Structures Using Finite Element Method. *Journal of Composite Materials*, 35, pp.188–201.
- Patel, N. & Lee, L.J. (1995) Effect of Fibre Architecture on Void Formation and Removal in Liquid Composite Moulding. *Polymer Composites*, 16(5), pp.386–399.
- Paul, J.T. & Thomson, J.B. (1965) The Importance of Voids in the Filament Wound Structure. In *SPI Composite Institutes 20th Annual Conference*. New York.
- Pearce, N., Guild, F. & Summerscales, J. (1998) A study of the effects of convergent flow fronts on the properties of fibre reinforced composites produced by RTM. *Composites Part (A)*, 29(97), pp.141–152.
- Potgieter, K. (2016) Planing Hulls. Available at: <http://www.navaldesign.co.za/articles> [Accessed October 28, 2016]
- Potter, K. (2012) *Resin transfer moulding*. Springer Science & Business Media, p.21.

- Radford, D.W. (1993) Cure Shrinkage-induced Warpage in Flat Uni-Axial Composites. *Journal of Composite, Technology and Research*, 15(4), pp.290–296.
- Ragondet, A. (2005) *Experimental Characterisation of the Vacuum Infusion Process*. PhD thesis, University of Nottingham.
- Rogozen M. B. (1982) Control Techniques for Organic Gas Emissions from Fiberglass Impregnation and Fabrication Processes, ARB/R-82/165, California Air Resources Board, Sacramento, CA.
- Rudd, C.D., Long, A.C., Kendall, K.N. & Mangin, C.G. (1997) *Liquid Moulding Technologies Resin Transfer Moulding, Structural Reaction Injection Moulding and Related Processing Techniques*, Cambridge: Wood head publishing.
- Russell, J.D., Madhukar, M.S., Genidy, M.S., Lee. A.Y. (2000) A New Method to Reduce Cure-Induced Stresses in Thermoset Polymer Composites, Part III: Correlating Stress History to Viscosity, Degree of Cure, and Cure Shrinkage. *Journal of Composite Materials*, 34(22), pp.1926–1947
- Sander, R. (1999) Compilation of Henry' s Law Constants for Inorganic and Organic Species of Potential Importance in Environmental Chemistry. Available at: www.rolf-sander.net/henry/henry.pdf.
- Schell, J.S.U., Deleglise, M., Binetruy, C., Krawczak, P., Ermanni, P. (2007) Numerical Prediction and Experimental Characterisation of Meso-scale Voids in Liquid Composite Moulding. *Composites Part A: Applied Science and Manufacturing*, 38(12), pp.2460–2470.
- Schilling, P.J., Karedla, B.P.R., Tatiparthi, A.K., Verges, M.A. & Herrington, P.D., 2005. X-ray computed microtomography of internal damage in fiber reinforced polymer matrix composites. *Composites Science and Technology*, 65(14), pp.2071–2078.
- Selvaraju, S. and Ilaiyavel, S. (2011). Applications of Composites in Marine Industry. *Journal of Engineering Research and Studies*, 3(2), pp.89-91.

- Shenoi, R.A. & Wellicome, J.F. (1993) *Composite Materials in Marine Structure* 1st ed., Cambridge: Cambridge University Press.
- Shepard, D.D. (1998) Resin Flow Front Monitoring Saves Money and Improves Quality. *SAMPE Journal*, 34, pp.31–35.
- Shokrieh, M.M. (2005) Theoretical and Experimental Studies on Residual Stresses in Laminated Polymer Composites. *Journal of Composite Materials*, 39(24), pp.2213–2225. Available at: <http://jcm.sagepub.com/cgi/doi/10.1177/0021998305053511> [Accessed September 26, 2011].
- Skordos, A.A. & Partridge, I.K. (2000) Dielectric flow sensing in resin transfer moulding of carbon fibre reinforced composites. In *Plastics Rubber and Composites* 29. pp. 391–394.
- Slusar, B., Flek, M., Yubtsov, R., Shevtsov, S. & Fomin, A. (2005) Mould Heating Distribution Control System Simulation for Polymerization of a Composite Spar for Helicopter Main Rotor Blade. In *Proceedings of Comsol Multiphysics User's Conference*. Stockholm.
- Smartfibre, (2016) *Fibre Bragg Grating (FBG) Optical Fibre Sensors for Zero Power, Intrinsically Safe Measurements.*: Available at: <http://www.smartfibres.com/fibre-bragg-grating.html> [Accessed October 20, 2016].
- Smith, R. A. (2009) Composite Defects and Their Detection. *Materials Science and Engineering*, (3) pp 103-143
- Song, X., Loos, A.C., Grimsley, B.W., Cano, R.J. & Hubert, P. (2004) Modelling the VARTM Composite Manufacturing Process. In *SAMPE Technical Conference*. pp. 469–491.
- Sorrentino, L. & Tersigni, L. (2010) A Method for Cure Process Design of Thick Composite Components Manufactured by Closed Die Technology. *Applied Composite Materials*, 19(1), pp.31-45.
- Sorrentino, L., Bellini, C., Carrino, L., Leone, A., Mostarda, E., Tersigni, L. (2009) Cure Process Design to manufacture composite components with variable thickness by a

- closed die technology. In *17th International Conference on Composite Materials*. Edinburgh, pp. 27–31.
- Stadtfield, H.C., Erninger, M., Bickerton, S. & Advani, S.G. (2002) An Experimental Method to Continuously Measure Permeability of Fibre Preforms as a Function of Fibre Volume Fraction. *Journal of Reinforced Plastics and Composites*, 21(10), pp.879–900.
- Summerscales, J. (2016) Composite Manufacturing for Marine Structures. *Marine Applications of Advanced Fibre-Reinforced Composites*, p.29.
- Stone, D.E.W. & Clark, B. (1975) Ultrasonic Attenuation as a Measure of Void Content in Carbon Fiber Reinforced Plastics. *Nondestructive Testing*, 8, pp.137–145.
- Thibaudeau, M. (2003) *Towards a Fully Integrated Resin Infusion Process*. PhD thesis, University of Southampton.
- Todd, M.D. (2013) *Fibre Optic Bragg Grating-based Sensing*. San Diego: University of California. Available at: http://www.sem.org/pdf/fiber_bragg_grating_sensing.pdf [Accessed October 27, 2012].
- Tsai, S.W. & H. T. Hahn (1980) *Introduction to Composite Materials*, Technomic Publishing Co.
- Tuncol, G., Danisman, M., Kaynar, A. & Sozer, E.M. (2007) Constraints on Monitoring Resin Flow in the Resin Transfer Moulding (RTM) Process by Using Thermocouple Sensors. *Composites Part A: Applied Science and Manufacturing*, 38, pp.1363–1386.
- Varna, J., Joffe, R., Berglund, L.A. & Lundström, T.S. (1995) Effects of Voids on Failure Mechanisms in RTM Laminates. *Composite Science Technology*, 53, pp.241–249.
- Verrey, J., Michaud, V. and Manson, J. (2006) Dynamic capillary effects in liquid composite moulding with non-crimp fabrics. *Composites Part A*:37(1), pp92-102.
- Walsh, B.J. (2011) Up in a Downtime. *Professional Boat Builder*, pp.26–37.
- Walsh, S.W. (1993) In-situ Sensor Method and Devices. U.S. Patent No. 5,210,499

- Wang, R., Zheng, S. & Zheng, Y. (2011) *Polymer Matrix Composites and Technology*. Wood Head publishing, Cambridge. Pp.174.
- Wielhorski, Y., Abdelwahed, A.B., & Bizet, L. (2012) Theoretical and Experimental Modelling of Bubble Formation with Connected Capillaries in Liquid Composite Moulding Processes, In: *11th International Conference Flow Processing in Composite Materials*, Auckland, New Zealand (2012)
- Williams, J.G., Morris, C.E.M. & Ennis, B.C. (1974) Liquid Flow Through Aligned Fibre Beds. *Polymer Engineering and Science*, 14(6), pp.413–419.
- Yamada, H., Mihata, I., Tomiyama, T. & Walsh, S.P. (1992) Investigation of Fundamental Causes of Pinholes in SMC Mouldings. In *SPI Composites Institute 47th Annual Conference*. New York.
- Young, W. (1996) The Effect of Surface Tension on Tow Impregnation of Unidirectional Fibrous Preform in Resin Transfer Molding. *Journal of Composite Materials*, 30(11), pp.1191-1209.
- Zhang, J., Xu, C. & Huang, P. (2009) Effect of Cure Cycle on Curing Process and Hardness for Epoxy Resin. *eXPRESS Polymer Letters*, 3(9), pp.534–541. Available at: http://www.expresspolymlett.com/articles/EPL-0001016_article.pdf [Accessed September 1, 2011].

10 Appendices

Appendix A-Princess Yachts Production Model Information

Current and Archived Production/ Development Models						
	P- Class		Length	Beam	Draught	Displacement
A2	Princess	40MY	40.16	8.02	2.29	230,000
A4	Princess	32MY	32	7.11	1.98	115,000
A3	Princess	72	22.35	5.49	1.68	45,000
Y7	Princess	95MY	30.12	7.06	1.83	106,000
Y8	Princess	P82	25.93	6.3	1.65	86,600
Y9	Princess	78MY	24.1	5.76	1.7	58, 500
Z5	Princess	62				
T9	Princess	60	18.61	4.83	1.27	30,500
N5	Princess	54	16.57	4.57	1.27	23,500
N4	Princess	50	15.37	4.57	1.27	22,900
R6	Princess	45				
R7	Princess	47				
R8	Princess	50				
M4	Princess	42	13.48	4.14	1.09	14,000
M9	Princess	(M4) 42 with IPS drives	13.48	4.14	1.09	14,000
B1	Princess	V57	17.88	4.65	1.27	22,900
B2	Princess	V65				
P6	Princess	V62	19.14	4.99	1.13	29,500
P7	Princess	V53	16.61	4.45	1.14	21,100
P8	Princess	V70				
P9	Princess	V85	25.98	6.27	1.81	74,000
S1	Princess	V78	23.83	5.66	1.65	47,500
S2	Princess	V72	22.26	5.38	1.06	42,000
X6	Princess	V50				
X7	Princess	V38	12.98	3.81	0.56	9,100
Y2	Princess	22M				
Y3	Princess	20M				
Y4	Princess	25m				
Y5	Princess	23m				
Y6	Princess	21m				
Z2	Princess	60				
Z3	Princess	65				
Z4	Princess	61				
Z6	Princess	67				
T6	Princess	56				
T7	Princess	57				
P5	Princess	V50				
T8	Princess	57 (upgrade)				

Table: 9 Princess yachts production models

Appendix B - Princess Yachts Hull Infusion Process and Material Data Sheets

The following procedure outlines the process that the laminating team at PYI follow when infusing a hull form.

1. Mould inspected for defects.
2. Mould cleaned and release wax applied.
3. Gelcoat hand rolled to the female mould.
4. Gelcoat cure.
5. Barrier coat hand rolled to the gelcoat.
6. Barrier coat cure.
7. Skin coat hand rolled to the barrier coat.
8. Skin coat cure.
9. Outer skin reinforcement laid into the mould with additional reinforcement added in specific areas as can be seen in Figure 160 where the additional reinforcement are called extras. 3M spray adhesive used to hold the reinforcement in the correct location.
10. Core kit laid into the mould with gaps filled with core foam.
11. Inner skin reinforcement laid into the mould.
12. Peel ply laid over reinforcement.
13. Infusion mesh laid over monolithic sections and at the resin inlet points, an example can be seen in Figure 81, identified by the green hatched areas.
14. Spiral cable laid on top of the infusion mesh, an example of the positioning of the infusion points can be seen in Figure 81.
15. Vacuum bag laid and sealed around the top of the mould using sealant tape.
16. Resin inlet tubes attached through the vacuum bag and sealed.
17. Vacuum applied.
18. Vacuum pressure monitored until pressure is below 10mb at all pumps.
19. Vacuum leak test performed where the vacuum pressure is monitored for 5 minutes with the vacuum pumps turned off. A leak rate below 10mb/minute must be achieved.
20. Vacuum pumps applied, the vacuum is measured in the mould and must be below 50mb.
21. The resin batch number, expiry date, resin temperature, viscosity and catalyst mixture are all measured and recorded, with the expected gel time also calculated.
22. Ambient temperature and mould temperature are recorded before the resin inlet at the keel is opened.
23. Keel resin inlet opened, Figure 81.
24. Visual monitoring of the flow location of the vacuum bag is used to open and close the resin inlets. The number of inlets is dependent on the size of the infusion, an example for a smaller component can be seen in Figure 81 where a keel, boost 1, chine and boost 2 resin inlet are shown. For larger infusions additional resin inlets will be placed between boost 1 and the chine and boost 2 and the top of the topside.
25. During the infusion, acoustic measurements are constantly taken to monitor the vacuum integrity of the bag, whilst vacuum bag temperatures are also recorded.
26. Once the infusion is complete the resin inlets area is closed and the vacuum pumps remains on during the cure and post cure. During the fibre optic infusion, the vacuum pumps were stopped 16 hours after the end of the infusion.
27. Post cure applied to moulds which use water controlled mould temperatures.

28. The vacuum bag and other consumables are removed from the component.
29. Lifting points are laminated on the hull at 4 locations to allow the component to be lifted from the mould.
30. 2 beams are attached to the top of the hull to support the structure once the component is released from the mould.
31. Component lifted and placed into a cradle and moved to the next stage of the production line.

The Data Sheets for the resin system and reinforcement used in this research can be found in the following pages.

CRYSTIC[®] 703PA

Polyester Resin for Vacuum Injection

Introduction

Crystic 703PA is a pre-accelerated, DCPD based polyester resin with low viscosity and controlled exotherm characteristics.

Approvals

Crystic 703PA is approved by Lloyd's Register of Shipping for use in construction of craft under their survey.

Applications

Crystic 703PA was developed primarily as a Vacuum Injection resin, but its properties make it suitable for use in other, similar techniques. The viscosity and exotherm characteristics of Crystic 703PA make it particularly suitable for the manufacture of large structures by Vacuum Injection methods.

Features and Benefits

Crystic 703PA has excellent mechanical properties and impact resistance. It is compatible with most reinforcement types.

Formulation

Crystic 703PA should be allowed to attain workshop temperature (18°C - 20°C) before use. It requires only the addition of a catalyst to start the curing reaction. The recommended catalyst is Catalyst M (or Butanox M50), which should be added at 1% - 2% into the resin. The catalyst should be thoroughly incorporated into the resin, using a low shear mechanical stirrer where possible. Geltimes of Crystic 702PAX and Crystic 702PA, using various catalyst levels, can be approximately determined from the table below.

Pot Life

Temperature	Pot Life in minutes using Butanox M50		
	Crystic 703PA		
	1.0% M50	1.5% M50	2.0% M50
Pot life in minutes at 15°C	318	196	140
Pot life in minutes at 20°C	205	124	84
Pot life in minutes at 25°C	128	84	64

The resin, mould and workshop should be at, or above 15°C before curing is carried out.

Additives

The addition of fillers or pigment pastes can adversely affect the Vacuum Injection process and also the properties of the cured laminate. Users should seek the advice of Scott Bader's Technical Service Department before making any additions.

Post Curing

Satisfactory laminates for many applications can be made from Crystic 703PA by curing at workshop temperature (20°C). For optimum properties, however, laminates should be postcured before being put into service. The laminate should be allowed to cure for 24 hours at 20°C, and then be oven cured for 16 hours at 40°C or 3 hours at 80°C.

Figure 148: Crystic 703pa Data Sheet page 1

Typical Properties

The following tables give typical properties of Crystic 703PA when tested in accordance with BS or BS EN ISO test method.

Property		Liquid Resin	
Appearance		Mauvish	
Viscosity at 25 °C	Poise	1.6	
Volatile Content	%	28	
Acid Value	Mg KOH/g	22	
Stability at 20 °C	months	3	
Geltime at 20 °C using 1.5% Butanox M50	minutes	124	
Property		Fully Cured* Resin (unfilled casting)	
		(1)	(2)
Barcol Hardness (Model GYZJ 034-1)		42	43
Deflection Temperature under load (1.80 MPa)	°C	59	64
Water Absorption 24 hours at 23°C	mg	-	11
Tensile Strength	MPa	49	38
Tensile Modulus	MPa	2758	3162
Elongation at Break	%	2.1	1.3

(1) Curing schedule – 24 hours at 20 °C, 16 hours at 40°C

(2) Curing schedule – 24 hours at 20 °C, 3 hours at 80°C

Property		C.S.M** Laminate
Glass Content	%	25
Tensile Strength	MPa	75
Tensile Modulus	MPa	6170
Elongation at Break	%	1.54
Flexural Strength	MPa	1185
Flexural Modulus	MPa	5180

** Made with 1 layer Rovicore 600 D3 600
Curing schedule – 24 hours at 20°C, 16 hours at 40°C

Figure 149: Crystic 703pa Data Sheet page 2

Storage

Crystic 703PA should be stored in the dark in suitable closed containers. It is recommended that the storage temperature should be less than 20°C where practical, but should not exceed 30°C. Ideally, containers should be opened only immediately prior to use.

Packaging

Crystic 703PA is supplied in 25kg, 225kg and 1.1 tonne containers. Bulk supplies can be delivered by road tanker.

Health & Safety

Please see separate Material Safety Data Sheet.

Version 2 : February 2013

All information on this data sheet is based on laboratory testing and is not intended for design purposes. Scott Bader makes no representations or warranties of any kind concerning this data. Due to variance of storage, handling and application of these materials, Scott Bader cannot accept liability for results obtained. The manufacture of materials is the subject of granted patents and patent applications; freedom to operate patented processes is not implied by this publication.

SCOTT BADER COMPANY LIMITED

Wollaston, Wellingborough, Northamptonshire, NN29 7RL

Telephone: +44 (0) 1933 663100

Facsimile: +44 (0) 1933 666623

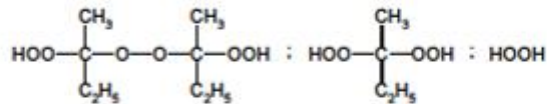
www.scottbader.com

Figure 150:Crystic 703pa Data Sheet page 3

Butanox[®] M-50

Product description

Methyl ethyl ketone peroxide, solution in dimethyl phthalate



CAS No. : 1338-23-4
 EINECS/ELINCS No. : 215-661-2
 TSCA status : listed on inventory

Specifications

Appearance : Clear and colorless liquid
 Total active oxygen : 8.8-9.0%

Characteristics

Density, 20°C : 1.180 g/cm³
 Viscosity, 20°C : 24 mPa.s
 Water content : max. 3.0%

Storage

Due to the relatively unstable nature of organic peroxides a loss of quality can be detected over a period of time. To minimize the loss of quality, Akzo Nobel recommends a maximum storage temperature (T_s max.) for each organic peroxide product.

For *Butanox M-50* T_s max. = 25°C

When stored under the recommended storage conditions, *Butanox M-50* will remain within the Akzo Nobel specifications for a period of at least three months after delivery.

Thermal stability

Organic peroxides are thermally unstable substances, which may undergo self-accelerating decomposition. The lowest temperature at which self-accelerating decomposition of a substance in the original packaging may occur is the Self-Accelerating Decomposition Temperature (SADT). The SADT is determined on the basis of the Heat Accumulation Storage Test.

For *Butanox M-50* SADT : 60°C

The Heat Accumulation Storage Test is a recognized test method for the determination of the SADT of organic peroxides (see Recommendations on the Transport of Dangerous Goods, Manual of Tests and Criteria - United Nations, New York and Geneva).

Major decomposition products

Carbon dioxide, Water, Acetic acid, Formic acid, Propanoic acid, Methyl ethyl ketone

Packaging and transport	<p>The standard packaging is a 30 l HDPE can (Nourytainer®) for 30 kg peroxide solution.</p> <p>In Asia Pacific the standard packaging is a 30 l HDPE can for 20 kg peroxide solution.</p> <p>Both packaging and transport meet the international regulations. For the availability of other packed quantities contact your Akzo Nobel representative.</p> <p><i>Butanox M-50</i> is classified as Organic peroxide type D; liquid; Division 5.2; UN 3105; PG II.</p>				
Safety and handling	<p>Keep containers tightly closed. Store and handle <i>Butanox M-50</i> in a dry well-ventilated place away from sources of heat or ignition and direct sunlight. Never weigh out in the storage room.</p> <p>Avoid contact with reducing agents (e.g. amines), acids, alkalis and heavy metal compounds (e.g. accelerators, driers and metal soaps).</p> <p>Please refer to the Material Safety Data Sheet (MSDS) for further information on the safe storage, use and handling of <i>Butanox M-50</i>. This information should be thoroughly reviewed prior to acceptance of this product. The MSDS is available at www.akzonobel-polymerchemicals.com.</p>				
Applications	<p><i>Butanox M-50</i> is a general purpose methyl ethyl ketone peroxide (MEKP) for the curing of unsaturated polyester resins in the presence of a cobalt accelerator at room and elevated temperatures.</p> <p>The curing system <i>Butanox M-50</i>/cobalt accelerator is particularly suitable for the curing of gelcoat resins, laminating resins, lacquers and castings; moreover the manufacture of light resistant parts may be possible contrary to the curing system benzoyl peroxide/amine accelerator.</p> <p>Practical experience throughout many years has proven that by the guaranteed low water content and the absence of polar compounds in <i>Butanox M-50</i>, this peroxide is very suitable in GRP products for e.g. marine applications.</p> <p>For room temperature application it is necessary to use <i>Butanox M-50</i> together with a cobalt accelerator (e.g. Accelerator NL-49P).</p>				
Dosing	<p>Depending on working conditions, the following peroxide and accelerator dosage levels are recommended:</p> <table border="0" style="margin-left: 40px;"> <tr> <td style="padding-right: 20px;"><i>Butanox M-50</i></td> <td>1 - 4 phr*</td> </tr> <tr> <td>Accelerator NL-49P</td> <td>0.5 - 3 phr</td> </tr> </table>	<i>Butanox M-50</i>	1 - 4 phr*	Accelerator NL-49P	0.5 - 3 phr
<i>Butanox M-50</i>	1 - 4 phr*				
Accelerator NL-49P	0.5 - 3 phr				

*phr = parts per hundred resin

TS 65421.05/June 2005
Page 2 of 4

Figure 152: Butanox M50 Data Sheet page 2

Cure Characteristics

In a high reactive standard orthophthalic resin in combination with Accelerator NL-49P (= 1% cobalt) the following application characteristics were determined:

Gel times at 20°C

2 phr *Butanox* M-50 + 0.5 phr Accelerator NL-49P 12 minutes
 2 phr *Butanox* M-50 + 1.0 phr Accelerator NL-49P 7 minutes

Cure of 1 mm pure resin layer at 20°C

The speed of cure is expressed as the time to reach a Persoz hardness of respectively 30, 60 and 120 s.

	Persoz:		
	30	60	120 s
2 phr <i>Butanox</i> M-50 + 0.5 phr Accelerator NL-49P	2.4	4.1	13 h
2 phr <i>Butanox</i> M-50 + 1.0 phr Accelerator NL-49P	1.7	3.0	9.5 h

Cure of 4 mm laminates at 20°C

4 mm laminates have been made with a 450 g/m² glass chopped strand mat. The glass content in the laminates is 30% (w/w).

The following parameters were determined:

- Time-temperature curve.
- Speed of cure expressed as the time to achieve a Barcol hardness (934-1) of 0-5 and 25-30 respectively.
- Residual styrene content after 24 h at 20°C and a subsequent postcure of 8 h at 80°C.

	Gel time (min.)	Time to peak (min.)	Peak exotherm (°C)
2 phr <i>Butanox</i> M-50 + 0.5 phr Accelerator NL-49P	13	36	44
2 phr <i>Butanox</i> M-50 + 1.0 phr Accelerator NL-49P	8	26	64

	Barcol		Res. styrene	
	0-5	25-30	24 h + 8 h	20°C + 80°C
	(h)	(h)	(%)	(%)
2 phr <i>Butanox</i> M-50 + 0.5 phr Accelerator NL-49P	3	15	6	0.3
2 phr <i>Butanox</i> M-50 + 1.0 phr Accelerator NL-49P		1	5	0.1

Figure 153: Butanox M50 Data Sheet page 3

Pot life at 20°C

Pot lives were determined of a mixture of *Butanox* M-50 and a non-preaccelerated UP resin at 20°C.

2 phr <i>Butanox</i> M-50	12 h
4 phr <i>Butanox</i> M-50	7 h

Solubility *Butanox* M-50 is miscible with phthalates and slightly miscible with water.

Colors *Butanox* M-50 is available in the colors blue, yellow-A, red-YM and red-YM 1/6.

Butanox and *Nouryliner* are registered trademarks of Akzo Nobel Chemicals BV or affiliates in one or more territories.

All information concerning this product and/or suggestions for handling and use contained herein are offered in good faith and are believed to be reliable. Akzo Nobel Polymer Chemicals, however, makes no warranty as to accuracy and/or sufficiency of such information and/or suggestions, as to the product's merchantability or fitness for any particular purpose, or that any suggested use will not infringe any patent. Nothing contained herein shall be construed as granting or extending any license under any patent. Buyer must determine for himself, by preliminary tests or otherwise, the suitability of this product for his purposes. The information contained herein supersedes all previously issued bulletins on the subject matter covered. The user may forward, distribute, and/or photocopy this document only if unaltered and complete, including all of its headers and footers, and should refrain from any unauthorized use. You may not copy this document to a website.



Akzo Nobel Polymer Chemicals BV
Amersfoort, The Netherlands
Tel: +31 33 467 6767
Fax: +31 33 467 6151
polymerchemicals.nl@akzonobel-pc.com

Akzo Nobel Polymer Chemicals LLC
Chicago, U.S.A.
Tel: +1 312 544 7000
1 800 825 7929 (Toll free US only)
Fax: +1 312 544 7188
polymerchemicals.us@akzonobel-pc.com

Akzo Nobel Polymer Chemicals Ltd.
Shanghai, PR China
Tel: +86 21 6279 3399
Fax: +86 21 6247 1129
polymerchemicals.ap@akzonobel-pc.com

www.akzonobel-polymerchemicals.com

Figure 154: *Butanox* M50 Data Sheet page 4



TECHNICAL DATASHEET

SAP No. 30000439 Article Description X-E-612g/m²-1270mm

Textile Structure 7000209 SAERTEX®

ARTICLE CONSTRUCTION (in accordance with EN 13473-1)

Layer	Construction	Areal weight	Tolerance	Material
4	45 °	300 g/m ²	+/- 5 %	E-glass 300 TEX
3	90 °	3 g/m ²	+/- 5 %	E-glass 68 TEX
2	0 °	3 g/m ²	+/- 5 %	E-glass 68 TEX
1	-45 °	300 g/m ²	+/- 5 %	E-glass 300 TEX
Stitching		6 g/m ²	+/- 1 g/m ²	PES [Polyester] 76 dtex

Fiber input can be determined individually

FURTHER CHARACTERISTICS

Gauge	5,0	Stitching pattern	warp	Width (nominal)	1.270 mm
Stitch length	2,02 mm	Total tolerance	5,1 %	Total areal weight	612 g/m ²

Labelling (Standard) Every roll is equipped with a label in the core. A further label is located outside on the foil or on the box.

Packaging (Standard) Every roll is wound on a cardboard core and wrapped in foil. Further packaging options can be determined individually.

Storage recommendation With original packaging: Temperature 15-35°C and 20-80% humidity. No moisture and direct sunlight. To avoid problems with humidity and electrostatic charge, fabrics to be conditioned 24 hours prior to processing, independent of storage conditions.

SAERTEX GmbH & Co. KG has been certified in accordance with ISO 9001:2002008 and has been awarded the 2016 Eco-Profit Award. The SAERTEX GmbH & Co. KG has its own DNV GL certified laboratory.

REINFORCING YOUR IDEAS



TECHNICAL DATASHEET

SAP No. 30000341 Article Description Q-E-986g/m²-1270mm

Textile Structure 7000171 SAERTEX®

ARTICLE CONSTRUCTION (in accordance with EN 13473-1)

Layer	Construction	Areal weight	Tolerance	Material
4	0 °	236 g/m ²	+/- 5 %	E-glass 600 TEX
3	45 °	251 g/m ²	+/- 5 %	E-glass 300 TEX
2	90 °	236 g/m ²	+/- 5 %	E-glass 600 TEX
1	-45 °	251 g/m ²	+/- 5 %	E-glass 300 TEX
Stitching		12 g/m ²	+/- 3 g/m ²	PES [Polyester] 76 dtex

Fiber input can be determined individually

FURTHER CHARACTERISTICS

Gauge	10,0	Stitching pattern	tricot-warp	Width (nominal)	1.270 mm
Stitch length	2,60 mm	Total tolerance	5,2 %	Total areal weight	986 g/m ²

- Labelling (Standard)** Every roll is equipped with a label in the core. A further label is located outside on the foil or on the box.
- Packaging (Standard)** Every roll is wound on a cardboard core and wrapped in foil. Further packaging options can be determined individually.
- Storage recommendation** With original packaging: Temperature 15-35°C and 20-80% humidity. No moisture and direct sunlight. To avoid problems with humidity and electrostatic charge, fabrics to be conditioned 24 hours prior to processing, independent of storage conditions.

SAERTEX GmbH & Co. KG has been certified in accordance with ISO 9001:2002008 and has been awarded the 2016 Eco-Profit Award. The SAERTEX GmbH & Co. KG has its own DNV GL certified laboratory.

REINFORCING YOUR IDEAS



TECHNICAL DATASHEET

SAP No. 30000448 Article Description X-S-E-1109g/m²-1270mm

Textile Structure 7000217 SAERTEX®

ARTICLE CONSTRUCTION (in accordance with EN 13473-1)

Layer	Construction	Areal weight	Tolerance	Material
4	CSM	300 g/m ²	+/- 10 %	E-glass
3	45 °	401 g/m ²	+/- 5 %	E-glass 600 TEX
2	0 °	1 g/m ²	+/- 5 %	E-glass 68 TEX
1	-45 °	401 g/m ²	+/- 5 %	E-glass 600 TEX
Stitching		6 g/m ²	+/- 1 g/m ²	PES [Polyester] 76 dtex

Fiber input can be determined individually

FURTHER CHARACTERISTICS

Gauge	5,0	Stitching pattern	tricot	Width (nominal)	1.270 mm
Stitch length	2,60 mm	Total tolerance	6,4 %	Total areal weight	1109 g/m ²

Labelling (Standard) Every roll is equipped with a label in the core. A further label is located outside on the foil or on the box.

Packaging (Standard) Every roll is wound on a cardboard core and wrapped in foil. Further packaging options can be determined individually.

Storage recommendation With original packaging: Temperature 15-35°C and 20-80% humidity. No moisture and direct sunlight. To avoid problems with humidity and electrostatic charge, fabrics to be conditioned 24 hours prior to processing, independent of storage conditions.

SAERTEX GmbH & Co. KG has been certified in accordance with ISO 9001:2002008 and has been awarded the 2016 Eco-Profit Award. The SAERTEX GmbH & Co. KG has its own DNV GL certified laboratory.

REINFORCING YOUR IDEAS



TECHNICAL DATASHEET

SAP No. 30000383 Article Description Q-E-1232g/m²-1270mm

Textile Structure 7000200 SAERTEX®

ARTICLE CONSTRUCTION (in accordance with EN 13473-1)

Layer	Construction	Areal weight	Tolerance	Material
4	0 °	319 g/m ²	+/- 5 %	E-glass 900 TEX
3	45 °	300 g/m ²	+/- 5 %	E-glass 300 TEX
2	90 °	307 g/m ²	+/- 5 %	E-glass 600 TEX
1	-45 °	300 g/m ²	+/- 5 %	E-glass 300 TEX
Stitching		6 g/m ²	+/- 1 g/m ²	PES [Polyester] 76 dtex

Fiber input can be determined individually

FURTHER CHARACTERISTICS

Gauge	5,0	Stitching pattern	tricot	Width (nominal)	1.270 mm
Stitch length	2,60 mm	Total tolerance	5,1 %	Total areal weight	1232 g/m ²

Labelling (Standard) Every roll is equipped with a label in the core. A further label is located outside on the foil or on the box.

Packaging (Standard) Every roll is wound on a cardboard core and wrapped in foil. Further packaging options can be determined individually.

Storage recommendation With original packaging: Temperature 15-35°C and 20-80% humidity. No moisture and direct sunlight. To avoid problems with humidity and electrostatic charge, fabrics to be conditioned 24 hours prior to processing, independent of storage conditions.

SAERTEX GmbH & Co. KG has been certified in accordance with ISO 9001:2002008 and has been awarded the 2016 Eco-Profit Award. The SAERTEX GmbH & Co. KG has its own DNV GL certified laboratory.

REINFORCING YOUR IDEAS



TECHNICAL DATASHEET

SAP No. 30000457 Article Description X-E-1212g/m²-1270mm

Textile Structure 7000227 SAERTEX®

ARTICLE CONSTRUCTION (in accordance with EN 13473-1)

Layer	Construction	Areal weight	Tolerance	Material
4	45 °	601 g/m ²	+/- 5 %	E-glass 1.200 TEX
3	90 °	3 g/m ²	+/- 5 %	E-glass 68 TEX
2	0 °	1 g/m ²	+/- 5 %	E-glass 34 TEX
1	-45 °	601 g/m ²	+/- 5 %	E-glass 1.200 TEX
Stitching		6 g/m ²	+/- 1 g/m ²	PES [Polyester] 76 dtex

Fiber input can be determined individually

FURTHER CHARACTERISTICS

Gauge	5,0	Stitching pattern	warp	Width (nominal)	1.270 mm
Stitch length	2,02 mm	Total tolerance	5,1 %	Total areal weight	1212 g/m ²

Labelling (Standard)	Every roll is equipped with a label in the core. A further label is located outside on the foil or on the box.
Packaging (Standard)	Every roll is wound on a cardboard core and wrapped in foil. Further packaging options can be determined individually.
Storage recommendation	With original packaging: Temperature 15-35°C and 20-80% humidity. No moisture and direct sunlight. To avoid problems with humidity and electrostatic charge, fabrics to be conditioned 24 hours prior to processing, independent of storage conditions.

SAERTEX GmbH & Co. KG has been certified in accordance with ISO 9001:2002008 and has been awarded the 2016 Eco-Profit Award. The SAERTEX GmbH & Co. KG has its own DNV GL certified laboratory.

REINFORCING YOUR IDEAS

Appendix C- Princess Yachts International Defects and Void Recording Sheets


	<p>Macrovoids</p>
	<p>Macrovoid clusters beginning to form between fabric layers</p>
	<p>Shrinkage voids caused by uneven through thickness cure shrinkage</p>
	<p>Bridging</p>

Figure 155 PYI Recorded Void Examples

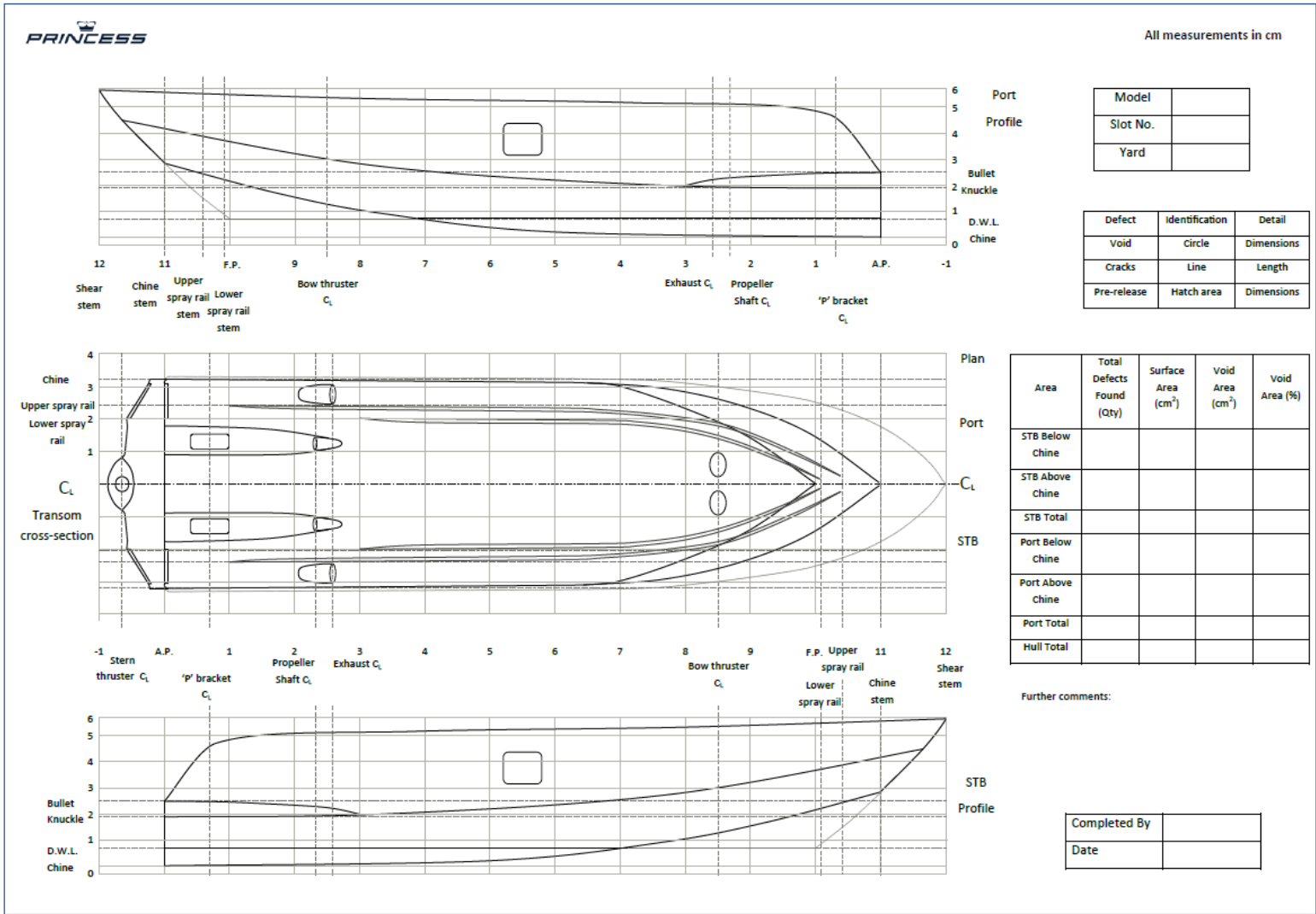


Figure 156 PYI Void Recording Sheet

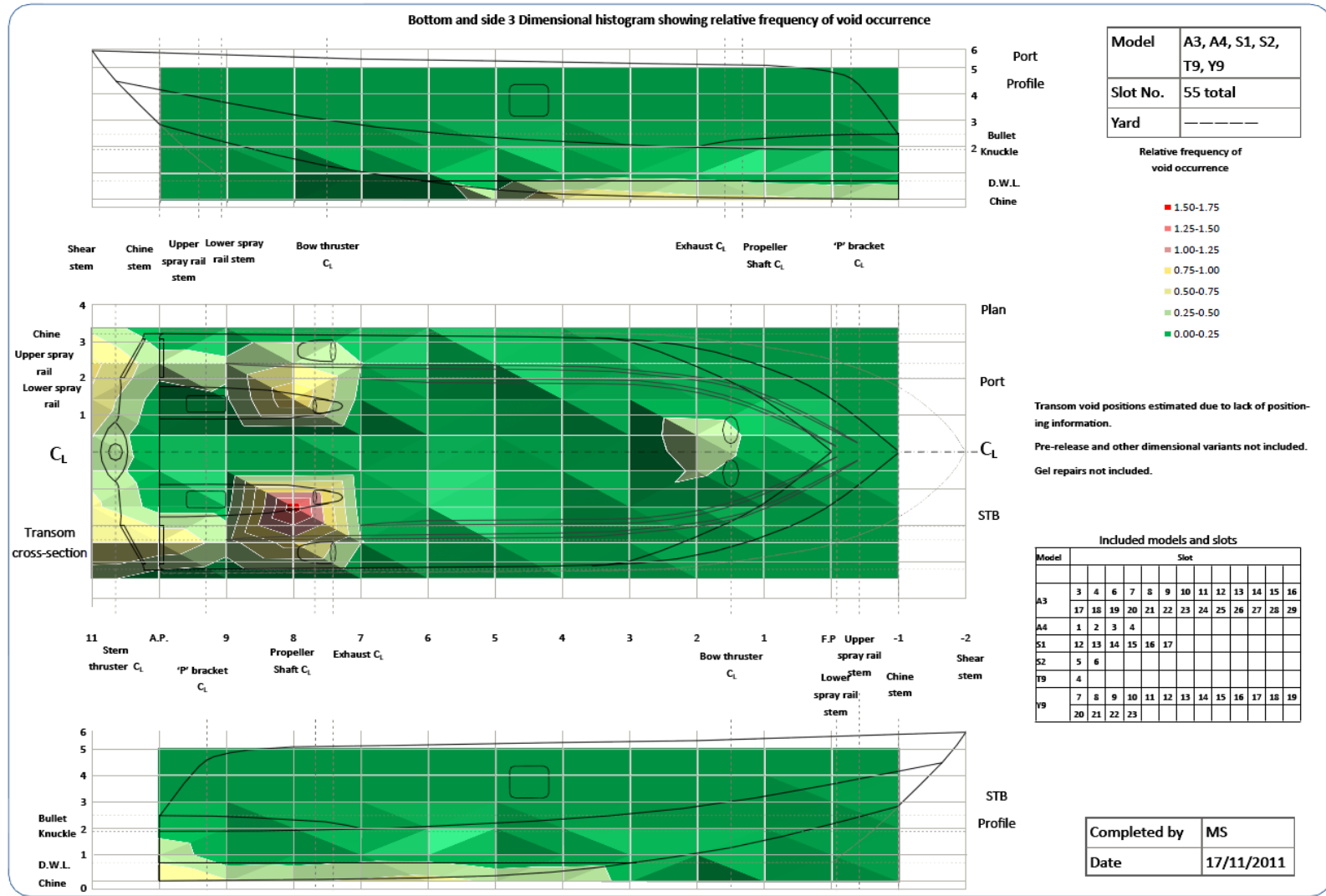


Figure 157 PYI Void Frequency of Occurrence and Location

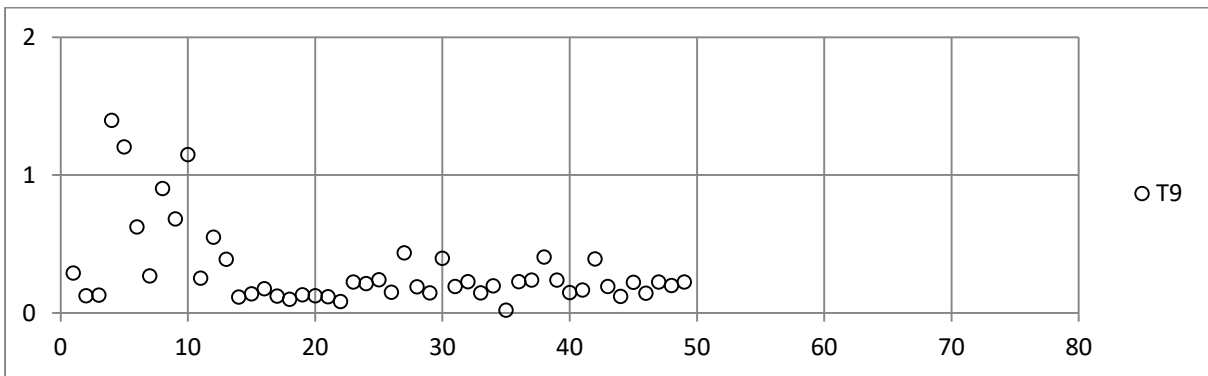
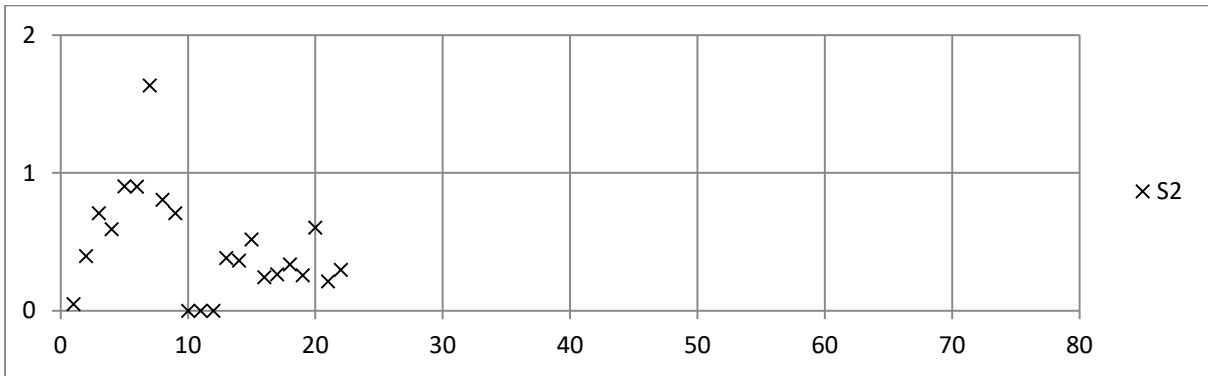
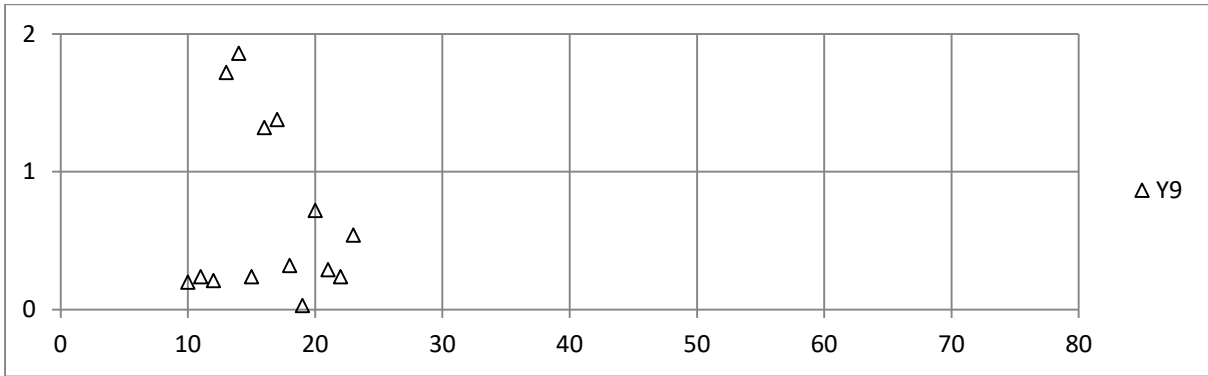
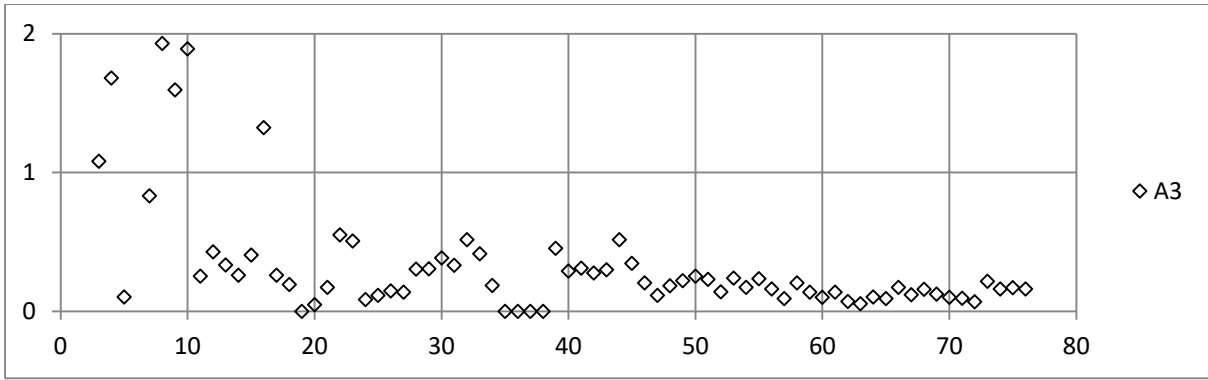


Figure 158 Void area (%) against build number for models A3, Y9, S2 and T9

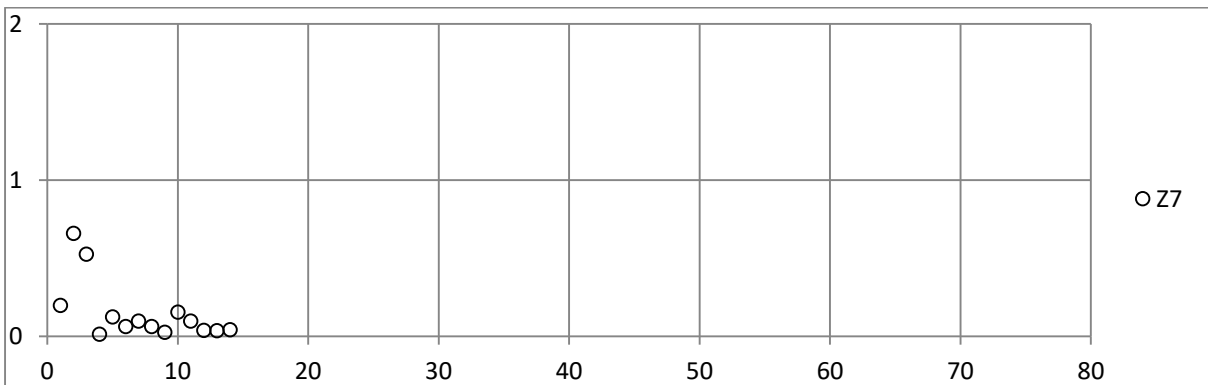
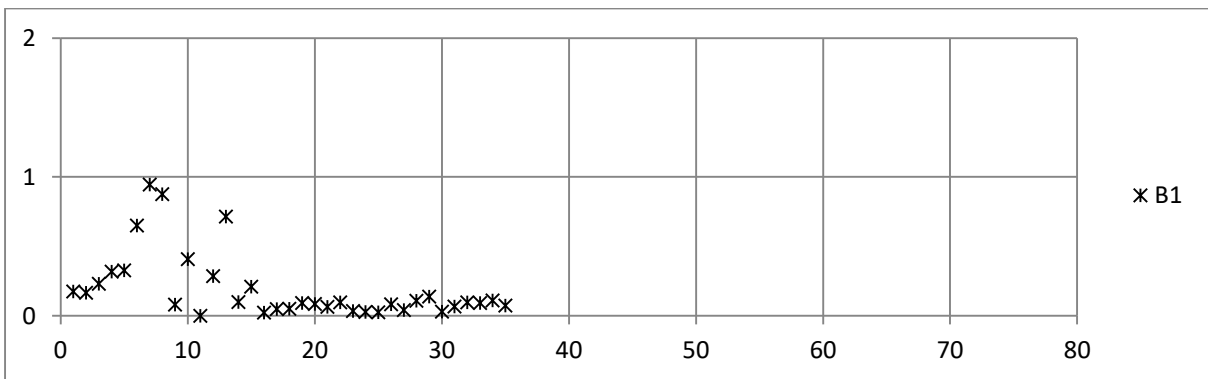
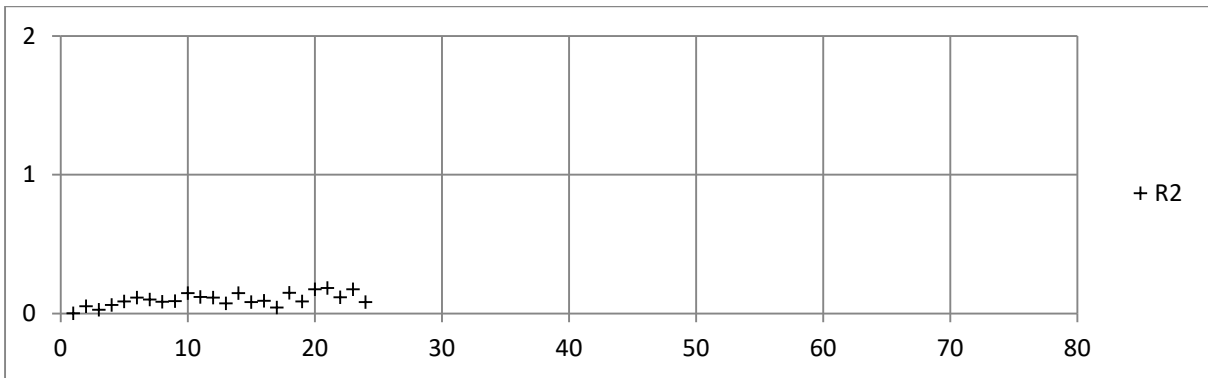
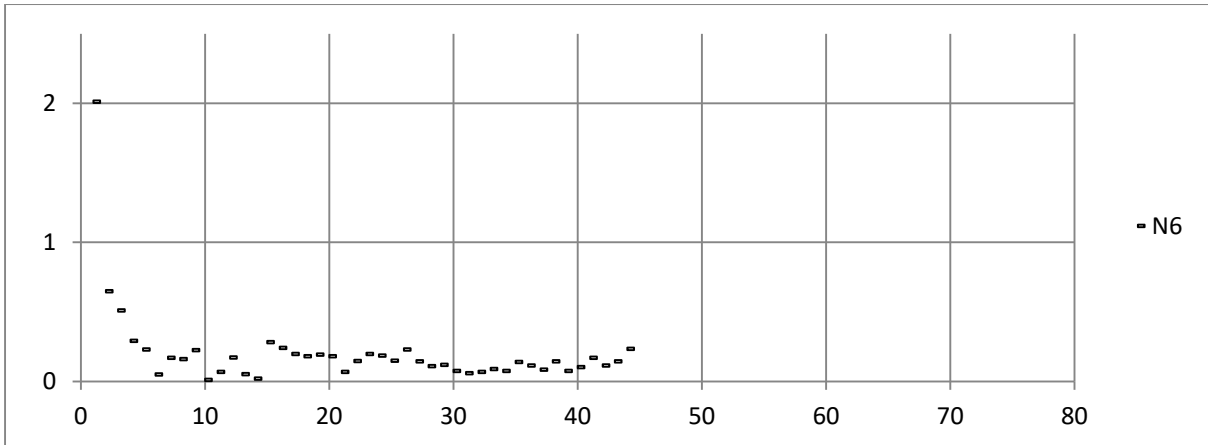


Figure 159 Void area (%) against build number for models N6, R2, B1 and Z7

Appendix D-Princess Yachts layup schematic

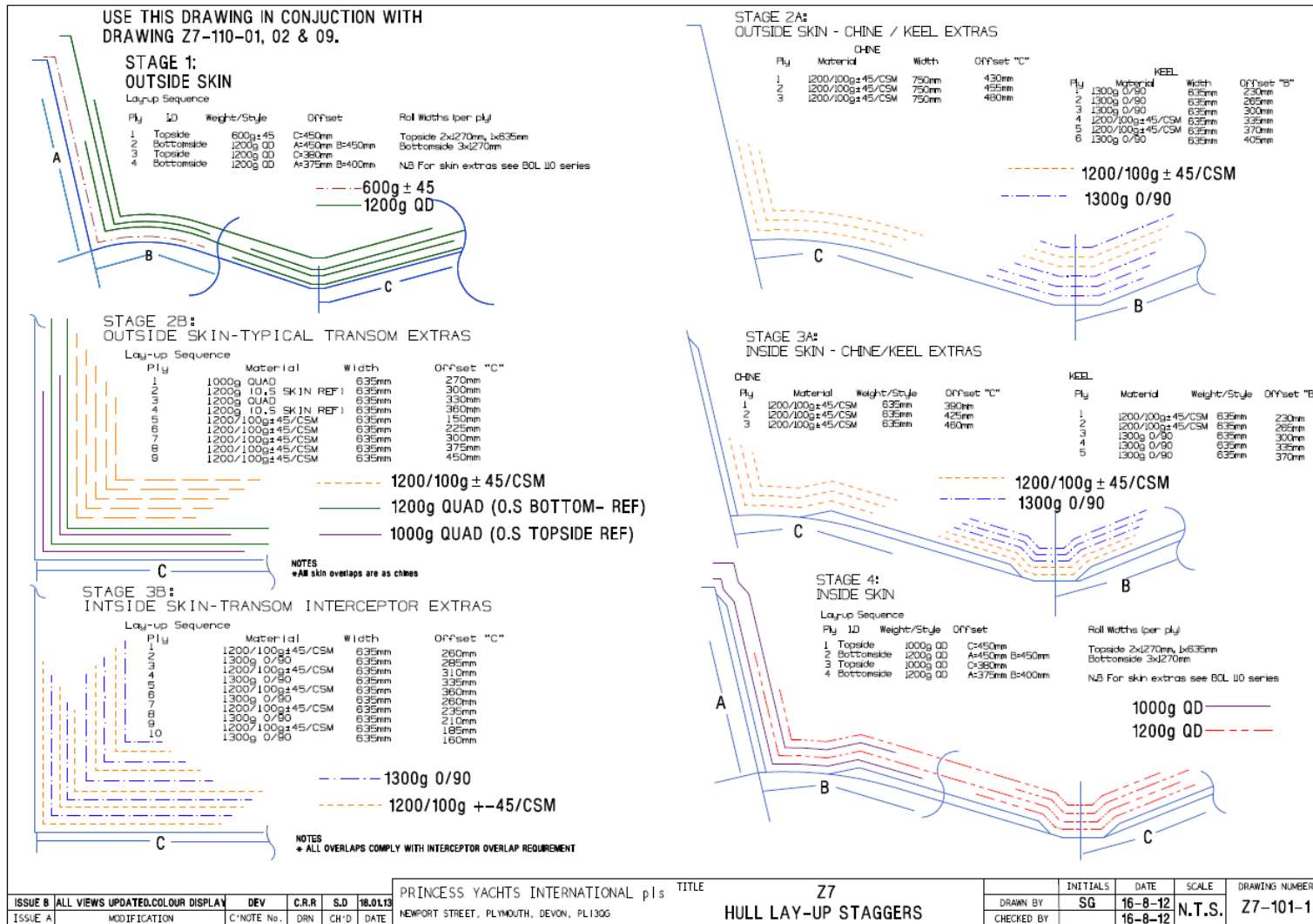


Figure 160: Hull layup schematic.

Appendix E- μ -CT Outer Skin Void Analysis Settings

The following settings have been included to allow for the μ -CT scans to be conducted using the same configuration and set-up.

The core samples were all scanned using the same settings during the same scan sessions. The samples were suspended in a Perspex tube at different heights so that the samples didn't need to be replaced after each scan.

University of Southampton 20-225kVp and 100-450kVP X-ray source Hutch μ -Ct scanner.

CT setting:

File Name=20130425_HMX_428_MS-Y9s8-2_01

OutputFolderName=20130425_HMX_428_MS-Y9s8-2_01

VoxelsX=2000

VoxelsY=2000

VoxelsZ=2000

VoxelSizeX=0.0363679198135462

VoxelSizeY=0.0363679198135462

VoxelSizeZ=0.0363679198135462

OffsetX=0

OffsetY=0

OffsetZ=0

SrcToObject=122.298038482666

SrcToDetector=672.56

MaskRadius=36.3679198135462

DetectorPixelsX=2000

DetectorPixelsY=2000

DetectorPixelSizeX=0.2

DetectorPixelSizeY=0.2

DetectorOffsetX=0.0

DetectorOffsetY=0

CentreOfRotationTop=0.0

CentreOfRotationBottom=0.0

WhiteLevel=60000.0
Scattering=0.0
CoefX4=0
CoefX3=0
CoefX2=0.25
CoefX1=0.75
CoefX0=0
Scale=1.32
RegionStartX=0
RegionStartY=0
RegionPixelsX=2000
RegionPixelsY=2000
Projections=3142
InitialAngle=4.99707508087158
AngularStep=0.11457670273711
FilterType=0
CutOffFrequency=2.4999999627471
Exponent=1.0
Normalisation=1.0
InterpolationType=1
Scaling=1.0
AutomaticCentreOfRotation=1
AutomaticCentreOfRotationOffsetZ1=0
AutomaticCentreOfRotationOffsetZ2=0
OutputType=0
TIFFScaling=1
ImportConversion=0
AutoScalingType=0
LowPercentile=0.2
HighPercentile=99.8

[Xrays]

XraykV=160

XrayuA=42

[CTPro]

Filter_ThicknessMM=0.250

Filter_Material=Aluminium

Shuttling=False

Appendix F-Resin Flow and Void Re-creation μ -CT Settings

The following settings have been included to allow for the μ -CT scans to be conducted using the same configuration and set-up.

University of Southampton 20-225kVp and 100-450kVp X-ray source Hutch μ -Ct scanner.

CT setting:

File Name=20130709_HUTCH_452_MS_slow_01

OutputFolderName=20130709_HUTCH_452_MS_slow_01

VoxelsX=2000

VoxelsY=2000

VoxelsZ=2000

VoxelSizeX=0.0488711767805634

VoxelSizeY=0.0488711767805634

VoxelSizeZ=0.0488711767805634

OffsetX=0

OffsetY=0

OffsetZ=0

SrcToObject=195.614398956299

SrcToDetector=800.5308

MaskRadius=48.8711767805634

DetectorPixelsX=2000

DetectorPixelsY=2000

DetectorPixelSizeX=0.2

DetectorPixelSizeY=0.2

DetectorOffsetX=0.0

DetectorOffsetY=0

CentreOfRotationTop=0.0

CentreOfRotationBottom=0.0

WhiteLevel=60000.0

Scattering=0.0

CoefX4=0.0

CoefX3=0.0
CoefX2=0.0
CoefX1=1.0
CoefX0=0.0
Scale=1.0
RegionStartX=0
RegionStartY=0
RegionPixelsX=2000
RegionPixelsY=2000
Projections=3142
InitialAngle=0
AngularStep=0.11457670273711
FilterType=0
CutOffFrequency=2.4999999627471
Exponent=1.0
Normalisation=1.0
InterpolationType=1
Scaling=1.0
AutomaticCentreOfRotation=1
AutomaticCentreOfRotationOffsetZ1=0
AutomaticCentreOfRotationOffsetZ2=0
OutputType=0
TIFFScaling=1
ImportConversion=1
AutoScalingType=0
LowPercentile=0.2
HighPercentile=99.8
[Xrays]
XraykV=80
XrayuA=87

[CTPro]

Filter_ThicknessMM=0.500

Filter_Material=Aluminium

Shuttling=True

Appendix G-In-situ Infusion μ -CT Settings

The following settings have been included to allow for the μ -CT scans to be conducted using the same configuration and set-up.

University of Southampton 20-225kVp and 100-450kVP X-ray source Hutch μ -Ct scanner.

CT setting:

File Name=20140430_HUTCH_599_MS_01

OutputFolderName=20140430_HUTCH_599_MS_01

VoxelsX=2000

VoxelsY=2000

VoxelsZ=2000

VoxelSizeX=0.0462927598264385

VoxelSizeY=0.0462927598264385

VoxelSizeZ=0.0462927598264385

OffsetX=0

OffsetY=0

OffsetZ=0

SrcToObject=185.689739227295

SrcToDetector=802.241

MaskRadius=46.2927598264385

DetectorPixelsX=2000

DetectorPixelsY=2000

DetectorPixelSizeX=0.2

DetectorPixelSizeY=0.2

DetectorOffsetX=0.0

DetectorOffsetY=0

CentreOfRotationTop=0.0

CentreOfRotationBottom=0.0

WhiteLevel=60000.0

Scattering=0.0

CoefX4=0.0

CoefX3=0.0
CoefX2=0.0
CoefX1=1.0
CoefX0=0.0
Scale=1.0
RegionStartX=0
RegionStartY=0
RegionPixelsX=2000
RegionPixelsY=2000
Projections=2401
InitialAngle=5
AngularStep=0.149937526030821
FilterType=0
CutOffFrequency=2.4999999627471
Exponent=1.0
Normalisation=1.0
InterpolationType=1
Scaling=1.0
AutomaticCentreOfRotation=1
AutomaticCentreOfRotationOffsetZ1=0
AutomaticCentreOfRotationOffsetZ2=0
OutputType=0
TIFFScaling=1
ImportConversion=1
AutoScalingType=0
LowPercentile=0.2
HighPercentile=99.8
[Xrays]
XraykV=80
XrayuA=154

[CTPro]

Filter_ThicknessMM=0.500

Filter_Material=Aluminium

Shuttling=False

Appendix H-Fibre Optic Results

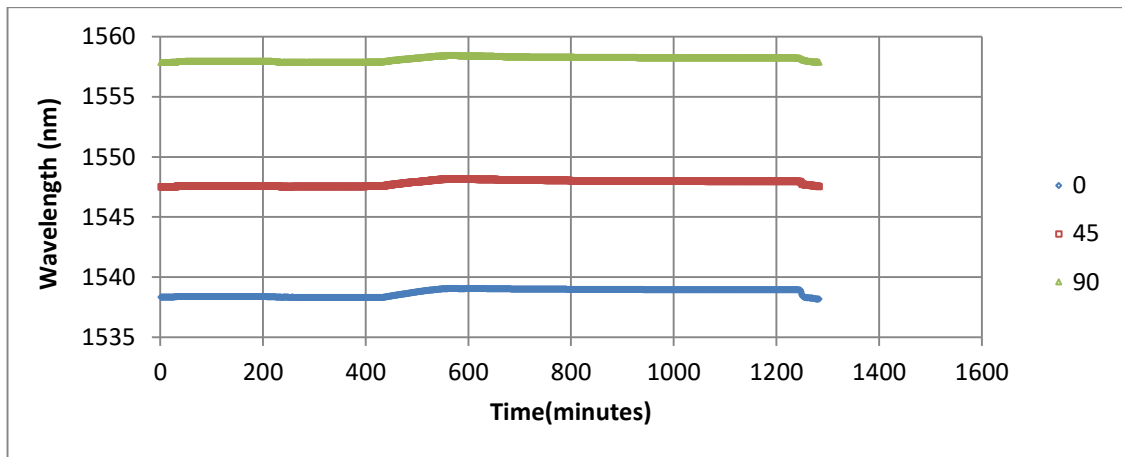


Figure 161: Fibre optic one wavelength measurements from vacuum to demoulding

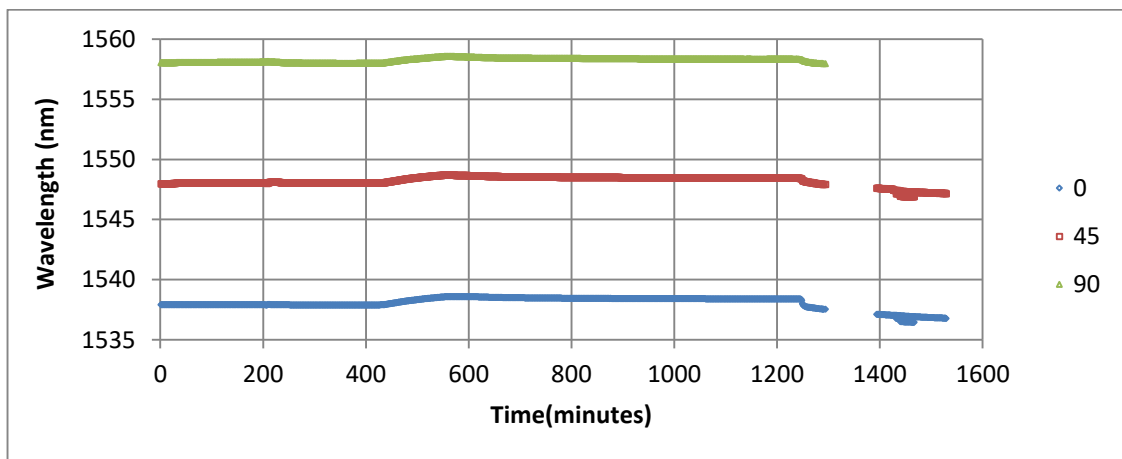


Figure 162: Fibre optic two wavelength measurements from vacuum to demoulding

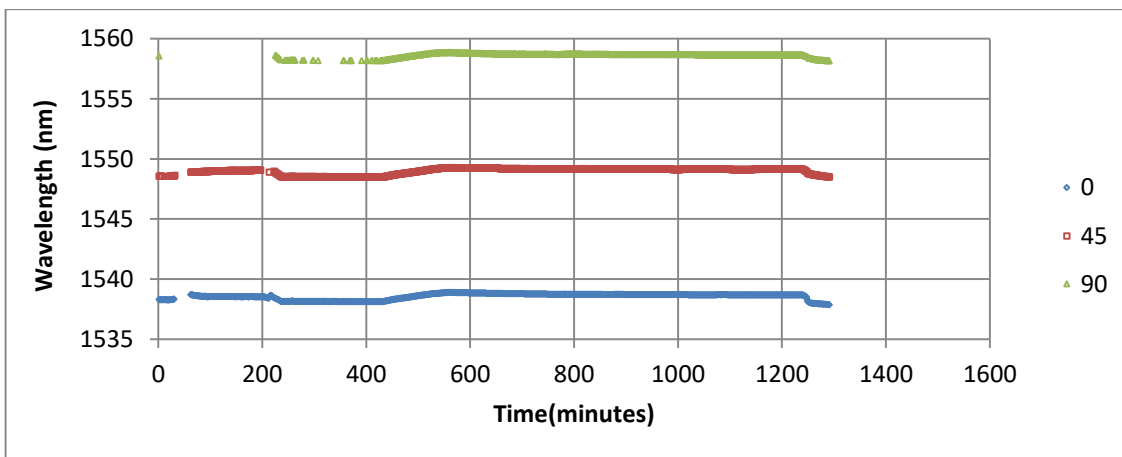


Figure 163: Fibre optic three wavelength measurements from vacuum to demoulding.